TR-152
1991

Particles in Surface Waters: Coagulation and Transport

G. Culkin
D. Lawler

Texas Water Resources Institute

Texas A&M University

TR-152

PARTICLES IN SURFACE WATERS: COAGULATION AND TRANSPORT

Gerald W. Culkin

Desmond F. Lawler

TEXAS WATER RESOURCES INSTITUTE

TEXAS A&M UNIVERSITY

AUGUST 1991

Technical Report No. 152

PARTICLES IN SURFACE WATERS: COAGULATION AND TRANSPORT

by

Gerald W. Culkin
Desmond F. Lawler

This report is a joint effort between the Texas Water Resources Institute, Texas A&M University, and the Center for Research in Water Resources, The University of Texas at Austin. It is also published in identical form by CRWR as Technical Report CRWR 232.

August, 1991

TEXAS WATER RESOURCES INSTITUTE
Texas A&M University
College Station, Texas 77843-2118

RESEARCH PROJECT COMPLETION REPORT

Project Numbers
G-1451-03
G-1592-03
(September 1, 1987 - August 31, 1988)
(September 1, 1988 - August 31, 1989)

Agreement Numbers
14-08-0001-G-1451
14-08-0001-G-1592

PARTICLES IN SURFACE WATERS: COAGULATION AND TRANSPORT

by

Gerald W. Culkin
Desmond F. Lawler

Center for Research in Water Resources
Bureau of Engineering Research
The University of Texas at Austin
Austin, Texas 78758-4497

The research on which this report is based was financed in part by the U.S. Department of the Interior, Geological Survey, through the Texas Water Resources Institute.

Technical Report No. 152
Texas Water Resources Institute
Texas A&M University
College Station, TX 77843-2118

Technical Report CRWR 232
Center for Research in Water Resources
10100 Burnet Road
Austin, TX 78758-4497

August 1991

ACKNOWLEDGEMENTS

This research was sponsored through a grant from the Texas Water Resources Research Institute. Dr. Wayne Jordan was the program manager and provided useful oversight.

The research was conducted in fulfillment of degree requirements for the first author. Dissertation committee members included Drs. Neal E. Armstrong, Randall J. Charbeneau, Howard M. Liljestrand, and Robert S. Schechter, of the University of Texas at Austin, and Dr. Donald J. O'Connor, of Manhattan College. Each member made important suggestions in the formation of this research. Although not a committee member, Dr. Kamy Sepehrnoori was particularly generous in his assistance with numerical methods. Other faculty who made major impressions on the research through their advice and teaching included Drs. Joseph F. Malina, David R. Maidment, and Edward J. Holley.

Dr. Mooyoung Han made a significant contribution to this research with his curvilinear flocculation model development. Tim Chan, Lawrence (Nubz) Newbury, and Bob Gloyd assisted in teaching 'C' so that Dr. Han's models could be modified. Dr. Norm Jones preparation and sharing of the contouring program that was used was extremely helpful.

PARTICLES IN SURFACE WATERS: COAGULATION AND TRANSPORT

Abstract

Conventional water quality assessment and simulation of particles in natural waters focus on bulk concentrations of the suspended solid phase. These analyses rely directly or indirectly on a linear, 'average particle' approach to describe processes that are nonlinear and highly size-dependent.

Size-dependent transport and transformation mechanisms were simulated in this research to identify conditions in which coagulation is important. Explicit finite difference schemes for two-dimensional, laterally-averaged, unsteady particle transport were developed to approximate the size-dependent particle transport processes, which included advection, dispersion, and settling. Coupled exchange of discrete particles between the water column and sediment bed was modeled using size-dependent particle sedimentation and resuspension. Simultaneous particle-particle flocculation was integrated over time in parallel with transport.

Model simulations of systems with idealized morphometry and forcing provided greater insight to competing processes that drive particle behavior in natural systems. Application of the model to a real system gave plausible results and suggested explanations for observed conditions.

TABLE OF CONTENTS

LIST OF TABLES

LIST OF FIGURES

LIST OF NOMENCLATURE

Symbol	Meaning
α, α_{chem}	Collision efficiency
β	Binary collision frequency
β	Derived coefficient for power law number distribution, number distribution exponent
γ	Curvilinear collision frequency function
ε	energy dissipation rate per mass of fluid
φ	Adjustment factor to convert rectilinear collision frequency function to curvilinear collision frequency function
μ	Absolute or dynamic viscosity of fluid
ν	Kinematic viscosity of fluid
ρ_s ρ_p	Density of solid, particle, or floc
ρ_f	Density of fluid
τ	A time scale
τ, τ_0	Actual shear stress at the bed
τ_c	Critical shear stress at the bed need to cause resuspension
A, A_s	Specific surface area of solid phase
A	Derived coefficient for power law number distribution, related to number concentration
B	Width of channel section
C	Courant number for numerical advection scale
C_d	A dimensionless drag coefficient
C_i	System "i" response, typically associated with numerical analysis
C_T, C_d, C_p	Bulk concentrations of contaminant: total, dissolved, particulate
D	Dispersion number for numerical dispersion scale
d, d_p	Particle diameter
E	Dispersion tensor
f	Friction factor for bed/water interface

f_c	Bed-Water friction parameter
f_d, f_p	Fraction of total contaminant as solute and as sorbate, respectively
f_k	Fraction of total bed mass in size k
g	Gravitational acceleration
G	Velociity gradient for collision by fluid shear
j_d	Particle number flux due to deposition
J_d	Particle mass flux due to deposition
j_R	Particle number flux due to deposition
J_R	Particle mass flux due to deposition
k	Boltzmann's constant
M	Dimensional (and empirical) bed mass flux rate constant
M'	Dimensionless bed mass flux rate constant
N or n	Discrete particle number concentration
P	Peclet number, ratio of physical or numerical advection to dispersion
R	Reaction rate of constituent
S	Discrete particle surface area concentration
t	Time
T	Temperature
U	Fluid velocity vector
u_B	Fluid velocity at be-water boundary layer
u_*	Friction or shear velocity parameter
v	Particle settling velocity relative to fluid
V	Discrete particle volume concentration

CHAPTER I

INTRODUCTION

1.1 NEED FOR RESEARCH

Suspended solid materials and trace dissolved contaminants are ubiquitous in natural aquatic environments. The transport, fate, and effects of the dissolved substances are each intimately related to the transport and fate of the solid phase. Models developed to date for the prediction of the solids-associated transport and fate use simplified representations of the processes controlling both solids transport and solids-contaminant association. These models give usable approximations for long-term problems but are unable to simulate the full range of transient system conditions. The increased attention being given to the fate and effects of contaminants in the aquatic environment calls for the development of refined tools for predicting solids and solids-associated contaminant behavior.

Nonpoint sources, *i.e.*, diffuse and indirect sources of pollution such as stormwater runoff, contribute 95% of the suspended solids loaded into the nation's waters (USEPA, 1984). Concerning contaminants from nonpoint sources, the National Urban Runoff Program documented the exceedance of water quality and health criteria for specific contaminants in the stormwater runoff from each of the nineteen urban areas studied (USEPA, 1983). Half of the States and six of the ten USEPA regions identified nonpoint sources as the major reason for the inability to attain water quality goals (USEPA, 1984). Various independent surveys of environmental managers, scientists, and engineers led to the conclusion that 75% of all lakes in the U.S. are seriously affected by nonpoint source pollution (USEPA, 1984).

The diameters of measurable particles in natural water systems span several orders of magnitude, and yet most water quality analyses treat the suspended solids phase as a uniform and unchanging commodity. Theoretical and experimental studies have shown, however, that particle composition, particle transport, and particle-particle and particle-contaminant interactions are all highly size-dependent. Although contaminant fate is intimately related to particle fate, no comprehensive transport and transformation model incorporates present understanding of the size-dependent particle and particle-contaminant behavior. A model which accounts for the mechanisms and effects of changes in the particle size distribution and the related nonlinear consequences would be expected to provide better predictions of solid and contaminant behavior.

Models in use for predicting solids transport and fate oversimplify the processes controlling particle transport and interaction. For example, solids sedimentation is described by a mass-mean particle settling velocity, or at best, a static distribution of settling velocities. Either approach ignores the dynamic, discrete particle coagulation mechanisms which profoundly affect the sedimentation of particles and sorbed contaminants. Models formulated to simulate the coagulation process in natural systems have typically assumed horizontal uniformity and also ignored interactions between the sediment bed and water column.

Models for simulating contaminant transport and fate rely on simplifications of the solid/solute distribution process, describing the association as dependent on sorbent mass concentration, *i.e.*, independent of sorbent surface area. Again, the influence that particle size plays in this process has been averaged away. These models are often able

to simulate average solids and contaminant behavior, but only within the limited range of system conditions described by time- or space-average solids parameters.

1.2 OBJECTIVES OF RESEARCH

This research was directed toward a more fundamental study of the role of particle coagulation in solids transport, the role of surface processes in contaminant fate, and their interrelationship. Mechanistic models were developed for the simulation of particle-particle interaction, particle-contaminant interaction, and their transport and fate in natural systems. To improve the physical foundation and increase the analytical ability of present sediment-contaminant transport and fate models, this research included the following objectives:

1) Formulate a two-dimensional, unsteady solids transport model that conservatively transports multiple classes of discrete size particles;

2) Couple particles in the water column and sediment bed through size-dependent sedimentation and resuspension transfer functions;

3) Couple to the particle transport model a transformation model of size-dependent coagulation;

4) By use of the model, evaluate the influence and interaction of coagulation, sedimentation, and resuspension on the transport and fate of solids in idealized and 'real' systems.

1.3 ORGANIZATION OF REPORT

Chapters 2 and 3 are devoted to background material. Chapter 2 is a review of the literature associated with particle behavior, especially in natural waters. Information and data pertaining to model study of the 'real' system, Town Lake, is given in Chapter

3; data there are summarized in a form consistent with the model formulation. Development of the particle transport-transformation model is presented in Chapter 4; the rationale for the various decisions made in model formulation is also discussed.

Chapters 5 and 6 contain model results and discussion. The model was first tested and used in 'idealized' settings, *i.e.*, systems with uniform rectangular morphometry, upstream inflow and load only, and steady flow. These simple systems made testing the sensitivity of model results to the inclusion (or exclusion) of certain particle phenomena, *i.e.*, coagulation, sedimentation, and resuspension, easier to interpret. These results, as well as parameter sensitivity studies, are in Chapter 5. The application to Town Lake, with its more complex morphometry and forcing, is presented in Chapter 6. Three types of conditions in Town Lake were considered: annual-average, steady-state forcing; seasonal-average, quasi-steady forcing for each of four seasons; and short-term, time-variable forcing of storm events. Finally, the results of the research are summarized in Chapter 7.

Throughout this research, a secondary objective was the formulation of a model that could be easily extended to include the interaction of soluble contaminants with particles via sorption mechanisms. Further, it was intended that the extension allow size-dependent particle-contaminant sorptive associations. Such an extended particle-contaminant model would account simultaneously for the behavior of the particles, the particle-bound contaminant, and the dissolved contaminant in a natural system. Appendix A contains a literature review providing the rationale for the development of the size-dependent particle-associated contaminant model. The expressions needed to relate the particle suspension to the equilibrium contaminant phase distribution are also presented there.

CHAPTER II

REVIEW OF LITERATURE

2.1 INTRODUCTION

A review and analysis of research on solids transport and fate are presented in this chapter. Relevant aspects include transport modeling of conservative substances and solids, coagulation theory and application. The review of related research in particle-associated contaminant transport, fate, adsorption theory, and modeling is presented in Appendix A.

2.2 TRANSPORT AND FATE OF PARTICLES IN NATURAL SYSTEMS

The transport of any contaminant is characterized by the motion of the bulk fluid and the behavior of the contaminant within that fluid. The simplest solids transport to imagine is that in which the solid particle behaves exactly like a fluid particle. A close approximation to this conceptualization is the ideal, infinitely dilute solution of a neutrally buoyant, conservative substance. Conditions necessary for solids to approach this behavior would include a zero density difference relative to the fluid, no reaction, gain, or loss, and insignificant inertial effects. The last condition is satisfied by Stokesian particles (Jobson and Sayre, 1970; Ludwick and Domurat, 1982), *i.e.*, where $Re < 0.5$. Similarly, particle relaxation times and characteristic turbulent eddy microtimes were compared by Sheng (1986b) to conclude that particles of radius less than 200 μm (at a particle density of 1.2 g/cm^3) would completely follow the motion of turbulent eddies in estuarine and coastal waters. Transport of neutrally buoyant solutes is presented, then, as the limiting case of solids transport.

2.2.1 Solute transport

The majority of research on contaminant transport in natural systems has focused on conservative, chemically discrete, neutrally buoyant, dissolved solutes, although temperature and group parameters such as salinity have certainly been employed to interpret mixing data. The problem is formulated as a set of simultaneous partial differential equations. In their most general form, these equations describe the instantaneous balance of force, conservation of mass (fluid and solute), and conservation of energy, all at a point.

Separate bodies of literature concerning the representation of relevant hydrodynamic processes have developed for each type of aquatic system. Marine and estuarine systems are not the focus of this research; rather, freshwater streams, lakes, and reservoirs are the concern. Fischer *et al.* (1979) provided one of the earliest syntheses of mixing and transport processes for these systems.

For riverine transport, Holley and Jirka (1986) gave an excellent and comprehensive presentation of the theory and experimental results applicable to initial and ambient mixing/transport in these systems. Initial mixing is the near field, active transport of material or energy via jets and/or plumes as fluid is discharged into a receiving body. It is characterized by the discharge's momentum and buoyancy fluxes as well as the properties of the receiving system, *e.g.*, boundaries, and density and flow profiles. Ambient mixing is the far field, passive transport of matter or energy which occurs after initial mixing. Initial mixing can often be represented as a diffusive (gradient-type) process. Although the two types of transport are relatively well represented as individual processes, a smooth and continuous representation of the transition between the two modes of transport does not currently exist.

Holley and Jirka gave particular attention to the development and applicability of spatially and temporally averaged representations of the complete instantaneous, three-dimensional solute transport equation. Theory and measurements from laboratory and field tests were presented for semi-empirical closure of the turbulence problem. Sufficient research has been completed to allow prediction of two-dimensional ambient response to steady input or one-dimensional ambient response to a pulse input with relatively good accuracy (within a factor of four) in rivers under certain conditions.

Although the same physics that applies to riverine transport also applies to lakes and reservoirs, the dynamics are usually quite different and more complex. These differences are due to the greater significance of meteorological forcing functions and large scale motions in lakes and reservoirs (Boyce, 1974). The hydrodynamic and solute transport equations for lakes and reservoirs are presented, along with simplifications, by many authors (Csanady, 1978; Lam, 1986; Lynch, 1986). Relatively large differences between and among lakes and reservoirs in their sources of energy influx and efflux, geomorphometry, and time and space scales result in significant differences in their behavior (Imberger and Hamblin, 1982). Because of the span in time and space scales, it is not possible to relate mixing to boundary conditions and flow properties through some universal turbulence closure scheme, so phenomenological modeling appears to be the best approach (Imberger *et al.*, 1987; Imberger and Hamblin, 1982). Mean fluid circulation and energy transport can be described well in certain circumstances (Lam, 1986), but the problem with this approach is that turbulent mass transport is not well resolved. Reviews of turbulence

closure schemes and laboratory and field measurements pertinent to reservoirs and lakes have been presented (Blumberg, 1986; Imberger *et al.*, 1987).

Simplification of the continuous partial differential solute transport equations via a discrete-volume spatial representation reduces the problem to the solution of ordinary differential equations, albeit with volumetric exchange flows used to represent the dispersion. This multiple box approach has been used widely in lake modeling (Kuo and Thomann, 1983; Thomann and Mueller, 1987) and to a lesser degree in river modeling (Stefan and Demetracopoulos, 1981). Some (Shanahan and Harleman, 1984; Shanahan and Harleman, 1985) have criticized the discontinuous box model representations because of their implicit numerical dispersion and because calibration cannot be tied to the physical lake hydrodynamics. Others (Kuo and Thomann, 1985) have justified certain applications of compartment modeling as a practical, necessary, and sufficiently accurate engineering analysis, contingent upon the appropriate system, dominant processes and scales, and available resources. One-dimensional box modeling for rivers was criticized (Holley and Jirka, 1986) because of its discontinuous spatial representation and its neglect of the significant transverse concentration variations which normally persist for long times (distances) in riverine settings.

2.2.2 Solids transport

The economic and social effects of erosion and sedimentation in water bodies have motivated vast research efforts directed toward the prediction of sediment transport. Recent progress has been presented for rivers (Wang *et al.*, 1986), reservoirs (Annandale, 1987; Frenette and Julien, 1986), lakes (Hakanson and Jansson, 1983; Sly, 1978), and estuaries (Partheniades, 1986). Past efforts have

generally treated sediment as a material with bulk properties, neglecting the explicit transport of solids-associated contaminants. Previous approaches have been highly empirical but generally adequate for the long term prediction of net sediment flux and distribution. For the prediction of short term flux and solids-associated contaminant fate, where the behavior and associations are very particle size-dependent, the empirical method is probably inadequate.

The sediment transport equation is similar to the conservative solute transport equation but with the complications of solids sources and sinks. Obvious sources include inflows and bed erosion, as well as biological production and inorganic precipitation. Obvious sinks include outflows and deposition, as well as biochemical reactions and inorganic dissolution. Not so apparent is that sedimentation is normally represented by the settling velocity of discrete particles, neglecting any particle interactions. Coagulation has been shown, however, to be a potentially important process in lakes (O'Melia and Bowman, 1984), estuaries (Edzwald *et al.*, 1974), and marine environments (Lerman, 1979; McCave, 1984).

Descriptions of unsteady, noncohesive sediment transport in turbulent fields, *i.e.*, averaging the instantaneous three-dimensional motion of sediment over time and space, have been developed for one-dimensional vertical fields (Dobbins, 1943) and for two-dimensional, laterally-averaged channel flows (Sayre, 1969). The analytical solution of these transport equations is not possible except for certain conditions, such as those imposed by Dobbins.

2.3 COAGULATION

The present theory of coagulation stems from early modern physics (von Smoluchowski, 1917). Particle-particle interactions are thought to occur via binary

collisions. The process is generally conceived as comprising two distinct steps, transport and destabilization (Hahn and Stumm, 1970), or transport and attachment (O'Melia, 1972). The transport step brings the two particles towards one another, within some very small distance of separation. The attachment step provides a stable or metastable bonding of the two particles that have collided, and it generally requires the destabilization of the particles to overcome electrostatic or steric repulsion.

2.3.1 Transport

The relative motion between two particles in a fluid can result in their collision or near collision. Any process that forces the particles to move relative to the fluid or that forces the fluid parcels to move relative to themselves results in particle transport in the coagulation sense. Transport mechanisms traditionally considered in aquatic coagulation analysis include Brownian motion, differential settling, and laminar or turbulent fluid shear. These are typically the dominant transport mechanisms in hydrosol flocculation, though any material or energy gradient would also result in particle transport. Examples of these mechanisms would include thermophoresis, electrophoresis, osmosis, and electroosmosis. As many as five transport mechanisms have been considered (McCave, 1984) in the marine aggregation of particles: the dominant three mentioned above, biogenic aggregation (via organism filtration, aggregation, and excretion), and turbulent inertial transport, borrowed from the aerosol literature (*i.e.*, Pruppacher and Klett, 1978). McCave (1984) showed that turbulent inertial coagulation would only be significant, relative to turbulent fluid shear, for particles differing in diameter by a half centimeter or more. Based on organism population densities and filtering rates, he also concluded

that biogenic aggregation was responsible for most of the 'coagulation' of particles larger than one micrometer in the upper ocean.

Three general approaches have been taken in modeling coagulation. These are referred to here as the similarity approach, the empirical approach, and the discrete particle approach. The methods are discussed in order, but emphasis is given to the latter since it is the method of choice in the research reported herein.

The similarity approach to coagulation modeling was introduced in studies of the evolution of aerosol size distributions (Friedlander, 1965). Friedlander presented the case for a self-similar particle size distribution which would be asymptotically approached at equilibrium. The key assumption in the similarity approach is that there is a constant volume flux through the particle size distribution at all times resulting from a continuous supply of particles and the quasi-equilibrium of coagulation mechanisms. Statistical moments of the analytical distributions can then be used to infer the dominant interactions, which Friedlander did for aerosols. The same approach was used to analyze marine interactions (Hunt, 1980). Others (Farley and Morel, 1986) have also used the constant volume flux assumption in a dimensional analysis of the self-preserving particle size distributions established in coagulation and sedimentation. Farley and Morel used micron-sized copper and goethite (γ-FeOOH) particles, with concentrations spanning several orders of magnitude, in experiments designed to calibrate their model.

Coagulation has also been modeled with empirical approaches, *i.e.*, as a process whose discrete dynamics are lumped together and determined experimentally. Coagulation in river impoundments was modeled using measured distributions of settling velocity (Hahn *et al.*, 1980; Uchrin and Weber, 1980). Mean settling

velocities for lake sediments have been derived from laboratory flume deposition/resuspension studies where concentration and bed shear stress were independent variables (Lick, 1982). Research on the Great Lakes (Richardson *et al.*, 1983) produced spatially distributed mean settling velocities for three "size classes" of solids (*i.e.*, light, heavy, and organic) in Saginaw Bay. Velocities were derived by calibration between predictions and field data. Modeling of estuarine coagulation, known to significantly affect particle interactions in that destabilizing environment, has also relied on empirical settling velocity distributions (Ariathurai and Krone, 1976). Recent work in estuarine sedimentation modeling (Hayter, 1987) employs an "apparent settling velocity," experimentally determined in the laboratory, as a function of concentration, salinity, and bed stress.

The discrete particle approach to coagulation modeling approximates the continuous particle number concentration as an explicit function of discrete size. The physical and chemical phenomena that govern particle interactions and fate can therefore be modeled mechanistically. Lawler formulated an unsteady, one-dimensional (vertical) model for analyzing particle coagulation and sedimentation (Lawler, 1979; Lawler *et al.*, 1980). The model integrates a set of ordinary differential equations, each describing the time rate of change in concentration of particles, in a fixed size range and in a particular vertical layer, due to flocculation (according to Smoluchowski), as follows:

$$\frac{dn_k}{dt} = \frac{1}{2}\alpha_{chem} \sum_{i+j=k} \beta(i,j)\, n_i\, n_j \; - \; \alpha_{chem}\, n_k \sum_{i=1}^{c} \beta(i,k)\, n_i \qquad \textbf{(2.1)}$$

The state variable, n_k, is the absolute particle number concentration in [#/cm^3]. In this equation, i, j, and k are integer indices denoting particle size class; c is

the maximum allowable value of i, j, or k; and t is time. The first term on the right hand side of the rate equation (2.1) describes the rate of gain of particles of size k by flocculation of two smaller particles, i and j. The second term describes the loss of particles of size k by flocculation with particles of size i, forming particles larger than k.

α_{chem} is the collision efficiency factor, *i.e.*, the fraction of predicted collisions that result in attachment. This probability of attachment, α_{chem}, depends upon microscopic interactions affected by solution and surface chemistry as well as by particle steric constraints. $\beta(i,j)$ is the composite collision frequency function that quantifies how often particles of sizes i and j do collide, a function of particle-fluid hydrodynamics with the effect of particle concentration extracted. The frequency function is a second-order number rate coefficient with dimensions for $\beta(i,j)$ of $[L^3T^{-1}]$.

The total collision frequency function, $\beta(i,j)$, is the linear sum of the interparticle frequency functions for the individual transport (collision) mechanisms considered in this model, *i.e.*, Brownian motion, differential settling, and turbulent fluid shear:

$$\beta(i,j) = \beta_{Br}(i,j) + \beta_{Ds}(i,j) + \beta_{Sh}(i,j). \qquad \textbf{(2.2)}$$

It is assumed that these mechanisms are independent of one another and therefore linearly additive.

Friedlander's classic text (1977) presented derivations for the so-called rectilinear collision frequency functions. These collisions stem from assumed rectilinear particle trajectories, *i.e.*, when particles do not hydrodynamically affect

each others' trajectories. The rectilinear collision frequency functions are presented below.

Hydrodynamic correction factors derived to convert the rectilinear collision frequency functions into curvilinear frequency functions have been presented (Han, 1989). Departing slightly from Han's nomenclature, let the rectilinear collision frequency kernel for a particular transport mechanism **x** be denoted as $\beta_x(i,j)$. Let the hydrodynamic correction factor needed to reconcile the rectilinear collision frequency with the curvilinear trajectories be denoted as $\varphi_x(i,j)$. Han called the curvilinear correction factor $\alpha_x(i,j)$, not to be confused with the chemical collision efficiency α_{chem}. Then the actual curvilinear collision frequency function, $\gamma_x(i,j)$ is the product of the rectilinear collision frequency kernel and the curvilinear correction factor, *i.e.*,

$$\gamma_x(i,j) = \varphi_x(i,j) \cdot \beta_x(i,j) . \qquad \textbf{(2.3)}$$

The three rectilinear collision kernels follow.

Brownian motion:

$$\beta_{Br}(i,j) = \frac{2\,k\,T}{3\,\mu}(d_i + d_j)^3 \left(\frac{1}{d_i} + \frac{1}{d_j}\right) \qquad \textbf{(2.4)}$$

where k is Boltzmann's constant, μ is the absolute viscosity, T is the absolute temperature, and d_i and d_j are the diameters of particles of sizes i and j. Han called the curvilinear correction factor, *i.e.*, the coefficient to apply to the rectilinear the β of (2.4), $\alpha_{Br}(i,j)$. He calculated the values by integrating Smoluchowski's rectilinear diffusion equation with hydrodynamic correction and interparticle forces.

Differential settling:

$$\beta_{Ds}(i,j) = \frac{\pi\,g}{72\,\mu}(\rho_s - \rho_f)(d_i + d_j)^3 \, |d_i - d_j| \qquad \textbf{(2.5)}$$

where ρ_s is the particle density, ρ_f is the fluid density, and g is gravitational acceleration. Note that the development for differential settling incorporates settling velocities for the two particles that are assumed to follow Stokes' solution for creeping flow around a sphere, Re < 0.5. Han called his curvilinear correction factor $\alpha_{Ds}(i,j)$ and tabulated the values from a curvilinear hydrodynamic trajectory analysis.

Laminar fluid shear:

$$\beta_{SH}(i,j) = \frac{G}{6}(d_i + d_j)^3 \qquad (2.6)$$

where $G = \frac{du_1}{dx_2}$, the magnitude of the local velocity gradient, u_1 is the velocity in direction 1, and x_2 is direction 2, normal to direction 1 in the plane of fluid flow. Note that a two-dimensional laminar shear flow is assumed in (2.6).

Turbulent fluid shear:

$$\beta_{Sh}(i,j) = \frac{\overline{G_m}}{6}(d_i + d_j)^3 \qquad (2.7)$$

$\overline{G_m}$ is a root mean square value of the local velocity gradient, a function of the energy dissipation rate per volume, *i.e.,* in two dimensions,

$$\overline{G_m} = \left[\frac{\phi}{\mu}\right]^{1/2} = \left[\frac{\partial u_i}{\partial x_j} + \frac{\partial u_j}{\partial x_i}\right]^{1/2} \qquad (2.8)$$

The original derivation of a mean velocity gradient for turbulent fluid shear (Camp and Stein, 1943) requires the temporal and spatial averaging of the local energy dissipation rate per mass, ε, and hence velocity gradients, too. Both these properties of the turbulent fluid field are highly variable. A recent review of the Camp and Stein approach criticized the two-dimensional development as inappropriate for the actual three-dimensional turbulent fluid field problem (Clark, 1985). The

frequency function for turbulent fluid shear developed against the meteorological backdrop (Saffman and Turner, 1956), while still a spatial and temporal average, is said to better represent the three-dimensional situation (Clark, 1985):

$$\beta_{Sh,t} = 0.160 (d_i + d_j)^3 \left(\frac{\varepsilon}{\nu}\right)^{1/2} \quad \textbf{(2.9)}$$

where ε is the local average energy dissipation rate per unit mass due to locally isotropic turbulence and ν is the kinematic fluid viscosity. In a practical sense, the parameter $\left(\frac{\varepsilon}{\nu}\right)^{1/2}$ differs from G_m only in the theoretical exactness of the derivation and the practical ability to estimate it.

The original (2.6) rectilinear form for collision by fluid shear, modified for curvilinear trajectories, is used in this research. Han called the curvilinear correction factor $\alpha_{Sh}(i,j)$, and he tabulated the values by interpolation of Adler's (1981) results, which included hydrodynamic correction and interparticle forces.

2.3.2 Factors affecting transport

As shown above for the rectilinear collision models, the principal variables affecting coagulation transport are the fluid properties (temperature, viscosity, density), the particle properties (size, density, concentration), and the fluid field properties (velocities, energy dissipation). Intrinsic fluid properties are known reliably, but natural system particle and fluid field properties are not as well defined.

A number of studies have pointed to the uncertain values for discrete particle settling velocity. For a particle Reynolds number $Re < 0.5$, the Stokes equation for creeping flow around a sphere predicts drag accurately within 2% (Happel and Brenner, 1983) or within 10% for $Re < 1$ (Panton, 1984) for quiescent settling. Many researchers have shown experimentally that turbulent shear flows (Jobson and Sayre,

1970; Sayre, 1969) and oscillating vertical flows (Ludwick and Dormurat, 1982) have negligible inertial effect on the drag coefficient and settling velocity of Stokes particles in water. Most particles and aggregates in natural systems satisfy the Stokes criterion (*e.g.*, $d_p < 120$ μm for $\rho_s < 2.5$ g/cm^3 at 20° C).

Unfortunately, the aggregate density is virtually impossible to measure, resulting in uncertainty concerning the floc settling velocities. In one study, discrete measurements were made of the individual settling velocities and floc sizes (2 to 100 μm) of 1800 lacustrine and marine aggregates (Chase, 1979). Measured bulk densities for the aggregates ranged from 1.035 to 1.055 g/cm^3. Chase concluded from theoretical vs. observed velocities that the predictions (Stokes equation) underestimated settling velocities by as much as an order of magnitude. Measurements using marine aggregates (Kajihara, 1971; Kawana and Tanimoto, 1976; Kawana and Tanimoto, 1979), estuarine flocs (Gibbs, 1985), gold sols (Weitz and Oliveria, 1984), and coagulated clay and sludge flocs (Tambo and Watanabe, 1979) have all shown that aggregate densities decrease with increasing floc size. The size-dependent density variation, not accounted for by Chase (1979), might explain some of the discrepancies obtained using those relatively small differential densities ($\rho_s - \rho_f$) at bulk values. Various empirical relations for floc density as a function of size were presented in the latter studies.

Fluid field properties can exert an appreciable but uncertain effect on coagulation transport of particles in natural waters. Measurements of energy dissipation in lake systems are few (Weilenmann *et al.*, 1989). O'Melia and co-workers have assumed mean velocity gradients in lakes of 1 to 10 s^{-1} in the well-mixed epilimnion, 0.1 s^{-1} in the more stable thermocline, and 0.5 to 1 s^{-1} in the

hypolimnion (O'Melia *et al.*, 1984; Weilenmann *et al.*, 1989). In the latter paper, the epilimnion velocity gradient for Lake Zurich was estimated as 1 s^{-1} on the basis of complete dissipation of the wind energy imparted to the lake, using the classic mixing model (Kraus and Turner, 1967). Most of this dissipation occurs in the viscous layer at the surface (on the order of 10 cm) in the open ocean, according to Krause and Turner. Weilenmann *et al.* (1989) concluded that fluid shear is an insignificant collision mechanism in Lake Zurich, except possibly during storms. The sensitivity of particle removal to velocity gradient assumptions was not presented. With the same mixing model, estimated mean velocity gradients in the ocean epilimnia range from 0.1 to 1 s^{-1} (Lerman, 1979). Dissipation rates in the ocean water column were cited that translate into turbulent velocity gradients of 0.01 s^{-1} in clear mid-ocean depths, 0.1 s^{-1} in the bottom mixed layer, and 1 s^{-1} in the surface waters (McCave, 1984). Away from coastal zones, one could expect dissipation rates in large, deep lakes (inland oceans) to be similar to the oceanic energy dissipation. In coastal zones and shallow inland seas (lakes), the dissipation rates would be greater.

Energy dissipation rates in open channel flow (rivers and riverine reservoirs) can be estimated on the basis of bed shear stress when other energy losses are relatively small. Bed shear losses can be significant. The parameter estimate of the average velocity gradient for a long reach of the Rhine in West Germany was 50 s^{-1} (Eppler *et al.*, 1975).

Experiments on lake sediments were performed in a Couette viscometer to examine the effects of laminar fluid shear and solids concentration on flocculation (Tsai *et al.*, 1987). Particle size measurements indicated that increasing bed shear rates (1, 2, and 4 dyne/cm^2) resulted in smaller median diameters and larger floc

densities at steady-state. Time to approach steady-state was also shorter with larger bed shear stress. Higher suspension concentrations (50, 100, 400, 800 mg/L) resulted in smaller mean diameters.

2.3.3 Attachment

Once particles have collided or been brought into near contact, many factors influence whether a permanent attachment will occur. Repulsive and attractive forces exist between particles in suspension, and attachment depends on the net energy of interaction as a function of separation distance. Good overviews of the origins of these forces, and quantitative descriptions for certain simple representations, are available (Lyklema, 1978 ; Overbeek, 1977).

Most particles in natural waters are stable, *i.e.*, resistant to attachment. A reduction in the energy barrier between the particles can be accomplished either by decreasing the repulsive forces or increasing the attractive forces or a simultaneous combination of the two. Destabilization is typically effected by reducing the repulsive forces, those due either to electrostatic repulsion or to steric repulsion.

O'Melia (1972) discussed four specific mechanisms of particle destabilization and attachment, *i.e.*, double layer compression (decreased repulsion), adsorption-charge neutralization (decreased repulsion), adsorption-polymer bridging (increased, albeit mediated, attraction), and precipitate enmeshment (possibly increased, mediated, attraction). Reviewing experimental and theoretical results on electrostatic repulsion, Lyklema (1978) concluded that destabilization can occur due to increased coagulant concentration, increased coagulant valence, or decreased particle radius. Overbeek (1977) stated, however, that experiments had shown no influence of particle size on stability. Although the processes causing destabilization in natural

systems are not under human control, as they are in engineered systems, each of these mechanisms is operative in natural systems.

2.3.4 Factors affecting attachment

As one measure of particle stability, electrostatic repulsion and stability can be measured indirectly by microelectrophoretic mobility experiments. A number of studies have been conducted using natural particles which indicate the qualitative influence of environmental factors on stability. Electrophoretic mobilities, u_m, measured for suspended particles from four estuaries and the North Sea (Hunter and Liss, 1979), demonstrated that a) all particles carried a negative surface charge, b) u_m became less negative with increasing salinity, and c) oceanic particles had a highly uniform u_m. In a subsequent analysis, the mobilities were shown to vary almost linearly with salinity (Hunter and Liss, 1982).

Aging in natural water definitely affects particle surface charge. Four particle types of divergent surface characteristics were exposed to seawater (Hunter, 1980). Regardless of the initial particle mobility sign (three of four initially positive) or magnitude in irradiated (organic free) seawater, subsequent exposure to seawater with natural dissolved organics caused convergence to similar magnitudes of negative mobility in all cases. This effect was attributed to adsorption of a tenacious polymeric film to the particle surfaces, whose ionized carboxylic functional groups established similar surface charge. Results thus indicated that increased ionic strength was most responsible for destabilization.

Particles and solution chemistries for 11 southeastern U.S. rivers and lakes were analyzed for u_m (Gerritsen and Bradley, 1987). Seven of the 11 systems were softwater, eight were acidic, and eight were high in dissolved organic carbon.

Regressions showed significant correlations between u_m and specific conductivity (positive), pH (negative), and dissolved organic carbon (negative). All particles possessed negative charge, so only increases in conductivity (ionic strength) were associated with destabilizing effects ; conversely, increased pH and DOC were associated with stabilizing effects.

The discrete particle coagulation models discussed above rely on the use of a collision efficiency parameter, α, to characterize the extent of particle destabilization and attachment. This parameter defines the fraction of those collisions predicted by transport theory which actually result in permanent attachment. A value of $\alpha = 0$ corresponds to perfect stability, whereas a value of $\alpha = 1.0$ indicates perfect instability or destabilization.

The parameter α originated with Smoluchowski. It was defined as the ratio of particle half life as predicted by the Brownian motion collision frequency function (T_{fast}) to the experimental particle half life (T_{slow}) (Overbeek, 1977). The concept presumes that the hydrodynamic collisions (transport) are predicted perfectly and that α accounts only for the uncertainty in physiochemical interactions. Although α can be estimated for certain electrostatic phenomena (Hahn and Stumm, 1970; Overbeek, 1977), current theory is inadequate for a theoretical prediction of particle instability in natural waters.

Values of α for suspended and sedimented particles in natural waters have been derived experimentally by many researchers. These studies have provided not only estimates of the field values of α, but the important factors influencing stability as well. All reported values of α rely on the assumption of perfect hydrodynamic collision frequency prediction, of course. Hahn and Stumm (1970) presented a

comparison of theoretically computed and experimentally determined values of α for different solids and coagulant concentrations. Edzwald *et al.* (1974) systematically determined α for three pure clay types and natural estuarine sediments, in buffered NaCl and synthetic seawater of equivalent ionic strength. For the ranges of salinity (1.8 to 17.5 ppt, parts per thousand) and ionic strength (36 to 343 meq/L) found in the estuaries studied, α increased with salinity. As expected, α was much more responsive to seawater of equal salinity but higher ionic strength, because of its divalent cations.

Collision efficiency results for natural sediments, with and without their natural organic coatings removed by NaOCl oxidation, have been published (Gibbs, 1983a). Both an organic-free synthetic seawater as well as a filtered, natural dissolved organic seawater were used as the suspending fluid. The uncoated particles coagulated much faster at the lower salinities but approached the same collision efficiencies as the coated particles at high salinity. The presence of small but undefined concentrations of natural dissolved organic carbon caused insignificant differences in coagulation relative to the removal of organic coatings (and any other surface modifications due to NaOCl) from the solids at the 150 mg/L concentration.

Gibbs' coating results (1983a) amplify those of Hunter (1980), whose seawater-exposed particles converged toward a uniform, negative electrophoretic mobility. The results of both Hunter (1980) and Gibbs (1983a) suggest that different size fractions of natural sediments do exhibit similar mobility and collision efficiency, as seen in Gibbs (1983b). For the special case of small, uncoated, charged particles, such as Gibbs' pure clays (1983b), the decreased stability observed for smaller particles is predicted by the simple electrostatic theory presented in Lyklema (1978).

Experimental methods can play an important role in the magnitude of α. A set of experiments, similar in conditions to those of Edzwald *et al.* (1974), were conducted in both blade and Couette reactors (Gibbs, 1983b). Gibbs achieved higher α values using lower shear rates when using the Couette reactor. He also found significantly higher α, and at lower salinities, than had Edzwald and his colleagues in corresponding blade reactor experiments. Gibbs attributed this finding to floc breakup during pipetting in the former study. Size-segregated, 1 to 2 μm, pure clay particles coagulated faster than 2 to 4 μm, pure clay particles; there were, however, no significant differences in α between the size fractions from the natural sediments. Since all of the pure clay size fraction experiments were conducted at the same particle mass concentrations (~150 mg/L), the results are open to debate; the greater number concentration in the smaller particle Gibbs experiments precludes a judgment of faster coagulation kinetics on the basis of size alone.

Collision efficiency experiments are not as abundant for natural freshwater particles. Five model inorganic solids and six organic (bacterial) solids were studied in both experimental solutions (with variations in concentrations of Na^+, Ca^{2+}, humic acid, fulvic acid, and lignosulfonic acid) and natural waters (Eppler *et al.*, 1975). The natural water samples were taken from five sites along 700 km of Rhine River, with a wide range of measured dissolved organic carbon. Results for kaolinite stability in 9 mM [Ca^{2+}] as a function of organic acid concentration (range: 1 to 100 or 1000 mg/L) were highly dependent on the acid concentration. The collision efficiency for kaolinite suspended in 9 mM [Ca^{2+}] with no organics was 0.35. Adding humic acid increased α from 0.35 to 0.45. Increasing fulvic acid concentration from 1 to 100 mg/L resulted in no change in α, but the value remained depressed at about $\alpha = 0.2$.

Increasing lignosulfonic acid concentration from 5 to 1000 mg/L decreased α from 0.15 to 0.05. The coagulation studies in filtered Rhine River water showed the kaolinite α increasing from 0.018 to 0.092 with distance downstream. Dissolved organic carbon concentrations increased in tandem with α, from 1.6 to 8.3 mg-C/L, but no other analyses of the river water solution chemistry were given.

Colloidal stability was measured for suspended particles and sediments from a softwater lake with low organic carbon concentration, Loch Raven Reservoir, Maryland (Ali *et al.*, 1984). The stability of suspended particles from the water column, preconcentrated for coagulation experimentation, was measured for samples taken over several months. Values of α, using the natural lake water ($[Ca^{2+}]$ = 0.5 mM, [organic carbon] = 2 mg/L) as solvent, ranged from 0.01 to 0.09; the geometric mean was 0.03.

Suspensions prepared from bed sediments taken near the Loch Raven Reservoir inflow were also coagulated with various concentrations of added calcium and/or fulvic acid. As with estuarine sediments, instability increased substantially (α from 0.035 to 0.39) with added calcium ($\Delta[Ca^{2+}]$ from 0. to 3.3 mM). Unlike others, (Gibbs, 1983a; Hunter, 1980), α decreased substantially (from 0.035 to 0.006) with added fulvic acid (Δ[FA] from 0 to 20 mg TOC/L) in the presence of no added calcium. With fulvic acid concentrations of 5 mg TOC/L, collision efficiencies were reduced about 75% compared to the calcium alone values. At these low ionic strengths, the relative change in organic macromolecule adsorption definitely inhibited collision efficiency. These observations do, however, parallel other results (Eppler *et al.*, 1975; Gerritsen and Bradley, 1987), where electrophoretic mobility and coagulation studies indicated increasing stability with increasing dissolved organic

carbon. Steric repulsion from the organic macromolecule adsorption is likely the cause at these lower ionic strengths.

Stability has also been measured in hardwater lakes in Switzerland (Weilenmann *et al.*, 1989). Collision efficiencies were measured for four lakes of differing calcium and dissolved organic carbon (DOC) concentrations. Results showed that α was dependent on both $[Ca^{2+}]$ and [DOC] concentrations. Moderate $[Ca^{2+}]$ (= 1.2 mM) and low [DOC] (= 1 mg/L) gave the largest α value, 0.09. In another lake with the same $[Ca^{2+}]$ but a high [DOC] (= 4 mg/L), the smallest α resulted, 0.01. Weaker $[Ca^{2+}]$ (= 0.9 mM) and [DOC] (= 1 mg/L) resulted in offsetting effects, producing an intermediate α of 0.06. Higher $[Ca^{2+}]$ (= 2 mM) and [DOC] (= 4 mg/L) also offset each other to result in an intermediate $\alpha = 0.05$. These results are consistent with freshwater studies discussed above (Ali *et al.*, 1984; Eppler *et al.*, 1975; Gerritsen and Bradley, 1987).

2.4 RESUSPENSION

Acting in opposition to sedimentation, which transfers particles and particle-associated contaminants out of the water column and into the bed, resuspension moves particles and contaminants out of the bed and into the water column. While sedimentation and erosion of solids have been problems of long-standing in inland and coastal waterways (Vanoni, 1975), bed resuspension in deeper water was considered relatively insignificant. Waves and currents are now known to resuspend particles at water depths of several hundred meters (Santschi, 1986).

The fate of particles in the sediment bed depends macroscopically on the applied shear stresses within the bed and the shear strength of the bed itself. Shear stress within the bed is created primarily by fluid motion in the overlying fluid

boundary layer. The fluid motion itself is the result of waves and currents. Bed shear strength is determined by microscopic interparticle forces, as influenced by the particle size distribution, bed porosity, solids density and composition, and interstitial water chemistry. The shear strength varies with depth and with time, both of which reflect the degree of compaction or consolidation.

Implicit in the magnitude of the shear strength is the extent and strength of particle aggregation. Analysis of river sediment transport has traditionally focused on noncohesive solids, *i.e.*, discrete particles (Lavelle and Mofjeld, 1987; Vanoni, 1975). This approach has been used for two primary reasons: first, because many of the problems of sedimentation in rivers have been the result of the mass accumulation of coarse and relatively non-flocculent solids, and second, because it avoids the complexity of fine particle flocculent behavior. The results of research on noncohesive solids resuspension are generally not applicable to this research because of the former's focus on bulk solids behavior dominated by the larger size fractions.

State of the art estuarine sediment transport modeling (most applicable to the dynamics of cohesive solids exchange) conceptually divides the cohesive sediment bed into four layers based on the physical form of the solids and the mode of erosion from the bed (Hayter, 1987). The four layers (from the bed/water interface down) are a) mobile suspension, b) stationary suspension, c) partially consolidated bed, and d) settled (or fully consolidated) bed. The first two layers are scoured by what Hayter termed "redispersion", a mass erosion of bulk solids from the bed. The deeper, partially and fully consolidated layers are scoured by what he called "resuspension", a surface erosion of discrete particles. Obviously, these deeper layers can only be eroded after the unconsolidated suspension bed above has been eroded. Though

resuspension is envisioned as acting on discrete particles, existing bed flux models, including Hayter's, describe only bulk solids erosion based on bulk properties. A discrete particle transport model could be used to overcome this inconsistency.

Hayter (1987) presented an application of cohesive sediment modeling for estuaries where the bed layers were divided into many sublayers to describe the highly variable rheological properties of the bed during the tidal cycle. Others (Bedford and Abdelrhman, 1987) have approached resuspension from the other side of the interface, *i.e.*, from the fluid boundary layer. These authors show that the time and length scales in the benthic boundary layer vary over six orders of magnitude, making analysis very difficult. For simplicity, the approach taken in this research has a single bed layer interacting with a single fluid layer by mass erosion. The bulk mass erosion from that uniform bed layer will be termed resuspension in the remainder of this paper.

The research on resuspension of sediments, notwithstanding the noncohesive alluvial and coastal work, is scant. Good summaries of the saltwater (Hayter, 1987) and freshwater (Fukuda and Lick, 1980; Lick, 1982) resuspension experiments exist. While the qualitative effects of various parameters on entrainment are known, quantitative prediction of entrainment is not possible without direct experiments. Research indicates that, other factors being equal, resuspension flux is linearly related to bed shear stress for consolidated sediments and exponentially related to shear stress for fresher, stratified sediments. Often the linear flux relation is expressed in terms of shear stress difference, *i.e.*, the difference between actual bed shear stress and a critical shear stress for the exposed sediment.

2.5 LITERATURE SUMMARY

From the research reviewed above, it is clear that particle and particle-particle behavior in natural waters is poorly understood. Such an understanding is critical, however, to our knowledge of how particles and adsorbable constituents behave in such systems. Past modeling of particle behavior has generally been limited to consideration of single size particles or the use of a few broad size ranges. Also, the modeling of substances sorbed onto natural particle surfaces (or into surface related matrices) cannot properly account for any particle size-dependency of such sorption and subsequent transport. The research reported herein was directed at the first of these gaps in our current understanding, the particle and particle-particle transport and fate.

With few exceptions, the research on particle behavior in natural systems has not accounted for the possibility of flocculation of the particles, and has assumed that particle sedimentation is a uniform and steady process. Particles can and do, however, flocculate in natural waters, changing their sedimentation characteristics as a result. Sedimentation is highly size-dependent. Since the influx of particles to a receiving system can have very different size characteristics under different conditions (*e.g.*, stormwater runoff vs. normal flow conditions), accounting for the size dependence in sedimentation would be an important advance in our ability to predict behavior under different conditions. In addition, particle-interaction modifications of the size distribution will vary with solution conditions such as pH, ionic strength, and organic macromolecule concentration. The model developed in this research accounts for the effects that changes in the size distribution have on the fate of particles in space and time.

CHAPTER III

TOWN LAKE APPLICATION BACKGROUND

3.1 INTRODUCTION

One of the major objectives of the research was the application of the particle transport and reaction model to a natural aquatic system in Texas. Town Lake, a 9.6 km impoundment of the lower Colorado River in Austin, Texas, was chosen for the application. The purpose of this chapter is to present the estimates of system conditions developed for that purpose. System-specific information presented includes characterizations of the watershed, lake morphometry and physiochemical conditions, particle loadings, and inflows. Much of this information was developed previously (Culkin, 1986).

In conjunction with characterization of the system's particle properties, limited measurements of particle size distributions are also presented. A short general introduction to the presentation and interpretation of particle size distributions is given as a preface to the Town Lake data.

3.2 TOWN LAKE WATERSHED

Characterization of the Town Lake watershed is necessary for estimating the fluid inflows and solids loadings driving the receiving system behavior. This section describes the watershed, its location, land uses, and tributaries. Conditions existing in 1980 are presented as the basis for simulation.

The immediate Town Lake watershed includes much of metropolitan Austin, from which several tributaries drain directly into the lake. Figure 3.1 depicts the general area and individual tributary drainage basins for Town Lake. Town Lake is the impoundment located between Tom Miller Dam and Longhorn Dam. Individual

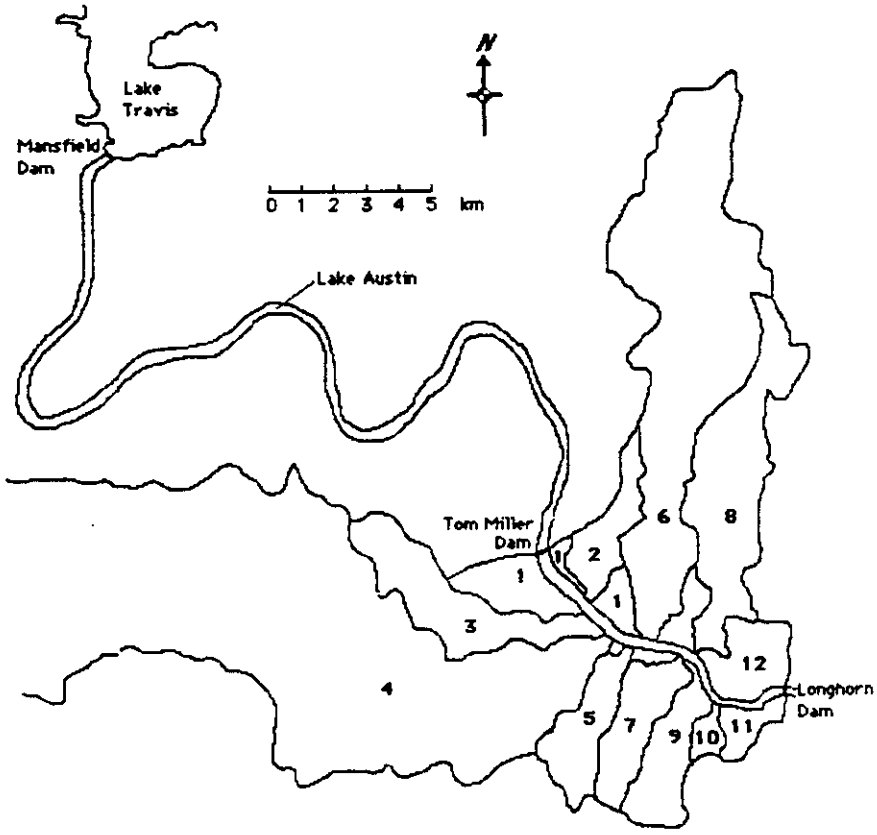

Figure 3.1 Town Lake Drainage Basins

creeks, as well as ambient water quality monitoring stations in the lake region, are shown in Figure 3.2.

Although the land adjacent to the Colorado River above Town Lake (and Austin) contributes substantially to the flow and contaminant loadings to Town Lake, upstream drainage has been lumped into a boundary condition for Town Lake. The Tom Miller Dam release thus specifies inflow and concentration at the head of Town Lake. Austin watersheds with direct discharges to Town Lake, however, are individually characterized in this section.

The rainfall-runoff coefficient was used in this research as a simple but effective means of predicting the quantity of runoff for sub-basins of the watershed. The runoff coefficient is actually the slope of the regression of watershed runoff on rainfall, and it is considered here to be a function of impervious cover only. Impervious cover is defined as the fraction of total land area that completely prevents infiltration of rainfall into the subsurface. An outline of the procedure used to develop runoff coefficients for each sub-drainage basin of a lake is as follows: estimate the amount of land in each type of land use within the sub-basin, estimate the equivalent impervious cover in each type of land use, calculate a weighted average impervious cover for the sub-basin, and finally, estimate a runoff coefficient for the basin based upon the runoff coefficient-impervious cover regression model.

Town Lake's watershed is moderately to heavily urbanized. The City of Austin Planning Department published demographic and land use data from 1980 (City of Austin, 1982). Tributary watersheds were individually characterized for the amount of land area in each of several land use types, detailed in Appendix B.

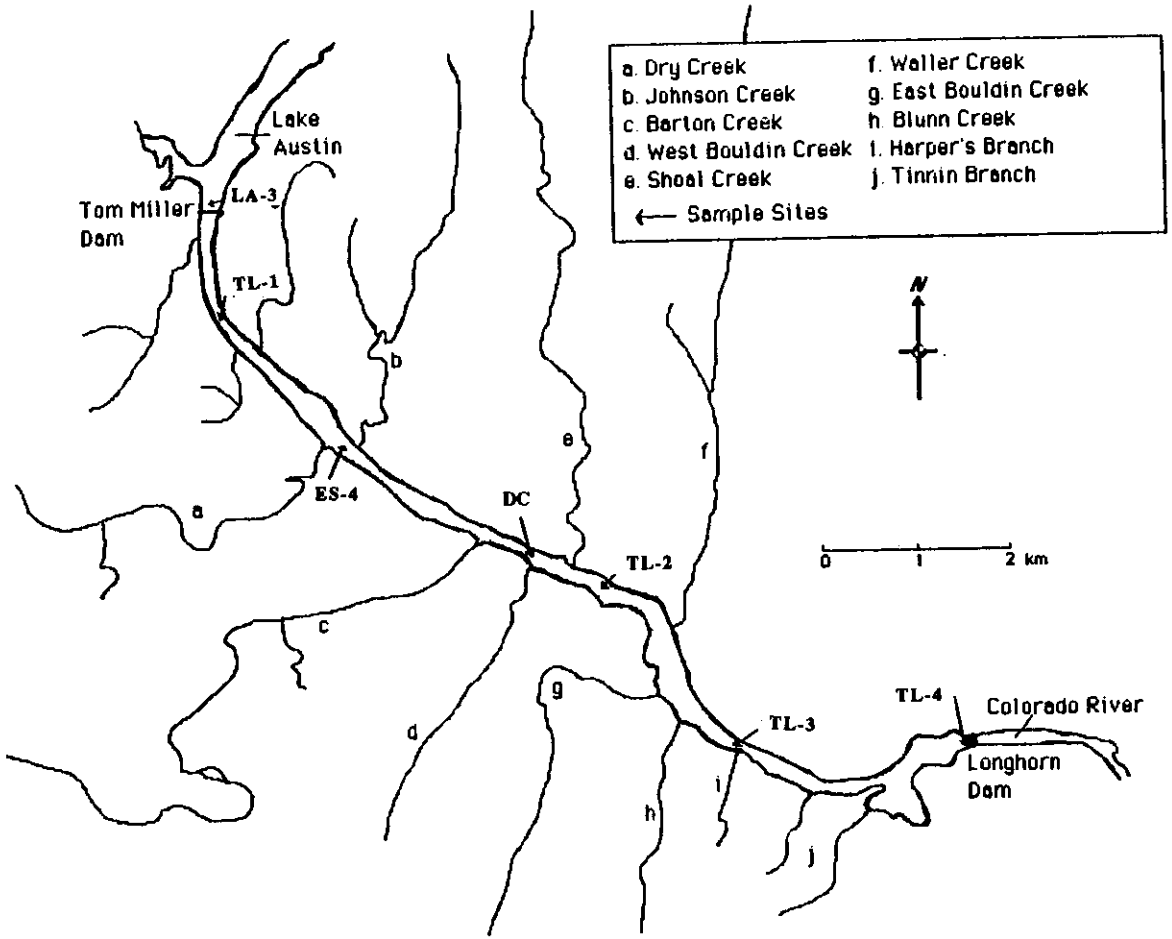

Figure 3.2 **Town Lake Tributaries and Sampling Sites**

Impervious cover estimates for different land use types were presented as part of an urban runoff assessment methodology prepared for use in the state of Texas (Hydroscience, 1976); these are cited in Appendix B. These impervious cover fractions were multiplied by land use areas in each tributary basin to estimate a weighted-average percent impervious cover for each sub-basin of the lake. Drainage areas and weighted-average impervious cover estimates for each sub-basin are presented in Table 3.1. The reach numbers correspond to the numerical grids in the research model, *e.g.*, Reach 1 extends downstream from the head of the lake at Tom Miller Dam for one-tenth of the total distance down the lake, Reach 2 extends from one-tenth to two-tenths of the total distance down the lake, *etc.* The major creeks draining into each reach, shown in Figures 3.1 and 3.2, are named in Table 3.1.

Estimated impervious cover from the methodology just described were compared against direct aerial photograph measurements of impervious cover for three watersheds. The estimated impervious covers were approximately 12% higher than the aerial survey measurements published (City of Austin, 1984c) for the Barton, Shoal, and Waller Creek watersheds. A linear regression of the estimated vs. measured impervious cover ($r^2 = 0.997$ for the three sub-basins) was then applied to the remaining basins as a calibration for the 1980 conditions. Actual values measured for the three basins directly measured were retained.

Rainfall-runoff data for Austin area creeks between 1976 and 1983 were analyzed by the City of Austin as part of a stormwater modeling study (1984c).The relationship between event-mean runoff coefficients and impervious cover, presented in that City of Austin report, is reproduced here as Figure 3.3. Actual mean runoff ratios from the report have been added to the figure as an illustration of

Table 3.1

SUMMARY OF TOWN LAKE WATERSHED CHARACTERISTICS

Segments Sub-basins	Area [km^2]	1980 Impervious Cover [%]	Runoff Coefficient
Reaches 1 - 2			
Lake Austin	238.	5.	0.12
Upper Town Lake	7.8	22.	0.25
Reaches 3 - 4			
Dry Creek	9.8	13.1	0.15
Johnson Creek	4.4	47.4	0.33
Reaches 5 - 6			
Barton Creek	324.	7.0	0.12
W. Bouldin Creek	7.8	46.4	0.33
Shoal Creek	40.7	46.4	0.27
Reaches 7 - 8			
Waller Creek	14.2	42.0	0.34
E. Bouldin Creek	4.9	49.5	0.36
Blunn Creek	3.6	43.1	0.31
Reaches 9 - 10			
Harper's Branch	1.6	51.4	0.38
Tinnin Branch	2.1	44.7	0.32
Lower Town Lake	6.0	45.	0.32

Note: 1.00 km^2 = 0.386
mi^2 = 247. ac

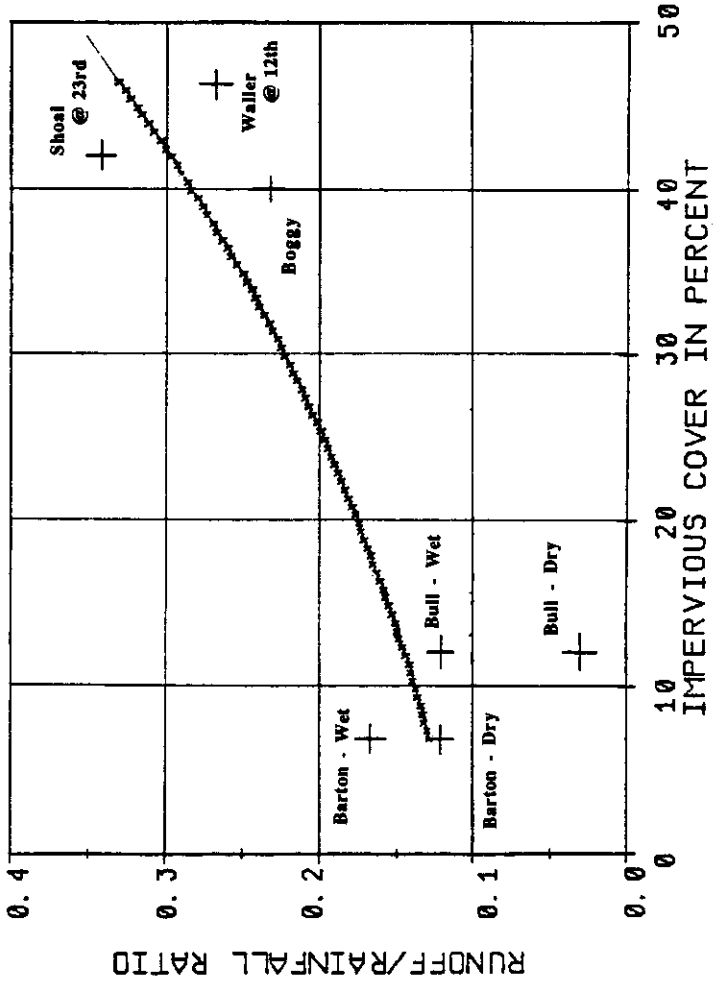

Figure 3.3 **Runoff Coefficient for Town Lake Watershed.** (City of Austin, 1984c)

the range of data. Runoff coefficients will vary dramatically from storm to storm for a given basin (notice the difference between the means for wet and dry antecedent periods, shown for Barton and Bull Creeks). For a preliminary analysis, such as the water quality modeling conducted in this study, the relationship for average runoff coefficient presented in Figure 3.3 was believed to be acceptable.

Detailed watershed characteristics for the years 1980 and 2005 are contained in Appendix B (the 2005 projections are listed for comparison). Total area, area in each type of land use, component impervious area from each land use, weighted impervious cover for the watershed, and resultant runoff coefficient are included for each of the named tributary watersheds.

Three points concerning the watershed calculations deserve mention. First, total watershed areas differ between the two sources cited for that data; watershed areas from the City of Austin Watershed Management Division (City of Austin, 1984a) were used, as the planning report areas (City of Austin, 1982) were intended primarily to describe water and sewer service areas rather than accurate drainage basin delineations. Second, the Lake Austin watershed characteristics are only rough estimates based on limited details in the City of Austin reports (1984a; 1984c). Errors in these estimates have no significant effect on the research reported herein, however. The effect is negligible because the Lake Austin watershed runoff is only a small fraction of the total Lake Austin inflow to Town Lake, and the Lake Austin watershed runoff is not used explicitly in the contaminant loading estimates. Third, a minimum of 9.3 km^2 of the Town Lake watershed area is not assigned to specific tributaries in the studies previously cited. Examining Figures 3.1 and 3.2, one sees several areas with no named streams for drainage. These were lumped into two basins labeled

"Upper Town Lake" and "Lower Town Lake" for this study, and their impervious cover and runoff coefficients were assigned based on areas of similar land use.

3.3 TOWN LAKE MORPHOMETRY

Application of the particle transport and transformation model to Town Lake requires spatial dimensions for the system. Transport processes and overall system response are dependent on the distribution of fluid, the locations of inflows, and the morphometry of the impoundment. Morphometric dimensions, *e.g.*, length, depth, cross-sectional area, surface area, and volume, are normally averaged over some portion of the physical system and used to represent that piece of the system. The process of subdividing the system into control volumes that satisfy the field data, modeling objectives, and computational constraints is known as segmenting the system. In the case of finite difference models, such as that used in this research, the process is called discretizing the system. The methods used to characterize morphometry and discretize Town Lake follow.

Town Lake was created as an impoundment of the lower Colorado River in 1960 by the construction of Longhorn Dam. The volume and surface area of the impoundment were plotted vs. stage, probably as part of its initial design (City of Austin, 1984a). These plots are shown in Figure 3.4. At 428 ft MSL, the nominal operating elevation of Town Lake, the volume and the surface area were reported to be 3520 ac-ft (4.34×10^6 m^3) and 416 ac (1.68×10^6 m^2). A lake-average depth of 2.58 m (8.5 ft.) would have been dictated. From 1960 to 1975, a sand and gravel dredging operation removed a considerable volume of bed material from the lake near Longhorn Dam. Following this period of dredging, the City of Austin Electric

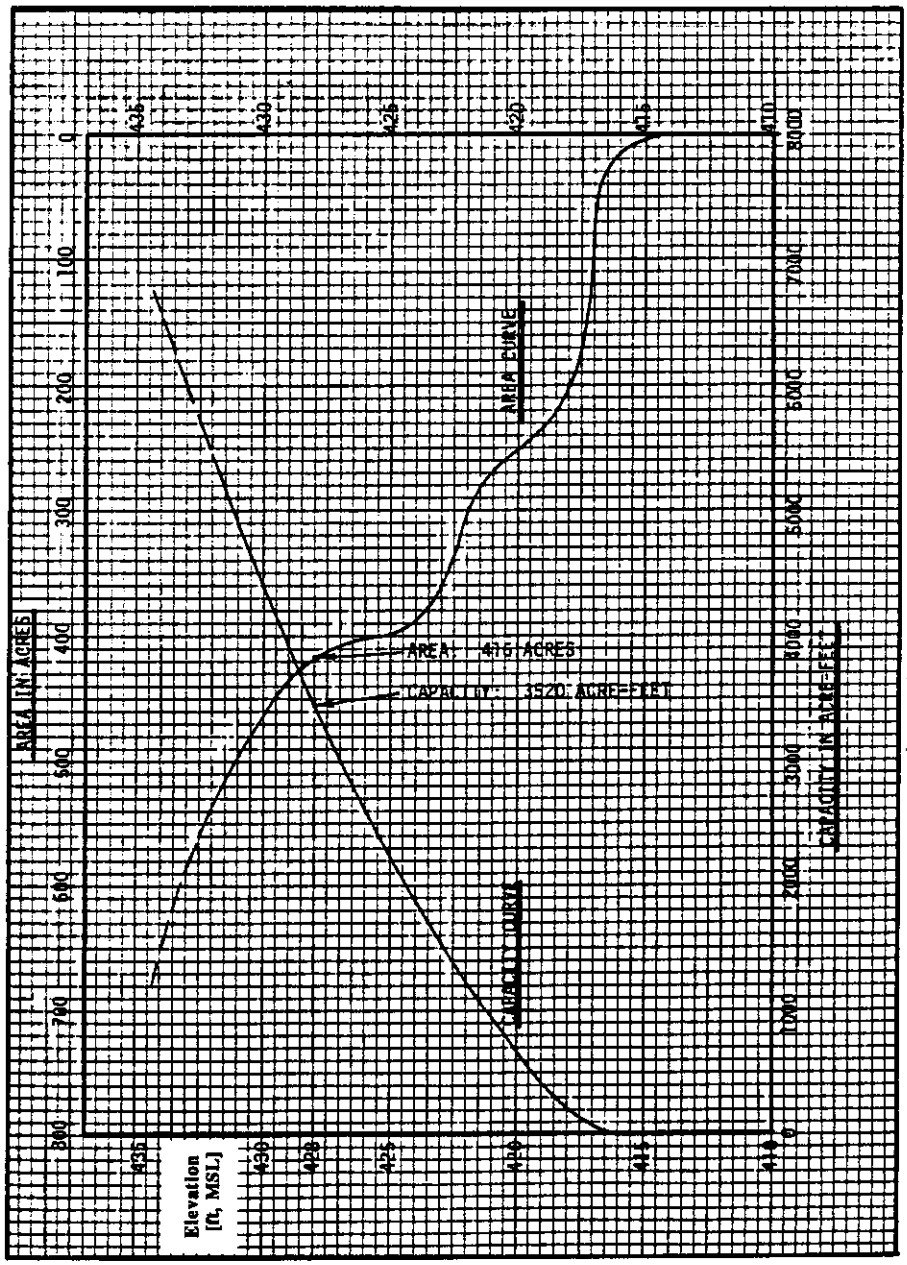

Figure 3.4. Town Lake Area-Capacity Curves, 1960. (City of Austin, 1984a)

Department (City of Austin, 1984b) estimated a new volume of approximately 6000 ac-ft (7.40×10^6 m^3) at the nominal operating elevation, a 70% increase over the 1960 impounded volume.

A bathymetric survey by depth soundings was conducted by the U.S. Army Corps of Engineers (USACE), Ft. Worth District office, ca. 1977. Cross-sectional areas and top-widths (bank to bank widths at the water line) vs. elevation (at 5 ft intervals) had been obtained for 39 cross sections in Town Lake. The reduced data were obtained from the University of Texas Center for Research in Water Resources (Oljay Unver, personal communication, 1985). The data were generally reported at elevations other than the nominal 428 ft MSL pool elevation. Therefore, (linear) interpolation was used to estimate the top width at the nominal pool elevation. For a concave-down, near-shore bed, linear interpolation would result in overestimation of both the top-width and the cross-sectional area. A concave-up, near-shore bed would cause underestimates. Survey cross-section locations were concentrated upstream and downstream of flow restrictions, *i.e.*, mainly near bridges; these concentrations probably make little difference in average calculated dimensions because of the relatively straight shorelines of Town Lake.

The procedures for estimating the dimensions of the segments between USACE cross-sections were as follows. The volume of a particular segment was estimated as the product of [the average of the two end cross-sectional areas] and [the longitudinal distance between the cross-sections]. The (air-water) surface area of a segment was estimated as the product of [the average of the two end top widths] and [the longitudinal distance between the cross-sections]. The average depth of a cross-section was estimated as the quotient of its cross-sectional area and top width.

A reduced summary of the lake morphometry data is given in Appendix C. Compare the increased total volume (6.38×10^6 m^3), surface area (1.54×10^6 m^2), and average depth (4.12 m) calculated from the post-dredging survey against the 1960 dimensions. These changes have substantial effects on both real and modeled transport, residence time, and particle fate within the system. Estimated cross-sectional areas from the survey measurements, and the cross-sectional average depths derived from those areas, are shown in Figure 3.5.

The reduced data for the 38 field segments were used in discretizing the 9.6 km reservoir. Ten segments or reaches of equal length (960 m) were actually used in the modeling. Reach boundary locations are generally set to separate a system into regions of similar forcing, similar physical or chemical properties, monitoring data extent, or desired spatial resolution. Load discontinuities such as major tributaries, or lake regions of significantly different properties, require establishment of spatial discretization. For example, Reach 3 includes two major creeks in developed (Johnson Creek) and developing (Dry Creek) areas; it is separated from the relatively low population density area just below Tom Miller Dam (Reaches 1 and 2). The Reach 3 segment of the impoundment also marks a transition from swifter, shallower flow into slower, deeper flow.

The choices for the lower reach boundaries were dictated by the uniform grid size chosen, but conformed closely to changes in impoundment morphometry, sample site locations, and watershed characteristics. The discretized cross-sectional areas used in the numerical application were averages over the appropriate intervals, taken from Figure 3.5.

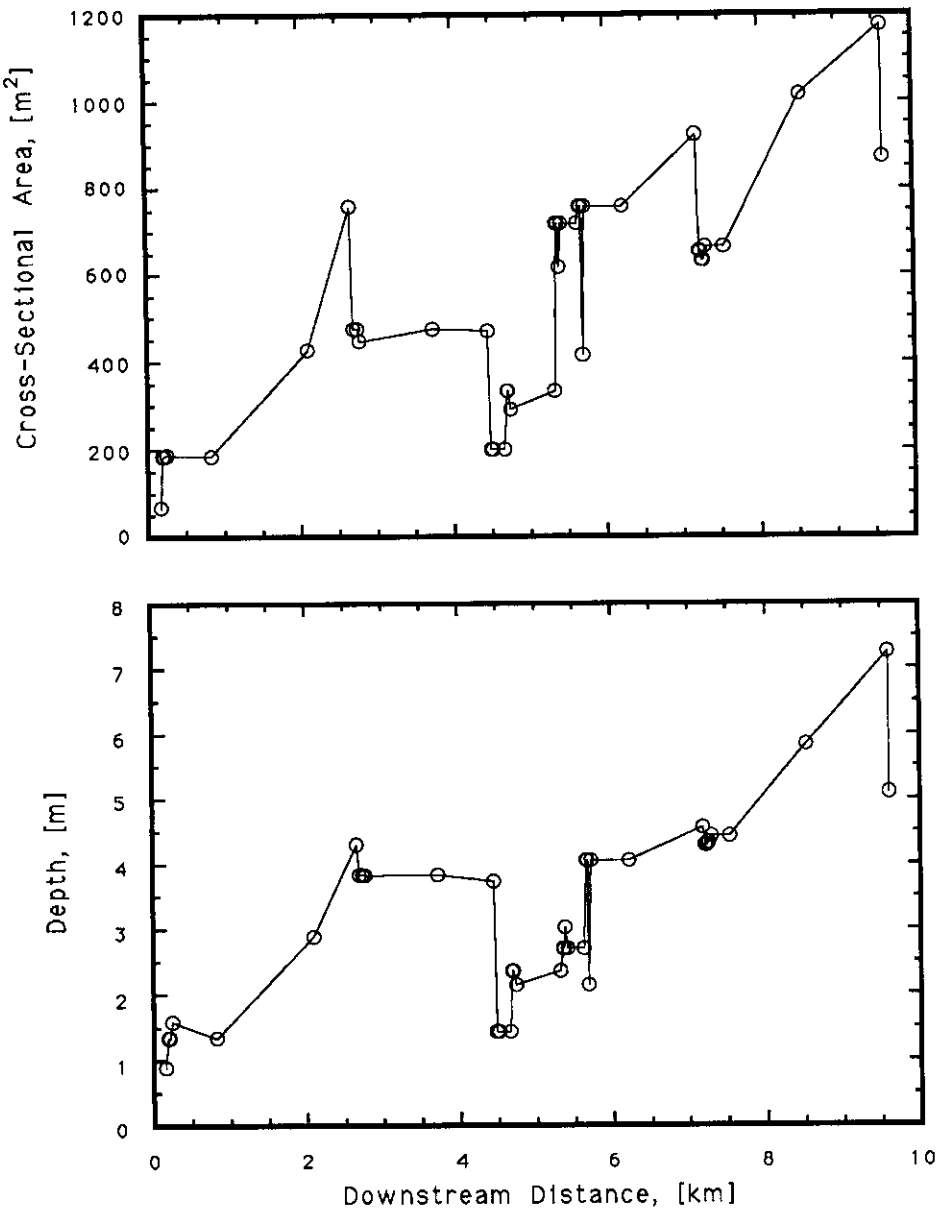

Figure 3.5 **Town Lake Cross-Sectional Areas and Depths**

3.4 TOWN LAKE HYDROLOGY

On the average, hydrologic inflow to Town Lake is dominated by releases from Lake Austin via Tom Miller Dam; however, storm runoff from immediate tributaries can become a significant, if not the dominant, inflow during and after storms (City of Austin, 1984a; City of Austin, 1984c; Espey, 1976). Since it was believed that these urban runoff events provide significant contaminant loadings on the system, careful attention was paid to their flowrates. Precipitation drives the runoff process, so analysis of precipitation records was made. Upstream water supply withdrawals divert clean water that would normally be flushing Town Lake, thereby affecting contaminant transport. Therefore, Austin water treatment plant withdrawals from Town Lake, Lake Austin, and Lake Travis were detailed.

Flowrates from these sources, as well as significant spring flow and rainfall-evaporation flow, were estimated individually, then combined, on a monthly basis. Seasonal- and annual-average flowrates, by reach, were then computed. The methods used in estimating each of the flowrates are described in Appendix D. A summary of the net inflows to Town Lake, as used in the modeling, is presented in Table 3.2. More detailed data are tabulated in Appendix D. With the provisos mentioned in Section 3.2, the estimates of Table 3.2 are believed to be reasonable long-term seasonally-averaged flowrates.

3.5 CHARACTERIZATION OF PARTICLE SIZE DISTRIBUTIONS

Information is presented in this section concerning particle size distributions. Methods to mathematically describe the particle size distribution are presented. Subsequently, particle size distribution data used to describe the Town Lake water column are presented.

Table 3.2

AVERAGE HYDROLOGIC INFLOWS TO TOWN LAKE

Watershed	Winter[1] Average [m^3/s][2]	Spring Average [m^3/s]	Summer Average [m^3/s]	Fall Average [m^3/s]	Annual Average [m^3/s]
Lake Austin	20.88	84.49	56.67	10.17	43.04
Reaches 1 - 2	0.038	0.066	0.039	0.047	0.047
Reaches 3 - 4	0.057	0.100	0.066	0.072	0.074
Reaches 5 - 6[3]	1.097	2.083	1.292	1.319	1.411
Reaches 7 - 8	0.124	0.218	0.120	0.157	0.155
Reaches 9 - 10	0.059	0.103	0.065	0.073	0.075

[1] Winter = January 1 to March 31
Spring = April 1 to June 30
Summer = July 1 to September 30
Fall = October 1 to December 31

[2] 1.000 m^3/s = 35.31 cfs

[3] Net inflow = (Total inflow - Green WTP withdrawal)

In discussing a heterodisperse suspension, it is necessary to describe mathematically the distribution of particles comprising the suspension. The following explanation was taken from Lawler (1979).

A cumulative size distribution is illustrated in Figure 3.6, where the cumulative number concentration, N, is plotted as a function of particle size. Particle size is expressed here in volumetric dimensions (v). N(a) denotes the total number concentration [#/cm^3] of particles that have a volume $v \leq a$ [μm^3], *i.e.*,

$$N(a) = \int_0^a dN(v) . \qquad (3.1)$$

The total number concentration for all particle sizes is shown in the figure as N_∞. The slope of this curve, $\Delta N/\Delta v$ (or dN/dv, as $\Delta v \rightarrow 0$), is one of several "particle size distribution functions" that are actually slopes of the various cumulative number distributions. In this case, the particle size distribution function is represented as n(v) and has units of [#/cm^3-μm^3]. By examining small ranges of v, incremental changes in the number concentration become the focus.

Particle volume is just one of three common measures of particle size. Particle surface area (s) and characteristic particle diameter (d_p) are also often used to characterize a particle's size, so that the three common particle size distribution functions can be defined:

$$\frac{\Delta N}{\Delta v} \approx \frac{dN}{dv} = n(v), \quad [\#/cm^3\text{-}\mu m^3] \qquad (3.2)$$

$$\frac{\Delta N}{\Delta s} \approx \frac{dN}{ds} = n(s), \quad [\#/cm^3\text{-}\mu m^2] \qquad (3.3)$$

$$\frac{\Delta N}{\Delta d_p} \approx \frac{dN}{dd_p} = n(d_p), \quad [\#/cm^3\text{-}\mu m] . \qquad (3.4)$$

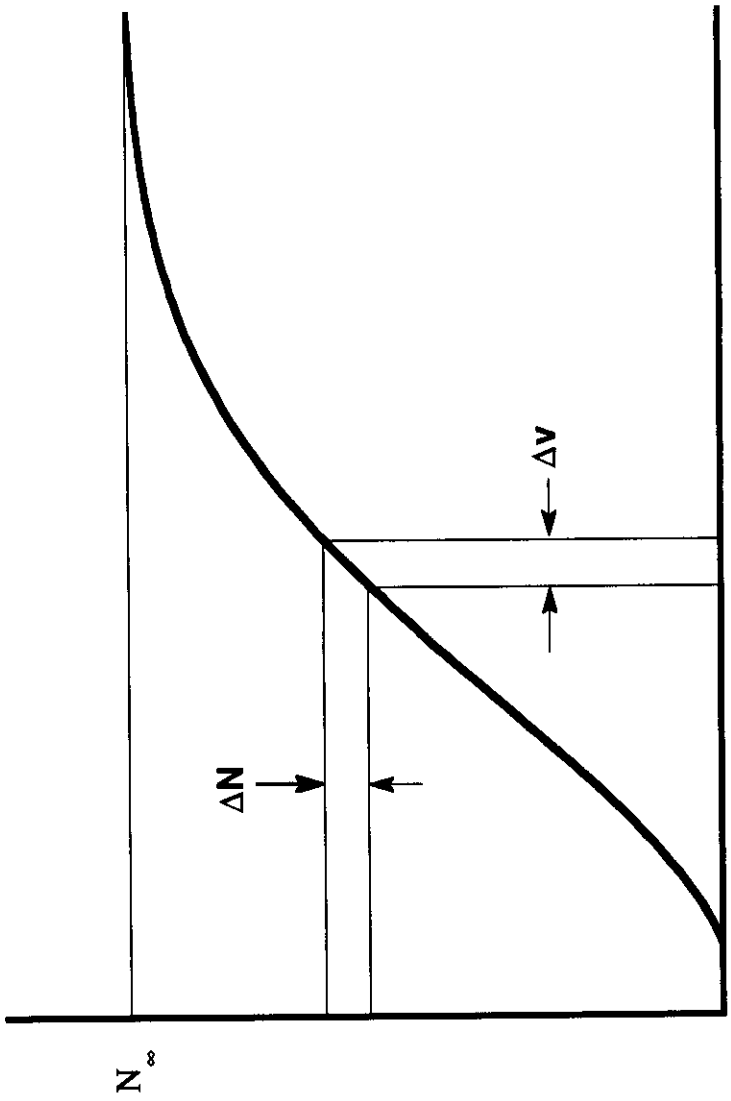

Figure 3.6 Cumulative Number Distribution

These particle size distribution functions can be used in conceptual and empirical studies of coagulation, particle transport, and separation processes. They are particularly useful for normalizing particle size distribution information from different experimental (particle counters) or simulation (model) studies.

There are other functions useful for analyzing particle size distributions that rely on distribution properties other than the cumulative number concentration. For instance, cumulative particle volume concentration, V [$\mu m^3/cm^3$], and cumulative particle surface area concentration, S [$\mu m^2/cm^3$], are also of great interest in the study of particle transport and transformation. Total particle volume concentration, V_∞, and total surface area concentration, S_∞, are used in Chapters 5 and 6 in analyzing simulation results.

Analysis of the distribution of cumulative particle volume leads to analysis of the discrete incremental particle volume. A function that normalizes the distribution of particle volume by the logarithm of particle diameter is called the "volume distribution." The volume concentration of all particles in the interval between size 1 and size 2 can be written as

$$V_{1\text{-}2} = \int_1^2 dV. \qquad \textbf{(3.5)}$$

Dividing and multiplying the right hand side of (3.5) by $d(\log d_p)$ yields

$$V_{1\text{-}2} = \int_1^2 \frac{dV}{d(\log d_p)}\, d(\log d_p). \qquad \textbf{(3.6)}$$

A plot of the volume distribution, $v(d_p) = dV/d(\log d_p)$, versus $\log d_p$ is illustrated in Figure 3.7. The volume concentration associated with all particles in the size interval

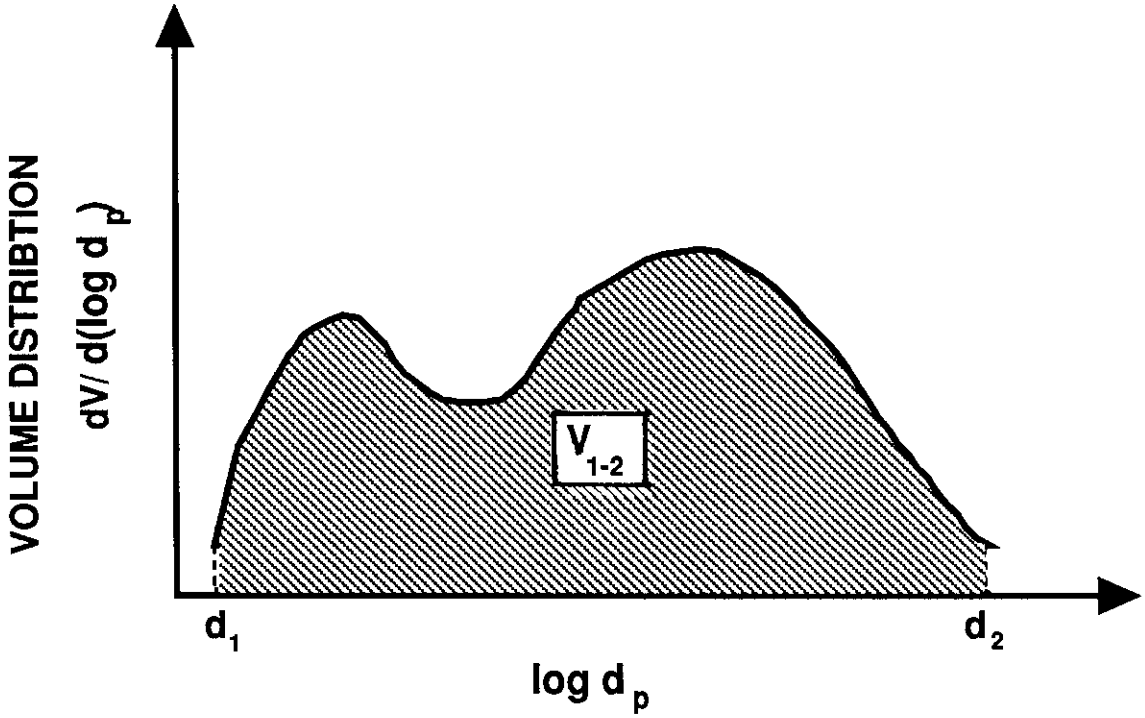

Figure 3.7 Particle Volume Distribution

from d_1 to d_2, as described by (3.5) and (3.6), is equal to the integrated (shaded) area in Figure 3.7. In preparing such plots from field measurements, it is frequently assumed that the particles are spherical. This assumption is made in this research.

The definitions of the cumulative number concentration N(v) and the particle size distribution function (volume basis) dictate that

$$dV = v\, n(v)\, dv. \tag{3.7}$$

Dividing by $d(\log d_p)$, one obtains the volume distribution,

$$\frac{dV}{d(\log d_p)} = \frac{v\, n(v)\, dv}{d(\log d_p)} = \frac{v\, n(v)\, dv}{d(d_p)} \frac{d(d_p)}{d(\log d_p)}. \tag{3.8}$$

Assuming spherical particles, $v = \pi\, d_p^3/6$, then $dv = (\pi\, d_p^2/2)\, d(d_p)$. Substituting these identities into the volume distribution (3.8) and noting that $d(\log d_p) = d(\ln d_p)/2.3 = d(d_p)/(2.3\, d_p)$, one obtains for the volume distribution:

$$\frac{dV}{d(\log d_p)} = \frac{2.3\,\pi^2}{12} d_p^6\, n(v)\,. \qquad \textbf{(3.9)}$$

The volume distribution as expressed in (3.9) contains particle dimensions of both diameter (d_p) and volume ($n(v)$), and it is often rearranged to include diameter as the only measure of particle size. Recall that $n(v) = dN/dv$ and, for spherical particles, $dv = (\pi\ d_p^2/2)\, d(d_p)$. Making these substitutions in (3.9) finally yields the

Volume distribution:

$$\frac{dV}{d(\log d_p)} = \frac{2.3\,\pi}{6} d_p^4\, n(d_p)\,. \qquad \textbf{(3.10)}$$

Similar distribution relationships can be derived for the surface area distribution and the number distribution. The results are

Surface Area distribution:

$$\frac{dS}{d(\log d_p)} = 2.3\,\pi\, d_p^3\ \frac{dN}{d(d_p)}\,, \qquad \textbf{(3.11)}$$

Number distribution:

$$\frac{dN}{d(\log d_p)} = 2.3\,\pi\, d_p\ \frac{dN}{d(d_p)}\,. \qquad \textbf{(3.12)}$$

For a plot of the surface area distribution, $dS/d(\log d_p)$, versus $\log d_p$ that is similar to Figure 3.7, the integrated area under the resulting curve from $\log d_1$ to $\log d_2$ would represent the total concentration of surface area in the suspension provided by particles in the size interval from d_1 to d_2. A plot of the number distribution, $dN/d(\log$

d_p), versus log d_p would provide analogous information about the total number concentration in various size ranges.

A very useful means of summarizing the particle size distribution is the log of the particle size distribution function (number basis), *i.e.*, $\log(n(d_p)) = \log\left(\frac{\Delta N}{\Delta d_p}\right)$ obtained from the log of (3.4). This function is employed for converting from one dimensional basis to another. In particular, the slope of the plot of log of number distribution vs. $\log(d_p)$ is often used to quickly determine how the particle volume, surface, and number concentrations vary with size (Lawler, 1979).

3.6 TOWN LAKE SUSPENDED SOLIDS

3.6.1 Mass concentrations

Suspended solids exert strong influences on many aspects of water quality, influencing optical properties by number (thus primary productivity) and benthic substrates by mass (thus benthic and higher communities). Particle surface interactions with strongly sorbing contaminants are believed to affect the behavior of those substances in Town Lake (Culkin, 1986) and many other systems. The presence of suspended solids concentrations in aquatic systems has generally been keyed to total mass concentrations. Data were compiled to analyze the spatial trends in suspended solids mass concentrations measured in Town Lake as total suspended solids, TSS (Armstrong *et al.*, 1985; TNRIS, 1983).

Spatially-distributed average TSS data and statistics for monitoring locations in Town Lake are presented in Table 3.3. Data from each given site from different monitoring programs (TNRIS, 1983) were pooled to develop joint means and

Table 3.3

SUSPENDED SOLIDS IN TOWN LAKE WATER COLUMN

System and Sampling Site	Distance D/S from Tom Miller Dam (km)	Sampling Period	No. Samples	Range [mg/L]	Mean [mg/L]	Standard Deviation [mg/L]
Lake Austin						
LA-1	-33.0	10/78 - 9/85	41	0 - 53	8.8	10.0
LA-3	-0.1	10/78 - 9/85	39	0 - 121	15.0	24.5
Town Lake						
Red Bud Trail	0.25	10/73 - 9/85	26	4 - 22	8.4	4.2
TL-1	1.0	2/75 - 9/85	54	0 - 133	12.7	25.2
DC	4.4	2/75 - 1/83	55	0 - 121	12.7	20.1
TL-4	9.6	10/73 - 9/85	87	0 - 120	17.0	24.9
Colorado River						
Montopolis	11.9	1/74 - 8/82	98	1 - 458	24.7	64.1

standard deviations. There was considerable variation about each of the means. There was a moderate trend of increasing concentrations in Town Lake in the downstream direction.

Figure 3.8 contains the measurements of total suspended solids concentration as a function of distance down the reservoir. Mean values are indicated by the symbols, and the error bars indicate values of the mean plus and minus two (2) times the sample estimates of standard deviation. The ranges bounded by the error bars do not encompass the entire spans of measured concentrations at any of the sites; there is, however, approximately a 95% probability that the upper and lower confidence levels defined by the error bars would contain a normally distributed TSS variable. Although the TSS concentrations are not likely to be normally distributed, the confidence limits on the mean are fairly good asymptotic approximations given the large number of observations at each site.

A caveat on the interpretations of lake monitoring data concerns their representativeness. Loading data presented below in Section 3.7.2 suggest that the observed data underestimated the true flow-weighted concentrations. This could have been caused by under-representation of large storm events, which are difficult to sample.

An unexpected observation from the monitoring data is the almost 50% decrease in mean suspended solids concentrations between the upstream (LA-3) and downstream (Red Bud Trail) sides of Tom Miller Dam. This statement is based on long-term mean concentrations of Table 3.3. Also, ten of the 16 monthly grab sample pairs from the Armstrong data (Armstrong et al., 1985) show this decrease (two of the months had identical upstream/downstream concentrations). Figure 3.9 was

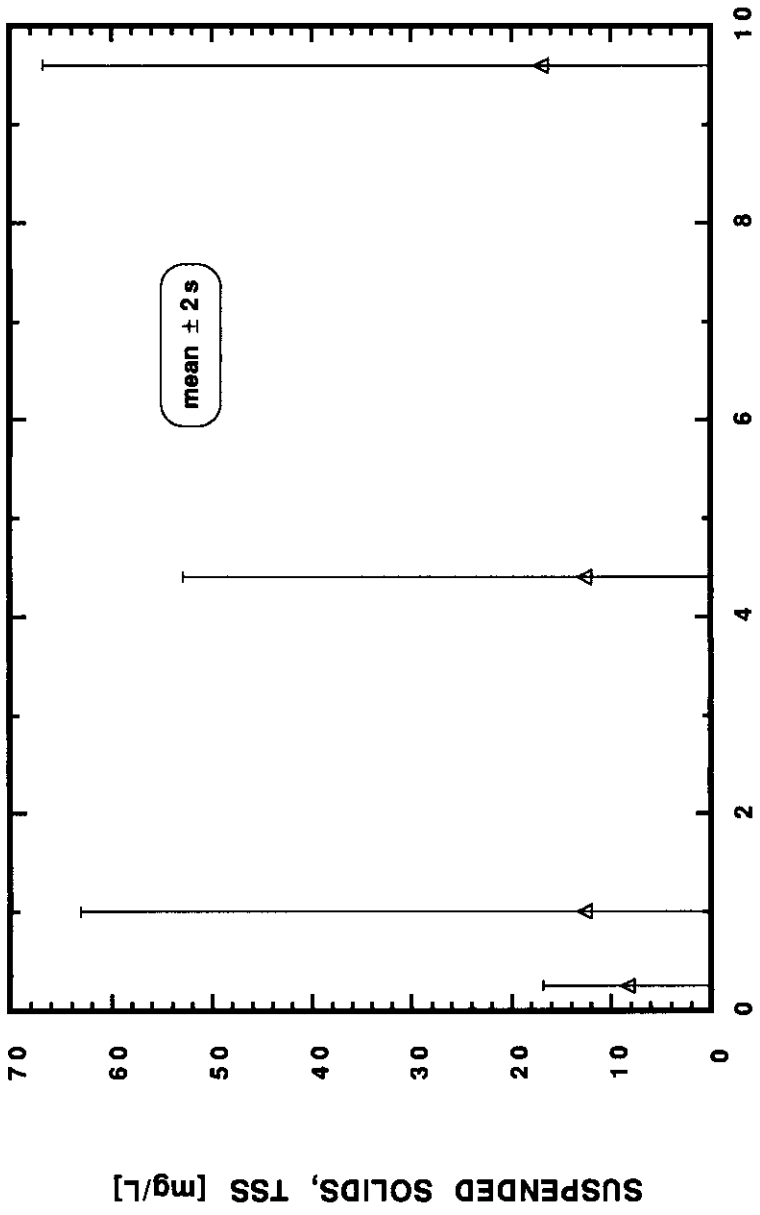

Figure 3.8 Average Observed TSS [mg/L] in Town Lake

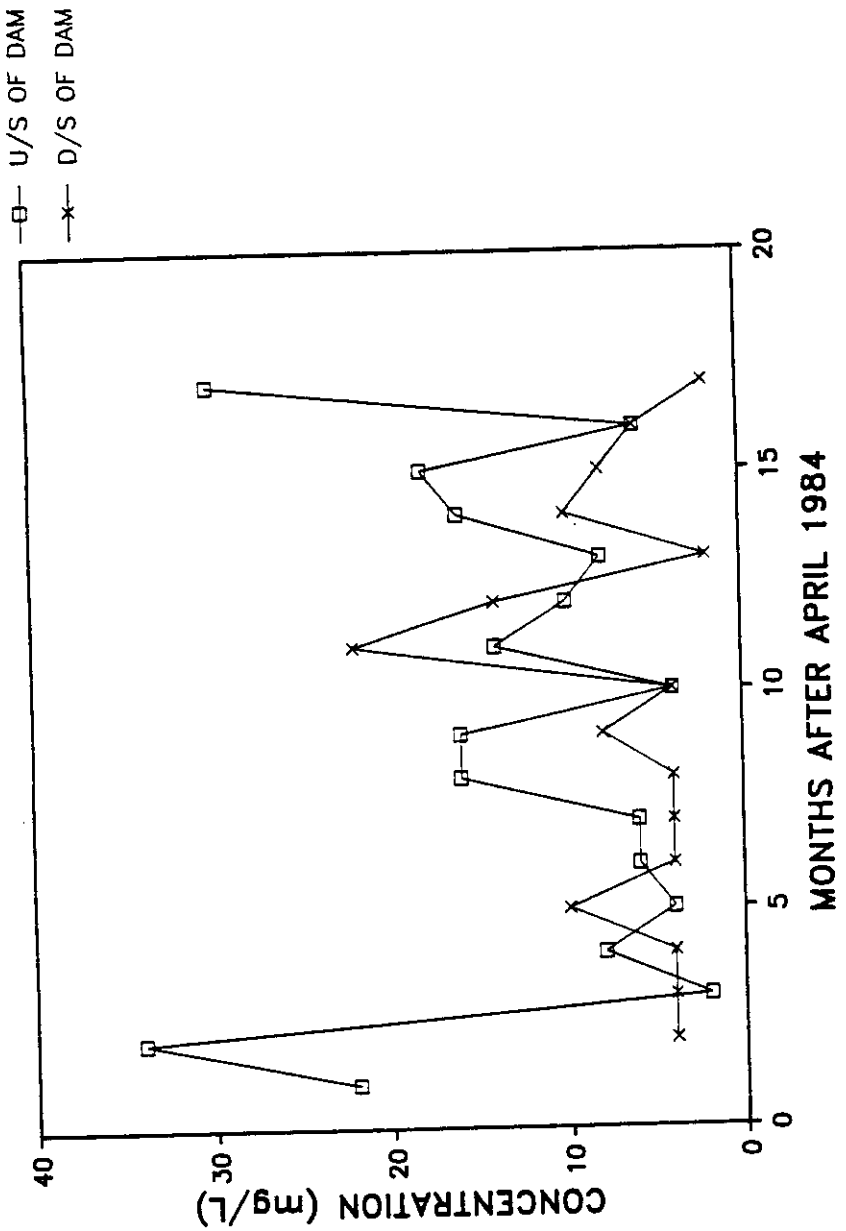

Figure 3.9 **Suspended Solids Upstream and Downstream of Tom Miller Dam**

plotted to illustrate these time-coincident results. Assuming that the two sets of samples were from different populations with different but unknown variances, the difference in the means is significant at the 90% confidence level.

Given the confidence that the TSS reductions across the dam were real, two theories are offered to explain the observation. First, it is possible that one or both of the sample sets were not representative of the time-average behavior of the spatially-averaged populations characterizing the two sites. For example, sample locations might have led to over- or underestimates of representative concentrations. The second theory is that coagulation in the lake, as described by O'Melia (1985), is taking place and resulting in lower solids concentrations in the bottom of the water column than the middle or top. Regardless of explanation, the result is a significant reduction of the apparent TSS concentration entering Town Lake.

A particle mass concentration of 9.8 mg/L was an implicit upstream boundary condition for the Town Lake simulations. Its derivation from a boundary condition on the inflow particle distribution is discussed in the following section.

3.6.2 Particle size distribution

The initial and upstream boundary conditions on the water column particle size distributions (PSD) in Town Lake were based on a characteristic PSD from Lake Austin in Austin, Texas. This 30 km, run of the river impoundment of the Lower Colorado River is formed by Tom Miller Dam, just upstream of Town Lake. Lake Austin is mesotrophic and has an annual mean detention time of seven days.

Samples of the water column from lower Lake Austin were taken from the raw water intake line to the Davis Water Treatment Plant in Austin, Texas in June and July, 1989 (Robert Cushing, University of Texas-Austin, personal communication).

The Davis WTP intake is a few kilometers upstream of Tom Miller Dam. Particle size distributions were analyzed within one day of collection on a Coulter Multisizer using 30 μm and 100 μm apertures (Coulter Electronics; Hialeah, Florida) (Cushing, 1990).

Several sets of PSDs were examined for data integrity, and the basic particle size distributions selected for this research were from samples collected 29 June, 1989. The log of the particle size distribution function (PSDF) from the two apertures analyzed is presented in Figure 3.10. These treated data were obtained from raw measurements by a) removing channels of zero particle count and obvious outliers (*e.g.*, log $d_p > 1.1$), and b) smoothing data by ensemble averaging of concentration data over each five-class interval, from minus two to plus two neighboring classes. A single log PSDF was then fitted to the two overlapped PSDF's of Figure 3.10 to give a single smooth and continuous function. The volume distribution derived from that particle size distribution function is shown in Figure 3.11 (the 'pseudo-peak' near log $d_p = 1.1$ was adjusted for the simulations).

Estimates of the particle volume and mass concentrations associated with the particle size distributions were needed. By numerically integrating the volume distribution, Figure 3.11, the total particle volume concentration was estimated to be approximately 1.37×10^6 $\mu m^3/cm^3$, or 1.37 ppmv. A reasonable estimate of suspended particle density of 1.35 g/cm^3 would yield a suspended solids concentration of 1.85 mg/L.

Lake monitoring data were used to conclude that the lake suspended solids concentration was about 2 mg/L at the time of sampling. Although the lake particle mass concentration was not measured for the samples analyzed by Cushing, turbidity was measured as approximately 1 NTU. The daily average turbidity of lake intake

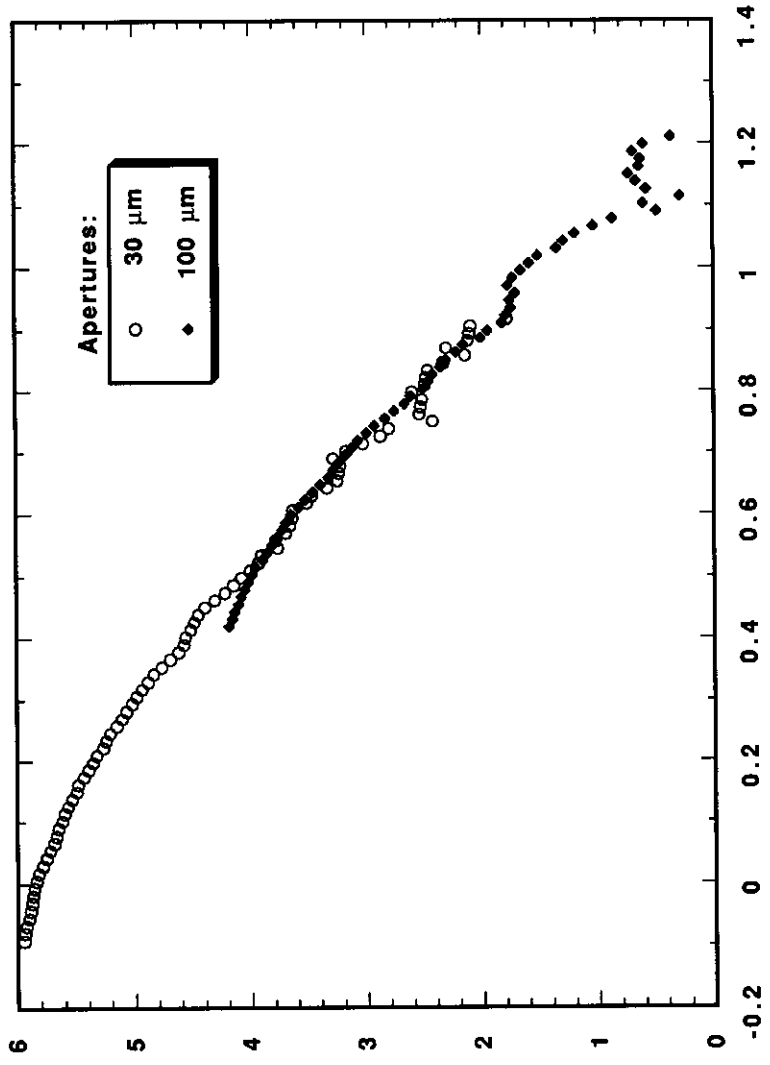

Figure 3.10 Measured Particle Size Distribution Functions for Lake Austin

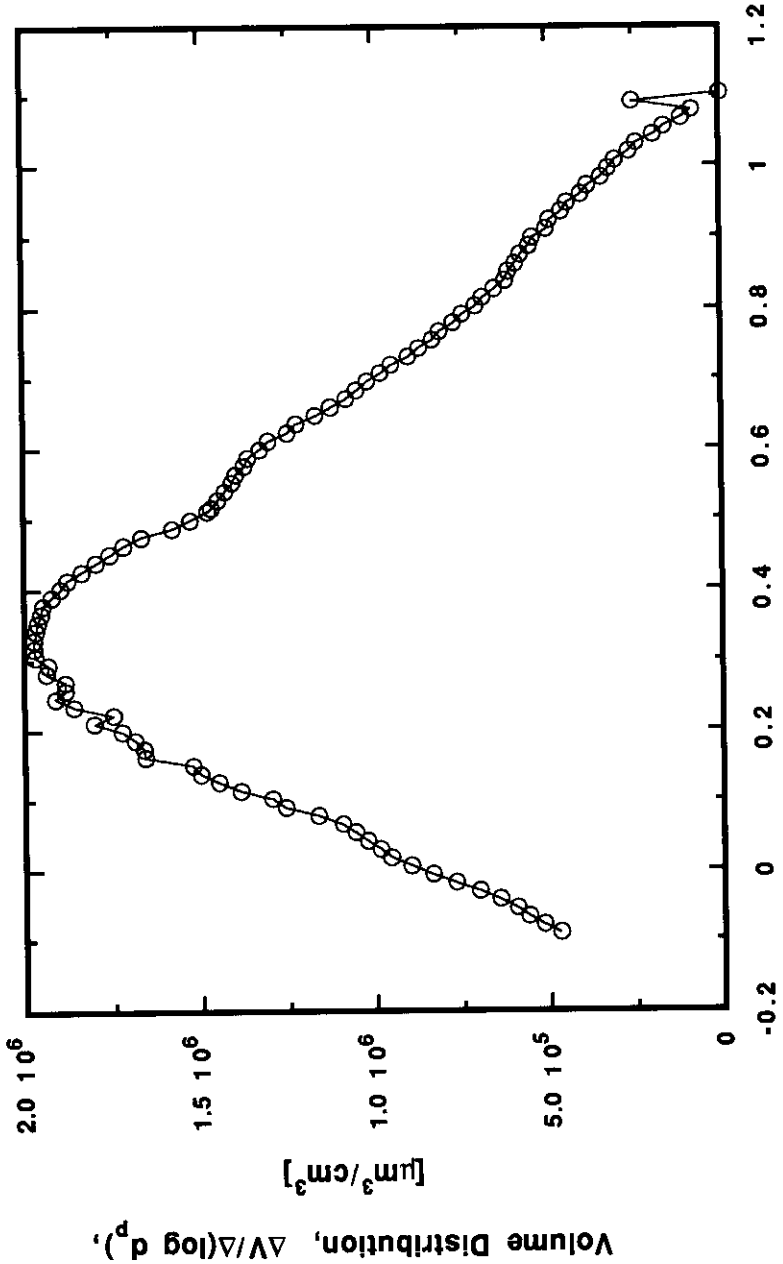

Figure 3.11 Derived Volume Distribution for Lake Austin

composite samples for 29 June, as reported by the Davis Water Treatment Plant laboratory, was 5.9 NTU, however. Also, on 26 June, the Lower Colorado River Authority had sampled Lake Austin at a 1' depth at Tom Miller Dam and found TSS of 2 mg/L and turbidity of 5.7 NTU (John Wedig, LCRA-Austin, personal communication). Because of the spatial and temporal proximity of the LCRA sampling and the conformance of results to the WTP turbidity measurements, it was assumed that the composite water quality in the lake at the time of sampling on 29 June was, approximately, TSS of 2 mg/L and turbidity of 6 NTU.

Another data set was examined to check the validity of the 2 mg/L assumption. Sixteen water column samples from lower Lake Austin were taken at two depths (near-surface and near-bed) from four different sampling stations on two days during Spring 1989 by the US Geological Survey. The samples were analyzed for suspended solids and turbidity (Helen Davidson, USGS-Austin, personal communication). The two days represented both a storm condition and a base flow condition. Regressions of the USGS suspended solids on turbidity were constructed. For the base flow event there was substantial scatter at different locations in the lake, and the regressions could not establish a significant correlation between measured turbidities and suspended solids concentrations. Therefore the assumption that solids concentration in the lake was about 2 mg/L was retained.

The log of the particle size distribution function corresponding to the measured volume distribution shown in Figure 3.11 was adjusted for use in the model to satisfy numerical and environmental (Town Lake upstream inflow) requirements. Although the modified distribution generally retained the characteristic shape as found for Lake Austin, it was modified in three ways. Specifically, the measured

particle size range was extrapolated, the number of distinct size classes was reduced, and the total volume concentration was increased.

First, the volume distribution was extrapolated to include smaller and larger size classes than actually measured. Extension to the left (smaller diameters) allowed smaller particles, known to be present, to be available as primary particles for coagulation. This extrapolation also caused the number distribution to approach closure. The size range was also extended to the right (larger diameters) so that larger particle size classes would be available for aggregate growth and because such classes were necessary for flux from boundary sources, *e.g.*, from bed resuspension or storm loading. The larger sizes did not receive any volume in the case of the Lake Austin inflow but were available for the reasons as stated.

Second, for computational economy, the number of size classes was consolidated from the original 100^+ classes, over the original size range, to 31 size classes over the expanded size range. Third, the log PSDF was shifted up such that the total particle mass concentration was 9.84 mg/L (assuming aggregate density of 1.35 g/cm^3). This TSS concentration is an appropriate long term average at the head of Town Lake, Austin, Texas.

Table 3.4 was prepared to illustrate some of the properties of the particle size distribution used as the initial and upstream boundary conditions for this research. (Time-variable upstream conditions considered in Chapter 6 did have the same relative PSD shape, but varied in absolute concentrations during the simulation). The particle model used discrete number concentrations for different size classes of particles, 31 sizes in this modeling. The absolute discrete number concentration, $\Delta N(k)$ in [#/cm^3], represents how many particles are present with diameters in the

Table 3.4

INITIAL AND UPSTREAM SIZE DISTRIBUTION FOR TOWN LAKE

Size Class	Mean Class Diameter	Minimum Class Diameter	Maximum Class Diameter	Class Δd_p	log of PSDF (psdf in)	Δ N(k)
k	[μm]	[μm]	[μm]	[μm]	[#/cm^3-μm]	[#/cm^3]
1	0.398	0.355	0.447	0.092	6.755	523345
2	0.501	0.447	0.562	0.116	6.735	630170
3	0.631	0.562	0.708	0.146	6.705	740206
4	0.794	0.708	0.891	0.183	6.662	840332
5	1.000	0.891	1.122	0.231	6.577	872192
6	1.259	1.122	1.413	0.291	6.352	654475
7	1.585	1.413	1.778	0.366	6.075	434992
8	1.995	1.778	2.239	0.460	5.729	246466
9	2.512	2.239	2.818	0.580	5.317	120345
10	3.162	2.818	3.548	0.730	4.823	48565
11	3.981	3.548	4.467	0.919	4.362	21150
12	5.012	4.467	5.623	1.157	3.838	7968
13	6.310	5.623	7.079	1.456	3.286	2813
14	7.943	7.079	8.913	1.833	2.770	1079
15	10.000	8.913	11.220	2.308	2.129	311
16	12.589	11.220	14.125	2.905	0.000	3
17	15.849	14.125	17.783	3.657	$-\infty$	0
18	19.953	17.783	22.387	4.604	$-\infty$	0
19	25.119	22.387	28.184	5.797	$-\infty$	0
20	31.623	28.184	35.481	7.298	$-\infty$	0
21	39.811	35.481	44.668	9.187	$-\infty$	0
22	50.119	44.668	56.234	11.566	$-\infty$	0
23	63.096	56.234	70.795	14.560	$-\infty$	0
24	79.433	70.795	89.125	18.331	$-\infty$	0
25	100.000	89.125	112.202	23.077	$-\infty$	0
26	125.893	112.202	141.254	29.052	$-\infty$	0
27	158.490	141.254	177.828	36.574	$-\infty$	0
28	199.527	177.828	223.873	46.044	$-\infty$	0
29	251.189	223.873	281.839	57.966	$-\infty$	0
30	316.228	281.839	354.814	72.975	$-\infty$	0
31	398.108	354.814	446.685	91.870	$-\infty$	0

range between the lower and upper diameters of class k. This absolute number concentration is the same concentration referred to in the discrete coagulation rate expression, Equation (2.1), as n_k.

Many problems can arise in interpreting results presented in terms of the discrete particle number (or volume, surface, mass, etc.) concentration. Obviously, the value of $\Delta N(k)$ is intimately dependent on the size interval chosen to represent class k. For reference, a constant $\Delta(\log d_p)$ of 0.1 was used throughout this research; therefore, corresponding Δd_p's increased continuously with particle size, as shown in the fifth column of Table 3.4. A normalized distribution corresponding to $\Delta N(k)$, *i.e.*, $\Delta N(k)/\Delta(\log d_p)$, transmits all of the information contained in the absolute number concentration, but in a form independent of experimental or model conditions. Other normalized distributions are used, such as the log of particle size distribution function, which is shown in the sixth column of Table 3.4. Distributions normalized by the class size produce numerical and graphical information that can be exchanged and interpreted freely and unambiguously, without regard to measurement or modeling conventions. In this study, the simulations were carried out using absolute discrete number concentrations (such as the last column of Table 3.4), and the results were presented and interpreted in normalized form.

Integral and statistical properties of the Town Lake PSD are used in later chapters. The integral concentrations are as follows: total number of $5.144 \times 10^6/cm^3$; total superficial surface area of 2.209×10^6 $\mu m^2/cm^3$ or 220.9 cm^2/L; and total volume of 7.286×10^6 $\mu m^3/cm^3$ or 7.286 ppmv. The weighted mean diameters are as follows: number-average diameter of 0.9929 μm; area-average diameter of 1.979 μm; and volume-average diameter of 2.986 μm.

3.7 TOWN LAKE SEDIMENT DATA

Sediment data for Town Lake and Lake Austin (as applicable) are presented in this section. Sediment properties and behavior are critical factors in the fate and distribution of solids contaminants in aquatic systems. The modeling framework used in this study required the estimation of key sediment parameters, namely sediment bulk solids concentration, particle size distribution, and porosity. Since the existing sediment data for Town Lake are limited, these parameters were derived using measured solids concentrations and certain assumptions.

Sediment organic content and percent solids data were presented for Town Lake and Lake Austin (Wallace, 1986). Four sites in Town Lake and three sites in Lake Austin were sampled. This information is presented in Table 3.5.

Percent solids is calculated as the quotient of the weight of dry solids and the weight of wet solids. One expects percent solids to generally decrease with distance down the length of an impoundment as denser solids will have settled out further upstream. Except for the segment 1 measurement, this was the case in Wallace's (1986) data. The segment 1 sediment sample was taken at site TL-1, Figure 3.2. This site is just downstream of Red Bud Isle near the headwaters of the lake. Field personnel reported no success in taking samples in the channels on either side of the island due to the rocky bottom and were forced to sample between the channels in the lee of the island.

Sampling from the sediments deposited in the wake of the island is believed to be the reason for a low solids content at TL-1. Indeed, the rocky bottom through most of the cross section at TL-1 had a very high solids content. The deep, highly scoured, small cross-sectional area channels found on the sides of the island near TL-1 might

Table 3.5
TOWN LAKE and LAKE AUSTIN SEDIMENT CHARACTERISTICS

Site	LA-3	TL-1	ES-4	TL-2	TL-3	TL-4
Lake	Austin	Town	Town	Town	Town	Town
D/S Distance from T. Miller Dam [km]	-0.1	1.0	2.8	5.4	7.3	9.6
%Solids[2]	43.24	47.70	-	50.79	44.81	40.56
%Solids[3]	63.67	-	57.7	60.3	-	68.7
%OrganicCarbon[2]	3.24	2.00	-	2.84	2.24	3.02
%Clay[3]	29.9	-	27.7	31.2	-	27.9
%Silt[3]	16.5	-	51.7	55.5	-	53.3
%Sand[3]	53.6	-	20.6	13.3	-	18.9

[1] Site designations per Figure 3.2.

[2] Wallace and Armstrong (1986). Values are averages of 2 samples per site, except 1/site at TL-2 and -4. Sampled May 1985.

[3] Engineering-Science, Inc. and City of Austin (1983). Values are averages of 3 samples per site. Sampled March 1981.

not represent the average conditions in the first segment. Large, shallow backwater areas exist between the dam and the island, and the flow slows considerably after the side-channels converge at the lee of the island.

The solids content data from the Nationwide Urban Runoff Program study in Austin (City of Austin and Engineering-Science, 1983), shown in Table 3.5, ran counter to the Wallace results. In certain years and seasons, however, heavy loads of channel-eroded sediments might create such a condition. The sediment size sieving analyses into sand, silt, and clay fractions were the only size distribution data for the lake sediments, but no consistent spatial trends appeared. The Town Lake bed, sampled at three points in the lateral cross sections of three locations (City of Austin and Engineering-Science, Inc., 1983), was composed of approximately 29% clay ($d_p < 2$ μm), 53% silt (2 μm $< d_p <$ 62 μm), and 18% sand (62 μm $< d_p$).

3.8 SOLIDS LOADING

The significant solids loading to Town Lake comes from upstream inflows and urban runoff from the immediate watershed. The upstream boundary conditions for Town Lake particle modeling are presented in the section above.

Tributary solids loads were calculated as the product of tributary inflow rates and boundary concentrations. Hydrologic inputs were discussed above. Tributary solids concentrations have been studied and shown to vary with the particular watershed and flowrates (City of Austin, 1984c). The solids concentrations were reported in those studies to vary from 600 to 1700 mg/L for storm events (Culkin, 1986). Given a complete lack of tributary particle size characterizations, however, a spatially and temporally uniform particle size distribution was used in this research for steady-state (annual and seasonal) simulations. Time-variable storm events did

have particle concentrations ramped up and down during the storm response periods. These considerations are presented in Chapter 6.

CHAPTER IV

MODEL DEVELOPMENT

4.1 INTRODUCTION

A mathematical model capable of simulating particle-particle interactions and behavior in natural aquatic systems was developed in this research. In this chapter the conceptual framework and numerical methods used in developing and applying the model are presented. Assumptions and limitations of the approaches taken are discussed, and an overview of the actual code is provided.

The model simultaneously simulates particle transport and reaction (coagulation). Size-dependent particle behavior is the focal point of the model. The transport framework allows unsteady, two-dimensional fluid flow and dispersion fields to be specified under laterally-averaged conditions. Water column and bed exchanges couple these dilute and concentrated phases, which enables the analysis of size-dependent transport processes such as sedimentation and erosion.

Particle-particle interaction is the phenomenon of primary interest in this research. The schematic presented in Figure 4.1 illustrates the major processes and behavioral pathways. Subsequent sections of this chapter explain the development of the particle transport framework and the particle-particle interaction model. An outline of the simulation code is then presented.

A particle-associated contaminant transport and fate model was also developed to explore the influence of solids behavior on dissolved, sorbable contaminants. The development of that model is presented and discussed in Appendix A.

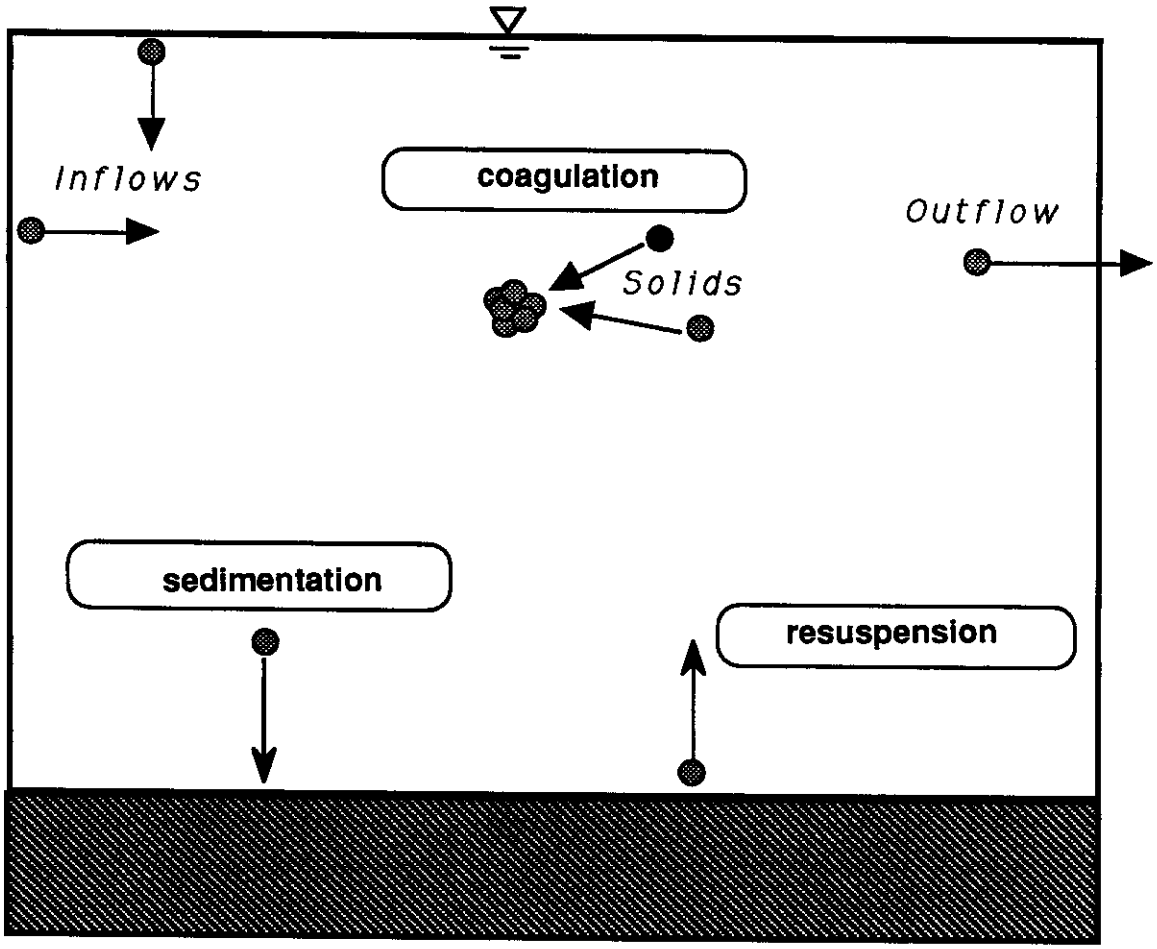

Figure 4.1 Conceptual Model Framework

4.2 PARTICLE TRANSPORT MODEL

4.2.1 Equations

Time-variable transport and reaction of heterodisperse particles in a multidimensional system are described mathematically with the conservative form of the advection-dispersion-reaction equation,

$$\frac{\partial n_k}{\partial t} + \frac{\partial}{\partial x_i}(U_i n_k) = \frac{\partial}{\partial x_i}\left(E_{ij}\frac{\partial n_k}{\partial x_j}\right) + R(n_k), \qquad (4.1)$$

or with the nonconservative form of the advection-dispersion-reaction equation,

$$\frac{\partial n_k}{\partial t} + U_i \frac{\partial n_k}{\partial x_i} = E_{ij} \frac{\partial^2 n_k}{\partial x_i \partial x_j} + R(n_k) . \qquad \textbf{(4.2)}$$

Considering only principal components of the dispersion tensor and ignoring reaction(s), the more familiar (nonconservative) advection-dispersion equation is

$$\frac{\partial n_k}{\partial t} + U_i \frac{\partial n_k}{\partial x_i} = E_{ii} \frac{\partial^2 n_k}{\partial x_i^2} . \qquad \textbf{(4.3)}$$

In the transport and transport-reaction equations (4.1) to (4.3) above, the number concentrations of size class "k" particles, n_k, are the state variables. The units for the absolute discrete particle number concentrations n_k are [#/cm^3]. In the general discussion of particle size distribution characterizations (Section 3.5), the absolute discrete particle number concentrations were denoted symbolically as $\Delta N(k)$. In subsequent sections of the report, n_k is used in model equations, and $\Delta N(k)$ (or just ΔN) is used for presentation of results.

Equation (4.3) describes particle transport alone. As stated previously, the spatial domain is two-dimensional (assumed laterally uniform). In the index notation used in equations (4.1) to (4.3), the index "i" represents both longitudinal or vertical directions; index "j" represents the direction perpendicular to direction "i." Consequently, state-variables and parameters are lateral averages. Distributed parameters U_i are the directional velocities for the particle, and distributed parameter E_{ij} is the turbulent dispersion tensor for the particle. The particle parameters U_i and E_{ij} might or might not be the same as those for the fluid.

The term $R(n_k)$ in equations (4.1) and (4.2) is a source/sink term. In this research, the term represents the coagulation reaction rate. Other particle production

and loss processes are ignored, as discussed in Section 2.2.5. To solve the advection-dispersion-reaction equation (4.2), the processes are numerically decoupled into independent though simultaneous transport and reaction steps. The validity of this decoupling is discussed further in Section 4.3 with the reaction model.

Size-dependent particle transport in the water column is readily described by the transport equation (4.3). As discussed in Chapter 2, Stokesian particles possess negligible inertia and follow the mean fluid flow. A constant depth was assumed in the modeling, and therefore mean vertical fluid velocities are zero. Particles are transported relative to the fluid due to gravity, however. Superimposing the non-zero, size-dependent, relative particle settling velocity, v_k, upon the size-independent vertical fluid velocity U_z (= 0) resulted in an absolute, size-dependent, vertical particle velocity $U_{z,k}$.

Size-dependent bed deposition and resuspension were addressed with a system of boundary conditions, as described in the next section. The size-dependent transport approach permits the identity and role of particle classes to remain distinguishable. This property is important in analyzing two conditions: a) steady-state conditions, in which the mean particle size and/or concentration (hence, behavior) vary substantially through space, and b) unsteady loads or perturbations on the system, in which even 'good' parameter estimates of mean properties can vary significantly during the unsteady period. It is also noted that this discrete particle approach will benefit the analysis of differential horizontal contaminant transport, which is due to the combination of size-dependent contaminant partitioning and size-dependent sedimentation (both commonly observed).

Finite-difference methods were used to numerically integrate the system of transport and reaction equations at discrete points in space. A two-dimensional rectangular grid was set up to represent the receiving system domain. The model and equations are formulated for a rigid lid, constant depth system. The grid is shown in Figure 4.2. The physical longitudinal dimension, x, is positive in the downstream direction. The numerical length in x is represented by the integer index "i" or the fractional system length "X". The vertical physical dimension, z, is positive down. The numerical depth in z is represented by the integer index "j" or the fractional system depth "Z".

Finite-difference approximations were substituted for the time and transport derivatives to convert the unsteady advection-diffusion transport equation (4.3) from a parabolic partial differential equation into an algebraic equation. Finite difference approximations can be made by any of several differential or integral methods (Jaluria and Torrance, 1986; Roache, 1982). Taylor series expansions were the primary means of derivation here, although the control volume approach was needed for the boundary condition at the bed-water interface. The algebraic solution of the set of equations resulting from these substitutions is discussed in Section 4.2.3.

The standard forward divided difference approximation has been used for the time derivative. In one spatial dimension, its finite difference equation (FDE) is written

$$\frac{\partial n}{\partial t} \cong \frac{n_i^{l+1} - n_i^l}{\Delta t} . \qquad \textbf{(4.4)}$$

Time level "l" is the current time, and time level "l+1" is at the projected time, *i.e.,* at one time step of Δt duration after the current time. Subscript "i" denotes the base

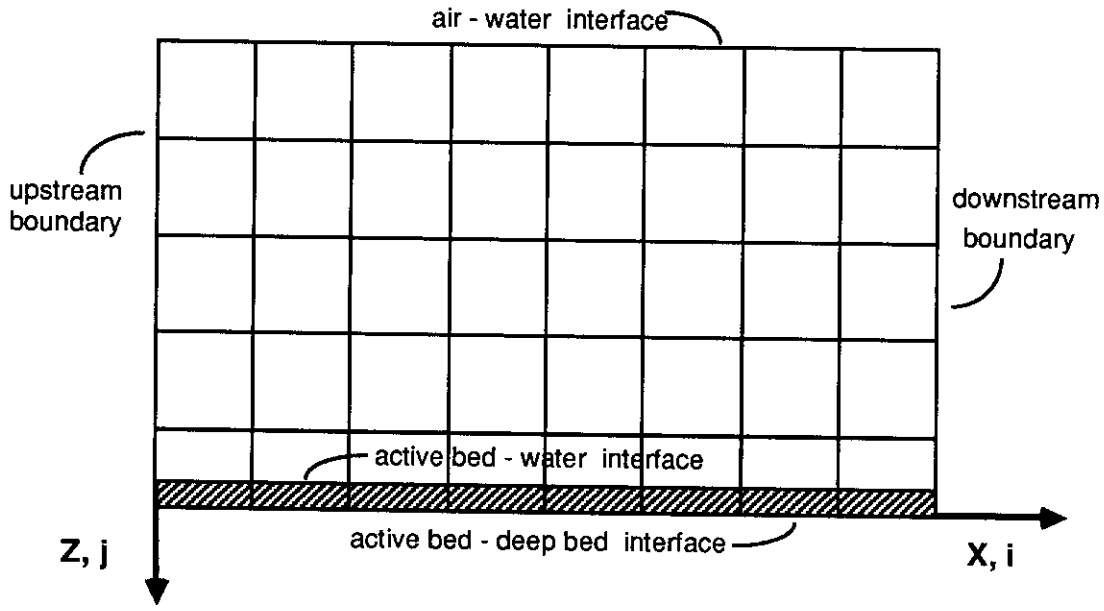

Figure 4.2 Computational Grid and Boundaries

point, where the derivative is being evaluated. The accuracy of the approximation is first order in time, which is written $\mathcal{O}(\Delta t)$.

The standard central difference approximation for the second derivative, and the representation used in this model, is

$$\frac{\partial^2 n}{\partial x^2} \cong \frac{n_{i+1} - 2n_i + n_{i-1}}{(\Delta x)^2} . \qquad (4.5)$$

Index "i" again marks the node where the derivative is being evaluated, and i+1 and i-1 are located plus one and minus one space step of Δx, respectively, from the base point. All terms are understood to be taken at the current time level l. Taylor series expansions were used to estimate function values at neighboring points to the desired accuracy. The standard central difference approximation is obtained by combining the

expansions for the function values at the base location plus one space step and at the base location minus one space step. After combining the two expansions to yield the central difference approximation (4.5), a remainder term is truncated. It consists of terms with derivatives of fourth order and greater, multiplied by coefficients of Δx^2, Δx^4, and so on. The combined remainder (error) term for the FDE is then of $\mathcal{O}(\Delta x^2)$ we say that the estimate of the curvature has accuracy that is second order in space, $\mathcal{O}(\Delta x^2)$.

Numerical approximations of the advective flux, those terms involving spatial concentration gradients, typically cause problems in transient finite difference transport models. These problems arise in advection-dominated flows, *i.e.*, where the grid Peclet number is greater than one. The dimensionless grid Peclet number is defined as the ratio of advective to dispersive transport, *i.e.*,

$$Pe_\Delta \equiv \frac{U_x \Delta x}{E_x}, \tag{4.6}$$

for the x direction. The grid Peclet number is obviously conditioned on the computational structure used in the problem solution, *i.e.*, the step or grid size chosen, as well as the physics of the transport fields. The grid Peclet number is itself the ratio of two dimensionless numbers, the Courant number, C_x, and the dispersion number, D_x. The dimensionless parameters are

$$Pe_\Delta \equiv \frac{C_x}{D_x} \tag{4.7}$$

where

$$C_x \equiv U_x \frac{\Delta t}{\Delta x} \tag{4.8}$$

and

$$D_x \equiv E_x \frac{\Delta t}{(\Delta x)^2}. \tag{4.9}$$

The Courant number is the fraction of a complete grid step traversed by advection during one time step. The dispersion number indicates the fraction of a complete grid step traversed by dispersion during one time step.

There are several simple approximations available to estimate the advective concentration gradient in equation (4.3). Backward differencing of the derivative gives the FDE

$$\frac{\partial n}{\partial x} \cong \frac{n_i - n_{i-1}}{\Delta x} . \qquad \textbf{(4.10)}$$

Forward differencing gives

$$\frac{\partial n}{\partial x} \cong \frac{n_{i+1} - n_i}{\Delta x} . \qquad \textbf{(4.11)}$$

Central differencing yields

$$\frac{\partial n}{\partial x} \cong \frac{n_{i+1} - n_{i-1}}{2\Delta x} . \qquad \textbf{(4.12)}$$

Each of these two-point gradient approximations can lead to disastrous results in accuracy, stability, or computational time for advection-dominated scalar transport (Leonard, 1979). For example, backward differencing smears the otherwise sharp front of a step input concentration gradient, whereas central differencing results in oscillations at the otherwise monotonal front of the step input. There are, of course, many other possible FDE approximations for the first derivative (Lapidus and Pinder, 1982). Even when bounds on the time step are placed to make explicit solutions more stable and accurate, however, numerical diffusion introduced by these methods often requires the use of physical dispersion coefficients which are severely understated in order to compensate for the numerical dispersion (Leonard, 1979).

A gradient approximation was derived to overcome the problematic solutions discussed above. Combining Taylor series expansions at x_i, x_{i-1}, x_{i-2}, and x_{i+1}, and grouping all terms of fourth order and higher derivatives into a single (and truncated) remainder term, the spatial gradients may be expressed as

$$\frac{\partial n}{\partial x} \cong \frac{2n_{i+1,j} + 3n_{i,j} - 6n_{i-1,j} + n_{i-2,j}}{6(\Delta x)} \qquad \textbf{(4.13a)}$$

or analogously in the vertical as

$$\frac{\partial n}{\partial z} \cong \frac{2n_{i,j+1} + 3n_{i,j} - 6n_{i,j-1} + n_{i,j-2}}{6(\Delta z)}. \qquad \textbf{(4.13b)}$$

Having truncated all fourth order and higher derivatives, which carry coefficients of Δx^3 and higher, the gradient approximations (4.13a and 4.13b) are accurate to $\mathcal{O}(\Delta x^3)$ and $\mathcal{O}(\Delta z^3)$. This accuracy can be compared to that of the standard two-point FDEs. Backward and forward approximations (4.10) and (4.11) are only first-order correct, and the central approximation (4.12) is only second-order accurate.

A similar but improved four-point gradient approximation was developed (Leonard, 1979), and it is known as "Leonard's method." Both steady-state (QUICK) and transient response (QUICKEST: Quadratic Upstream Interpolation for Convective Kinematics - Estimated Streaming Terms) variations were presented. Leonard's method was derived using the control volume approach rather than by Taylor series expansion. Scalar (mass, in this case) conservation is thus assured within the domain. A Taylor series derivation of Leonard's method was shown to be equivalent to the QUICKEST algorithm (Basco, 1984). Basco converted second- and third-order time derivatives and space-time cross-derivatives into spatial derivatives, then incorporated them into the Taylor series expansions, to recover Leonard's FDE.

A more useful computational form of the one-dimensional FDE was also presented by Basco (1984):

$$
\begin{aligned}
n_i^{l+1} \cong\ & n_i^l \\
& + n_{i+1}^l \left[-\frac{C}{2} + D + \frac{C^2}{2} + \frac{C}{6}(1 - C^2 - 6D) \right] \\
& + n_i^l \left[-2D - C^2 - \frac{C}{2}(1 - C^2 - 6D) \right] \\
& + n_{i-1}^l \left[\frac{C}{2} + D + \frac{C^2}{2} + \frac{C}{6}(1 - C^2 - 6D) \right] \\
& + n_{i-2}^l \left[-\frac{C}{6}(1 - C^2 - 6D) \right] .
\end{aligned}
\tag{4.14}
$$

Equation (4.14) is the basic FDE for one-dimensional transport. It is second-order accurate in time and third-order accurate in space. Note that the FDE returns pure grid to grid advection, *i.e.*, $n_i^{l+1} = n_i^l$, whenever the Courant number C = 1 and the dispersion number D = 0, regardless of concentrations n_i, n_{i+1}, or n_{i-2}. This result demonstrates the value (mass conservation) of the control volume approach used in the original derivation. Useful plots of the regions of stability and phase errors for this form of Leonard's method were also given by Basco (1984).

Direct substitution of derivative approximations for time (4.4), gradient (4.13), and curvature (4.5) in the one-dimensional transport equation (4.3) gives

$$
\begin{aligned}
n_i^{l+1} \cong\ & n_i^l \\
& + n_{i+1}^l \left[-\frac{U_x \Delta t}{3 \Delta x} + \frac{E_x \Delta t}{(\Delta x)^2} \right] \\
& + n_i^l \left[-\frac{U_x \Delta t}{2 \Delta x} - \frac{2 E_x \Delta t}{(\Delta x)^2} \right] \\
& + n_{i-1}^l \left[\frac{U_x \Delta t}{\Delta x} + \frac{E_x \Delta t}{(\Delta x)^2} \right] \\
& + n_{i-2}^l \left[-\frac{U_x \Delta t}{6 \Delta x} \right] .
\end{aligned}
\tag{4.15}
$$

In contrast to Leonard's method (4.14), one does not generally recover step to step advection with equation (4.15) using $C_x = 1$ and $D_x = 0$. Only under the general condition of uniform concentration at all nodes (zero gradient and curvature), or some unique concentration distribution, would step to step advection be assured. Mass conservation in advection-dominated flow, particularly if it is unsteady, is thus problematic when using (4.15). Also, even although this method is third-order accurate in space, it is only first-order accurate in time. Leonard's method, with its third-order accuracy in time, is thus preferred. Nonetheless, the straight forward Taylor series approach (4.15) has been successfully used in unsteady 3-D petroleum reservoir transport and phase behavior simulations (Saad, Pope, and Sepehrnoori, 1989), using relatively small Courant ($C \leq 0.05$) and grid Peclet ($Pe_\Delta \leq 50$) numbers.

The one-dimensional version of the transport FDE (4.14) was substituted for the partial differential equation (4.3). The resulting set of algebraic equations was solved in a one-dimensional test simulation of a step input to a fixed-lid rectangular reservoir with Dirichlet (constant scalar value) boundary conditions. The first nodes internal to the domain must use the backward difference FDE (4.10) instead of the four-point gradient. Comparisons showed excellent agreement between analytical and numerical solutions.

Saad *et al.* (1989) used the same approach to test alternative FDEs for the first derivative accuracy in finite difference (oil and gas) reservoir simulators. These authors presented analytical and numerical solutions for the 1-D problem that showed remarkable agreement between the four point gradient method (4.13) numerical solutions and analytical solutions, using grid Peclet numbers at least up to 10.

Solutions using other FD approximations for the gradient departed very noticeably at smaller grid Peclet numbers.

The transport equation using Leonard's method (4.14) is still subject to potential instabilities and inaccuracy (Basco, 1984; Hall and Chapman, 1985; Leonard, 1979). Although the acceptable grid Peclet number illustrated by Saad *et al.* (1989) was at least 10, the Courant number used was low ($C \approx 0.05$). Values of Courant number much less than 1 are normally used in surface water transport (Leonard, 1979), but Basco (1984) presented stability and accuracy guidelines illustrating potential use up to a Courant number of 2.

The extension of Leonard's method to multiple dimensions can be straightforward when one-dimensional advection dominates. A simple superposition of the two (vertical and longitudinal) 1-dimensional transport FDEs using Leonard's method (4.14) was initially used in the model. The seven point, 2-D computational stencil used is shown in Figure 4.3. The z-axis orientation, affecting the expression of the derivative approximation, was chosen positive down, as indicated in Figure 4.2. Net long term vertical advective flux is assumed toward the bed, which is the case for lacrustine cases and most instances where coagulation is important.

A simple superposition of two 1-D FDEs (4.14) was employed by Davis and Moore (1982) in a 2-D simulation of closed channel flow around a rectangular block, but the authors noted potential errors in ignoring the spatial cross-derivatives. They concluded that simple superposition was adequate for their work because nearly unidirectional flow made cross-derivatives negligible. Hall and Chapman (1985) cautioned against superimposing 1-D finite difference approximations for advective

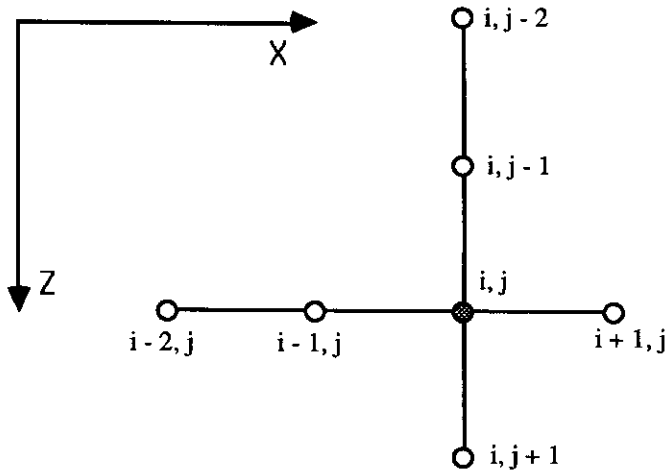

Figure 4.3. Computational Stencil for 2-D Differencing

terms in 2-D estuarine modeling, however, because depth-averaged fluid velocities in longitudinal and lateral directions are comparable, which makes the cross-derivative terms significant.

Two conditions prohibited the simple superposition of two 1-D FDEs (4.14) in this research. The first condition was the voiding of 1-D advective dominance when large particle settling velocities are present, and the second condition was the treatment needed for lateral averaging.

Advective transport of particles, even those fine particles considered in this work, is not one-dimensionally dominant under all circumstances. Given the constant system depth mentioned above, vertical fluid velocity is zero; mean horizontal fluid flow is thus assured. Larger, denser particles in the water column can have a significant vertical settling velocity component relative to their fluid-imposed horizontal velocity, however. Inclusion of cross-derivative corrections to the superimposed 1-D FDEs is thus needed. The additional terms needed to recover second-order time accuracy have been given as (Davis, 1984)

$$\frac{\Delta t}{2}\left[\frac{\partial}{\partial x}\left(u\,v\,\frac{\partial n}{\partial z}\right)+\frac{\partial}{\partial z}\left(u\,v\,\frac{\partial n}{\partial x}\right)\right]^{1}. \qquad \textbf{(4.16)}$$

Differences of products must be carefully treated to avoid numerical errors by noting that the exact expansion

$$d(uv) = u\,dv + v\,du \qquad \textbf{(4.17a)}$$

must be converted to the approximation

$$d(uv) \cong (uv)_{j+1} - (uv)_{j-1}\,. \qquad \textbf{(4.17b)}$$

As stated by Abbott (1979), "... of the infinity of possible (consistent) difference approximations to..." (the differential, 4.17b), "...there is, essentially, one and only one difference *equality*:"

$$(uv)_{j+1} - (uv)_{j-1} \equiv \left(\frac{u_{j+1}+u_{j-1}}{2}\right)(v_{j+1}-v_{j-1}) + \left(\frac{v_{j+1}+v_{j-1}}{2}\right)(u_{j+1}-u_{j-1}) \qquad \textbf{(4.18a)}$$

Therefore, the finite difference equation becomes

$$d(uv) \cong \left(\frac{u_{j+1}+u_{j-1}}{2}\right)(v_{j+1}-v_{j-1}) + \left(\frac{v_{j+1}+v_{j-1}}{2}\right)(u_{j+1}-u_{j-1})\,. \qquad \textbf{(4.18b)}$$

Abbott (1979) noted that it is not possible to incorporate this particular (4.18b) FDE approximation for cross-derivatives in most (implicit) numerical schemes. The explicit approach employed in this model is, however, amenable to the use of (4.18b). Although the presence of three functions within the derivatives of the cross-derivative corrections terms (4.16) makes the approximations much lengthier to write and compute than those of (4.18), the principles are the same. The two-dimensional version of the transport FDE (4.14), with appropriate terms for cross-derivatives, was substituted for the model partial differential equation (4.3).

The constant-depth FDEs, even with cross-derivatives incorporated as just described, still cannot be applied in systems of variable width. Given the lateral averaging of concentration and system parameters such as fluid velocities and dispersion coefficients, each concentration term in the defining transport equations (4.1 to 4.3) must be multiplied by the cross-sectional width, B. Adjustment of the algorithms to include the appropriate nodal width factors thus completed the development of the two-dimensional, laterally-averaged (constant depth), unsteady transport model. These considerations are discussed at the beginning of Chapter 6.

4.2.2 Boundary conditions

Finite-difference approximations for the boundary conditions (BCs) have been derived and incorporated in the transport equations. A set of unique approximations for the bed-water interface, describing bed deposition and resuspension, have been derived. This approach has not been used before, and it provides a way to utilize bulk mass flux experimental results (those typically reported for flume erosion studies) in the discrete particle number modeling framework.

Unlike ordinary differential equations (ODE), the nature of boundary and initial conditions for a partial differential equation (PDE) determines its unique solution and is thus of dominant computational importance (Roache, 1982). The transport equation is a second-order PDE in both x and z directions. Two boundary conditions in each direction are therefore needed for its solution. Specifying both BCs at the same interface would lead to an ill-posed problem (Jaluria and Torrance, 1986), so boundary conditions for a given direction are established at opposite interfaces of the domain. Boundaries considered were depicted in Figure 4.2. Vertical BCs are discussed first, followed by horizontal BCs.

In the vertical, a standard zero-flux condition,

$$v_k n_k - E_z \frac{\partial n_k}{\partial z} = 0, \qquad \textbf{(4.19)}$$

is set at the air-water interface. This is a homogeneous, Robbins (or mixed) boundary condition. The distinctive property of this BC is that it is particle size dependent. The BC states that a dynamic equilibrium exists at the free surface between positive (down) particle flux due to gravitational settling and negative flux due to gradient-type dispersion. This equilibrium is both physically and computationally valid. The no-flux condition at the interface does not imply zero flux over the control volume or steady-state at the interface. The particle size-dependent boundary condition (4.19) is rewritten as

$$\frac{\partial n_k}{\partial z} = \frac{v_k}{E_z} n_k \, . \qquad \textbf{(4.20)}$$

This form was substituted directly in the transport equation for the air-water interface nodes. Note that conditions of purely quiescent settling, *i.e.*, $E_z = 0$, are not computationally possible. Brownian motion (described by a molecular diffusion-like coefficient, $D_m \neq 0$) prevents this from being of physical or numerical concern in fluid water, however.

A finite difference form of this boundary condition must be used to extract an approximation for the curvature in the transport FDE (4.14). Using a backward difference approximation for the gradient (4.10)

$$\frac{\partial n}{\partial x} \cong \frac{n_i - n_{i-1}}{\Delta x}$$

and noting that the vertical (z) transport is at the interface, $j = 1$,

$$\frac{\partial n}{\partial z} \cong \frac{n_1 - n_0}{\Delta z} \, . \qquad \textbf{(4.21)}$$

Concentration n_0 is a fictitious concentration at the imaginary node j = 0. The node is positioned outside the physical domain in order to have a concentration for central differencing at the interface. Given the explicit constraint on the gradient (4.20), the utility of the backward difference gradient estimate is in approximating the curvature (4.5) at the air-water interface. Equating the backward difference approximation (4.21) with the air-water interface boundary condition (4.20) gives

$$n_0 \equiv n_1 \left(1 - \frac{v \Delta z}{E_z}\right). \qquad \textbf{(4.22)}$$

This imaginary concentration estimate can now be used in the central difference approximation to the second derivative at the interface.

At the bottom of the water column, we consider two sediment compartments, one of which enters into the boundary condition interaction of the water column with the sediment bed. The sediment layer at the sediment-water interface is conceived as actively exchanging particles with the overlying water column. Beneath the active sediment-water interface is an active bed-deep bed interface, shown at the very bottom of Figure 4.3. For the shorter time-scale problems investigated using this model, the two compartments are considered isolated; the evolution of the deep bed is not considered, nor is it allowed to interact with the active bed above it. In a sense, zero-flux BCs are assumed at the active bed-deep bed interface. Since there is no change taking place within the deep bed, nor any exchange taking place between the deep and shallow beds, there is no need to establish a formal mathematical linkage between the two compartments via boundary conditions.

Given the near total absence of size-dependent experimental erosion data for fine, cohesive sediments, the boundary condition at the bed-water interface is the

most difficult to formulate. A general nonequilibrium boundary condition has the following form:

Deposition Flux - Erosion Flux = Net Deposition Flux to Bed, *i.e.*,

$$J_D - J_R = \Delta J , \tag{4.23}$$

where the absolute deposition and resuspension fluxes are denoted J_D and J_R, respectively. This conservation BC could be established on the basis of discrete particle numbers, total particle mass, or other unique bases. For the size-dependent particle transport simulated here, the flux at the bed-water column interface is formulated as the net result of mass deposition and mass erosion.

In integral terms, the deposition mass flux is

$$J_D = \sum_{k=1} v_k \, n_k \frac{\pi \, d_k^3 \, \rho_k}{6} , \, [M/L^2\text{-}T] \tag{4.24}$$

and the resuspension mass flux is

$$J_R = -\sum_{k=1} E_z \frac{\pi \, d_k^3 \, \rho_k}{6} \frac{\partial n_k}{\partial z} , \, [M/L^2\text{-}T] ; \tag{4.25}$$

v_k is the appropriate particle settling velocity, and d_k and ρ_k are the particle diameter and density. E_z is a turbulent dispersion coefficient which must describe the flux due to turbulent velocity and concentration fluctuations in the near-bed region. Aside from practical difficulties in characterizing the turbulent flow field, the coefficient must also account for the physicochemical nature of the interfacial region, *i.e.*, the degree of sediment cohesiveness. As such, it is not a property of the flow field as depicted, and it is not a good conceptual model.

An alternate approach, and the path chosen for this research, is to use empirical relations derived from bulk resuspension mass flux measurements. One such expression, a linear relationship based on excess shear stress, is

$$J_R = M(\tau_0 - \tau_c). \quad \textbf{(4.26)}$$

The bed shear stress, τ_0, is the shear stress imposed by the fluid flow on the bed. The critical bed shear stress, τ_c, is the shear stress that causes resuspension of the bed. The rate coefficient, M [T/L], is the proportionality factor relating the observed mass flux and excess shear stress. This linear relation (4.26) was found to represent the resuspension process for deposited, cohesive sediments (Ariathurai and Arulanandan, 1978). Other descriptions have also been used in modeling resuspension from different cohesive sediment types (Hayter, 1987).

In discrete terms, the deposition mass flux for a single size class is

$$J_{D,k} = v_k n_k \frac{\pi \rho_k}{6} d_k^3, \ [M/L^2\text{-}T]; \quad \textbf{(4.27)}$$

the deposition number flux for a single size class is

$$j_{D,k} = v_k n_k, \ [\#/L^2\text{-}T]. \quad \textbf{(4.28)}$$

The absolute discrete particle or mass deposition fluxes, $j_{D,k}$ or $J_{D,k}$, are readily found by applying the known (assumed) particle properties to the concentration just above the bed.

Translating the bulk mass resuspension flux into discrete particle fluxes is not as straightforward as the *a priori* depositional fluxes. To convert bulk resuspension mass flux J_R into discrete particle resuspension mass flux $J_{R,k}$, we define f_k as the fraction of J_R composed of size k particles. Thus,

$$J_{R,k} = f_k J_R \quad \textbf{(4.29)}$$

This construct can take two different forms, but either form requires three key assumptions, discussed below.

First, we assume that an active and well-mixed bed exists, *i.e.*, there are no vertical concentration gradients (for the entire size distribution) through this active layer. A practical requirement for this assumption to be valid is that size-dependent deposition mixes vertically through the active layer(s) in a time much less than the characteristic resuspension time. The assumption is questionable, given current knowledge of sediment layer dynamics, except under two conditions: a) the layer(s) is confined to a relatively thin segment, perhaps 1 cm or less, or b) the depositional rate (sedimentation velocity) is slow.

Second, it is assumed that the aggregates are unconsolidated enough to be available for independent behavior both before and after resuspension. Thus, significant post-deposition compaction is not allowed. Again, this assumption is doubtful unless we consider thin sediment layers, short time periods, weak floc strength, stable suspensions, or a combination of these factors.

Last, we assume that coagulation ceases in the active bed. This assumption is made even though it is not necessary for computational purposes and the aggregation process is sure to proceed by some mechanism(s) over some time scale(s). The restriction is placed because of the extreme uncertainty about how to specify the flocculation process in concentrated suspensions, even in controlled laboratory thickening systems.

Given the premises of a shallow, active, homogeneous layer of stable, independent particles acting over short time scales, we can make the first-order assumption: the erosion rate of size k particles from the bed is proportional to the

concentration of k-size particles in the bed. This is a first approximation. Whether a mass or number proportionality is assumed establishes two alternative expressions:

a) Assume the resuspension mass fraction, $f_k \propto$ Number concentration of size k particles in bed, *i.e.*:

$$f_k \equiv \frac{n_k}{N_{Tot}} \tag{4.30a}$$

where

N_{Tot} = Total number concentration in bed, [#/L^3], *i.e.*, $\sum_j n_j$,

or

b) Assume the resuspension mass fraction, $f_k \propto$ Mass concentration of size k particles in bed, *i.e.*:

$$f_k \equiv \frac{m_k}{M_{Tot}} \equiv \frac{n_k \left(\frac{\pi\, d_k^3\, \rho_k}{6}\right) V_{bed}}{\sum_j n_j \left(\frac{\pi\, d_j^3\, \rho_j}{6}\right) V_{bed}} \tag{4.30b}$$

or

$$f_k = \frac{n_k\, d_k^3\, \rho_k}{\sum_j n_j\, d_j^3\, \rho_j}. \tag{4.30c}$$

If the floc density (ρ) is independent of size, the mass fraction expression (4.30b) simplifies to

$$f_k = \frac{\pi\, \rho\, d_k^3\, n_k}{6\, \rho\, (1 - \Phi)} = \frac{\pi\, d_k^3\, n_k}{6\, (1 - \Phi)}, \tag{4.30d}$$

where Φ is the porosity of the bed-water interface.

When solids erode via bulk resuspension, the mass fraction approximation for f_k (4.30d) is the appropriate form of choice. This behavior is commonly observed (and measured) in the study of freshly deposited cohesive sediments. Not surprisingly, it is

seen also in the study of turbulent bursting phenomena in the resuspension of noncohesive sediments. It is apparent from the outset that the assumptions leading to (4.30) violate conditions which lead to bed armoring, bed layering, and bed consolidation, phenomena which have been observed over longer time and space scales.

The discrete resuspension number flux can now be stated as

$$j_{R,k} = \frac{\#\text{-}k}{\text{mass-}k} \frac{\text{mass-}k}{\text{bulk mass}} \frac{\text{bulk mass}}{\text{area-time}} \qquad \textbf{(4.31a)}$$

or

$$j_{R,k} = \frac{1}{\frac{\pi \rho d_k^3}{6}} f_k \frac{\text{bulk mass}}{\text{area-time}} = \frac{n_k}{\rho (1 - \Phi)} \frac{\text{bulk mass}}{\text{area-time}}. \qquad \textbf{(4.31b)}$$

Inventories of bed particle mass and number are maintained over time during the simulation. Thus, initial conditions establish the maximum potential bed erosion. This limitation to active or interfacial bed interaction alone would be inadequate for certain hydrological events such as prolonged and extreme bed shear.

The horizontal boundary conditions on the water column are standard. The upstream boundary condition is a simple Dirichlet condition, *i.e.*, the concentration is constant over a given time step. For this application, that boundary concentration is the tributary inflow concentration. Although this BC is necessarily constant over the computational time step, it can vary with time. In the unsteady storm simulations discussed in Section 6.4, the upstream BC is ramped up and down over the course of the storm.

The downstream boundary condition is a homogeneous Neumann (derivative) condition stating that dispersive flux across the boundary is zero,

$$E_x \frac{\partial n_k}{\partial x} = 0 . \qquad (4.32)$$

Given the zero gradient, the boundary node is specified in terms of the upstream node. Horizontal transport out of the system is thus limited to advection only. To estimate the curvature at the downstream boundary with a finite difference approximation, a derived value for the imaginary node beyond the physical domain is used, as with the curvature at the air-water interface.

Although it is not discussed in detail here, consistency requires that most of the boundary-specific BCs extend away from the boundaries and into the computational domain. This condition is due to the fact that the 4-point Leonard's method stencil 'reaches' backward and forward to the boundaries and imaginary nodes. The net result is that, for the relatively small number of computational meshes used in this research, almost all of the nodes have unique algorithms expressing concentration at the next time level as a function of neighboring and boundary nodes. Only the innermost part of the domain actually uses the same algorithm, as unaffected by boundary influences.

4.2.3 Solution method

The solution method is largely dictated by the choice of discretizations chosen to approximate the transport equation (4.14). Particle number concentration for any size and space combination at the next time step is expressed explicitly as a function of neighboring concentrations at the current time step. The technique is a direct solution since all derivative approximations are explicit in time. Solution of the set of transport equations (4.14), one equation for each particle size at each grid point, is accomplished by marching forward in time from the set of initial conditions. For several reasons, the derived finite difference equations are long, complicated, and

many: two-dimensional geometry, the use of Leonard's method, multiple size-dependent boundary conditions, and the numerous terms added to accommodate cross-derivatives for bidirectional flow.

The advantage of the explicit method is the relative simplicity of its direct solution. Because of this particular application, *i.e.*, an advection-dominated (sometimes), two-dimensional system with unusual boundary conditions, simplicity of solution was the deciding factor in selecting the explicit technique. The disadvantage of the explicit method is that restrictive time step limits are necessary for computational stability. Certain multi-dimensional, implicit methods can overcome the time step limitation; however, even efficient splitting methods such as A.D.I. (alternating direction-implicit) can have their inherent stability advantage offset by the need for iterative solution of the linear system of equations. Also, time splitting requires a much more complex discretization (two separate sets of FD equations, each in a different direction and at a different time level, with different sets of boundary conditions) and simultaneous system solution technique.

In this research, a uniform Cartesian grid, shown in Figure 4.2, was used to model the structure of the system. For future model application to real systems with highly variable depth, there is a need to characterize depth variations. Although this research does not accommodate depth variations, there are two methods which enable more realistic finite difference models of varying morphometry (*e.g.*, depth). The first and more traditional technique uses constant, fixed-size, vertical grids as in Figure 4.2, but staggers them in discontinuous steps to approximate depth variations as a function of longitudinal distance. Boundary region finite difference equations for transport must be tailored to specific system geometry, and more care must be

exercised that local velocities satisfy the continuity equation. As has been noted (Sheng, 1986a), the general flow field may be well-represented using this approach, but there is usually insufficient resolution in the near-shore region. More important, distortion of the bed geometry results in misrepresentation of the the near-bed velocities and shear stress needed for sediment transport prediction.

A second technique, the fitting of nonorthogonal grids from prototype system dimensions to Cartesian model coordinates, is available. The basic approach used to transform prototype equations and dimensions to the vertically-stretched, rectangular grid system has been outlined (Sheng, 1986b). This method is more general, more easily extended to complex geometries, and more promising for future research.

4.3 PARTICLE-PARTICLE REACTION MODEL

The approach taken in this research numerically decouples the advection-dispersion-reaction process, stated in equation (4.3), into independent though simultaneous transport and reaction steps. This decoupling approach is strictly valid only for linear processes. Flocculation is not a linear process; however, the use of relatively short reaction time steps can satisfy the quasi-linear assumption needed to superimpose, with acceptable accuracy, the independent integrals of the reaction and transport differentials. For the kinetics typical of natural system coagulation, relative concentration changes due to transport dominate in the determination of numerical integration time steps, and the time steps taken for reaction are thus sufficiently short to assume accurate superposition.

4.3.1 Equations

The reaction term $R(n_k)$ in the advection-dispersion-reaction equation (4.2) expresses the kinetics of the coagulation reaction. These kinetics are described in the

model by the well-known Smoluchowski equation, expressing the Lagrangian rate of change in particle number concentration. The rate is a function of the particle size, concentration, and density, as well as the fluid physiochemical properties. In discrete form, the time rate of change in particle concentration, introduced in Chapter 2, is

$$R(n_k) = \frac{1}{2}\alpha_{chem} \sum_{i+j=k} \beta(i,j)\, n_i\, n_j \; - \; \alpha_{chem}\, n_k \sum_{i=1}^{c} \beta(i,k)\, n_i \,. \qquad \textbf{(2.1)}$$

In the reaction rate equation (2.1), the dependent variable n_k is the particle number concentration.

4.3.2 Initial conditions

The initial conditions for the reaction are the known or assumed number concentration distributions existing at each discrete point in the ambient receiving system. The reaction rate is not an explicit function of location but of particle number concentration, temperature, and system dependent solid/solution parameters affecting α_{chem} and $\beta(i,j)$. Integration of the reaction rate equation (2.1) projects a new concentration from an 'initial' condition at each location. Each set of 'final' concentration distributions thus becomes the initial condition for the next time step.

For the decoupled transport-reaction system, the initial conditions for the transport and reaction processes are identical. First, transport is allowed to proceed over a defined time interval (one time step). Coagulation then proceeds from the same initial conditions used for transport. The concentration changes due to flocculation are then added to the final concentrations from the transport step for a total net change.

4.3.3 Assumptions and limitations

Smoluchowski's coagulation equation in its discrete form (2.1) is merely a statement of mass conservation, albeit with a lot of physics implied in the

mechanisms, rate parameters, and methods of quantization. The discretization and solution of the equation require simplifications, however, which vary in degree of justifiability. In this section, the assumptions used are identified, and their degree of uncertainty is estimated.

The foundational assumption in this model is that all particles can be adequately represented (geometrically, kinematically, and dynamically) as spheres of constant density. For example, binary coalescence of primary spheres to form spherical flocs (rather than multiple-body collisions and/or formation of non-spherical, variable density aggregates) is assumed. These assumptions are idealizations required by the present state of knowledge in fluid mechanics, that is, multiple-body hydrodynamic interactions have been solved completely only for the two-spherical body case. Single body kinematics for more complex particle shapes are known, but the results are applicable in neither flocculent nor non-dilute suspensions. The limitation in this case is that experimental observations must be made in terms of equivalent spherical properties, and that system behavior can be described using those observations. This has been possible, with calibration, for certain engineered systems (Lawler and Wilkes, 1984), and suspensions of natural particles are also expected to respond to this treatment.

In conjunction with the sphericity/density assumptions, size discretization assumptions are necessary for computational reasons. Particle size classes, finite in number, are equally spaced on a logarithmic diameter scale to approximate the continuous distribution of particle properties. Because of constant density, coalescence of particles of size i and j to form a particle of size k results in a floc of volume that conserves mass but usually lies somewhere between the discrete sizes of

the model. A technique for apportioning the volume of resultant floc k into integral size classes, and the problems it solves, have been described well (Lawler *et al.*, 1980). Finite discretization is only a limitation if too gross (*e.g.*, poor representation of a class property by the midpoint size) or too fine (*e.g.*, computationally difficult or inefficient); the log-linear floc volume apportionment devised by Lawler should only create problems for gross discretization.

The number of solids size classes can be varied depending upon the particle size distributions of inflow and receiving system water/bed, as well as computational considerations. A first-order uncertainty analysis was performed using a power law number distribution of the form

$$n(d_p) = A\, d_p^{-\beta} \qquad \textbf{(4.33)}$$

with a variable exponent β. For β increasing in a log-linear fashion from a value of 0 at $d_p = 0.6$ μm to a value of 5 at $d_p = 100$ μm, 20 size classes are sufficient to represent the distribution with minimal error (< 0.1 %) in describing the function $n(d_p)$. The desired lower and upper diameter limits for this research were 0.6 μm and 200 μm. For these limits and a log diameter increment of 0.1, *i.e.*,

$$\log\left[\frac{d_{k+1}}{d_k}\right] = 0.1, \qquad \textbf{(4.34)}$$

26 initial size classes would be needed. Two smaller size classes, for number distribution closure, were appended. Three larger size classes, for negligible growth control of the particle size distribution, were also appended. A total of 31 discrete size classes, $0.4 < d_p < 400$ μm, were thus used. Errors in the estimation of actual coagulation kinetics stemming from the use of large particle size increments is another issue which must be answered by experience and actual data.

4.3.4 Solution method

The advection-dispersion-reaction equation (4.2) was decoupled and solved in separate transport (4.3) and reaction (2.1) steps.

The particle interaction model is based on an existing model for simulating changes in the particle size distribution during flocculation and sedimentation processes. Solution of the discrete Smoluchowski equation (2.1) is based on logic originally developed by Lawler (1980). Significant hydrodynamic modifications to the original collision frequency functions were made, as described in Section 2.3.1 (Han, 1989). The explicit derivatives for each size class are calculated directly from the rate equation (2.1). The number concentration derivatives are integrated over time using a modified (predictor-corrector) Euler method. The method is $\mathcal{O}(\Delta t^2)$ accurate in time, compared to the Euler method which is $\mathcal{O}(\Delta t)$. Lawler (1980) originally integrated the set of ordinary differential equations in a thickening model by using Gear's method for stiff systems. The system is certainly stiff, but Lawler (personal communication) later found that simple Euler integration gave comparable accuracy with much faster execution, at least for dilute suspension flocculation modeling. Predictor-corrector methods have been largely supplanted by other methods, except in the unusual case where "high precision solution of very smooth equations with very complicated right-hand-sides" is necessary (Press, Flannery, Teukolsky, and Vetterling, 1986).

4.4 PROGRAM OVERVIEW

4.4.1 Code description

The program listing is presented in Appendix E, but a short narrative is given in this section. The overall computational control, particle transport routines, and I/O

functions were written in Fortran. The coagulation routines were written in C and called by the Fortran routine. These coagulation routines came from a self-contained coagulation-sedimentation model (Han, 1989); sedimentation and other nonessential functions were stripped from the code; argument lists and array subscripting were modified to communicate between the Fortran and C routines. Since most of the subroutines are commented within their respective listings, the focus here is that of an overview.

- MAIN.FOR

  This routine opens input and output files, initializes arrays and variables, and calls the subroutines and functions as needed. MAIN allocates all dynamic storage needed by the Fortran and C codes.

IN() Input data are read and echoed by this subroutine.

PARTCL() Based upon the input data, particle properties are assigned by this subroutine.

CONCIC() Initial conditions for particle number concentrations are calculated by this subroutine.

- FRCGAM()

  This C function is called as a subroutine by the Fortran main only at time zero. Arrays containing derivative indexing bounds and collision frequency factors are returned for later use by the COAG() subroutine.

  The frcgam.c function serves as a controller in that it calls other C subfunctions, described below, that make the array assignments. These functions were excerpted from Han's (1989) model, SEDMOD.C, for flocculent sedimentation of dilute suspensions. FRCGAM() shares dynamic memory for arrays in common with the Fortran main. FRCGAM() also opens and closes its own output files.

fraccalc() This C subfunction calculates the arrays used to discretize the volumes obtained in particle coagulation. Lawler (1980) developed and described the logic to make the fundamental calculation, and Han (1989) generalized the logic to accommodate arbitrary log volume step size for the particle size distribution.

gammacalc() This C subfunction calculates either rectilinear or curvilinear collision frequency functions for interparticle transport by Brownian motion, fluid shear, and differential sedimentation. A curvilinear collision frequency function is the product of both the rectilinear collision frequency function and a hydrodynamic correction factor.

FLOWI() Initial fluid velocities and dispersion coefficients are assigned by this subroutine.

STABLE() The time step used to achieve numerical stability is calculated by this subroutine, based upon transport conditions and grid size.

RAMPQN() New flows and particle number concentrations are calculated for tributaries, as needed, by this subroutine.

BCN() Boundary conditions for upstream tributary particle number concentrations are calculated, as needed, by this subroutine.

SOURCE() Source terms due to tributary particle loading are calculated, as needed, by this subroutine.

ERODE() Gross potential mass flux of solids from the bed is calculated by this subroutine.

BEDXCH() Net mass flux of solids from the bed to water column is calculated by this subroutine.

TRANSP() Size-dependent advection and dispersion of particles by fluid flow and gravitational settling are calculated (without reaction) by this subroutine.

- COAG()

  This C function is called as a subroutine by the Fortran main. Smoluchowski's equation (2.1) is integrated over the time step just used in transport; initial conditions are those concentrations, that existed at the start of the last transport step. The array returned is the matrix of concentration changes due to coagulation alone.

  The coag.c function serves as a controller in that it monitors time and calls other C functions, described below, which perform the integration. COAG() shares dynamic memory for arrays in common with the Fortran main. COAG() also opens and closes its own output files.

euler_pcm() For a given integration step size received from COAG(), this subfunction controls the integration of the reaction term (2.1).

diffun() The reaction rate at any time is calculated on the basis of particle concentrations and system parameters.

TOTAL() Computations are made to convert number concentration results to other forms.

OUTPT() Select results at requested times are written to output files.

4.4.2 Development and application environments

The model codes were developed, tested, and used in several operating and computing environments. The primary computational platform was the Cray Research X-MP EA/14 se, located at the Center for High Performance Computing, University of Texas at Austin. The Cray X-MP is a vectorized, single processor machine, and used the UNICOS 5.1 operating system. The front-end computer for the Cray was the Digital Equipment Corporation VAX-8600, with VMS 5.3 operating system. Cray's standard vectorizing compilers, the CFT-77 Fortran compiler and the SCC C

compiler, created separate object codes which were subsequently linked by a segment loader.

The majority of subroutine development was performed on an Apple Computer Macintosh Plus using DCM Data Product's Mactran Plus Fortran compiler.

4.4.3 Considerations in linking Fortran and C

Fortran and C have different array storage conventions, regardless of the operating environment. These considerations and the manner in which they were addressed are described in this section.

The names of C subroutines called by the Fortran program, as well as the names of the arguments shared between them, must all be capitalized to be consistent with the Cray, Inc. Fortran (CFT) implementation. This is because all variables and arrays passed between the object codes reside in shared memory. All that is actually "passed" from one to the other is the pointer address for the first element of the shared variable or array in memory. Shared array dimension sizes in C should be made the same as those initially declared in Fortran.

For the purpose of linking object codes written in Fortran and C, array storage is the primary difference between the two languages for this implementation. Fortran uses column major storage and C uses row major storage. Passing vector arguments between the languages presents no problem; however, a conflict exists when passing multidimensional matrix arguments. The simple solution is to reverse subscripts when passing the arguments. For example, general array A(i,j,k) in Fortran should be dimensioned and addressed as array A(k,j,i) in C.

Subscript addressing is another difference between the two languages. The default initial address of a vector (or matrix) is element 1 in Fortran but element 0 in

C. User-defined subscript definition of arrays is available in Fortran but not in C. Again, the simple solution is to recognize this and index matrix operations accordingly. As a simple example, a vector dimensioned for NK elements in Fortran which has been passed to a C subroutine cannot be dimensioned in C for NK elements and then addressed for elements 1 to NK. The C routine has allocated NK words of memory, but the pointer subscripts are from 0 to NK-1. This situation arose in both of the C subroutines in this research.

For complex index algebra or where index value has a tangible physical meaning, both true for these codes, it can be preferable to index the elements from 1 rather than 0. In this case, the array must first be dimensioned for NK+1 in both routines. Second, the array must have all elements shifted up one when entering the C subroutine from the Fortran main. Third, the array must have all elements shifted back down one element before leaving the C routine and returning to the Fortran main. Rewriting the indexing within the C algorithms would be an obvious advantage where the double reassignments at each subroutine call become too time consuming. Han's coding, with algorithms to allow variable $\Delta(\log d_p)$, is quite complex, and it was left in its untransformed, original state.

Character strings are much more difficult to transfer between linked subroutines in the two languages than are numeric values, but this was not required in this model.

CHAPTER V

PARTICLE BEHAVIOR IN IDEALIZED SYSTEMS

5.1 INTRODUCTION

This research was conducted to examine the importance of coagulation in particle and contaminant transport and fate. In conjunction with this aim, identification of those transport and chemistry conditions which call for the explicit modeling of particle coagulation was desired. Parametric modeling studies were conducted numerically, using the model developed in the first phase of the research, to discern these conditions.

Particle transport and transformation simulations of idealized systems were conducted, and the results are presented and discussed in this chapter. As discussed more fully in Chapter 3, the prototype under consideration is Town Lake, Austin, Texas. The choice of specific values for each parameter in the model is presented first. A base case analysis of an idealized Town Lake is then presented and discussed. This base case is reflective of the actual system, but the geometry has been simplified to facilitate analysis. A more realistic model application to Town Lake is presented in Chapter 6. The analysis of the base case is presented in two section, one focused on integral measures of particle concentration, and the other on discrete particle size distributions. With the base case established as a reference point, the second half of this chapter focuses on process comparisons and parameter sensitivity analyses.

Variations in system conditions were simulated and analyzed to determine characteristic particle behavior and interaction in response to alternate system conditions. First, individual physical processes were numerically turned on and off in the simulations to examine the relative importance of transport, sedimentation,

resuspension, and coagulation in the fate of particles. Following the process analyses, physical system and particle parameters were systematically varied to examine their effects on particle behavior. Realistic, *i.e.*, naturally occurring, parameter values were chosen to represent a range of natural systems, responses, and limiting conditions.

5.1.1 Conceptual approach

Natural system behavior is the complex response to the spectra of highly variable forcing functions and parameters: hydrology, meteorology, chemistry, biology, and morphometry. For static, idealized systems with simple properties and limited linear processes, it is possible to obtain transfer functions using systems analysis techniques. For dynamic natural systems, however, only the grossest scale behavior can be analyzed in this fashion.

The scaling concept arose from the study of dimensional analysis. The original purpose, still valid, was to reduce the number of conditions and parameters to be varied independently in laboratory experiments. The scaling approach is also used where exact or numerical solutions for a particular system are not possible. In fluid mechanics, for instance, very few systems exist where exact solution of the equations of motion is possible. By comparing the magnitudes of characteristic time or length properties (or their normalized counterparts) for each component of the process, both significant and insignificant aspects of the problem can be identified. Ignoring less important processes may result in approximation of the real system with a simplified, but realistic and solvable problem statement.

While engineers have always sought ways to simplify complex problems to achieve valid solutions of acceptable accuracy, the formal use of the scaling concept in mathematical water quality modeling is rather recent. Boyce (1974) and others (*e.g.*,

Imboden and Lerman, 1978; Imboden and Schwarzenbach, 1985) have illustrated the application of scaling in determining model time and length scales. The systematic use of scaling to evaluate the relative importance of different transport and reaction mechanisms aids in identifying those processes to retain or eliminate. The scale concept was used in this research to aid in identifying parameter ranges for sensitivity analysis and to aid in the identification of dominant and negligible processes.

The responses of the simulation state variable, discrete particle number concentration, and its associated distributions were examined with two basic approaches. Integral analysis was used first, and discrete analysis was then used.

The integral approach was used first to grasp an understanding of system response over the entire particle size range. Derived response variables thus included total number, area, and volume concentrations. Integral particle mass concentrations serve in place of integral particle volume concentrations throughout most of the results presentations of Chapters 5 and 6. Given the (assumed) size-independent floc density, the integral mass concentration can be used interchangeable in place of the integral volume concentration when considering the results. The greater intuitive appeal of the mass concentration and its importance in contemporary water quality modeling and assessment both argue for the use of suspended solids concentration as the default reference for particle volume/mass. It must be clearly understood, however, that particle volume served as the conservative property in the transformation framework, and that discrete number concentrations served as the conservative property in the transport framework.

Discrete analysis, the second approach, is designed to understand the system response within individual and relative particle size classes. Variables thus include

discrete number concentrations n(k) [#/cm^3], as well as derived particle distributions. Normalized particle number, area, and volume (or mass) distributions, as well as the particle size distribution function, are presented and discussed.

5.2 IDEAL SYSTEM CONDITIONS

Ideal systems are the topic of this chapter. As mentioned above, Town Lake is the prototype. Base case simulation parameters reflect the best estimate of average conditions present in Town Lake, notwithstanding the inherent idealizations described below. Parameters used in the process and parameter sensitivity studies use the same basic system, with controlled changes reflective of natural variations in other systems.

Temporal variations in loads and kinetic parameters were ignored in the base case. Thus, the simulation was propagated from initial conditions, under steady (annual-average) forcing, until a steady-state water column response to the boundary conditions and operative physics was achieved. Spatial irregularity was simplified by assuming a rectangular parallelepiped morphometry, *i.e.*, the lake was assumed to have constant depth and width. The rigid lid model dictates a constant system volume. Also, it was assumed that lateral tributary inflows along the length of the reservoir contribute negligible fluid and particle loads. These rectangular and tributary restrictions were relaxed in the application to the prototype, presented in Chapter 6.

System properties to be examined in the idealized transport and coagulation behavior studies include the fluid transport system (advection, system dimensions, residence times, and dispersion and turbulence), the particle characteristics, bed resuspension, and the solution chemistry.

5.2.1 Fluid transport system

Characteristic fluid transport and system morphometric parameters were varied to examine their influence on particle transport and fate. Properties included the receiving system dimensions, fluid velocities and dispersivities, and resulting residence times.

Receiving water systems considered in this research include rivers, reservoirs, and lakes. Typical vertical dimensions are in the order of 1 to 100 meters for small, shallow systems to very large, deep lakes (Boyce, 1974; Imboden and Schwarzenbach, 1985). Typical horizontal dimensions are in the range 0.1 to 100 km for small reservoirs to very large lakes.The prototypical base case system has the following mean dimensions: depth of 4.1 m, longitudinal length of 9.6 km, and transverse width of 164 m.

As pointed out by Holley (1969) and Boyce (1974), the distinction between advective and dispersive flux is arbitrary at all length scales except the molecular. Advection, then, can be thought of as the transport providing larger scale motion, whereas dispersion provides the small scale, residual mixing which is superimposed on the advection. Obviously the time scale is inversely related to the space scale. For larger dimensions of interest, *e.g.*, the length or width of a lake basin or the length of a river, advection normally dominates contaminant transport (Imboden and Schwarzenbach, 1985).

The range of magnitudes for surface water advective velocities is quite large. Lerman (1979) estimates the fluid velocity range in the order of 1 to 100 cm/s for all types of surface water systems. For large lakes such as the Great Lakes, Boyce (1974) characterizes basin-wide and coastal horizontal currents on the order of 10 cm/s. Boyce also estimated the localized vertical fluid velocities due to upwelling, downwelling, and

Langmuir circulation to be on the order of 1 cm/s. Though the model's transport framework can accommodate a prescribed vertical velocity field, vertical fluid flux is not included in these analyses.

A vertical distribution of longitudinal velocity was prescribed for the idealized and actual system shear flows incorporated in the model for the systems of Chapters 5 and 6. The logarithmic velocity profiles were defined by sectional parameters of mean longitudinal velocity, depth, and friction factor. The prototypical base case system has a mean longitudinal velocity of 6.54 cm/s and a Darcy-Weisbach bed friction factor of 0.02. Town Lake's mean Reynolds number of 2.7×10^5 based on depth, coupled with the chosen friction factor, imply a flow in the transitional region between hydraulically smooth and fully rough (for turbulent, uniform, open-channel flow).

System fluid residence times are determined by their characteristic length and velocity scales. Typical whole lake water residence times are on the order of 10^1 to 10^4 days (Imboden and Schwarzenbach, 1985). Many small reservoirs (Brune, 1953) and rivers can have characteristic residence times (*i.e.*, characteristic length/advective velocity) of a day or less. The prototype system residence time was 1.7 d.

It was mentioned above that the division between dispersion and advection is arbitrary, defined by the ability to resolve the advective scale. Holley (1969) also discussed the relatively arbitrary distinction between diffusion and dispersion as being solely related to spatial and temporal averaging scales, except at the molecular level.

For large scale simulations, the gradient type dispersion inherent in the model transport equation (3.3) has proven adequate, if not ideal, for horizontal lake mixing (Blumberg, 1986). The dispersion coefficient E_x is then typically in the range of 10^3 to 10^5 cm^2/s. Representations of both longitudinal and lateral components are available,

but further progress requires that improved representations be related to mean flow and turbulence parameters. For vertical lake mixing, Blumberg (1986) and Imberger *et al.* (1987) have suggested, however, that the small time and space scale processes responsible for vertical mixing in open waters cannot be parameterized by the empirical eddy viscosity concept. When used, the vertical dispersion coefficient E_z is typically in the range of 10^{-1} to 10^3 cm^2/s (Imboden and Schwarzenbach, 1985). Three-, two-, and one- dimensional mixing analyses for smaller scale (in the vertical) rivers were examined theoretically and experimentally by Holley and Jirka (1986). Dispersion coefficients presented for riverine mixing were dependent on river velocity, depth, width, and roughness. In contrast to lake dispersion, rather satisfactory parameterizations of vertical and transverse riverine mixing are available. Despite its name, Town Lake has many riverine characteristics. Default dispersion coefficients used for the prototype system were 10^3 cm^2/s for longitudinal mixing and 8.9 cm^2/s for vertical mixing.

Energy dissipation is an important measure of fluid turbulence, reflecting both passive particle and contaminant dispersion as well as dynamic interparticle collision contacts by fluid shear. Values of energy dissipation can be expressed in several alternate forms, but the most useful for this work is the mean velocity gradient, G. The range of G in natural systems is typically 0.01 to 10 s^{-1} (Lerman, 1979; Sheng, 1986b; Weilenmann *et al.*, 1989) for deep 'stagnant' hypolimnia to coastal areas and open water storm events, respectively. Greater shear takes place in some rivers, *e.g.*, the Rhine's 50 s^{-1} (Hahn *et al.*, 1980). The mean velocity gradient chosen for the prototype system was 10 s^{-1}.

is normally used to relate shear stress at the bed to the fluid velocity at the turbulent boundary layer, u_B. The dimensionless skin friction factor f_c is typically on the order of 0.004 (Sheng, 1986a).

For vertically averaged flows, where $\overline{u_x}$ is the vertically-averaged horizontal velocity, an alternate quadratic stress law parameterization is often used for geostrophic flows:

$$\tau_0 = C_d \rho \overline{u_x}^2 . \qquad (5.3)$$

The dimensionless drag coefficient C_d is typically on the order of 0.003 to 0.004. The relation between the boundary layer (5.2) and vertically-averaged (5.3) expressions for shear stress is obvious. Stratified flows (of either type) require modification of the basic form to account for the suppressed momentum transport.

Bedford and Abdelrhman (1987) cited average values of 10^{-2} dyne/cm^2 for bed shear stresses in Lake Erie (calm) and the deep ocean and values of 1 dyne/cm^2 for bed shear stresses in Lake Erie (storm) and on the continental shelf. Periodically, shear stresses can be much greater in shallow depths, however. Sheng and Lick (1979) and Sheng (1986b) reported current and wave induced bed shear stresses in Lake Erie shallows and Mississippi Sound shallows of 14 and 15 dyne/cm^2, respectively.

In open channel flow, characteristic of rivers and many reservoirs and estuaries, the turbulent bed shear stress is normally parameterized as

$$\tau_0 = \rho_f u_*^2 , \qquad (5.4)$$

where u_* is the shear velocity or friction velocity. Specification of the shear velocity (and thus the bed shear stress) is based upon the cross-sectionally averaged longitudinal fluid velocity $\overline{u_x}$ and the dimensionless Darcy-Weisbach bed friction factor f:

$$u* = \overline{u_x} \sqrt{\frac{f}{8}} . \qquad (5.5)$$

The mean longitudinal fluid velocity is readily estimated, and the open channel types of flow being examined in this research allow the use of this approach. A typical value for the bed friction factor under a wide range of turbulent flows is 0.02. This value was used for the prototype system. Very high Reynolds numbers or small roughness elements result in smaller friction factors; smaller Reynolds numbers or relatively rough beds result in larger friction factors. The friction factors examined in the parameter sensitivity studies included 0.015 and 0.025, corresponding to hydraulically smooth and fully rough turbulent flows.

Critical shear stress for fine cohesive bed sediments is on the order of 1 dyne/cm^2, with values generally in the range 0.2 to 20 dyne/cm^2 (Sheng, 1986b). Sheng presented experimental erosion results for Mississippi Sound deposits that had a critical shear stress of 0.9 dyne/cm^2. Raggio and Jirka (1988) reported a critical shear stress of 10 dyne/cm^2 (1 Pa) for cohesive sediments taken from the bed of the Buffalo River in Buffalo, New York. A review was provided by (Hayter, 1987) of the experiments conducted to determine cohesive sediment shear strength (and density) as a function of the depth in the bed, the bed shear rate at the time of deposition, the time since deposition, and the solution salinity. Shear strength throughout the depth of flow-deposited kaolinite beds were in the same relative range as for the surface layers, though the magnitude increased with depth. The prototype system's critical shear stress was set at 1 dyne/cm^2.

For the resuspension flux parameterization suggested by (5.1), the rate constant M (g/cm^2-s) can be experimentally determined along with the critical shear stress. (Ariathurai and Arulanandan, 1978) conducted erosion tests of more than 200 samples

of compacted sediments of natural and pure clay. These authors found virtually all values of the rate constant in the range of $5 \times 10^{-5} < M < 5 \times 10^{-4}$ g/cm^2-s.

Instead of normalizing the excess shear stress, as in the parameterization of (5.2), the flux can be expressed equivalently as

$$J_r = M' (\tau_0 - \tau_c) . \qquad (5.6)$$

The modified rate constant M' is obtained by dividing the original rate constant by the critical shear stress, *i.e.*, $M' = M/\tau_c$. The rate constant M' is on the order of 1×10^{-6} to 2×10^{-5} s/cm (Sheng, 1986b). In accord with the large critical shear stress cited above for the Buffalo River bed, Raggio and Jirka (1988) reported a small rate constant (determined by model calibration) of only 5×10^{-7} s/cm. The rate constant M' used for the prototype system was 1×10^{-6} s/cm . Values of 0.0, 1.0×10^{-7}, and 1.0×10^{-5} s/cm were examined in parametric studies.

5.3 BASE CASE: INTEGRAL SOLID PHASE BEHAVIOR

The base case idealizations were made to better isolate the influences of individual processes on particle behavior. Temporal variations in loads and kinetic parameters were ignored in the base case. Thus, the simulation was propagated from initial conditions, under steady (annual-average) forcing, until a steady-state water column response to the boundary conditions and operative physics was achieved. Spatial irregularity was simplified by assuming a 3-dimensional rectangular morphometry, *i.e.*, the lake was assumed to have constant depth and width. Also, it was assumed that lateral tributary inflows along the length of the reservoir contribute negligible fluid and particle loads. These restrictions were relaxed in the application to the prototype, presented in Chapter 6.

It is useful to begin the base case analysis with an inspection of the integral behavior of the particle distribution because the results clearly show the overall behavior of the solid phase. Total (*i.e.*, summed over the entire size distribution) particle concentrations of mass, number, and superficial surface area are presented in this section. Initial conditions within the water column domain were equivalent to the upstream boundary condition. Results given are steady-state responses for the water column, *i.e.*, at a time of three mean system residence times (evidence is given below to justify this assertion). Changes from the initial condition can be attributed to the parallel processes of advection, dispersion, sedimentation, resuspension, and coagulation.

Because concentrations in the system vary in both longitudinal and vertical directions, a display of the two-dimensional, spatially-distributed concentrations at steady-state is valuable for analyzing the integral results. As an example of the integral contour plots to be discussed in this section, consider Figure 5.1. The isopleths present the steady-state contours of constant total particle number concentration, as a function of longitudinal and vertical location in the water column. Given the 2-D modeling framework, this longitudinal/vertical slice of the water column represents laterally-averaged system response. Contours were constructed by linear or cubic interpolation from the discrete nodal concentrations at the 55 spatial mesh points (11 longitudinal by 5 vertical). This grid, corresponding to the generic grid presented in Figure 4.2, was used for all simulations in the research. The 55 mesh points are also shown in Figure 5.1.

Transport equations were written in dimensional form, but nondimensional distances are used to present the simulation results. The following conventions were used for physical and numerical spatial dimensions. The upstream system boundary, at

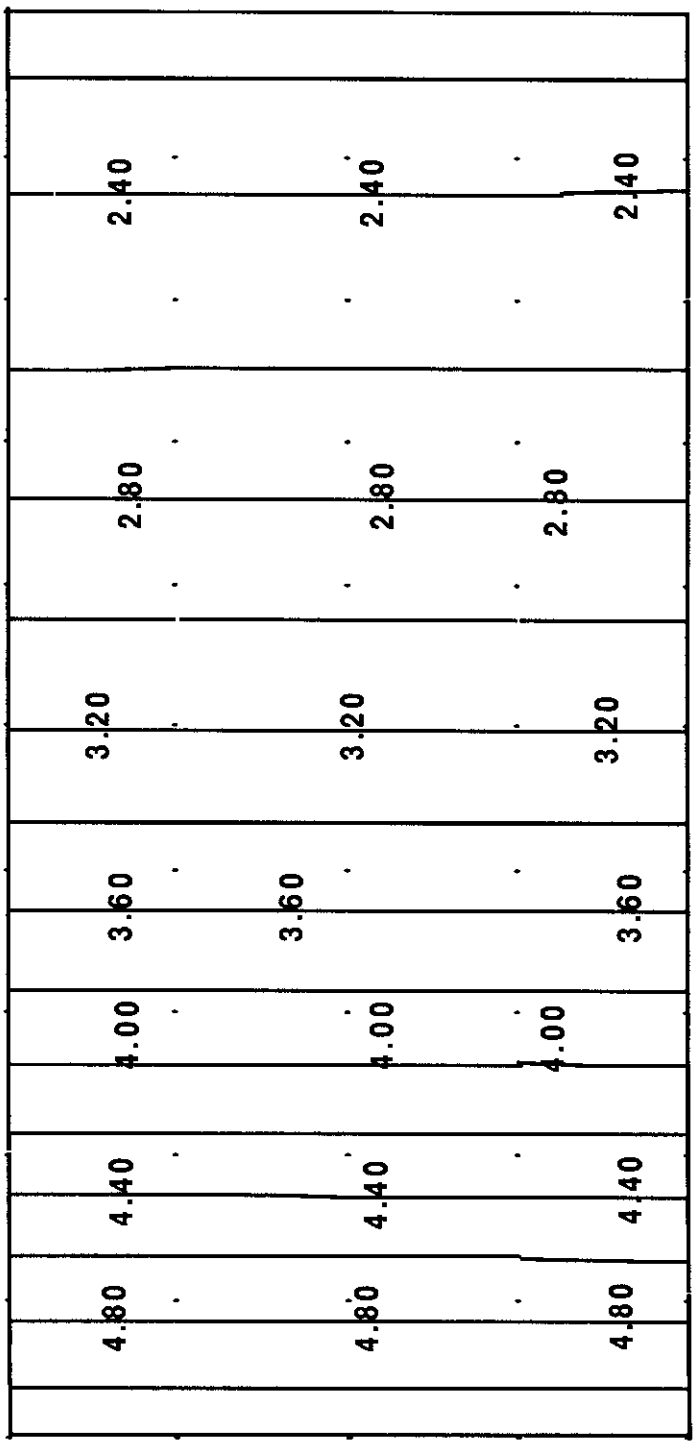

Figure 5.1 Base Case Number Concentration Isopleths at Steady-State. [10^6 /cm^3]

a physical distance x = 0.0 km, corresponds to the left boundary of the computational domain; the corresponding dimensionless longitudinal distance, X, is 0. The dimensionless longitudinal distance is just the fractional downstream distance, X = x/L, where L is the length of the reservoir. The right boundary of the computational domain (X = 1.0) corresponds to the downstream system boundary (x = L = 9.6 km); fluid flow is from left to right.

In the vertical, the air-water interface defines the vertical physical origin, z = 0.0 m. The upper boundary of the computational domain shown in the figure (dimensionless depth Z = 0.0) is the vertical computational origin. The bottom boundary of the computational domain that is revealed represents the deepest water column grid (Z = 0.8, depth z = 3.3 m). Dimensionless depth is just the fractional depth, Z = z/H, where H is the water column depth to the bed-water interface (4.1 m). The bed-water interface (at Z = 1.0) behaves as a separate phase from the water column.

5.3.1 Total number

Total particle number concentration behavior is presented first. Referring again to Figure 5.1, the steady-state response isopleths represented a simulation time of three mean residence times. The initial condition for the domain, as well as the upstream boundary condition for the entire simulation, was a total number concentration N (analogous to N_∞ in Figure 3.6) of 5.14 x 10^6 [particles/cm^3].

One of the more distinctive features of the response for this system was the nearly homogeneous vertical distribution of total number. The system appeared to display 1-dimensional behavior: vertically uniform, with longitudinal variation only. Factors which could cause this uniformity are those which promote vertical mixing. In

this system these included the relatively shallow water column of 4.1 m and the moderately high vertical dispersion coefficient of 8.9 cm^2/s. Recall that the Stokesian particles considered in this research possess the same turbulent mixing coefficient(s) as the fluid itself, *i.e.*, the vertical mixing is size-independent. Size-dependent processes affecting the vertical distribution, *e.g.*, sedimentation and coagulation, did not appear to exert a dominating influence on the vertical number distribution. The characteristic vertical mixing time, $\tau_{dz} = H^2/E_z$, was only 5.2 hr, small relative to the mean lake detention time of 41 hr. Since only the integral behavior is shown in Figure 5.1, it is probable that large numbers of small particles, which can be readily mixed from top to bottom, obscured any vertical stratification of the larger particles.

A second distinctive feature of the total number response was the substantial reduction in total particle number down the length of the reservoir. A continuous decrease in number concentration with distance is clearly evident in Figure 5.1. A plot of number concentration as a function of longitudinal distance, at constant depth (Z = 0.4), is presented in Figure 5.2. Approximately 60% of the total number of particles entering the system was lost from the water column before reaching the outflow boundary of the system.

It should be noted that, for the ideal system of constant flowrate and cross section, *i.e.*, constant velocity, differences in longitudinal distance are synonymous with travel time. This makes the overall kinetics directly apparent from the longitudinal response.

Potential number sinks included coagulation and sedimentation. Either one of the processes could have produced the observed number reduction independently, *i.e.*, without the other. In the absence of mass concentration results, presented further

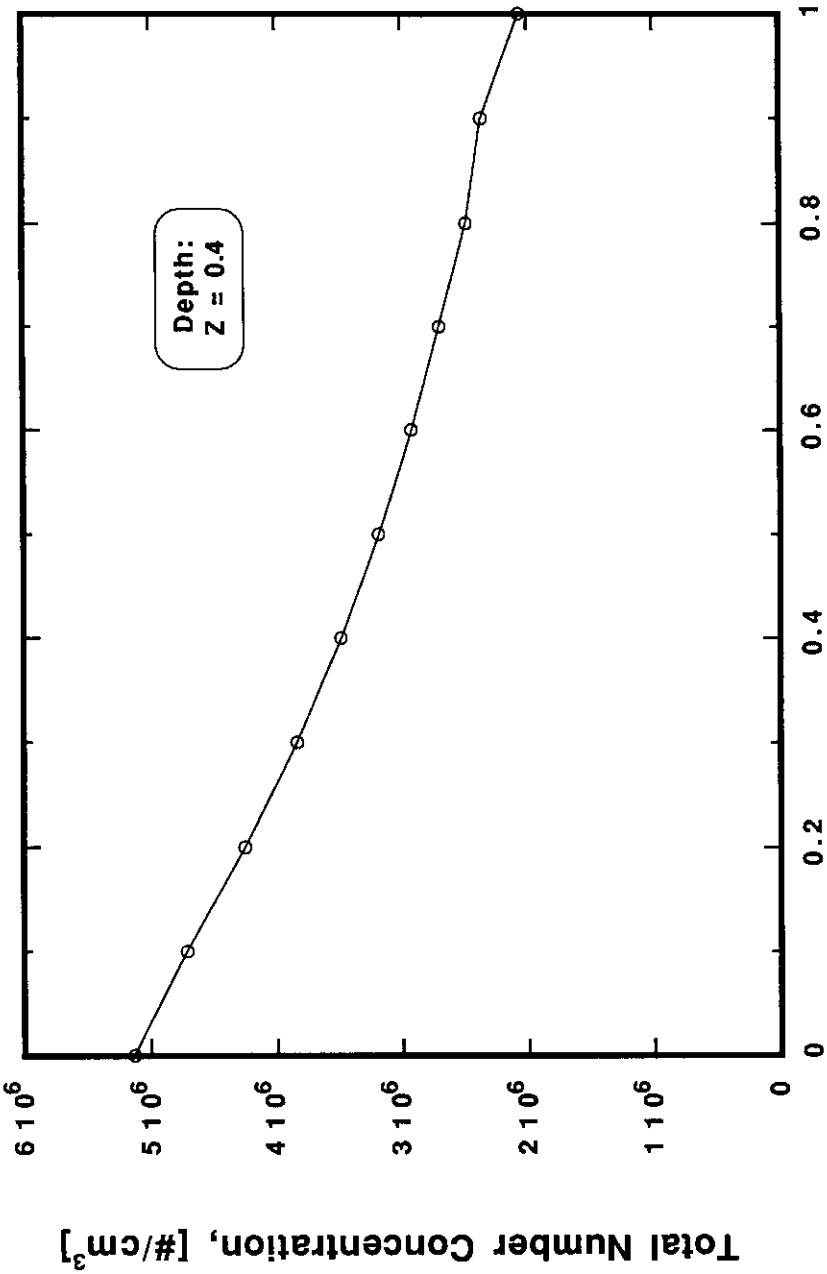

Figure 5.2 Longitudinal Profile of Base Case Number Concentration at Steady-State

below, one cannot determine whether the number decrease was due to coagulation, sedimentation, or a combination.

The kinetics of the changing number concentration can be qualitatively and quantitatively examined using the simulation results. For example, the rate of concentration change was obviously decreasing with time; the concentration isopleths spreading out with distance, seen in Figure 5.1, demonstrate this. The familiar exponential decay curve appearing in Figure 5.2 suggests an overall first-order loss of particle number concentration. Exponential loss is the basis for most water quality modeling of sedimentation and resuspension: a net rate constant (the net sum of all rate constants) applicable to all particle sizes over a vertically mixed water column. The standard variable in water quality modeling is mass concentration, however.

The sudden drop in number concentration at the downstream boundary (X = 1.0) was unexpected. Given the numerically consistent formulation of downstream boundary conditions, the reason for the concentration drop at the boundary is not known. The drop does have a small direct influence (causes some decrease in concentration) at the node upstream of the boundary; much smaller indirect influences are propagated upstream.

The number decay rate can be quantitatively assessed. For simple first-order kinetics, and acknowledging the direct relation between travel time and distance ($x = t/U_x$) in the ideal system, a linearized plot of total number concentration,

$$\ln \frac{N}{N_0} = - k t , \qquad (5.7)$$

would plot as a straight line. Since coagulation dynamics are generally acknowledged to be second-order in particle number concentration, a second-order rate expression for the loss of particle number could also be considered. The linearized response is

$$\frac{1}{N} - \frac{1}{N_0} = k t , \qquad (5.8)$$

where N_0 is the initial total number concentration.

Linear regression plots of both the first-order and second-order decay models were examined, and both fit the results quite well at dimensionless depth Z = 0.4. Excluding the outflow boundary concentrations, both model regressions gave correlation coefficients of 0.998, with insignificant difference between the two models. On the basis of these results, one cannot dismiss the traditional, overall first-order decay model as a means for describing total number concentration response. It would be desirable to use a lumped first-order decay model in place of the full transport/coagulation model, with its complex and expensive reaction kinetics. Unfortunately, the comparison between 1^{st} - and 2^{nd} -order models was only possible because of the mechanistic coagulation modeling. Since there is no *a priori* means of determining the net 1^{st} -order rate coefficient, this modeling analysis could only be used after field study or full coagulation modeling. These potential uses of the 1^{st} -order particle model could be invalidated if other conditions upset the net balance of processes, such as those that appear to be present in the base case. These conditions could include a shift in process dominance towards coagulation, for example, or spatial or temporal inhomogeneities in system parameters of forcing.

Because all of the computational analyses required time-variable evolution to a steady-state, it was important to judge the simulation time needed to reach numerical and physical steady-state response. The total number concentration response after 3 residence times of simulation was compared to the response after 2 residence times of simulation to judge the numerical convergence to a steady-state response.

The comparative simulation began from a uniform initial particle number distribution everywhere throughout the water column domain, with a total concentration of 5.14 x $10^6/cm^3$. The Dirichlet condition at the upstream boundary (X = 0) was maintained at this concentration for the entire duration of the simulation. Number concentrations at the end of simulation for the two cases (two vs. three mean residence times) were identical, to five significant figures; total suspended solids concentration comparisons of the two simulation times had equivalent agreement. The domain approached the steady-state distributions between one and two mean residence times, *i.e.*, significant changes took place between one and two mean residence times, particularly in the downstream end of the system.

The simulation time needed to propagate boundary conditions throughout the domain to achieve steady-state distributions depends not only on boundary conditions, but on transport and kinetic rates within the domain. Recall from above that the characteristic vertical cross-mixing time (fluid transport only) is a short 5 hr. The system considered is highly advective (longitudinally), and the characteristic advection time is one mean residence time: $\tau_{ax} = L_x/U_x$ is 1.7 d or 41 hr. Thus, steady-state boundary conditions can propagate longitudinally in approximately 41 hr and vertically in approximately 5 hr.

To propagate, by transport, the sum of steady horizontal and vertical fluid fluxes through the domain should take approximately 46 hr. total (41 plus 5). This is a little over one residence time, as seen in the simulation results just discussed. The reason for the series-like response rather than a parallel-like response is because the transport is in two different directions, *i.e.*, longitudinally and vertically. Following propagation of a perturbation through one dimension, this new perturbation must be

propagated through the other dimension. In reality, the propagations take place simultaneously, and the time needed to reach an effective (near-) steady-state can be somewhat less than the sum of the independent process time scales.

It is not possible to deduce directly from simulation results the estimates of the individual characteristic times for the source and sink processes and fluxes that influence vertical transport (*i.e.*, coagulation, resuspension, and sedimentation); however, the kinetics of total number reduction give some idea of these time scales.

Although we cannot deduce from the total number results the individual time scales for the heterodisperse suspension in two-dimensional space, it is possible to determine an overall response time. To analyze the characteristic time scale of source and sink processes, assume that coagulation, resuspension, and sedimentation can be represented by independent (*i.e.*, parallel) rate expressions which are each first-order in total number concentration. Then an overall rate expression is the sum of the linearly additive first-order expressions, so that an equivalent overall rate coefficient is the sum of the individual first-order rate coefficients. An estimate of the characteristic time $\tau_{s/s}$ for the lumped, first-order, source/sink decay process is

$$\tau_{s/s} = \frac{N}{\left|\frac{\partial N}{\partial t}\right|}, \qquad (5.9)$$

The partial derivative of total number in (5.9) can be estimated from the slope of the linear regression of the first-order expression for longitudinal decay of total number concentration (5.7). Using conditions at the upstream boundary to evaluate the concentration and its derivative, the characteristic time $\tau_{s/s}$ is approximately 1.5 d or 36 hr. This time scale is valid at steady-state at one point in the field.

In general, the characteristic time varies in space because both the concentration and the time derivative of concentration are functions of space. For the case of a first-order process, however, both the concentration and its derivative change at the same rate. Therefore, the characteristic time remains constant throughout the system.

For a system subject to unidirectional parallel processes, such as

$$\begin{aligned} &\overset{k_1}{A \rightarrow B} \\ &\overset{k_2}{A \rightarrow B} \\ &\vdots \end{aligned} \qquad \textbf{(5.10)}$$

the overall rate of decrease of A and increase of B will be at least as fast as the fastest individual process (the largest k_i and smallest characteristic time) will allow. In contrast, for a system subject to bi-directional parallel processes, such as

$$\begin{aligned} &\overset{k_1}{A \rightarrow B} \\ &\overset{k_2}{A \rightarrow B} \\ &\overset{k_3}{A \leftarrow B} \\ &\vdots \end{aligned} \qquad \textbf{(5.11)}$$

it is not true in general that the overall rates of change of A and of B are at least as fast as the fastest individual process allows. It cannot even be said whether the overall conversion is forward, backward, or at equilibrium.

The important conclusion from the preceding discussion concerns scale. Although resuspension acts to increase total number concentration in the water column, coagulation and sedimentation act counter to that effect, and the overall process is one of net number reduction. It can be concluded that, for the ideal system just discussed, coagulation and sedimentation reduce particle number concentration faster than erosion

can add. It is also concluded that a simulation time of two residence times is sufficient to achieve steady-state system response for the typical conditions tested. For the remaining steady-state results in Chapters 5 and 6, the results are presented after two residence times of simulation unless otherwise noted.

5.3.2 Total mass

As mentioned at the beginning of the chapter, particle volume and mass are directly related by particle density and are used interchangeably in this study. The integral mass concentration is commonly referred to as total suspended solids, abbreviated TSS, with conventional units of [mg/L]. In this section the integral particle mass concentration response of the base case simulation is examined.

Steady-state total mass concentration (TSS) isopleths, shown in Figure 5.3, were derived from the number distributions. Simulations began from a uniform initial condition of particle number distribution, throughout the water column domain, which was equivalent to a total particle mass concentration of 9.84 mg/L. This concentration was maintained as a Dirichlet condition at the upstream boundary ($X = 0$).

Compared to the number response illustrated by Figure 5.1, it is obvious that TSS behavior was qualitatively different than total number behavior. Two differences can be seen. First, the spatial variation of TSS response was not uniform in the longitudinal or vertical directions. Second, mass concentration generally increased in the downstream direction, whereas the number concentrations decreased.

The increase in the mass concentrations in the downstream direction is illustrated along a single grid at mid-depth ($Z = 0.4$) in Figure 5.4. The overall increase in suspension concentration was approximately 4% between inflow and outflow. Mass concentration appeared to asymptotically increase down the length of the system,

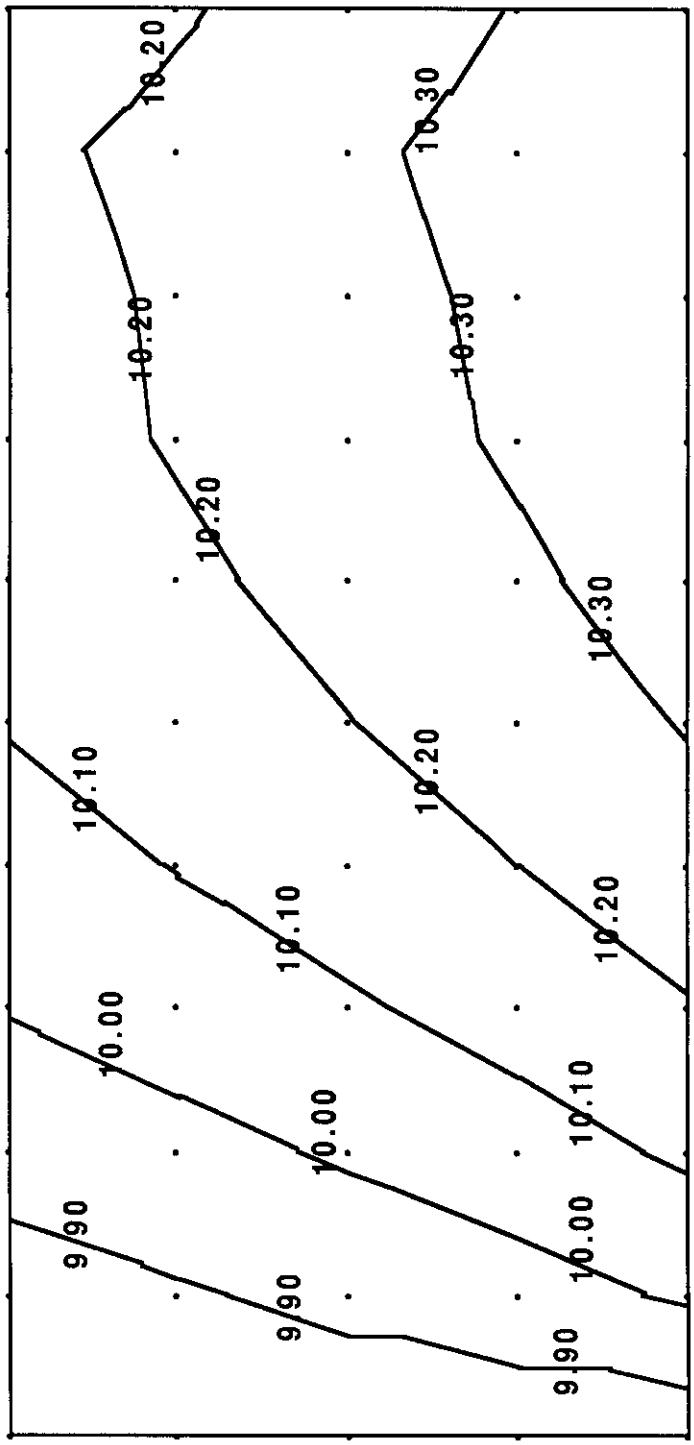

Figure 5.3 Base Case TSS Concentration at Steady-State. [mg/L]

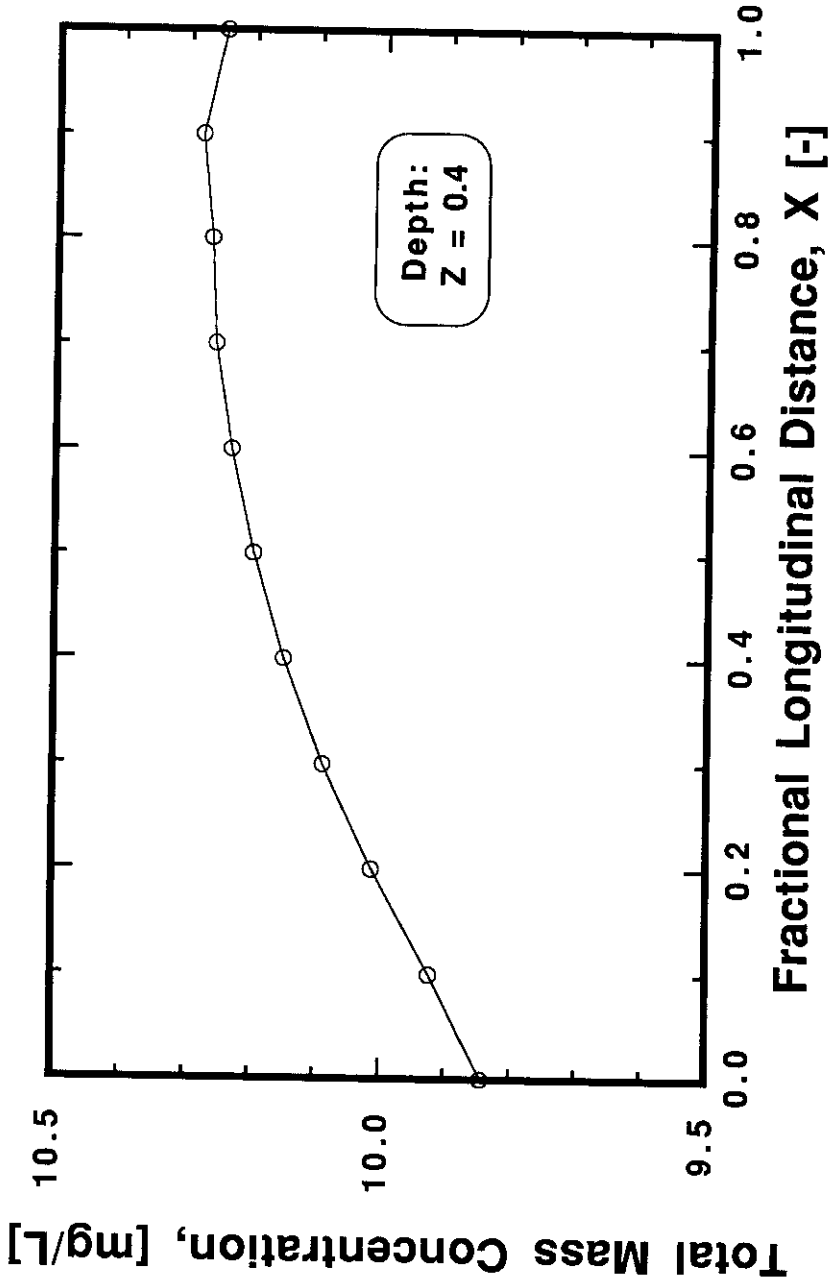

Figure 5.4 Longitudinal Profile of Base Case Mass Concentration at Steady-State

approaching an equilibrium value. The minor concentration decrease near the downstream boundary was caused by the accelerated rate of number concentration decrease at the boundary, as discussed above.

Assume a first-order increase in concentration as suggested in Figure 5.4, increasing from the boundary value at x = 0.0 km to a value approaching equilibrium. At constant depth, we have

$$TSS(x) = TSS(0.0) + [TSS_{equil} - TSS(0.0)]\ [1 - \exp(-k\,x)]\,, \qquad \textbf{(5.12)}$$

where

$TSS(0.0)$ = the boundary concentration

TSS_{equil} = the equilibrium concentration

k = a lumped first-order rate constant .

The exponential increase suggested in Figure 5.4 and equation (5.12) is the response of a one-dimensional system subject to a (longitudinally) distributed source. Linearization of (5.12) results in

$$-\ln\left(1 - \frac{TSS(x) - TSS(0.0)}{TSS_{equil} - TSS(0.0)}\right) = k\,x\,; \qquad \textbf{(5.13)}$$

the simulation results and linear regression line are plotted in Figure 5.5. From Figure 5.4, the magnitude of the apparent equilibrium concentration was estimated to be 10.3 mg/L. Overall, there was reasonable conformance of the assumed one-dimensional (longitudinal) first-order mass concentration increase at a constant depth (5.13) to the observed simulation results.

As with the longitudinal behavior, the two-dimensional steady-state isopleths of mass concentration response revealed interesting and direct contrasts between the vertical number and mass responses; compare Figures 5.1 and 5.3. Unlike the isoconcentration lines of total number, which were vertical, the isoconcentration lines

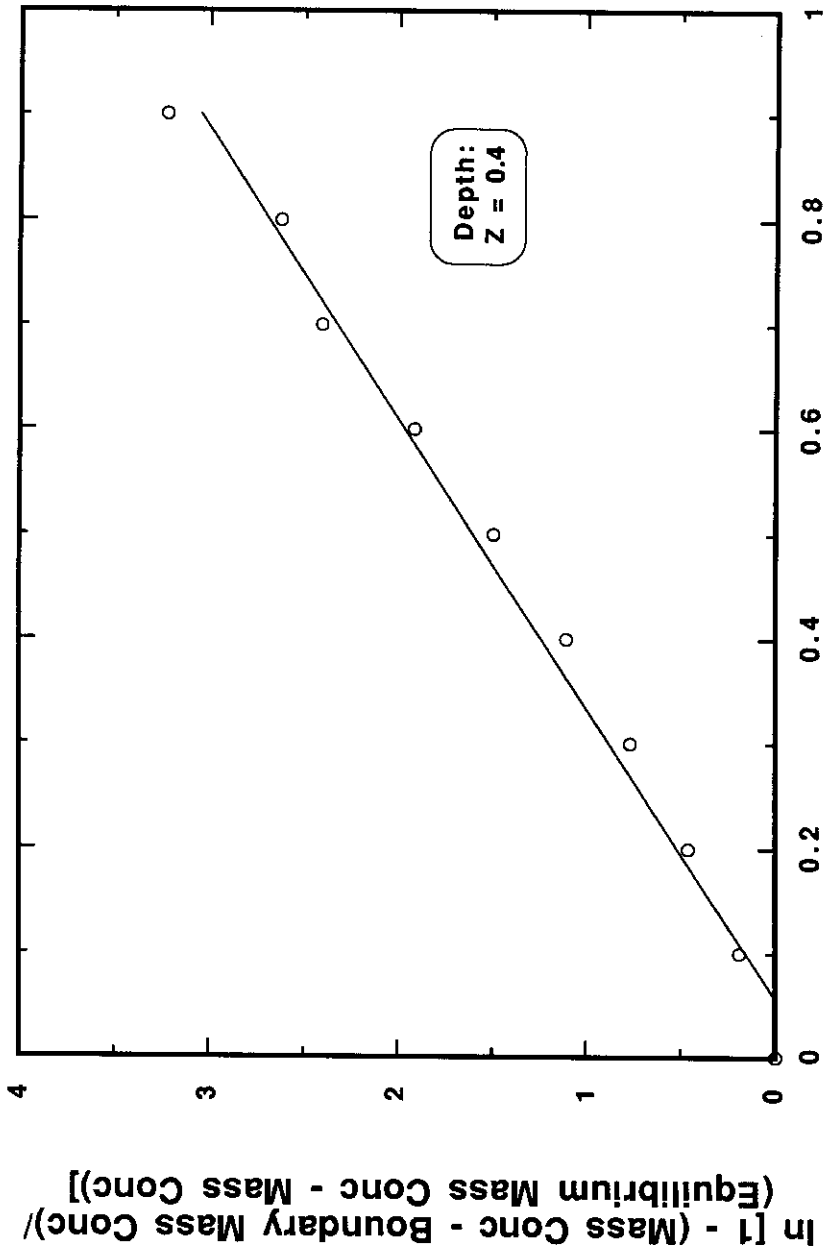

Figure 5.5 Regression of Base Case TSS Concentration against Linear, Lumped Model

of total mass appeared to bend downstream, tracing out a path that appeared to traverse from the bed-water interface to the air-water interface.

At any given longitudinal coordinate of Figure 5.3, the mass concentration decreased from the bed up. To illustrate this, a vertical profile of the mass concentration at mid-lake (X = 0.4) is presented in Figure 5.6. Again, an exponential distribution of mass appeared evident. In steady two-dimensional flow, with homogeneous vertical dispersion (as modeled in this research) and homogeneous particles of uniform (mass-average) settling velocity, the steady-state vertical balance between sedimentation and vertical dispersion is described by equating the two fluxes,

$$\mathrm{TSS}(z)\,\overline{v_{sm}} + E_z \frac{\partial\,\mathrm{TSS}(z)}{\partial z} = 0\,, \qquad \textbf{(5.14)}$$

where $\overline{v_{sm}}$ is the mass-average settling velocity. With a vertical boundary condition of $\mathrm{TSS}(z\,@\,a) = \mathrm{TSS}_a$ near the bed (*i.e.*, at a distance of 'a' above the bed), the solution to (5.14) is (Vanoni, 1975)

$$\left[\frac{\mathrm{TSS}(z)}{\mathrm{TSS}_a}\right] = \exp\left[-\frac{\overline{v_{sm}}}{E_z}\,(z-a)\right]. \qquad \textbf{(5.15)}$$

A linearization of the vertical profile (5.15) is

$$\ln \mathrm{TSS}(z) = \ln \mathrm{TSS}_a + \frac{\overline{v_{sm}}\,a}{E_z} - \left(\frac{\overline{v_{sm}}}{E_z}\right) z\,. \qquad \textbf{(5.16)}$$

A plot of linear regression indicated a reasonable fit of the simulation results to the suggested first-order vertical response.

One cannot infer the two bed boundary condition parameters (location-height and concentration) from the single correlation fitted to the solution (5.16). It is possible to isolate and estimate the coefficient ($-v_s/E_z$) from the regression slope, however. The

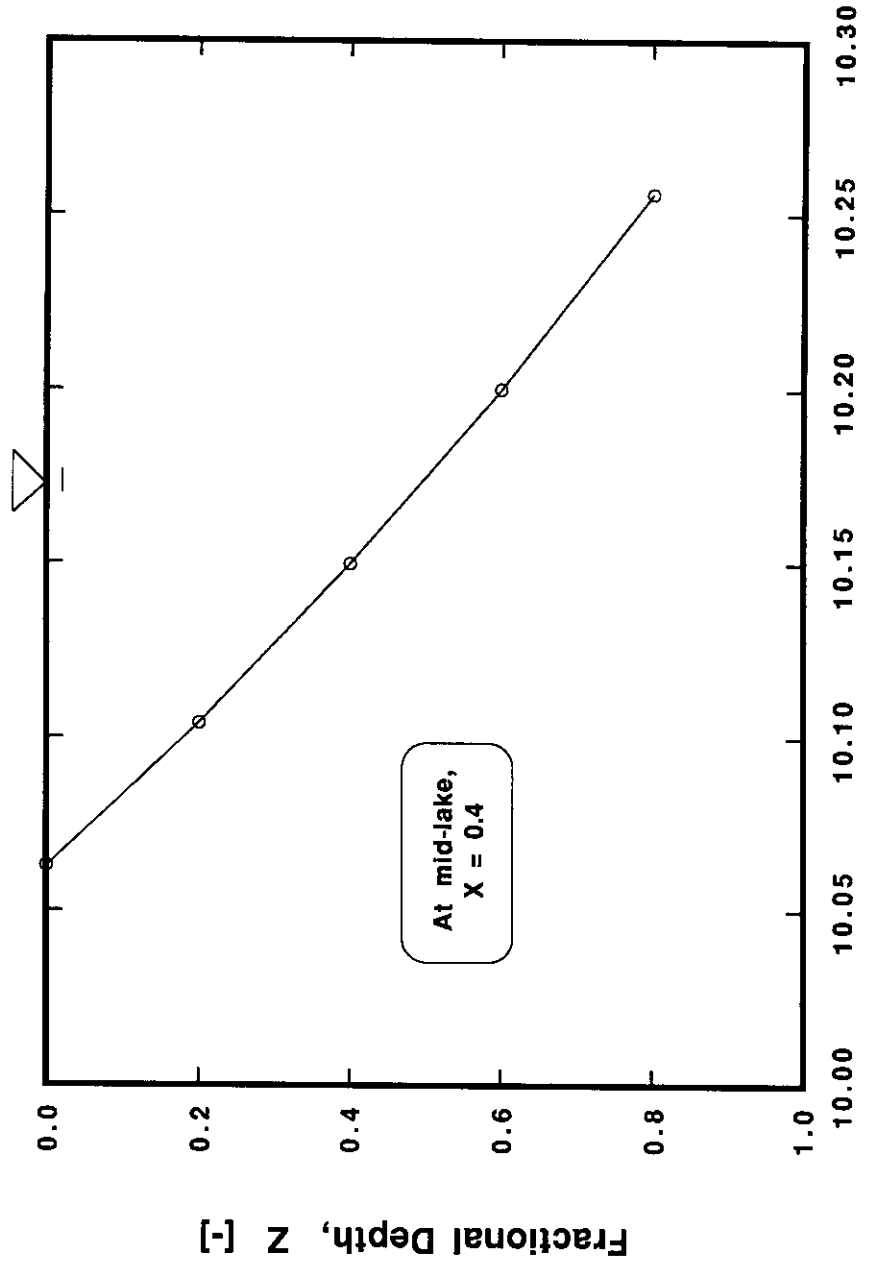

Figure 5.6 Vertical Distribution of Base Case Mass at Steady-State

slope was -5.92×10^{-5} cm^{-1}. The vertical dispersion coefficient for the base case simulation was a constant 8.94 cm^2/s. An estimate of the mass-average settling velocity is the product of the regression slope and the dispersion coefficient, or 5.30×10^{-4} cm/s. The mass-average Stokesian particle diameter from the regression, corresponding to this Stokes velocity, would be 1.24 μm.

Mass-average particle diameters calculated from the simulation output particle size distributions for each depth at X = 0.4 did not, however, agree well with the mass-average diameter estimated from the regression. The mass-average particle diameters from simulation increased from 3.64 μm at the air-water interface (Z = 0.0) to 3.76 μm near the bed-water interface (Z = 0.8), a modest 3.4% increase. These mass-average diameters were much larger than predicted from the regression. (For comparison, the number-average diameters increased from 1.097 μm at the air-water interface to 1.099 μm near the bed-water interface, a minute 0.18% increase.)

Two possible physical explanations for the lack of agreement between mass-average regression and simulation diameters are (a) the vertical distribution was not at equilibrium and (b) the integral behavior of the heterodisperse particles is not accurately describable by a single, lumped, mass-average settling velocity.

Concerning the first explanation, the vertical distribution at mid-lake (X = 0.4) was clearly not at equilibrium. This fact can be seen in the mass concentration isopleths (Figure 5.3), where isoconcentration lines were not yet parallel to the flux boundary (the bed). Nonequilibrium was even more evident in Figure 5.4, where the beginning of the horizontal isoconcentration line at mid-depth (Z = 0.4) was not approached until near the downstream end of the lake (X = 0.9).

The reason for the underestimated mass-average settling velocity from the regression slope is easily explained by referring to the original differential equation for flux (5.14) and to the mass concentration isopleths (Figure 5.3). First, the mathematical sedimentation flux is forced to equal the mathematical dispersive flux by the assumption of the ODE (5.14) and its solution (5.15). When physical dispersion dominates in a nonequilibrium situation, an underestimated mathematical settling velocity will result given a fixed dispersion. As shown in Figure 5.3, the isoconcentration lines at mid-lake were rising with distance, relative to the bed; this could only result from dispersion domination over sedimentation.

A ratio of particle dispersive to sedimentation mass fluxes can be estimated by the ratio of the actual velocity to the forced (regression) velocity. This ratio can be estimated from the square of the actual to regressed mass-average diameters. In the base case at X = 0.4, the ratio indicates that the dispersive flux is approximately 8.9 times the sedimentation flux. The dispersive:sedimentation mass flux ratio will approach unity as vertical equilibrium is approached, *i.e.*, near the downstream end of the system. Note also that the number flux ratio has no direct relationship to the mass flux ratio, since particle sedimentation is strictly and strongly size-dependent.

Concerning the second explanation, which is the possible inability of a mathematically lumped settling velocity to describe the distributed mass behavior, a definitive answer cannot be given at this point. In general, a lumped velocity would be fine for integral mass analysis if the size distribution was unchanging. That condition was not met in the base case, as evidenced by the substantial loss of number concentration and simultaneous increase in mass concentration. Coagulation and sedimentation in conjunction with resuspension is the only combination of processes

that can explain both observations. Simulations presented in the latter sections of this chapter examine the explicit effects of each of these processes.

5.3.3 Bed mass

The integral behavior of the bed mass amplifies the above conclusions concerning resuspension and attainment of equilibrium. Active bed mass [g/cm^2] as a function of longitudinal distance, at a simulation time of three mean residence times, is presented in Figure 5.7. The simulation had began with a uniform active bed mass down the length of the system. After three mean residence times, the bed was degrading with time, while the water column had reached steady-state.

In response to the steady and uniform bed shear stress, which exceeded the critical bed shear strength, bed mass was continuously resuspended into the water column. Except for the upstream boundary (X = 0), all nodes lost the same absolute amount of bed mass during the period of the simulation, based strictly on excess shear stress. The upstream boundary bed mass was fixed so that no resuspension could occur to affect the overlying (Dirichlet) water column boundary concentrations. Despite identical absolute mass resuspension fluxes from each node, the net mass flux varied noticeably and consistently down length of the bed, as less net loss of bed mass from downstream nodes.

Bed mass response shown in Figure 5.7 is the cumulative response to all positive and negative fluxes. Greater bed mass in succeeding downstream bed nodes is not a reflection of smaller resuspension flux but a demonstration of greater sedimentation flux. Fundamentally, the (number) sedimentation flux is merely the product of (number) concentration and discrete settling velocity. Given that discrete settling velocities are not a function of distance, the increasing near-bed water column

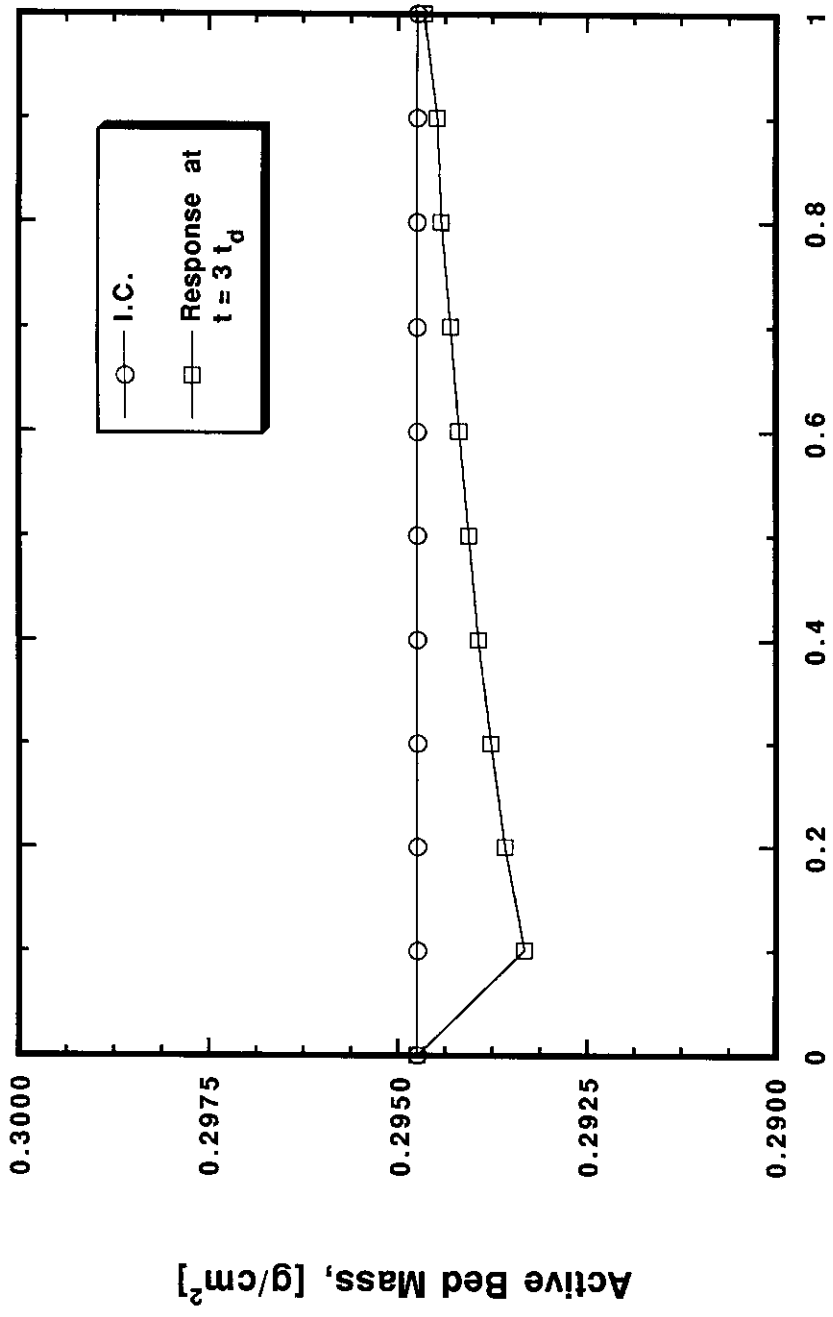

Figure 5.7 Base Case Active Bed Mass after 3 Mean Detention Times

concentrations present at downstream locations had to be responsible for the larger downstream sedimentation fluxes to the bed.

As discussed above in conjunction with the water column number and mass concentration isopleths (Figures 5.1 and 5.3), mass concentrations increased with downstream distance, but number concentrations displayed the opposite behavior. Resuspension, coupled with an imbalance between sedimentation and dispersion (*i.e.*, the net flux up), serves to increase mass concentrations in the near-bed fluid. These relatively small longitudinal gradients in mass concentration provided the longitudinally increasing sedimentation fluxes that are apparent. Given enough distance, a balance between absolute fluxes will be achieved such that the net bed flux is zero, neither aggrading nor degrading.

It is interesting to note that resuspension cannot be considered one of the parallel vertical flux processes operating on the water column suspension, despite the contrary assumptions discussed above. Resuspension is a boundary flux. As such, it operates in series with the water column processes. Particles from the bed must be transferred from the inventory of bed solids into the water column before they are available for coagulation and sedimentation.

For processes in series, the slowest one determines the overall rate of progress. The mass concentration isopleths (Figure 5.3) clearly show that resuspension was not rate determining in this system. Bed mass that eroded into the near-bed water column accumulated there faster than it could be mixed away by dispersion. This was evidenced in two ways: first, by the increasing concentration with distance in the near-bed region (an accumulation), and second, by the 'trajectories' or isoconcentration lines

leaving the bed and sweeping eventually up to the air-water interface. Both results demonstrate that resuspension was faster than vertical mixing.

The 2-dimensional simulation also highlighted interaction between the vertical processes. Based upon the system parameters defined *a priori*, it was stated above that the characteristic vertical mixing time of H^2/E_z was only 5.2 hr, or approximately 0.13 mean residence times. It is interesting that this characteristic time can also be observed in the simulation results, despite the potential confusion of interpreting the results from competing series/parallel, forward/backward, and longitudinal/vertical processes.

Specifically, the characteristic vertical mixing time can be inferred from Figure 5.3 in the region where vertical dispersion flux dominated sedimentation flux. This region extended between fractional longitudinal distances X = 0.1 and X = 0.3, spanning the region of initial resuspension and dispersive dominance. Thus the travel time taken for the first developed isoconcentration line (9.9 mg/L) to travel from the near-bed to the air-water interface was equal to the characteristic vertical mixing time. Further downstream, the apparent speed of vertical mixing was offset by the increased sedimentation flux; travel time for isoconcentration lines to traverse the water column depth increased. Beyond the point of established vertical flux equilibrium (horizontal isoconcentration lines), vertical particle mixing would not be discernible via the concentration isopleths.

5.3.4 Total surface area

Steady-state total particle surface area concentration isopleths, shown in Figure 5.8, were also derived from the number concentrations. It is assumed that the superficial surface area of the spheres gives a representative idea of the potential

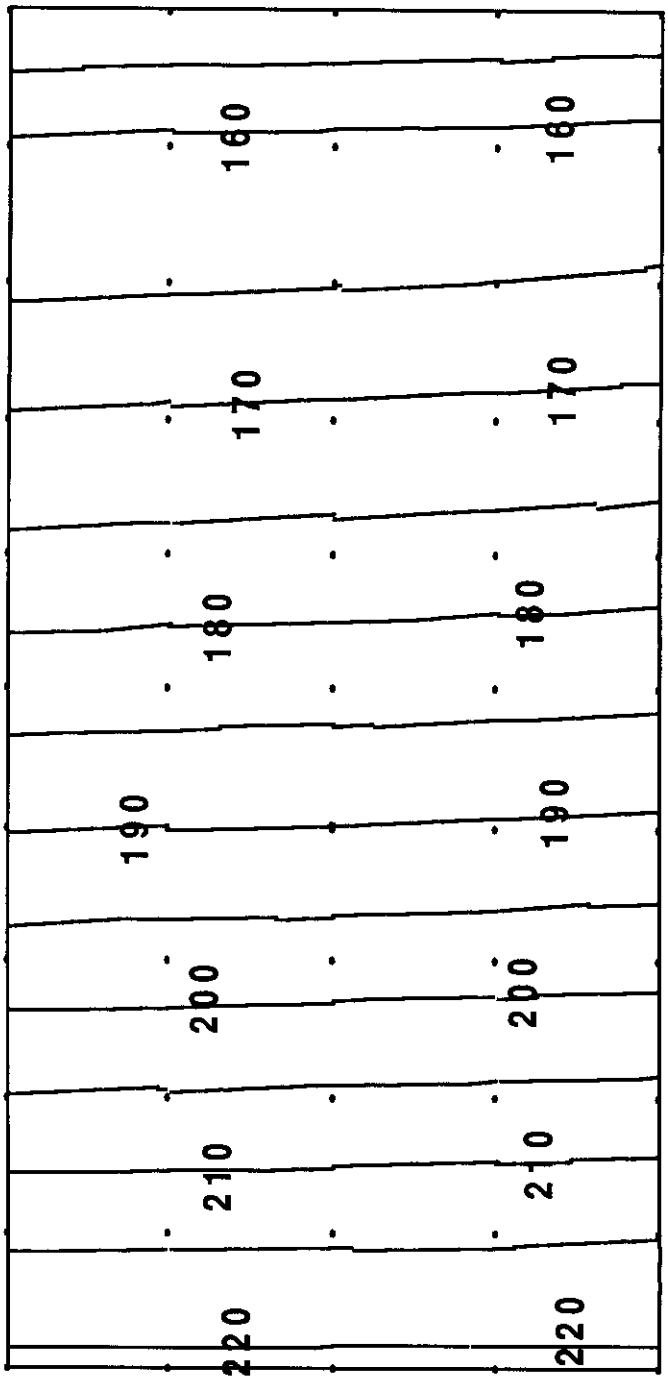

Figure 5.8 Base Case Total Surface Area Concentration Isopleths at Steady-State [cm^2/L]

same sign. The illusion is caused by the relative opposition of their longitudinal gradients.

5.3.5 Integral summary

A review of integral particle behavior results reveals the important strengths and limitations of the integral approach. The major strength is that each individual integral measure provides some indication of (net) processes taking place. For example, the total mass concentration isopleths clearly demonstrate the dominance of resuspension. This strength is based, however, upon the integration of the discrete particle distributions, a procedure unavailable to traditional water quality modelers.

The weakness of the integral approach is that a single integral measure, taken alone, cannot enable conclusions differentiating the simultaneous process influences. For example, the surface area concentration isopleths cannot differentiate coagulation effects, which are driven by number concentrations, from sedimentation and resuspension effects, which are driven by mass concentrations. This limitation is true for any single integral property of a dynamic and heterogeneous particle size distribution.

Without information about the particle size distribution, one cannot determine relative process influences. Without a deterministic knowledge of cause and effect, based upon process insight and mechanistic description, system modeling is hopelessly confined to case by case calibration. Discrete particle modeling offers the ability to assess competing process influences.

sorptive media available. This use of the particle distribution is a key element in the particle-associated contaminant model presented in Appendix A.

Recall that the simulation was initialized with the default particle size distribution, uniform throughout the water column domain. The total particle surface area concentration was 221 cm^2/L. The initial particle size distribution, with the assumptions of sphericity and effective density, has a specific (superficial) surface area of 2.24 m^2/g.

Comparing the surface area isopleths of Figure 5.8 with number and mass isopleths (Figures 5.1 and 5.3), it can be observed that total surface area response was qualitatively intermediate between the number and mass behavior. Particular likenesses and differences existed between area and number as well as between area and mass.

As did the total number concentration, the total surface area concentration decreased in the longitudinal direction. The decrease was approximately 32% between inflow and outflow. The surface area loss was expected, given the relatively large number concentration decreases (60%) and the relatively small mass concentration increases (4%). Because of the small mass concentration increase in conjunction with loss of surface area, the specific area reduction was slightly more than the surface area concentration reduction; the specific surface area was decreased approximately 34% to 1.47 m^2/g.

A vertical gradient of surface area concentration is noticeable in the isopleths of Figure 5.8. This behavior is similar to that of the total mass concentration. Although the vertical gradients of the surface area isoconcentration lines appear to be opposite to those of the mass isoconcentration lines (Figure 5.3), both sets of gradients have the

5.4 BASE CASE: DISCRETE PARTICLE BEHAVIOR

Following completion of the integral analysis of the base case in the previous section, analysis of the discrete behavior of the particle distribution can now provide further amplification. Viewed from the more fundamental particle level, the steady-state system response under base case conditions can be more completely understood. Elements of particle size distribution description were introduced in Section 3.6.

5.4.1 Discrete number

Absolute discrete number concentrations served as state variables in the transport-transformation model and were used to derive the integral particle measures presented in Section 5.3. This absolute, discrete particle number concentration ($\Delta N(k)$ in Section 3.6 notation and this chapter, or n_k in Chapter 4 notation) is a function of four independent dimensions, *i.e.*, time level (l), particle size class (k), longitudinal node (i), and vertical node (j). At a fixed time, the two spatial dimensions and one particle concentration dimension form a three-dimensional array. Presentation of these 3-D arrays cannot be easily accomplished in two dimensions. Therefore, all size distributions are presented here either at a point or as a function of one spatial dimension.

The dynamics of base case particle behavior are fully discussed below, but the mechanics of the size distribution are illustrated first. The curves in Figure 5.9 represent three "number distributions". These number distributions normalize the absolute number concentrations discretized in modeling and experimental analyses. Lawler (1987) has argued that the absolute discrete (*i.e.*, finite size range class) particle concentrations of whatever measure (number, volume, mass, or surface area) must be

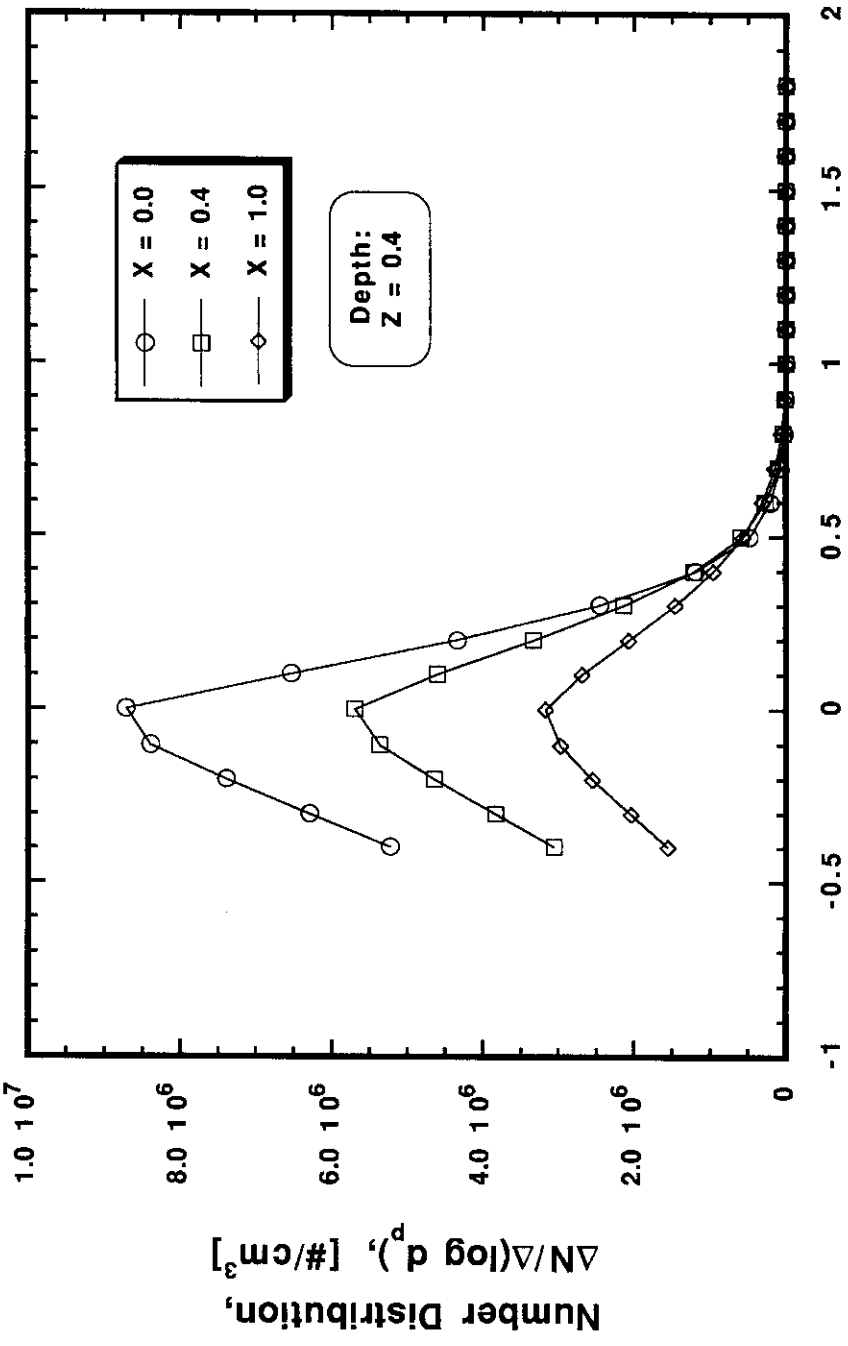

Figure 5.9 Longitudinal Evolution of Base Case Number Distribution at Steady-State

normalized by the diameter increment of the discrete size class. As an example, the (state variable) absolute number concentration for each size class is normalized by the log diameter increment for that size class. The symbolic magnitude of the number distribution for a size class k, at a point, is $\Delta N(k)/\Delta(\log d_p)$. The number distributions of Figure 5.9 were obtained by such normalization.

Normalization performs two useful functions (Lawler, 1987). First, since these distributions are normally presented as a function of equally spaced intervals of log diameter, the distribution may be more easily integrated to give incremental, cumulative, and total concentrations. This normalization allows convenient visual integration. A second and more important reason is that normalization makes the function independent of the specific value of the log diameter interval that is used. The $\Delta(\log d_p)$ available in certain experimental particle size counters is fixed, although in modeling and the other particle size counters it is adjustable. Without the normalization by $\Delta(\log d_p)$, function values are relative measures rather than true absolutes, which limits the utility of the work to others. In the modeling performed in this research, the $\Delta(\log d_p)$ used was 0.1.

The three number distributions in Figure 5.9 correspond to the three standard longitudinal locations at inflow, mid-lake, and outflow (X = 0.0, 0.4, 1.0), all at the standard mid-depth (Z = 0.4). Two facts are apparent. The first is the obvious loss of particle number, *i.e.*, the integral of the number distributions. Integrating under the inflow and outflow curves, the same 60% loss cited in the integral analysis is found. The second and more telling observation is that the relative loss of particles was much greater in the small sizes than in the larger sizes. Coagulation is the only mechanism that could accomplish both; subsequent analysis will examine process competition.

Number concentrations decreased with distance for all but the larger particle sizes, $\log(d_p) \geq 0.5$. Although not demonstrated well by number distributions, the number concentrations increased for the largest particles, and accounts for the increasing total mass concentrations, discussed in the integral analysis section.

On the arithmetic ordinate scale of Figure 5.9, all of the concentrations at the larger sizes appear to be zero; this is a problem, but there is a solution. A log ordinate scale is the customary remedy for this problem. The functional normalization is accomplished in a slightly different manner, *i.e.*, by Δd_p instead of by $\Delta(\log d_p)$. The log of the "particle size distribution function," or log PSDF, is calculated as $\log(\Delta N(k)/\Delta d_p)$. The log PSDF corresponding to Figure 5.9 is plotted in Figure 5.10.

The log PSDFs in Figure 5.10 express the conditions at the three standard longitudinal locations at mid-depth. Particle number reductions occurred during travel between the upstream boundary and mid-lake for particles smaller than 2.5 μm ($\log d_p \leq 0.4$); for larger diameters, concentrations increased during travel. The number concentration also were reduced between mid-lake and the downstream boundary for particles smaller than 3 μm ($\log d_p \leq 0.5$); for larger diameters, concentrations increased.

The log PSDFs in Figure 5.10 conclusively demonstrate that coagulation was taking place. Consider the potential mechanisms causing the net loss in particle number concentration (flocculation, sedimentation, and resuspension/dispersion). Bed resuspension was not responsible for the substantial number loss because it obviously would have acted counter to the decrease. Sedimentation was not responsible for the number loss: the settling velocities of those particles actually lost ($d_p \leq 2.5$ μm) were insufficient to cause observable sedimentation loss. Only flocculation could have

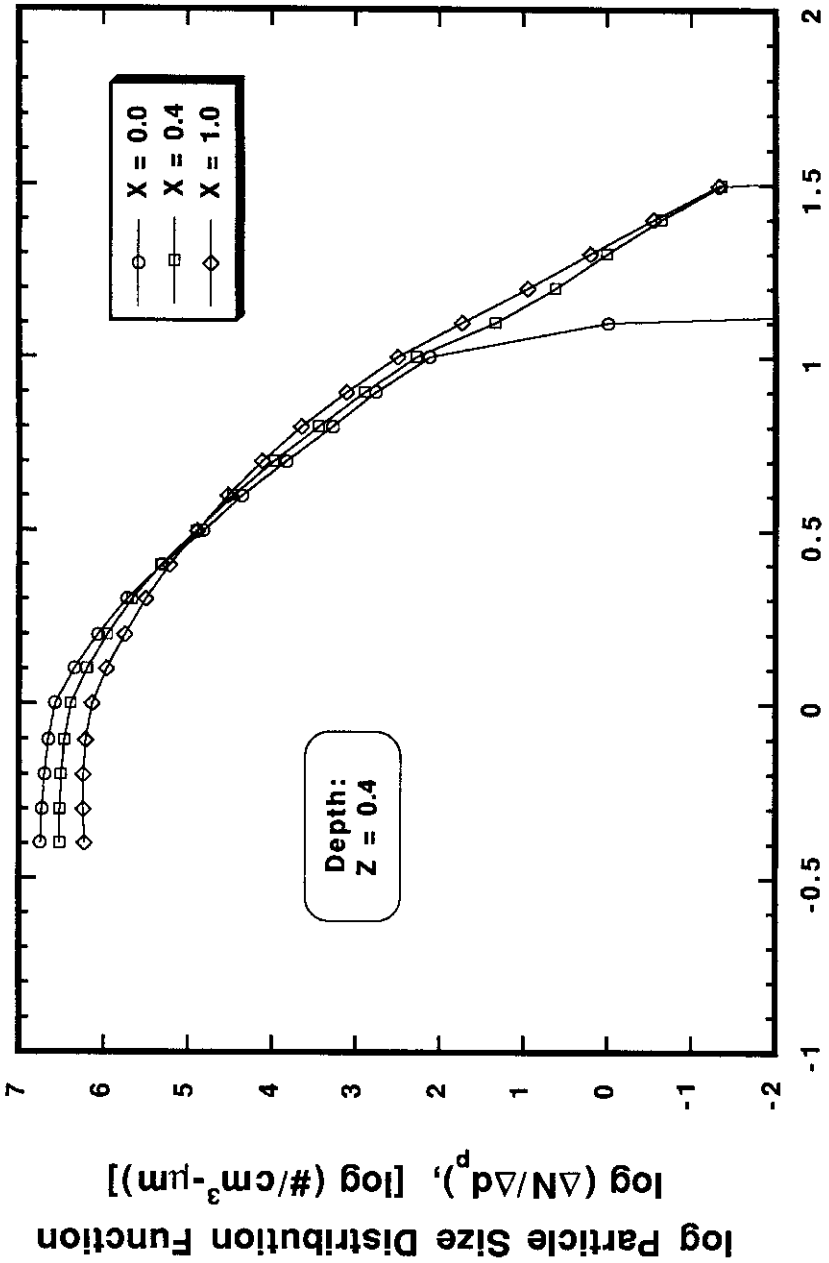

Figure 5.10 Longitudinal Evolution of Base Case Particle Size Distribution Function at Steady-State

produced the loss of particle number concentration, evidenced in the smaller diameters, as shown in the upstream vs. downstream comparisons of Figure 5.10. The cause for the loss of total number accompanied by a gain of total mass, which could only be guessed with the integral results, is revealed by discrete particle analysis.

The PSDFs in Figure 5.10 illustrate some other interesting effects, probably due to bed resuspension. Erosion is suggested by the appearance of inflection points in the PSDFs, as well as by the new concave-up regions that span the several largest size classes; this behavior was present between the mid-lake and downstream outflow locations. It seems that the particles that a) were small enough to be dispersed (vertically) faster than they settled and b) existed in concentrations large enough in the bed to supply the process, caused this unusual behavior (diameters of $1.1 \leq \log d_p \leq 1.5$). This behavior resembles the superposition of two different parent particle size distributions, which it actually is. This behavior has not been reported in previous modeling and experimental studies (*e.g.*, Lawler and Wilkes, 1984; O'Melia and Bowman, 1984; Weilenmann *et al.*, 1989). The clear distinction is that those studies incorporated only a single size distribution inflow, *e.g.*, no bed-water boundary fluxes.

5.4.2 Discrete volume

Volume distributions of the base case simulation are presented in this section. These distributions are analogous to the number distributions of the previous section in their origin and normalization.

Evolution of the volume distribution is shown for the standard longitudinal profile in Figure 5.11. Virtually every longitudinal response presented in the integral and discrete analyses is dramatically evident in this figure. First, the loss of the smaller particle volumes with distance confirms the coagulation conclusion. At the $\log d_p = 0$.

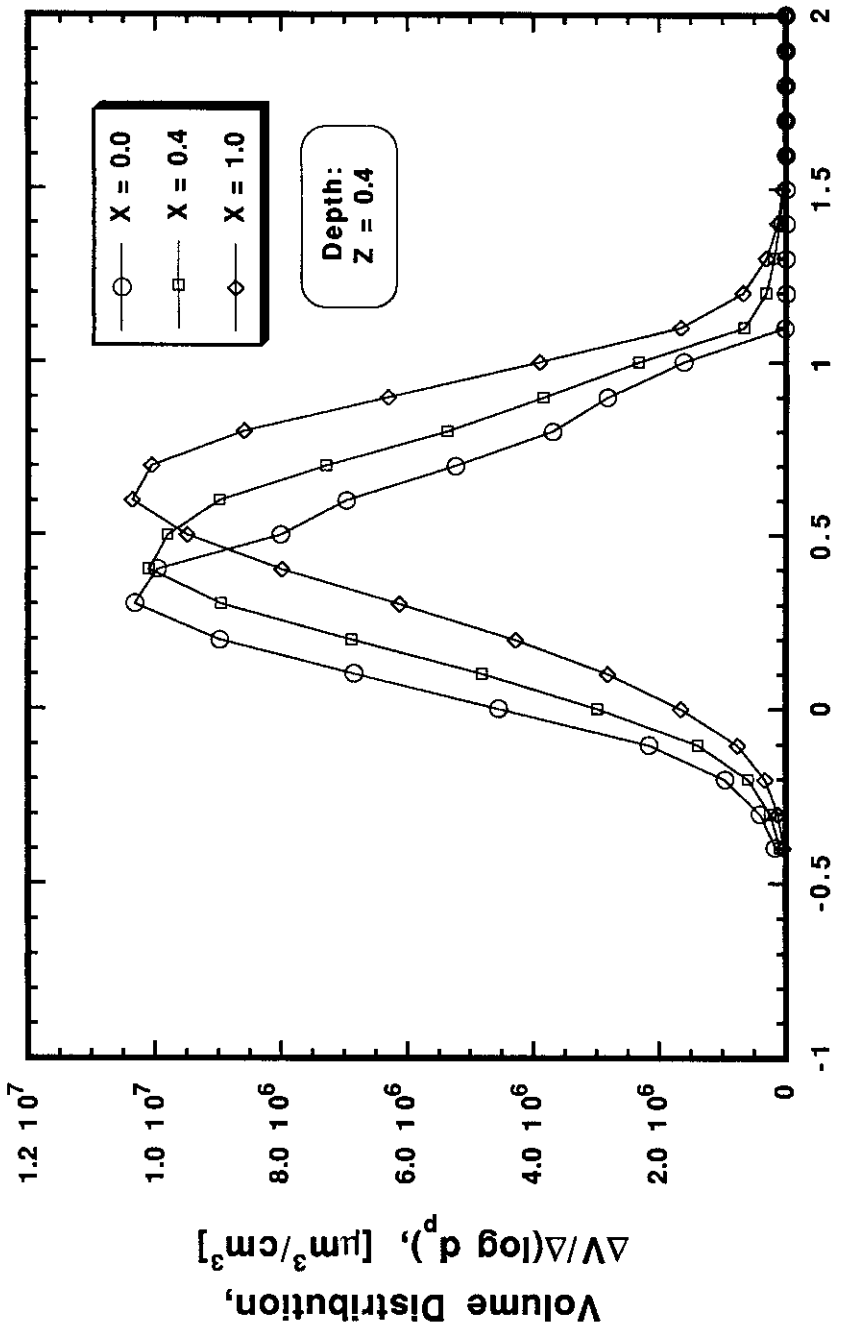

Figure 5.11 Longitudinal Evolution of Base Case Volume Distribution at Steady-State

size class, for example, approximately two thirds of the particle volume present at inflow has been removed. Second, volume in the larger size classes increased with distance. At the log $d_p = 0.7$ size class, for example, the particle volume present at inflow has almost doubled due to coagulation and perhaps resuspension. Third, the peak of the volume distribution (the volume modal diameter) shifts markedly to larger sizes as one progresses down the lake. The inflow peak is increased from log $d_p = 0.3$ to log $d_p = 0.6$ at the outflow. The shift in peak is again indicative of coagulation and perhaps resuspension. Last, the total volumes (the integrated areas under the distributions), proportional to the total mass, are almost constant with distance, as indicated previously.

The slight increase of total mass (volume) occurred by the introduction of large particles (log $d_p \geq 1.1$) that were not initially present. By shifting the mode, the addition of larger particles via resuspension also resulted in pronounced skewing of the distribution, from positive to negative.

5.4.3 Discrete surface area

Surface area distributions, shown for the standard longitudinal profile in Figure 5.12, displayed the intermediate behavior expected from the previous analyses. Total superficial surface area concentrations, equal to the integrated area under the area distributions, decreased down the length of the system. The decrease of total area occurred by the loss of small and intermediate size particles (log $d_p \leq 0.3$) by flocculation. The absolute surface area concentration of larger particles increased with distance due to resuspension. The combination of area gain and loss increased the modal diameter of the area concentration distribution from log $d_p = 0.2$ at the upstream

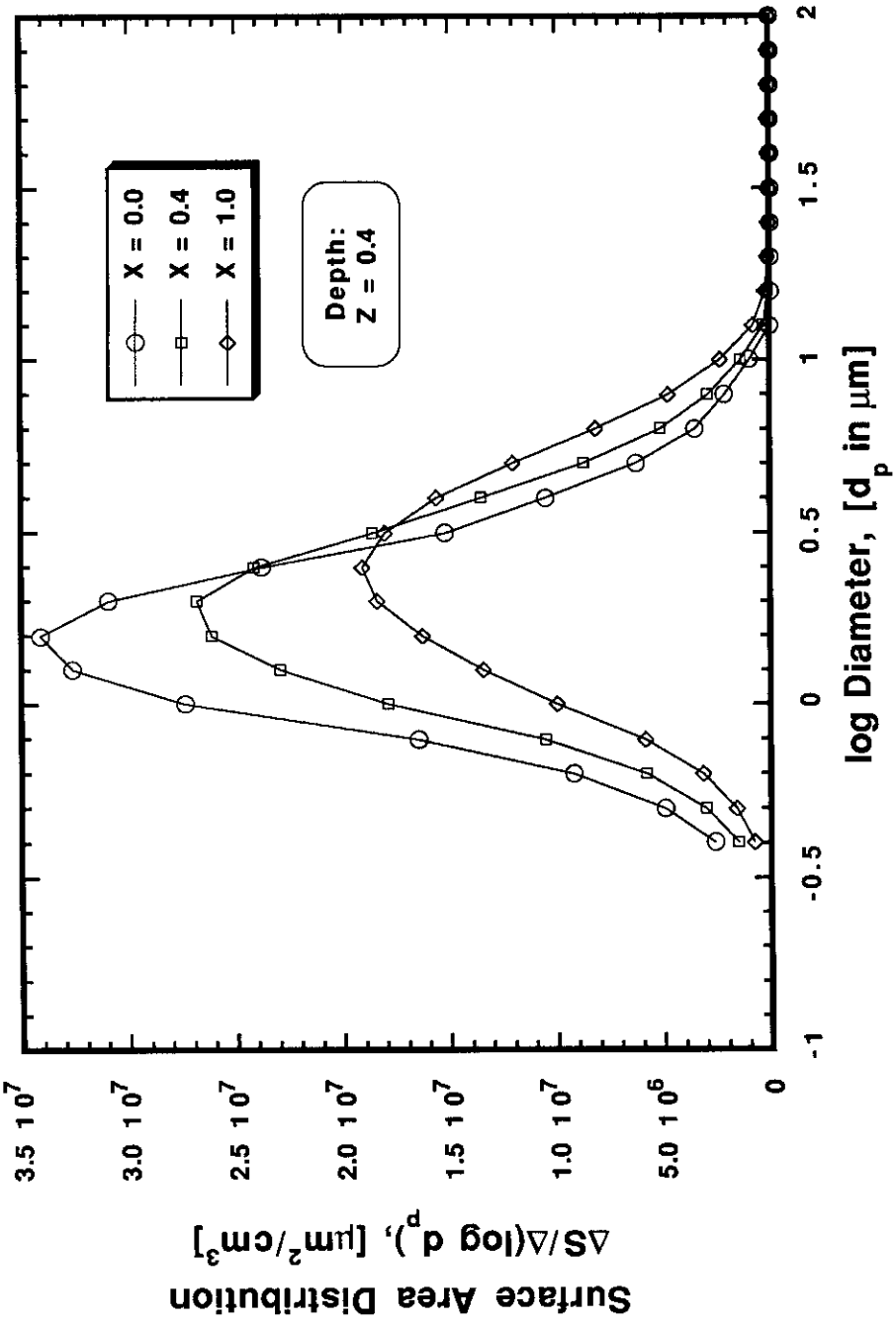

Figure 5.12 Longitudinal Evolution of Base Case Surface Area Distribution at Steady-State

boundary to log d_p = 0.4 at the downstream boundary. By shifting the mode, coagulation and resuspension resulted in a reduced skewness of the distribution.

5.4.4 Discrete vertical response

The two number distributions in Figure 5.13 correspond to two vertical locations in the mid-lake (X = 0.4) water column, at the air-water interface (Z = 0.0) and near the bed (Z = 0.8). There is no discernible difference between the two number distributions. Visually integrating the number distributions qualitatively confirms the vertical uniformity of total number concentration, as discussed in Section 5.3 on integral behavior. Because of the near identity of the two distributions at larger sizes, and the lack of resolution there, the larger mass concentrations near the bed cannot be detected using the number distributions.

Examination of the PSDFs does, however, provide the sensitivity to detect the relatively small vertical differences in the number concentrations. Figures 5.14 (a) and (b) contain the near-surface and near-bed PSDFs at mid-lake and at the downstream boundary, respectively. Larger number concentrations of the larger particles (log $d_p \geq$ 1.1) were apparent near the bed as compared to the air-water interface. These particle size distributions provide a size-dependent demonstration of how an exponential mass distribution (Figure 5.6) is generated, especially for a heterogeneous suspension, and exactly which particles are vertically segregated by the gravitational and dispersion forces, *i.e.*, only the larger particles. The vertical differences were greater at mid-lake than at the downstream boundary. These longitudinal changes are another indication of the vertical nonequilibrium between resuspension and sedimentation which was seen in the integral mass analysis. With size-dependent information, the reason for and extent of the nonequilibrium is more explicit with discrete particle distributions.

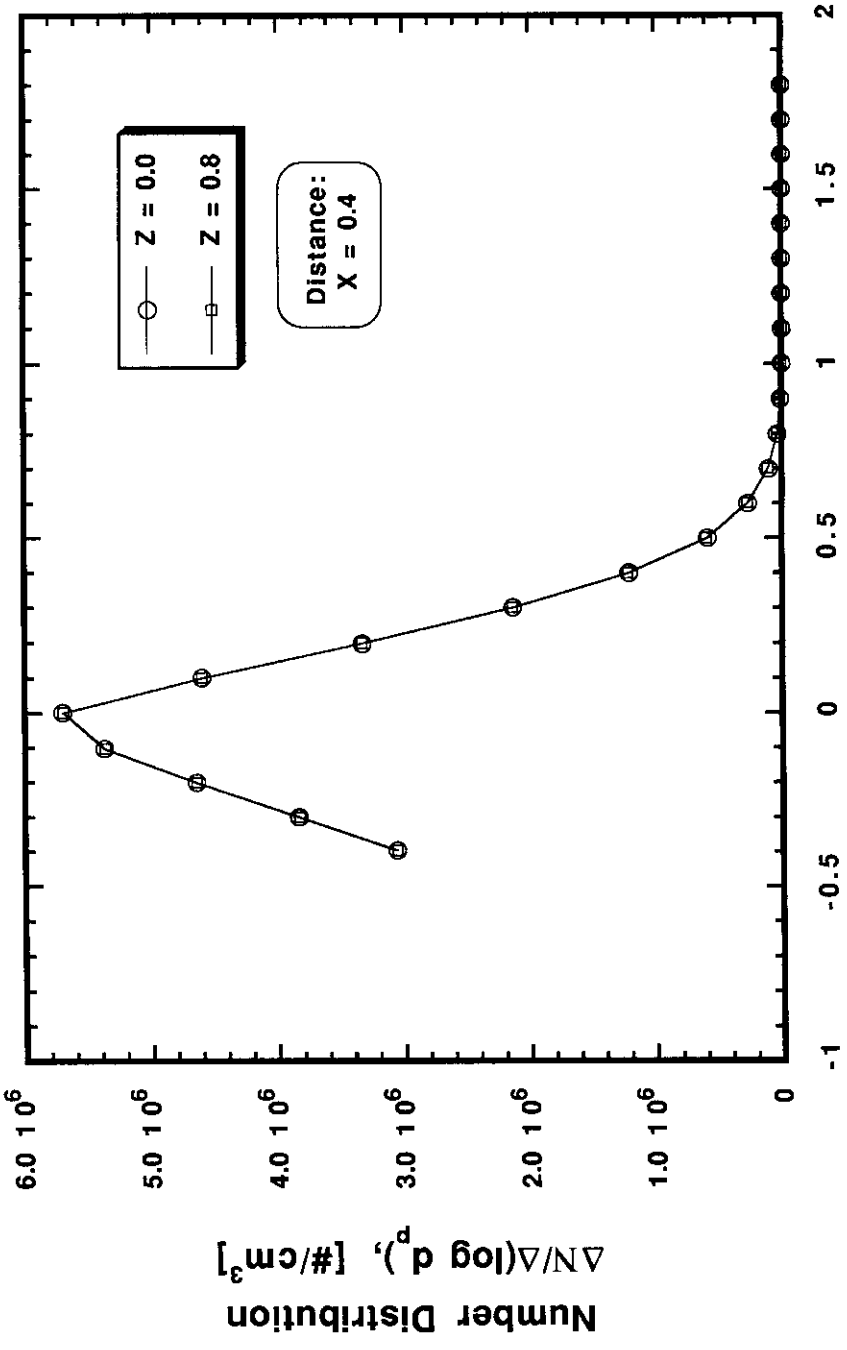

Figure 5.13 Vertical Distribution of Base Case Number Distribution at Steady-State

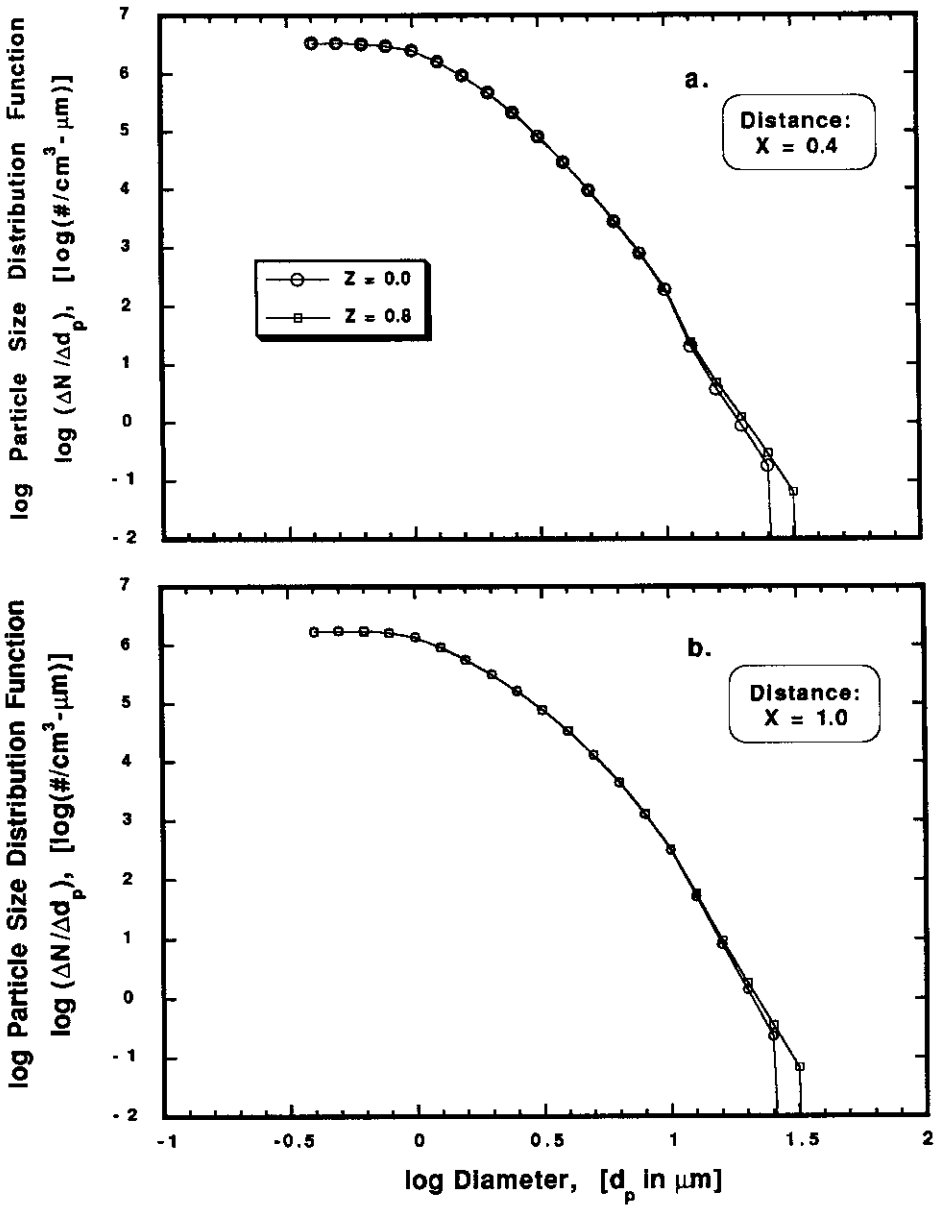

Figure 5.14 **Longitudinal Evolution of Vertical PSDF Profiles at Steady-State**

5.4.5 Discrete response summary

A review of discrete particle analyses reveals the important advantages of the discrete approach. First, the discrete approach provides all of the information obtainable from integral analysis. The advantage presented by the discrete approach is that it goes beyond integral analysis to provide size-dependent distributions of the suspension. It is these data that provide the platform for understanding the explicit processes, with different time scales, competing to change the overall size distribution of the suspension. Some might argue that, if mechanisms can be lumped into a composite process, the discrete distributions provide more information that one needs. This might be true in situations where conditions are unchanging, or when only a single integral parameter is of interest. However, the use of discrete analysis is actually more efficient than constructing a new model for new conditions; discrete analysis avoids constructing and then trying to link (non-mechanistically) three individual models for the three individual integral responses of particle volume (mass), number, and surface area.

5.5 PROCESS INFLUENCES

The processes involved in changing the particle size distribution within a control volume advected in a Lagrangian reference frame are coagulation, bed resuspension, and sedimentation. The effects upon the size distribution due to combination of these three principal processes (in conjunction with fluid transport) were examined in the previous section, the base case. In this section, the effects that the individual processes have upon integral and discrete behavior are examined. Process intercomparisons are presented, and the base case results serve as a point of reference.

The effect of an individual process upon the spatially varying PSD is of central concern. Although the typical solids modeling approach ignores coagulation and often lumps settling and resuspension into a net, depth-averaged, first-order process, the three mechanisms actually operate in an independent and nonlinear manner. The overall nonlinear response is the result of processes (gravitational settling and reaction kinetics) which are nonlinear, with respect to discrete particle size particle size, acting on a heterodisperse suspension. Traditional mass-based modeling schemes cannot capture these nonlinearities with a linear approach. Isolation of individual process influences thus provides insight concerning their particular significance.

System responses were simulated, process by process, assuming either the sole presence or the total absence of that individual process. Comparisons of results, a) with the process operating (either the base condition or as the sole process) vs. b) without the process operating, are presented and analyzed. A summary of the integral behavior is given in Table 5.1, and this table is referenced in conjunction with the discrete particle discussions in the process subsections below. System responses to relative degrees or rates (parameter sensitivity, Section 5.6) is the topic of the next section.

Integral results summarized in Table 5.1 are for the six process conditions which are discussed in this section. Two other conditions are also presented for reference, *i.e.*, the base case and the fluid-transport-only case. Response of the system was measured in three integral parameters, dealing with total particle number, volume, and area concentrations. These parameters are the ratios of the concentrations at mid-depth at the outflow boundary (an approximation for the outflow concentration averaged over the depth) to their respective concentrations at the inflow. Ratios

Table 5.1

SUMMARY OF INTEGRAL BEHAVIOR: IDEALIZED PROCESS COMPARISONS.

(Using system response concentrations at mid-depth outflow relative to upstream boundary concentrations)

	Processes Considered			N (1.0,0.4) / N (0.0,Z)	V (1.0,0.4) / V (0.0,Z)	A (1.0,0.4) / A (0.0,Z)
Simulation	**C**	**S**	**R**	Relative Number Concentration	Relative Volume Concentration	Relative Area Concentration
Base Case	√	√	√	0.402	1.042	0.683
No Coagulation	-	√	√	1.012	1.081	1.009
Coagulation Alone	√	-	-	0.407	0.9999	0.680
No Resuspension	√	√	-	0.395	0.888	0.635
Resuspension Alone	-	-	√	1.028	1.334	1.107
No Sedimentation	√	-	√	0.416	1.334	0.760
Sedimentation Alone	-	√	-	0.992	0.921	0.964
Fluid Transport Only	-	-	-	1.001	1.001	1.001

Key: **C** = Coagulation; **S** = Sedimentation; **R** = Resuspension

N = Total Number Concentration; **V** = Total Volume Concentration; **A** = Total Area Concentration

Fractional Coordinates (X, Z):
X = x/L
Z = z/H

represent the average fractions remaining, although values can be greater than 1.0 due to boundary fluxes.

5.5.1 Coagulation

The influence of particle coagulation was examined by isolating coagulation (in conjunction with transport) as the only operative process, as well as by eliminating coagulation from the simulation. Isolation of coagulation was accomplished in the simulation by numerically forcing sedimentation and resuspension fluxes to zero. Sedimentation fluxes were forced to zero by setting the |particle - fluid| density difference to zero; resuspension fluxes were forced to zero by setting the erosion rate constant to zero. Excluding coagulation was accomplished by two equivalent approaches. The first method was to make the particles completely stable, *i.e.*, by setting the chemical collision efficiency α_{chem} to 0.0. Thus the actual collisions between particles (collisions which are known to occur via the thermal, gravitational, and turbulent mechanisms discussed in Chapter 2) were still simulated, but attachment and changes in the size distribution were suppressed. As a check, the coagulation process could be completely bypassed in test simulations, and this was done to verify that the same results were achieved with either method.

The effects of coagulation on the particle size distributions were substantial. These consequences are illustrated most dramatically by comparing plots of the evolution of the size distribution resulting from sedimentation and resuspension only (*i.e.*, without coagulation) with the base case evolution. Comparisons with simulations including coagulation only then follow.

First, in the absence of coagulation, relatively small changes in the PSDs over space were observed. Longitudinal PSD evolution plots are presented in Figure 5.15.

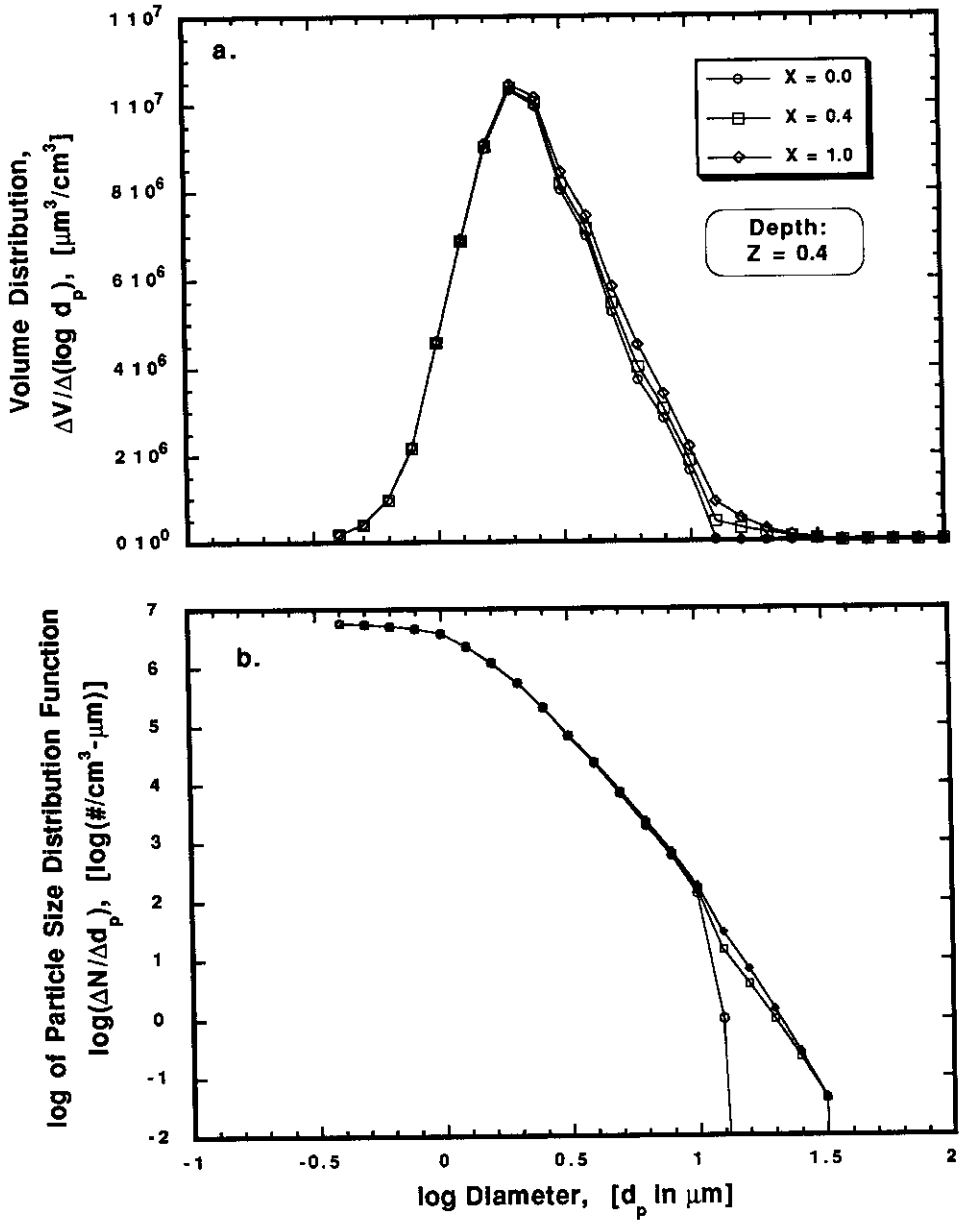

Figure 5.15 **Longitudinal Response of Ideal System with No Coagulation**

As shown in Figure 5.15(a), particle volume was essentially constant with distance for the smaller sizes, those smaller than the distribution mode (log $d_p \leq 0.3$). For all sizes larger than the distribution mode, volume was added to the PSD with distance. The relative increases of particle volume were substantial only in the largest sizes ($d_p > 10$ μm). Because the integrated volume distribution increased rather than decreased with distance, one can conclude that the net changes were due to bed resuspension outweighing sedimentation. The mode of the volume PSD remained unchanged with distance, however, and the volume-mean diameter was affected little.

The longitudinal profiles of the log of the particle size distribution function (Figure 5.15b) confirmed that insignificant changes in the number distribution occurred throughout most of the distribution (log $d_p \leq 1.0$, or $d_p \leq 10$ μm). Plots of log PSDF accentuate the arrival of the larger particles from the bed and their subsequently increasing concentration, with distance, in the water column. Also, the inflection points in the log PSDFs at log $d_p = 1.1$ signal the initial discontinuity, as well as the gradual approach to equilibrium, between the original bed and water column PSDs.

Integral results for the no-coagulation case, presented in Table 5.1, provide an additional perspective on the particle behavior. The total number concentration change from system inflow to outflow was only +1.2% (c.f. the base case change of -59.8%); comparatively large resuspension-induced increases in the PSDF at the large end of the size spectrum were actually small relative to the concentrations of small particles. The modest total volume increase, +8.1%, is important in that it was twice as large as the base case volume increase of +4.2%. By not flocculating small particles into larger particles that could be settled more easily, the conditions enabled more mass to remain in suspension at small sizes. The longitudinal total area concentration increase of 0.9%

was smaller than either the number or volume increases. That the area concentration results did not fall intermediate between the number and volume results was contrary to the coagulation-sedimentation expectation based on size-dependent physics. Resuspension caused this seeming contradiction.

The converse situation, coagulation operating alone, provides the complementary perspective to the no-coagulation scenario discussed above. The coagulation-alone volume distribution was compared with both the no-coagulation case and the base case results. In Figure 5.16, results at the downstream boundary for the three cases are shown. The plot labeled 'Base' represents all three mechanisms operative (C - coagulation, S - sedimentation, and R - resuspension), the case discussed in Sections 5.3 and 5.4. The plot labeled 'No C' represented no coagulation but sedimentation and resuspension operative. The plot labeled 'C only' represents conditions of no sedimentation or resuspension but coagulation occurring. Recognize that the 'coagulation-only' case was achieved in part by suppressing sedimentation, *i.e.*, by setting particle density equal to fluid density. Interparticle collisions by differential sedimentation were also suppressed. Thus, specific coagulation rates for this case were smaller than in the base case.

With coagulation alone, the entire volume distribution was shifted to larger sizes, just as in the base case. Minor differences between the coagulation-alone case and base case distributions in Figure 5.16(a) substantiated that most of the volume distribution shifting observed in the base case was the result of coagulation rather than bed-water exchange. Superimposing the effect of net resuspension flux on top of the coagulation-only response revealed that perceptible amounts of volume were added to the distribution (comparing Figure 5.16(a) coagulation-only vs. base). These increases

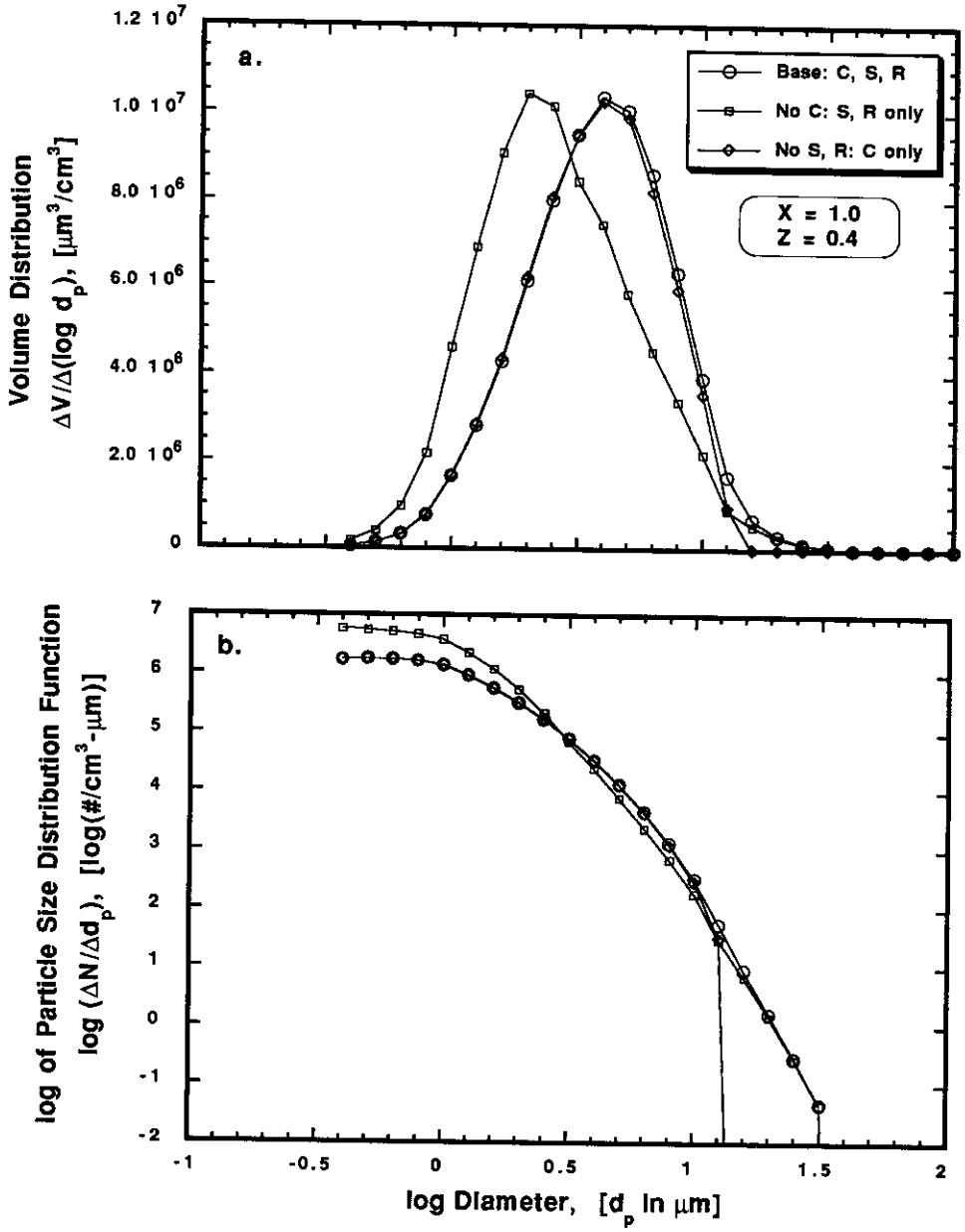

Figure 5.16 **Effect of Coagulation on Ideal System Response at Outflow**

took place only at particle sizes larger than the distribution mode. As in the no-coagulation case, relatively large volume distribution increases occurred only at the very largest particle sizes.

The interesting difference between the volume PSDs in the coagulation-only and coagulation-absent cases was that the modal diameters were separated by three discrete size classes. This separation was very large: the factor of 2 in the diameter mode difference would be a factor of 8 in the equivalent volume/mass mode difference. The lack of shift in the volume PSD for the case without coagulation (but resuspension) reflected the potential contribution of the bed mass eroded and mixed vertically through the water column. The probable reason that perceptible increases in the volume PSD of the no-coagulation case did not occur at diameters smaller than the boundary distribution mode ($\log d_p = 0.3$) was that these particles were not transferred from the bed fast enough to produce such a change. A plausible explanation for the fact that perceptible differences were not detected between the coagulation-alone volume PSD and the coagulation plus resuspension (base case) volume PSD in the small size ($-0.4 \leq \log d_p \leq 0.6$) range is this: the resuspended particles that were smaller than the volume distribution mode became quickly consumed by coagulation and transferred up the distribution, so that no accumulation appears.

The particle size distribution functions (Figure 5.16b) confirmed the effects observed above concerning the volume PSD. An observation is suggested by the intersection of the coagulation-only and coagulation-absent log PSDFs at the particle size $\log d_p = 1.1$. This point marked the diameter at which resuspension and coagulation resulted in equivalent modifications of the PSDs. In general, it is not correct to say that at that point the two different processes in the two different cases

were exerting the same effect on that size particle, much less the two entire PSDFs. Rather, the process equivalence would have to be interpreted in the context of integrated or cumulative effects, as the diameter of PSDF equivalence would change in space.

The integral responses for the coagulation-only case were nearly the same as those of the base case, as shown in Table 5.1. With no resuspension or sedimentation acting to remove particles from the water column, the simulated fractional volume remaining result of 0.9999 was essentially equivalent to the value of 1.0000 theoretically expected for volume conservation. The slight difference was due to numerical error. Smaller integral volume for the coagulation-only case, relative to the base case, was expected because of the net erosion in the base case. The larger (relative to the base case) integral number for the coagulation-only case might not be expected, given its absence of net erosion, but two factors could explain it. Most likely, the lack of collisions by differential sedimentation maintained higher number concentrations. Alternately, the lack of fine particle flux from the bed could have slowed the coagulation kinetics.

5.5.2 Bed resuspension

Resuspension of bed mass into the water column also had substantial effects upon the water column PSDs. The magnitude of the process's impacts on the PSD was estimated by simulating and comparing two conditions: no resuspension (*i.e.*, coagulation and sedimentation) and resuspension alone. For engineered systems, ideal sedimentation tank analysis typifies the first case, and natural system conditions of no significant gross (as opposed to net) resuspension are physically plausible. In the second case of resuspension alone, it is doubtful that natural systems exist at steady-state with resuspension but no settling or coagulation. The comparisons are valuable for

process insight, though, so the volume distribution evolution resulting from the two cases are contrasted in Figures 5.17 (a) and (b).

The longitudinal evolution of the volume distribution without resuspension (Figure 5.17a) bears both similarities and dissimilarities to the base case results. The primary similarity to the base case is the shifting of the volume PSD to larger diameters. In the absence of resuspension, this shift was surely the result of coagulation. The modal diameter increased three size classes, just as the base case had.

There were more dissimilarities than similarities, however, between the case of no resuspension and the base case. An obvious deviation from the base case volume PSD evolution was that particle settling, no longer offset by resuspension flux, resulted in net sedimentation and the loss of mass from the water column. The final average diameter was smaller than in the base case due to the absence of the largest particles supplied by the bed. Another difference from the base case was the increased skew of the outflow volume distribution; the inflow volume PSD was positively skewed, and both outflow volume PSDs were negatively skewed, but suppression of resuspension accentuated the skewness.

The integral behavior of the no-resuspension case is summarized in Table 5.1. Integral number and area reductions across the system were similar to those of the base case. Coagulation and sedimentation (rather than resuspension), which were operating in both scenarios, certainly dictated reduction of number and area. Integral volume behavior was markedly different from the base case, however. Small numbers of large particles, with relatively small surface area, were entrained in the water column by base case resuspension, and these large particles added the volume not seen in the no-resuspension case.

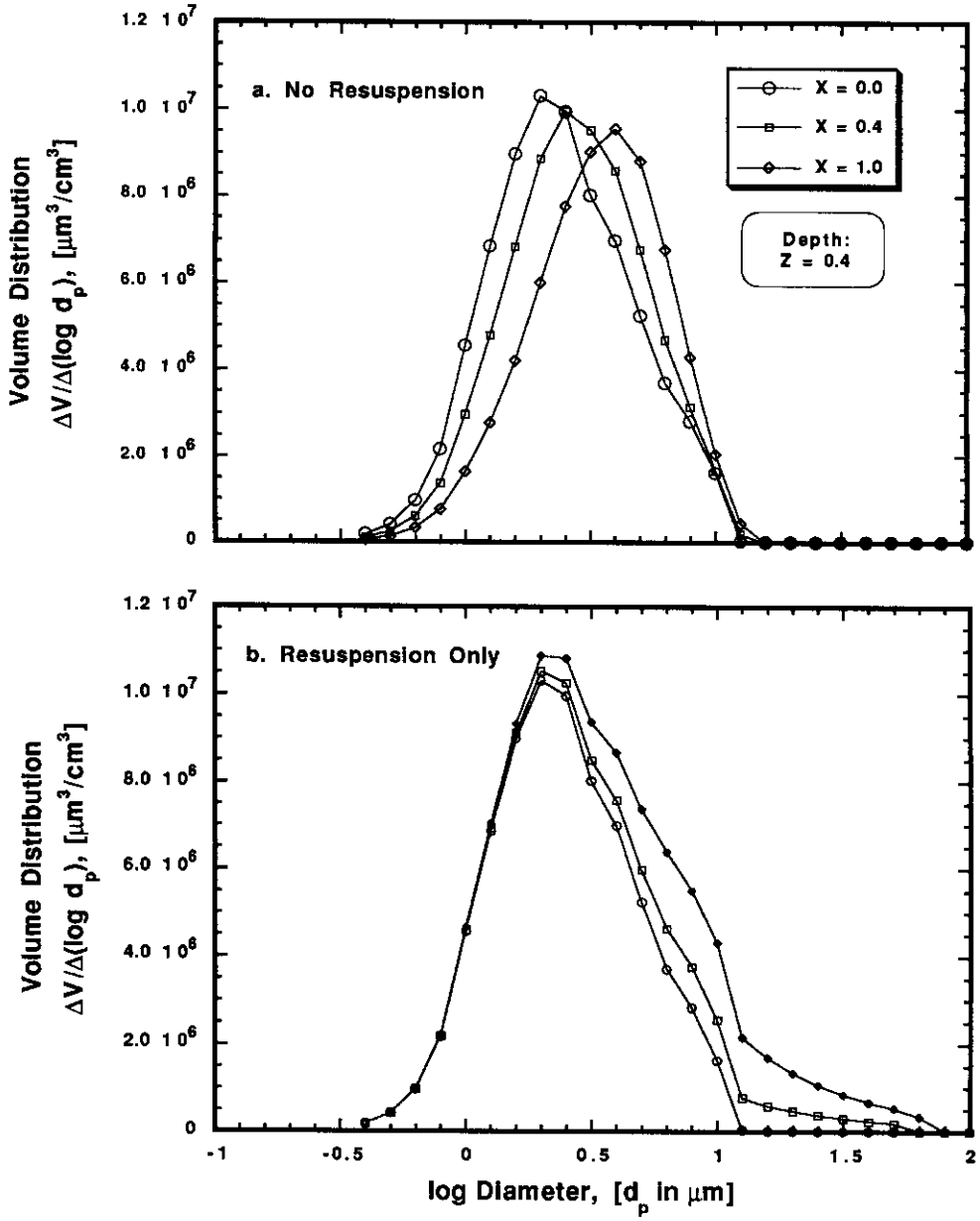

Figure 5.17 **Effect of Resuspension on Longitudinal Evolution of Particle Size Distributions**

How great an impact resuspension itself has on the PSD can only be inferred by eliminating the processes competing with it. System response with resuspension alone was also simulated. With direct competition from sedimentation removed, and without the PSD modifications caused by coagulation, resuspension can be seen to cause considerable change in the volume PSD, as shown in Figure 5.17(b).

The longitudinal evolution of the volume PSDs with resuspension alone clarifies the role of bulk resuspension in water column response. Substantial mass was added to the water column by resuspension; approximately 33% more was suspended in the outflow than in the inflow to the system. The peak volume concentration increased marginally. The increases in the volume distribution, confined almost exclusively to sizes equal to and larger than the mode of the water column volume distribution, were determined by the mass fraction in the bed for each d_p. Thus, although the outflow's discrete volume distribution modal diameter remained constant, resuspension increased the volume in larger size classes substantially.

Particle size distributions at the system outflow, shown in Figure 5.18, illustrate two resuspension effects more clearly. First, resuspension did not influence the concentrations of small particles to any appreciable degree. Concentrations were essentially the same with or without resuspension, provided that coagulation took place. Both the volume PSDs (Figure 5.18a) and the PSDFs (Figure 5.18b) illustrate these small particle effects. Second, resuspension greatly increased the concentrations of the larger particles, *i.e.*, those larger than the bed volume peak. Actually, the resuspension-induced increase is seen at $\log d_p = 1.1$, and the assumed bed volume peak was a plateau that spanned three size classes, $0.8 \leq \log d_p \leq 1.0$. The marked

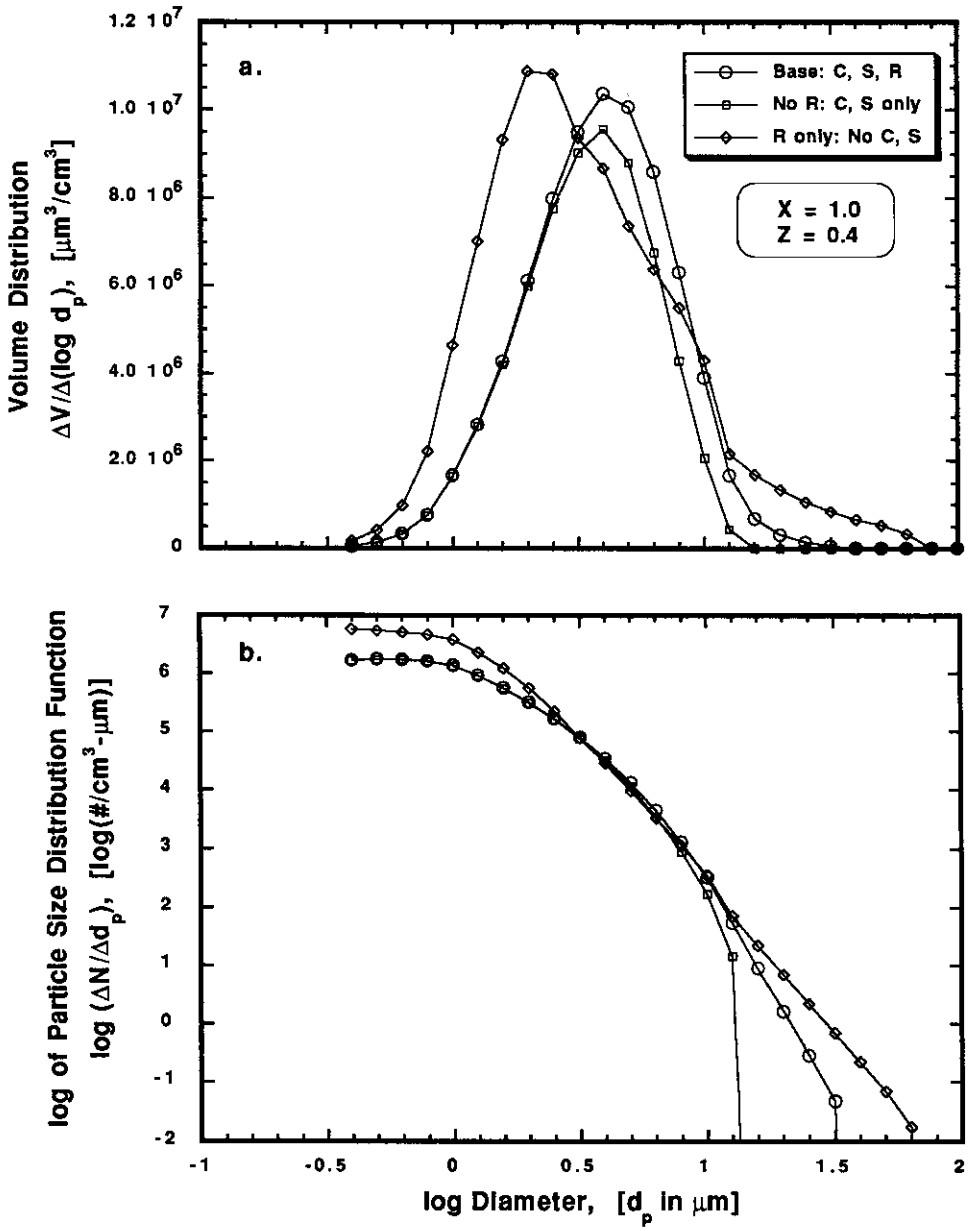

Figure 5.18 **Effects of Resuspension on Particle Size Distributions at Outflow**

abundance of the largest particles concentrations due to resuspension is particularly clear in the log PSDF.

The particle process mix in the resuspension-alone simulation influenced the integral responses as would be expected. As shown in Table 5.1, total particle number, area, and volume concentrations each increased across the system, more than the base case and substantially more than the no-resuspension case.

5.5.3 Sedimentation

Sedimentation of particles from the water column produced substantial effects upon the water column PSD responses, just as its companion processes had. The magnitude of the process's impacts on the PSD were estimated by simulating conditions of sedimentation alone vs. coagulation and resuspension alone. Conditions of negligible (net) sedimentation are present in many turbulent flows of fine particle suspensions; however, silt and sand sized particles do have consequential settling velocities, and a flocculating, eroding system with no sedimentation is not physically probable. Cases of steady-state sedimentation alone, *i.e.*, with negligible resuspension and coagulation, would be more likely than the converse.

The general form of the longitudinal evolution of the volume distribution without sedimentation (Figure 5.19a) appears as an exaggeration of the base case results. There was the same characteristic shift of the volume PSD to larger diameters. As in the base case, the shift was primarily due to coagulation. The modal diameter shifted an additional size class (four compared to three), however, since sedimentation did not act to counter the largest particles emanating from the bed.

One can see from Figure 5.19(a) that the total volume increased substantially in the absence of sedimentation. As reported in Table 5.1, the integral volume increased

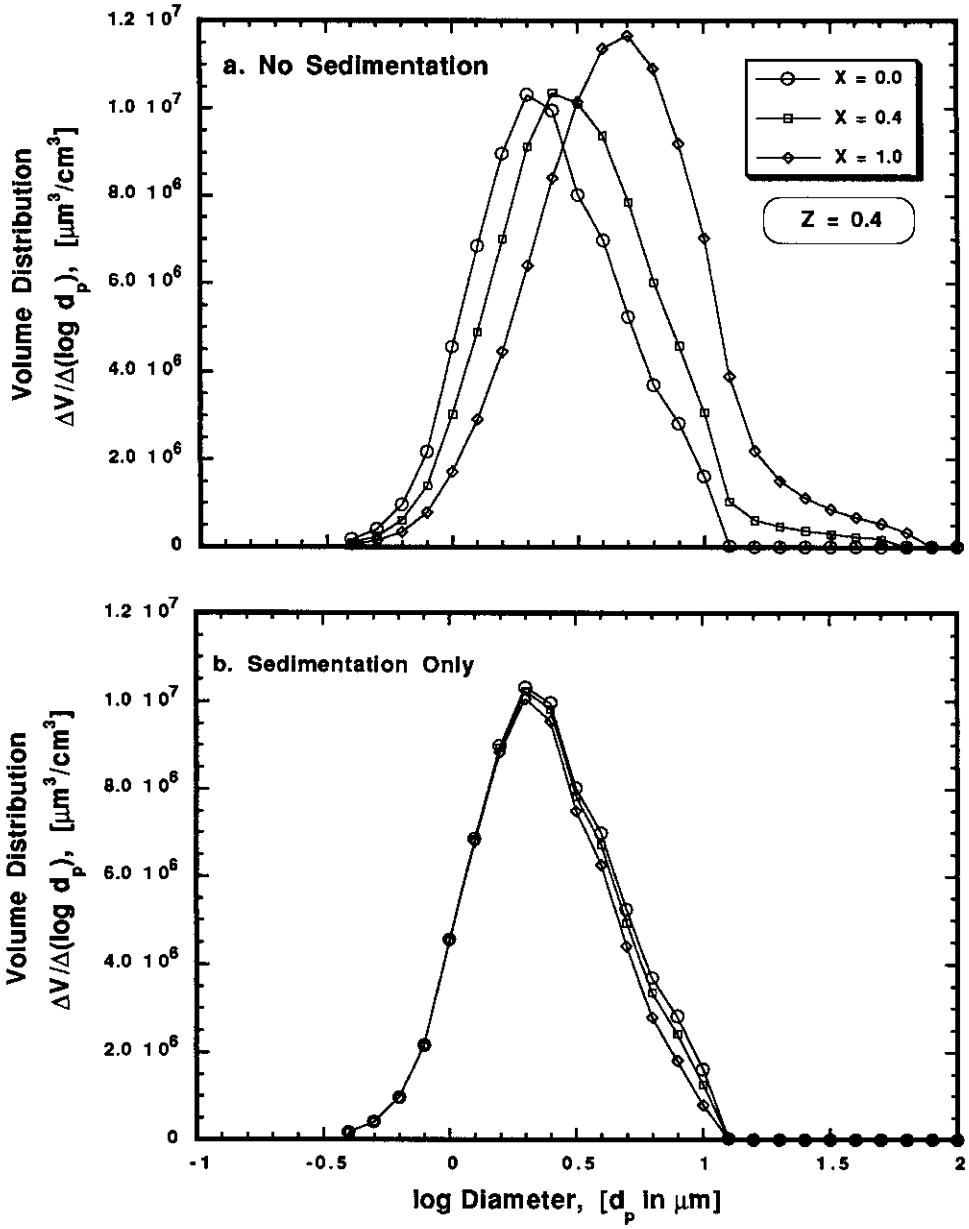

Figure 5.19 **Effects of Sedimentation on Longitudinal Evolution of Particle Size Distributions**

approximately 33% between inflow and outflow, even while total number decreased 58%. Since coagulation does not produce added volume, the volume increase was due strictly to resuspension, and this case produces the same volume response as the resuspension-only case in Section 5.5.2. Thus, the total volume increase with no sedimentation was identical to the total volume increase under resuspension only. Because coagulation was present in one case and absent in the other, the forms of the volume distributions and the total number concentrations obviously differed.

The plots of volume distribution results for sedimentation without resuspension or coagulation (Figure 5.19b) are most similar to those for sedimentation and resuspension without coagulation (Figure 5.15a). Their common feature is that neither case has coagulation to bring about particle growth. In both cases, small particle ($d_p \leq$ mode) values of the two sets of volume PSDs remain constant through space. For larger sizes in the former case (with sedimentation alone), the volume distribution gradually decreased due to net sedimentation flux. For larger sizes in the latter case (with resuspension), the volume distribution gradually increased due to the net resuspension flux. Without coagulation and resuspension, the sedimentation-only conditions did not result in the appearance of any very large particles, *i.e.*, particles larger than those present in the inflow distribution.

5.6 IDEAL SYSTEM PARAMETER SENSITIVITY

Varying degrees of state variable response can be elicited (mathematically and physically) from different systems subject to different forcing functions and system conditions. In the last section, the ideal rectangular system was examined in the context of absolute process influences. Steady-state system responses to size-dependent particle transport and reaction processes were analyzed. The method used was to consider the

effects of on-off process combinations. For this section, all three processes remained active. Analysis was of steady-state system response to relative variations in the conditions controlling process action. In other words, the model was subjected to a sensitivity analysis. Conditions included key process parameters and system descriptors.

5.6.1 Sensitivity analysis approach

Sensitivity analysis allows the identification of the parameters which have significant impact in the simulated response of a state variable. This analysis is of great value in aiding the decisions of when or where to allocate resources in parameter measurement, estimation, or experimentation; occasionally, sensitivity analysis can aid in the identification of significant vs. insignificant processes. In water quality modeling, the state variable is usually a contaminant species concentration. The parameters are coefficients which describe quantitatively the process kinetics and the system structure. The parameters can be lumped or distributed in space as well as constant or variable in time. The modeling framework employed for this and previous sections has used lumped and steady-state parameters.

The sensitivity coefficient measures the normalized change in state variable response relative to the normalized parameter change. The approach of Beck (1983) has been used in this analysis. The standard response and parameter values are those embodied in the base case, which was described above. In defining the sensitivity coefficient S_{ij} for response variable 'i' to parameter 'j,' the following notation is used:

$$S_{ij} \equiv \frac{\Delta C_i / C_i}{\Delta \beta_j / \beta_j} \qquad (5.17)$$

where

$\overline{C_i}$ ≡ Standard (base case) system response of state variable i

C_i ≡ Non-standard (test case) system response of state variable i

ΔC_i ≡ $C_i - \overline{C_i}$

$\overline{\beta_j}$ ≡ Value of standard (base case) parameter j

β_j ≡ Value of non-standard (test case) parameter j

$\Delta\beta_j$ ≡ $\beta_j - \overline{\beta_j}$

The magnitude of the sensitivity coefficient indicates the importance of accurately estimating a particular parameter. For parameters causing a linear system response, the sensitivity coefficient would have a value of 1.0. For example, doubling the standard parameter value would result in a doubling of the standard state variable system response. A small value of the sensitivity coefficient, *i.e.*, a value much less than unity, indicates either little difference in system response (when using the alternate vs. the standard parameter value), very large relative parameter change, or both.

Note that individual process significance cannot, in general, be ruled out solely on the basis of a small magnitude sensitivity coefficient for that process. The coefficient is based upon the response of the overall system, and a significant process could produce a component response that is exactly offset by the component response from a competing process. If, however, the parameter sensitivity coefficient value is very small given a (physically conceivable) parameter value that corresponds to an inoperative process, then the process can be judged to have negligible effect on system response.

Equation (5.17) can be rearranged and expressed as the product of a constant, positive fraction and a variable, positive or negative slope, *i.e.*,

$$S_{ij} \equiv \left[\frac{\overline{\beta_j}}{\overline{C_i}}\right]\left[\frac{\Delta C_i}{\Delta \beta_j}\right]. \qquad \textbf{(5.18)}$$

This expression reveals that the sensitivity coefficient will vary if the system response is nonlinear, *i.e.*, when $\Delta C_i/\Delta\beta_j$ is not constant. An example of this behavior is given in Figure 5.20, which shows the nonlinear variation of the response/parameter slope with different parameter values. At smaller values of parameter β_j, the sensitivity appears to be of great (negative) magnitude, but at larger values of β_j the sensitivity appears to be of small (negative) magnitude. The sensitivity in the neighborhood of the standard parameter value, indicated by the solid tangent line, is in between the two extremes. Approximating the standard case sensitivity (*i.e.*, as $\Delta\beta_j \rightarrow 0$) using the lower and upper parameters yields underestimates and overestimates, respectively, using the two-point estimates of (5.17).

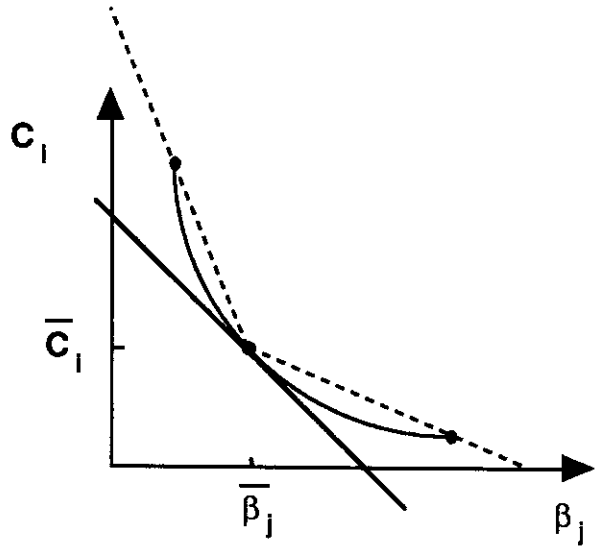

Figure 5.20 Variation in Sensitivity Coefficient with Parameter Value.

Any of the integral or discrete measures of particle concentration that have been previously presented could be selected as the state variable to represent steady-state system response. The integral particle number, surface area, and volume (mass) concentrations were chosen for this study. Each of these concentrations represents a different aspect of particle behavior that bears on particle and particle-associated behavior. In addition, the point in space chosen for comparison purposes was the mid-depth, downstream outflow node (X = 1.0, Z = 0.4) used in sections above. This location is well-suited to use in the sensitivity analysis for its ability to reflect the cumulative system response.

Parameters considered for sensitivity analysis are discussed in four groups: fluid properties affecting coagulation kinetics, particle properties affecting both coagulation and transport, transport system properties, and bed-water transport coupling properties.

5.6.2 Fluid properties

Many of the model parameters indirectly affect coagulation, but this section focuses on fluid properties that directly affect the kinetics of flocculation. These parameters describe physical and chemical properties of the fluid or the flow field that determine either the interparticle transport or the attachment probability. This group of parameters includes solid-solution interfacial chemistry (particle collision efficiency), fluid temperature, and velocity gradient. The particle collision efficiency is determined by both the solution chemistry and the surface chemistry so could be considered either a "fluid property" or a "suspension property;" it was decided to include this parameter on this section on fluid properties. Table 5.2 includes the results for this first group.

Table 5.2

SENSITIVITY ANALYSIS for FLUID (COAGULATIVE) PROPERTIES.

(Using system response concentrations at mid-depth outflow, [X, Z] = [1.0, 0.4])

	Condition	Base Case	Alpha-1	Alpha-2	G-1	G-2	Temp-1	Temp-2
Parameter	**[Units]**							
α_{chem}	[-]	0.2	**0.0**	**1.0**	0.2	0.2	0.2	0.2
G	[s^{-1}]	10	10	10	**1**	**50**	10	10
T	[° K]	293	293	293	293	293	**277**	**303**
ρ_f	[g/cm^3]	0.998	0.998	0.998	0.998	0.998	**1.000**	**0.9956**
μ	[g/cm-s]	0.0100	0.0100	0.0100	0.0100	0.0100	**0.0157**	**0.00798**
$\nu = \mu/\rho_f$	[cm^2/s]	0.0100	0.0100	0.0100	0.0100	0.0100	**0.0157**	**0.0080**
Response								
TNUM	[#/cm^3]	2.066 e6	5.200 e6	5.087 e5	2.929 e6	1.213 e6	2.475 e6	1.847 e6
TAREA	[cm^2/L]	151.1	227.6	63.22	190.1	92.86	163.9	143.2
TSS	[mg/L]	10.26	10.64	7.930	10.59	9.106	10.91	9.823
Sensitivity		{basis =>}	{α_{chem}}	{α_{chem}}	{G}	{G}	{ν}	{ν}
S_{ij} - TNUM	[-]		-1.517	-0.188	-0.464	-0.103	0.348	0.527
S_{ij} - TAREA	[-]		-0.506	-0.145	-0.287	-0.096	0.149	0.259
S_{ij} - TSS	[-]		-0.037	-0.057	-0.036	-0.001	0.111	0.212

Key:
(Parameters defined in text.)

TNUM = Integral (Total) Number Concentration
TAREA = Integral (Total) AreaConcentration
TSS = Integral (Total) Mass Concentration

Particle collision efficiency effects have already been addressed in the on/off approach of Section 5.5; considered here is the relative sensitivity to the parameter α_{chem}, the collision efficiency coefficient. This coefficient has a theoretical range of 0.0 (no collisions produce attachment) to 1.0 (where every predicted collision produces attachment). The base case parameter value used was 0.2, a magnitude whose selection was discussed in sections above.

The sensitivity of the system total number concentration response to α_{chem} was of the type illustrated in Figure 5.20, *i.e.*, both nonlinear and negative. System response was very sensitive in the low range of parameter values, as reflected in the sensitivity coefficient of -1.571, confirming the results reviewed in Section 5.5 for coagulation turned off. By virtue of the two-point estimate, the coefficient was actually underestimated. The coefficient reported had the largest (albeit negative) magnitude of any of the total number concentration/parameter sensitivity coefficients in this study. The system response was not as sensitive to values of the parameter chosen from the upper end of the feasible range, with S_{ij} of -0.188. It is believed that a monotonal system response exists and that in the mid-range (values of α_{chem} near the base case), the system response is moderately sensitive to the parameter value.

By the nature of the particle size distribution, the sensitivity of the total area and mass (derived from volume) concentration responses to α_{chem} was less than for the total number concentration. Changing the collision efficiency value had obvious impacts on the absolute area and mass concentrations as noted in Table 5.2. This simulation illustrates that small sensitivity coefficients do not necessarily mean that system response changes are also small. Surface area concentrations were modified substantially in response to α_{chem} changes. Mass concentrations did not change

substantially in the absence of coagulation because of resuspension dominance, which was discussed in Section 5.5. Conditions producing perfect attachment, however, reversed the net vertical flux such that mass concentrations were reduced absolutely (with longitudinal distance) as well as relative to the base case.

In both absolute and relative terms, *i.e.*, in absolute system concentration responses as well as in sensitivity coefficients, variations in the velocity gradient parameter G did not produce as much influence as had α_{chem}. A reduced G of 1.0 s^{-1} represents an average condition in the upper water column of a lake or marine system. The conditions represented by a velocity gradient of 50 s^{-1} could be encountered in a turbulent coastal environment, a shallow lake during a storm, or a large, swift river.

Reduction of G from 10.0 s^{-1} to 1.0 s^{-1} caused substantially less coagulation to occur; the resulting number, surface area, and mass concentration system responses were thus all greater than in the base case. Sensitivity of the number concentration was again the most responsive to the parameter change. The effect of reduced velocity gradient on the mass concentration was relatively weak, while the effect on surface area concentration was moderate.

Compared against the decreased velocity gradient outcomes, the increased velocity gradient caused larger absolute changes in concentration responses but smaller relative changes in sensitivity coefficients. Enhanced coagulation reduced the number concentrations seen in the base case. Larger flocs which were created were also able to settle out of the system to a greater extent. The surface area associated with the larger, remaining particles was also reduced.

Simulations conducted with temperature as the controlling parameter were actually influenced by several kinetic and transport characteristics and rate expressions.

As noted in Table 5.2, included among the fluid properties are the density ρ_f, absolute (dynamic) viscosity μ, and kinematic viscosity ν. These fluid properties directly affect settling velocities as well as collision frequencies due to Brownian motion and differential sedimentation. Because of the predominance of fluid transport effects, kinematic viscosity was treated as the model parameter. In the environmental temperature range examined, 4° to 30° C, the viscosity ν undergoes a much greater relative change than the absolute temperature.

The most interesting observation associated with the temperature responses and sensitivity coefficients concerns the mass concentrations. Although the absolute TSS responses did not change substantially from the base case, the sensitivity of TSS to viscosity was larger than its sensitivity to α_{chem} or G, as can be seen in Table 5.2. It is noted that the relative changes in the viscosity parameter were small, at least in comparison to the relative collision efficiency and velocity gradient changes discussed above. In this case, the product of a small relative parameter change and a large sensitivity coefficient yielded a small relative system response.

5.6.3 Particle and suspension properties

Properties describing the particle and suspension include the effective particle density (ρ_p) and the initial particle size distribution (PSD). The floc density is a strict parameter, and its effect on system response was indirectly examined in the no-sedimentation ($\rho_p = \rho_f$) process analysis in Section 5.5. Initial PSD is not a process or system parameter, but an initial condition for the propagation or evolution of the PSD in the system. Development of the base case particle density and initial PSD from field information was presented above.

Integral concentration and sensitivity analysis results for the density and PSD simulations are presented in Table 5.3, and the density findings are discussed first. All density cases used the same PSD at the upstream boundary as their initial condition, so their number, area, and volume PSDs were identical at the boundary. Differences among the particle densities in the four simulations (including the base case) yielded different initial mass concentrations, which are reported in Table 5.3.

Special treatment was needed for the mass response analysis. The absolute integral mass concentration responses could be directly compared, if desired, as long as normalization for density is made. Alternately, the fractional loss (gain) through the system (upstream to downstream) for each case could be compared directly using the individual values given for TSS initial conditions and TSS responses. The adjustment for density must be made for a legitimate sensitivity analysis of "TSS" response. These normalizations of the "TSS" response were made to arrive at the TSS sensitivity coefficients reported in the table. The TSS sensitivity coefficients presented actually correspond to total volume concentration responses, which is a more rational test of the density influence.

Sensitivity analyses for the densest particle case, $\rho_p = 2.0$, showed the negative coefficients expected for the integral responses. As density increased, all integral concentrations decreased. Although the absolute number concentration decreased for the denser solids, the change was relatively small. The change was likely the result of greater net sedimentation rather than substantially enhanced flocculation by differential sedimentation. This statement is made because of the much larger sensitivity coefficient obtained for TSS (volume). The 'normal' relationship between the sensitivity coefficients (most cases have $S_{TNUM,j} > S_{TSS,j}$) is reversed in the dense particle case,

Table 5.3

SENSITIVITY ANALYSIS of PARTICLE & SUSPENSION PROPERTIES.

(Using system response concentrations at mid-depth outflow, [X,Z] = [1.0, 0.4])

	Condition	Base Case	Den-1	Den-2	Den-3	Wconc-1	Wconc-2
Parameter	**[Units]**						
ρ_p	[g/cm^3]	1.35	**2.0**	**1.06**	**0.998**	1.35	1.35
ρ_f	[g/cm^3]	0.998	0.998	0.998	0.998	0.998	0.998
Initial PSDs	[-]	Base	Base	Base	Base	**Base x 10**	**Base / 10**
TSS @ B.C.	[mg/L]	9.844	14.58	7.729	7.277	**98.44**	**0.9844**
Response							
TNUM	[#/cm^3]	2.066 e6	1.954 e6	1.451 e6	2.140 e6	2.401 e6	5.337 e5
TAREA	[cm^2/L]	151.1	131.5	136.6	168.1	309.4	34.10
TSS	[mg/L]	10.26	11.83	9.603	9.707	45.01	2.465
Sensitivity		{basis =>}	{ρ_p}	{ρ_p}	{ρ_p}	{B.C. Concentrations}	
S_{ij} - TNUM	[-]		-0.112	1.386	-0.138	0.018	0.824
S_{ij} - TAREA	[-]		-0.269	0.445	-0.432	0.116	0.860
S_{ij} - TSS	[-]		-0.460	-0.894	-1.074	0.376	0.844

Key:
(Parameters defined in text.)

TNUM = Integral (Total) Number Concentration
TAREA = Integral (Total) Area Concentration
TSS = Integral (Total) Mass Concentration

and this reversal can only arise from the significantly enhanced net sedimentation from the water column. Enhanced sedimentation does not mean reduced coagulation or even diminished importance of coagulation, which could only be established with a simulation of dense, stable particles.

Although the very low density, no-sedimentation case ($\rho_p = \rho_f = 0.998$) was analyzed in Section 5.5.3, it was not done in the context of parameter sensitivity. Again, the expected sensitivities (negative) were found; a reduction in density produced larger system responses. Like the greater density case above, the mass (volume) sensitivity was larger than the number sensitivity. Total collision frequencies were not changed so markedly by the absence of differential sedimentation as to cause strong modification of the base case total number concentration. The relative system mass response was very sensitive to the density reduction, however, with a sensitivity coefficient magnitude greater than unity.

The intermediate density simulation ($\rho_p = 1.06$) produced interesting, yet seemingly contradictory results. The absolute mass concentration increased through the system as expected, due primarily to net resuspension dominance. The total number and area concentrations both decreased substantially, however. Obviously, the smallest particles were flocculating to a considerable degree to reduce number and area, while resuspension was adding mass that could not be effectively removed by sedimentation. These distinctions, when compared with the no-density difference case just reviewed, call for a revised interpretation that identifies a much greater importance on collision by differential sedimentation. Though the absolute density difference between the two

and this reversal can only arise from the significantly enhanced net sedimentation from the water column. Enhanced sedimentation does not mean reduced coagulation or even diminished importance of coagulation, which could only be established with a simulation of dense, stable particles.

Although the very low density, no-sedimentation case ($\rho_p = \rho_f = 0.998$) was analyzed in Section 5.5.3, it was not done in the context of parameter sensitivity. Again, the expected sensitivities (negative) were found; a reduction in density produced larger system responses. Like the greater density case above, the mass (volume) sensitivity was larger than the number sensitivity. Total collision frequencies were not changed so markedly by the absence of differential sedimentation as to cause strong modification of the base case total number concentration. The relative system mass response was very sensitive to the density reduction, however, with a sensitivity coefficient magnitude greater than unity.

The intermediate density simulation ($\rho_p = 1.06$) produced interesting, yet seemingly contradictory results. The absolute mass concentration increased through the system as expected, due primarily to net resuspension dominance. The total number and area concentrations both decreased substantially, however. Obviously, the smallest particles were flocculating to a considerable degree to reduce number and area, while resuspension was adding mass that could not be effectively removed by sedimentation. These distinctions, when compared with the no-density difference case just reviewed, call for a revised interpretation that identifies a much greater importance on collision by differential sedimentation. Though the absolute density difference between the two cases (Den-2 and Den-3) was small, substantially much more flocculation occurred in the Den-2 case ($\rho_p = 1.06$) as evidenced by the differences in the number and area

concentrations; coagulation by differential sedimentation was the lone process capable of causing the differences between these two cases.

The initial condition PSD was also examined in a simple way to determine its influence on state variable response sensitivity. Using the same relative size distributions that have been used in all simulations and discussions to this point, their absolute concentrations were adjusted in two simulations. A 'high' initial condition PSD was obtained by multiplying all discrete, base case concentrations by a factor of 10, and a 'low' initial condition PSD was obtained by dividing the base case concentrations by a factor of 10. The actual initial integral mass concentrations for the two cases are shown in Table 5.3. These two conditions could correspond to a very concentrated suspension inflow and a very dilute suspension inflow.

Absolute concentration responses due to modifications of initial PSD are readily analyzed, following the approach discussed in the density cases above. All initial concentrations would be 10 (or 1/10) times the base case initial concentrations. Because the PSD modifications were not modifications of a strict parameter value, but an initial condition, sensitivity coefficient analysis followed a different approach than in the density cases. The relative change in initial conditions (PSD) was treated as a relative change in a system perturbation, and this perturbation performs the same function as a process parameter in (5.17).

In the 'high' concentration case, the relative perturbation change (for each of the three system response concentrations) was a factor of nine, as in

$$S_{ij} \equiv \frac{\Delta C_i / C_i}{\Delta PSD / PSD}$$

or

$$S_{ij} \equiv \frac{\Delta C_i / \overline{C_i}}{(10 - 1)/1} .$$

In the 'low' concentration case, the analogous relative perturbation change was a factor of -0.9, as seen in

$$S_{ij} \equiv \frac{\Delta C_i / \overline{C_i}}{(0.1 - 1)/1} .$$

The coagulation reaction is a second-order reaction. The consequences of this second-order nature, manifest in the results for higher and lower initial concentrations, were that the fractional removals through the system changed as compared to the base case. For the higher initial PSD case, the accelerated kinetics increased fractional removals for all integral concentrations. For the lower initial PSD case, the slower kinetics decreased fractional removals for all integral concentrations.

Sensitivities to the PSD changes were generally as anticipated, *i.e.*, the coefficients were positive in all cases. Magnitudes of the low PSD coefficients were all greater than their high PSD counterparts, which resulted because of its smaller normalized perturbation. As with the largest and smallest (but not the intermediate) density cases, the mass responses for the modified PSD were generally more sensitive than the number and area responses. Again, the direct connection of the modified PSD to the sedimentation flux, on top of the flocculation influence, reversed the sensitivity order which had been seen in the primarily coagulation-dominant sensitivity simulations for collision efficiency, velocity gradient, and temperature.

5.6.4 Fluid transport properties

Parameters considered to be properties of the fluid transport system include mean longitudinal advective velocity, dispersion coefficients, and system depth. These properties are discussed in this section. Longitudinal advection and dispersion are presented first, followed by vertical depth and dispersion.

Changes in the longitudinal advective velocity yielded pronounced changes in the integral particle concentrations. Table 5.4 contains a summary of the relevant parameter values, system responses, and sensitivity coefficients. All parameters listed in the table are mean values. The vertical profile of longitudinal velocity actually used in the transport model (U_x) had the logarithmic distribution characteristic of open channel flow. As a result of the logarithmic velocity profile in open channel flow, the vertical mixing coefficient (E_z) should also be vertically distributed, but in a parabolic profile, symmetric about the mid-depth, H/2. Due to numerical difficulties, however, a constant, depth-averaged value of the vertical mixing coefficient was used in the transport model. The mean vertical mixing coefficient is, for a constant channel depth, linearly related to the mean longitudinal velocity. For purposes of discussing the effects of velocity on system responses, it can be noted here that the small changes in vertical mixing coefficient would have insignificant effect on system responses.

Reducing the fluid velocity to one-half of the base case value produced marked decreases in all system concentrations. In response to the low mean velocity, the induced shear stress at the bed was less than the empirically set critical bed shear stress, the threshold for bed resuspension. A no-resuspension case was thus the result of reduced velocity. System response sensitivities were all substantial, decreasing in magnitude from number to area to mass. For conditions such as the cessation of

Table 5.4

SENSITIVITY ANALYSIS of LONGITUDINAL FLUID TRANSPORT.

(Using system response concentrations at mid-depth outflow, [X, Z] = [1.0, 0.4])

		Base Case	Ux-1	Ux-2	Ex-1	Ex-2
Parameter	**[Units]**					
U_x	[cm/s]	6.54	**3.27**	**13.08**	6.54	6.54
H	[cm]	410.	410	410	410	410
E_x	[cm^2/s]	100.	100	100	**10**	**10,000**
E_z	[cm^2/s]	8.94	**4.47**	**17.88**	8.94	8.94
Response						
TNUM	[$\#/cm^3$]	2.066 e6	1.220 e6	4.064 e6	2.065 e6	2.075 e6
TAREA	[cm^2/L]	151.1	101.9	453.7	150.88	151.2
TSS	[mg/L]	10.26	7.451	51.88	10.25	10.25
Sensitivity		{basis =>}	$\{U_x\}$	$\{U_x\}$	$\{E_x\}$	$\{E_x\}$
S_{ij} - TNUM	[-]		0.819	0.967	0.0005	0.000
S_{ij} - TAREA	[-]		0.651	2.003	0.002	0.000
S_{ij} - TSS	[-]		0.547	4.057	0.001	0.000

Key:
(Parameters defined in text.)

TNUM = Integral (Total) Number Concentration
TAREA = Integral (Total) Area Concentration
TSS = Integral (Total) Mass Concentration

resuspension and an increased residence time in the system, this trend indicates that flocculation's influence in system response increased more than sedimentation's influence.

Increasing the system fluid velocity to double the base case velocity caused even greater absolute and relative concentration changes than halving the velocity had. The system area and mass concentration sensitivities of 2.0 and 4.0 were the largest seen in all of the sensitivity analyses. The bed shear stress is proportional to the square of the fluid velocity. Since the higher velocity produced greater bed shear stress and enhanced the resuspension flux, the mass-based flux would be expected to create strong response in mass concentration.

Longitudinal mixing coefficient, E_x, had virtually no effect on the (absolute and relative) system responses. This was expected. In this system, at steady-state and with gradual particle fluxes and reaction rates, only small longitudinal concentration gradients existed. The product of the longitudinal concentration gradient and the longitudinal mixing coefficient must be large, however, for a substantial dispersive flux. Given the small longitudinal concentration gradients, even radical changes in longitudinal mixing coefficient produced physically and numerically insignificant differences in the two-dimensional behavior of the particles.

The depth, H, and vertical mixing coefficient, E_z, parameters were varied to examine their influence on system response. Simulation parameters and results are presented in Table 5.5. In order to compare results on an equivalent travel time basis, the mean longitudinal velocity was identical in all cases, equal to the base case velocity. As mentioned above, the vertical mixing coefficients used in the transport simulations

Table 5.5

SENSITIVITY ANALYSIS of VERTICAL FLUID TRANSPORT PROPERTIES.

(Using system response concentrations at mid-depth outflow, [X, Z] = [1.0, 0.4])

		Base Case	Depth-1	Depth-2	Ez-1	Ez-2	Ez-3	Ez-4	Ez-5
Parameter	**Units**								
H	[cm]	410	**820**	**205**	410	410	**820**	**2050**	**2050**
E_z	[cm^2/s]	8.94	**17.88**	**4.47**	**89.4**	**1.0**	**1.0**	**1.0**	**0.1**
$\tau = H^2/E_z$	[s]	1.87 e4	3.761 e4	9.402 e3	1.880 e3	1.681 e5	6.724 e5	4.202 e6	4.202 e7
$P_e = Hv(d_m)/E_z$	[-]	1.917 e-2	1.875 e-2	1.918 e-2	1.903 e-3	1.538 e-1	2.719 e-1	1.041	10.11
Response									
TNUM	[#/cm^3]	2.0657 e6	2.052 e6	2.094 e6	2.135 e6	2.065 e6	2.061 e6	1.479 e6	1.485 e6
TAREA	[cm^2/L]	151.10	149.6	153.1	153.6	149.7	147.2	126.2	126.2
TSS	[mg/L]	10.259	10.11	10.40	10.32	9.96	9.50	9.78	9.71
Sensitivity		{basis=>}	$\{H^2/E_z\}$	$\{H^2/E_z\}$	$\{H^2/E_z\}$	$\{H^2/E_z\}$	$\{H^2/E_z\}$	$\{H^2/E_z\}$	$\{H^2/E_z\}$
S_{ij} - TNUM	[-]		-0.007	-0.027	-0.0001	-0.0001	-0.0001	-0.001	-0.0001
S_{ij} - TAREA	[-]		-0.010	-0.027	-0.001	-0.001	-0.0007	-0.001	-0.0001
S_{ij} - TSS	[-]		-0.014	-0.028	-0.004	-0.004	-0.002	-0.0002	0.0000

Key:
(Parameters defined in text.)

TNUM = Integral (Total) Number Concentration
TAREA = Integral (Total) Area Concentration
TSS = Integral (Total) Mass Concentration

were vertical averages. The open channel relation between velocity and vertical mixing was bypassed in the model for this sensitivity analysis.

Because of the competing effect of depth and vertical mixing on the rate of vertical transport, a composite parameter was used to relate the system conditions to responses. The characteristic vertical mixing time, noted in the table amongst the parameters as H^2/E_z, is indicative of the time required for fluid turbulence to mix mass from the air-water boundary to the bed-water boundary or vice versa. For comparison, the characteristic time for longitudinal fluid/particle advection through the system, L/U_x, was 1.47×10^5 [s].

The two depth cases provided a good illustration of the important factors influencing vertical particle behavior. Their respective depths, dispersion coefficients, and mixing times were twice and half those of the base case. For these parameter values, the absolute concentration changes were only in the 1% range, and the sensitivity coefficients were only in the 0.1 to 3% range. Greater depth, with its correspondingly larger open channel flow vertical mixing coefficient, showed concentration decreases in all responses. Having a greater depth to dilute the resuspension flux (constant for all cases) would explain the decreases. Taking a longer time to vertically mix from the bed through the water column would also be an explanation. The shallower depth case, with a reduced mixing coefficient but also a reduced time for vertical mixing, produced larger concentrations. The greatest sensitivity was in the mass concentration response, and this would support either of the two bed flux related arguments.

Five combinations of depth and (velocity-independent) vertical mixing coefficient were used to focus on the vertical mixing process; the characteristic vertical

mixing time is treated as the model parameter. All cases possessed negative sensitivity coefficients for all responses. As with the depth cases, larger characteristic mixing times produced concentration reductions, and shorter characteristic mixing times produced concentration increases. The key determinant in system response appeared to be the characteristic time to disperse bed mass up rather than the depth or the mixing coefficient.

Simulations of deep conditions, cases Ez-4 and Ez-5, produced the smallest number and area concentration responses; these cases thus represented the greatest reductions of the upstream boundary concentration. The deep water column depths and small vertical mixing coefficients established very long characteristic vertical mixing times, time scales that were orders of magnitude longer than the system residence time (*i.e.*, the longitudinal advective time scale). Such large mixing times limited the influence of bed resuspension on the overlying water column. The clearing from the water column of large fractions of smaller particles, evidenced in the small number and area concentration responses at the mid-depth outflow, was certainly assisted by the insufficient time to achieve vertical mixing to that depth.

An integral mass isoconcentration plot of results for case Ez-5, which had the longest vertical mixing time, is presented in Figure 5.21(a). Comparison with the isoconcentration contours for the base case (Figure 5.3) illustrates three important effects for the deep reservoir. First, the base case behavior of net resuspension flux progressing up through the entire water column (via vertical mixing), within the system residence time, did not happen in the deep reservoir of limited mixing. Given the balance of sedimentation and vertical dispersion acting on the particle size distribution

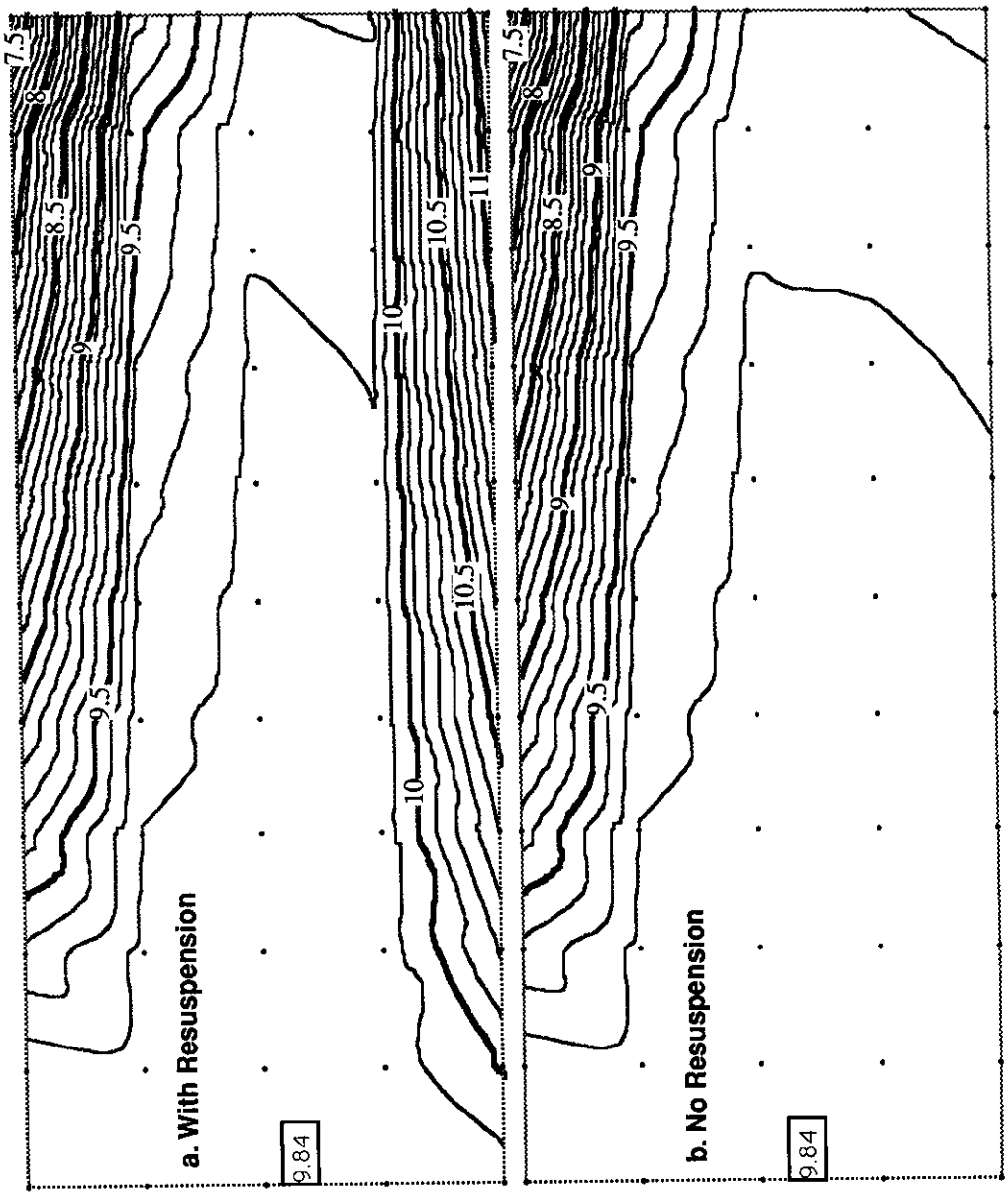

Figure 5.21 Response to Resuspension in Deep Reservoir

in the near bed region, the large vertical gradient of mass concentration would be expected to continue in a reservoir that was extended longitudinally.

A second effect in the deep reservoir, suggested by the mid-depth region of small vertical concentration gradient, was that of stratified flow. Although the uniform vertical dispersion coefficient resulted in a uniform rate of vertical fluid dispersion, conditions in the system actually established a stratified-particle system. The boundary particle flux normal to the fluid flowfield and the counter-dispersive force of gravity on the particles both served to stratify the particles. The water column mid-depth also became a buffer region between regions of net particle mass loss (upper water column) and net particle mass gain (lower water column). In this zone of dynamic equilibrium, loss of mass due to coagulation and sedimentation was offset by sedimentation flux from above and (limited) dispersive resuspension flux from below. Despite the nearly constant mass concentration in the buffer region, the particle size distribution was significantly modified; as mentioned above, the particle number and area concentrations were substantially reduced from inflow to outflow.

The apparent buildup of particle mass in the lower depths of the water column of the deep reservoir with small vertical mixing was not expected, and this raises questions about the influence of coagulation. Although the simulation was specifically designed to evaluate parameter sensitivity, the behavior in such physical systems was also of interest. Lake coagulation modeling results (O'Melia and Bowman, 1984; Weilenmann *et al.*, 1989) have demonstrated reduced particle mass concentrations at depth, in conformance with many field observations. Both of those simulations had incorporated particle production in the epilimnion, however, via implicit or explicit (phytoplankton photosynthesis and death, precipitation, and tributary inflow) source

terms. Both simulations were steady-state solutions, and neither framework included bed resuspension. These are appropriate approaches for evaluating the long-term behavior of most lakes, which function as sediment traps.

The apparent buildup of mass in the deep reservoir was due to resuspension; insufficient vertically mixing time allowed the apparent particle accumulation in the lower depths. This conclusion was confirmed with a numerical simulation of the same system without resuspension, as shown in Figure 5.21(b). The simulation isocontours in the upper half of the water column remained the same as those resulting from resuspension. In the lower half of the water column, however, the bed flux influence was gone and mass concentration was relatively homogeneous. The contours had even begun inverting, as expected for a flocculent sedimentation system. Given sufficient residence time, an upper water column particle source(s), and limited resuspension, it is expected that a decreasing concentration gradient from top to bottom would be realized, as found by others (O'Melia and Bowman, 1984; Weilenmann *et al.*, 1989).

Table 5.5 also includes values of the vertical, mass-mean particle Peclet numbers. The nondimensional Peclet number is commonly used in physical (*e.g.*, reactor transport analysis) and computational (*e.g.*, finite difference solution of advection-dispersion equation) studies to characterize the relative ratio of advection to dispersion. This vertical Peclet number, P_e, has the form

$$P_e \equiv \frac{\overline{v_s} H}{E_z}, \qquad \textbf{(5.19)}$$

where the settling velocity is is the Stokes velocity for the mass-mean diameter and other terms are as previously described.

The Peclet number can also be expressed as

$$P_e \equiv \frac{H^2/E_z}{H/v_s} = \frac{\tau_{disp}}{\tau_{set}}, \qquad (5.20)$$

where the numerators of the fractions are the characteristic time for vertical mixing and the denominators are the characteristic time for particle settling. Obviously there is a Peclet number for each particle size and, given orders of magnitude difference in the heterogeneous particle settling velocities, these discrete Peclet numbers will also vary by orders of magnitude.

For $P_e << 1$, mass-average particle behavior will be dispersion-dominated and will tend to be vertically well-mixed. When $P_e >> 1$, mass-average particle behavior will be advection-dominated (settling-dominated), and particles will tend to settle out. The deep reservoirs of Ez-4 and Ez-5 were the only simulations of moderate to large P_e. As expected, then, these advection-dominated cases had the smallest total number and area concentration responses.

5.6.5 Bed resuspension

Parameters characteristic of bed resuspension include the resuspension rate coefficient and the bed friction factor. The influence of these parameters on system response is presented in this section.

As described in Section 5.2.3 by the bulk mass resuspension flux equation (5.6), the mass flux is assumed to be linearly proportional to the excess shear stress, *i.e.*,

$$J_R = M'(\tau_0 - \tau_c). \qquad (5.6)$$

The flux is zero for a non-positive excess shear stress. A rate coefficient of M' = 0.0 [s/cm] was used for a simulation discussed in Section 5.4 to evaluate the effect of resuspension on the base case system. Variations in the rate coefficient are examined in

this section, as are the indirect effects of friction factor (through the shear velocity) on resuspension flux. Results are summarized in Table 5.6.

Variations in the resuspension rate coefficient produced system responses as expected. Number concentrations, as measured by both integral responses and sensitivity coefficients, were influenced little. As the resuspension flux is modeled as a mass phenomenon, integral number concentration changes are secondary effects. This would indicate that changes in resuspension would produce only small changes in coagulation itself. Of course, sensitivity would be significant in the particular (large diameter) particle classes most affected by resuspension, and the relative dominance of collision mechanisms (particularly differential sedimentation) would be affected.

As mentioned before, all of the results discussed in this chapter represented steady-state responses in the water column, while the sediment bed was not, in general, at steady-state. Net resuspension cases continuously depleted the bed particle inventory, and net sedimentation cases continuously added to the bed inventory. The quantities of all size particles in the bed were so abundant that the relatively insignificant numbers added by sedimentation were ineffective in changing the size distribution. Indeed, the log PSDF of the bed remained constant for the length of all the simulations conducted for this chapter.

The sediment bed particle size distribution effectively represented a Dirichlet (constant function value) boundary condition, and its initial specification thus determined in large part the system response to resuspension. Recall that the bed PSD was assumed, and established, to have larger diameter particles than the normal tributary inflows. A system with a finer bed PSD would thus have a greater impact on

Table 5.6

SENSITIVITY ANALYSIS of BED RESUSPENSION PROPERTIES.

(Using system response concentrations at mid-depth outflow, [X, Z] = [1.0, 0.4])

		Base Case	Rate-1	Rate-2	Rate-3	Fric-1	Fric-2
Parameter	**Units**						
M'	[s/cm]	1.0 e-6	**0.0**	**1.0 e-7**	**1.0 e-5**	1.0 e-6	1.0 e-6
f	[-]	0.020	0.020	0.020	0.020	**0.015**	**0.025**
E_z	[cm^2/s]	8.94	8.94	8.94	8.94	7.74	9.99
Response							
TNUM	[#/cm^3]	2.0657 e6	2.031 e6	2.035 e6	2.354 e6	2.024 e6	2.055 e6
TAREA	[cm^2/L]	151.10	140.4	141.5	237.5	140.1	146.0
TSS	[mg/L]	10.259	8.74	8.90	23.43	8.73	9.51
Sensitivity		{basis=>}	{M'}	{M'}	{M'}	{f}	{f}
S_{ij} - TNUM	[-]		0.017	0.017	0.016	0.082	-0.020
S_{ij} - TAREA	[-]		0.071	0.071	0.064	0.291	-0.136
S_{ij} - TSS	[-]		0.148	0.147	0.143	0.595	-0.293

Key:
(Parameters defined in text.)

TNUM = Integral (Total) Number Concentration
TAREA = Integral (Total) Area Concentration
TSS = Integral (Total) Mass Concentration

number concentrations than did these cases. This system with finer solids in the bed would thus establish a closer link between coagulation and resuspension.

Surface area concentration responses were relatively minor in the cases of zero or low rate coefficient. Surface area concentration response did increase substantially in the high rate case, however, reflecting the increased presence of larger particles.

Mass concentration responses were similar to, but larger than, area concentration responses. The system mass response to the small rate coefficient was not easily distinguished from the case with no resuspension at all. In contrast, the high rate coefficient resulted in a more than doubling of the base case response.

The dimensionless bed friction coefficient, f, determines the magnitude of the shear velocity, the bed shear stress, the resulting vertical profile of longitudinal velocity, and the vertical mixing coefficient. The smaller value of f used, corresponding to a hydraulically smooth bed, yielded a bed shear stress smaller than the critical shear stress. The lack of bed flux into the water column, in conjunction with a reduced vertical dispersion coefficient, gave high positive sensitivities in all integral particle concentrations. With reduced mixing, the system responses were smaller than with no resuspension.

Interestingly, the larger friction factor yielded negative sensitivities and produced smaller system responses than the base case, despite the larger shear stress and faster vertical mixing generated. The effect of the friction factor on the velocity profile is believed to be the cause of this anomaly. Greater friction decreases the near-bed fluid velocities while increasing the near-surface velocities; the mean velocity and volumetric flowrate remain the same regardless of the friction factor (in the rigid-lid

model). With smaller near-bed velocities and larger gross bed fluxes, larger concentrations of particles would be expected to accumulate in the near-bed region.

5.7 SUMMARY OF PARTICLE BEHAVIOR IN IDEAL SYSTEMS

Variations on the idealized prototype allowed several different steady-state analyses to be conducted using the particle transport-transformation model. Following is a summary of the general findings.

Integral analysis of the system particle response can be accomplished, given the spatially distributed particle size distribution. The integral properties of the size distributions allow insight concerning the overall behavior of the suspended and bed solid phases. In certain cases, lumped concentration results appear to follow simple first-order transport-transformation models. The qualitative effects of competing processes that are acting upon the discrete particles can be inferred in certain integral analyses, but quantitative influences due to individual mechanisms cannot be fully determined.

Discrete analyses expose the full power of the discrete particle modeling approach. Size-dependent, mechanistic descriptions of particle behavior lead to deterministic solutions that are best suited to size-dependent analyses. Simple longitudinal and vertical profiles can characterize the important behavior over the domain, as well as the interactions within the suspension and between the bulk water column and bed phases.

Process analyses provided a test of the model itself, as well as the reasonableness of system responses under certain extreme scenarios. Given the ability to turn on or off the primary transport and transformation mechanisms within the model, the model can be applied with greater confidence in divergent types of systems,

where particular mechanisms may be absent. Coagulation, a size-dependent process, was seen to be important in system response in virtually all scenarios.

Parametric studies of the model allowed identification of those parameters whose definition appears most critical in the application of the model. These parameters included the influent size distribution, the collision efficiency and velocity gradient, and the resuspension-related parameters, *i.e.*, the shear velocity (as expressed by friction factor), the critical shear stress, and the bed mass flux rate coefficient. Given these sensitivities, available data can be used with a greater appreciation of its limitations, and process and field studies to support water quality research and management efforts can be planned in a more optimal manner.

CHAPTER VI

MODEL APPLICATION TO REAL SYSTEMS

6.1 INTRODUCTION

The simulations discussed in Chapter 5 were instructional in allowing careful discrimination of individual process effects. Idealized systems of uniform and rectangular cross-section, with only a single, steady inflow, were the basis for those analyses. Those ideal lakes also received boundary particle fluxes at the bed-water interface. In addition to upstream inflow and loading, however, real lakes are subject to the following conditions:

- longitudinal variation of the lake width and depth
- longitudinal spatial distribution of tributary inflow and loading
- temporal variation of upstream and tributary forcing
- inflows enter the system in confined vertical layer.

These additional complexities in geometry and forcing result in significant differences compared to the ideal systems of the previous chapter. The variable morphometry results in acceleration and deceleration of flows. Lateral tributary inflows and loading result in longitudinal concentration responses not seen from simple upstream inflows. Almost regardless of how the lateral boundary tributary loads are distributed over the water column depth, there are vertical concentration responses different from those in the ideal lake considered in Chapter 5. Temporal variations in inflows and loading result in time-variable system accumulation and depletion of mass.

In this chapter, results of the application of a revised model to a real lake are discussed. The lake, Town Lake, is the run-of-the-river impoundment of the Colorado River in Austin, Texas. Town Lake, its watershed, and its hydrologic and particle

conditions and forcing were described in Chapter 3. The simulation results examined in this chapter include lake responses to variable cross-section, longitudinally distributed suspension inflows, quasi-steady annual and seasonal forcing, and unsteady storm flows.

6.2 Approach and Conditions

As for the idealized, uniform, rectangular systems simulated in the previous chapter, ten equally-spaced longitudinal segments were used for the model applications to Town Lake. The cross-sectional areas used for these simulations approximated the variations in the real lake; data are presented in Appendix C and discussed in Section 3.3. The system depth was represented by the lake-average hydraulic depth, as in the uniform cross-section cases. Inflows of fluid and particles were added as source terms at alternating grids, approximating the distribution of the actual major tributaries to the reservoir. Given the very shallow depths of the tributaries, the particle source terms were distributed over the top 30% of the water column.

In the vertical dimension, a rigid lid model was assumed, *i.e.*, the depth was not spatially-variable; lake volume was also considered to be constant in time. Variable system depth was not incorporated for two reasons: first, the bed slopes are relatively mild over the domain, and second, the construction of a new 2-D mesh and difference equations would have been required. Laterally-uniform, logarithmic, vertically-distributed profiles of longitudinal velocity were specified on the basis of the individual cross-sectional average velocities.

Although concentrations were still assumed transversely uniform, modification of the transport equations was required to accommodate the transverse dimension variations. Revised finite difference equations, written for conservation in a prismatic

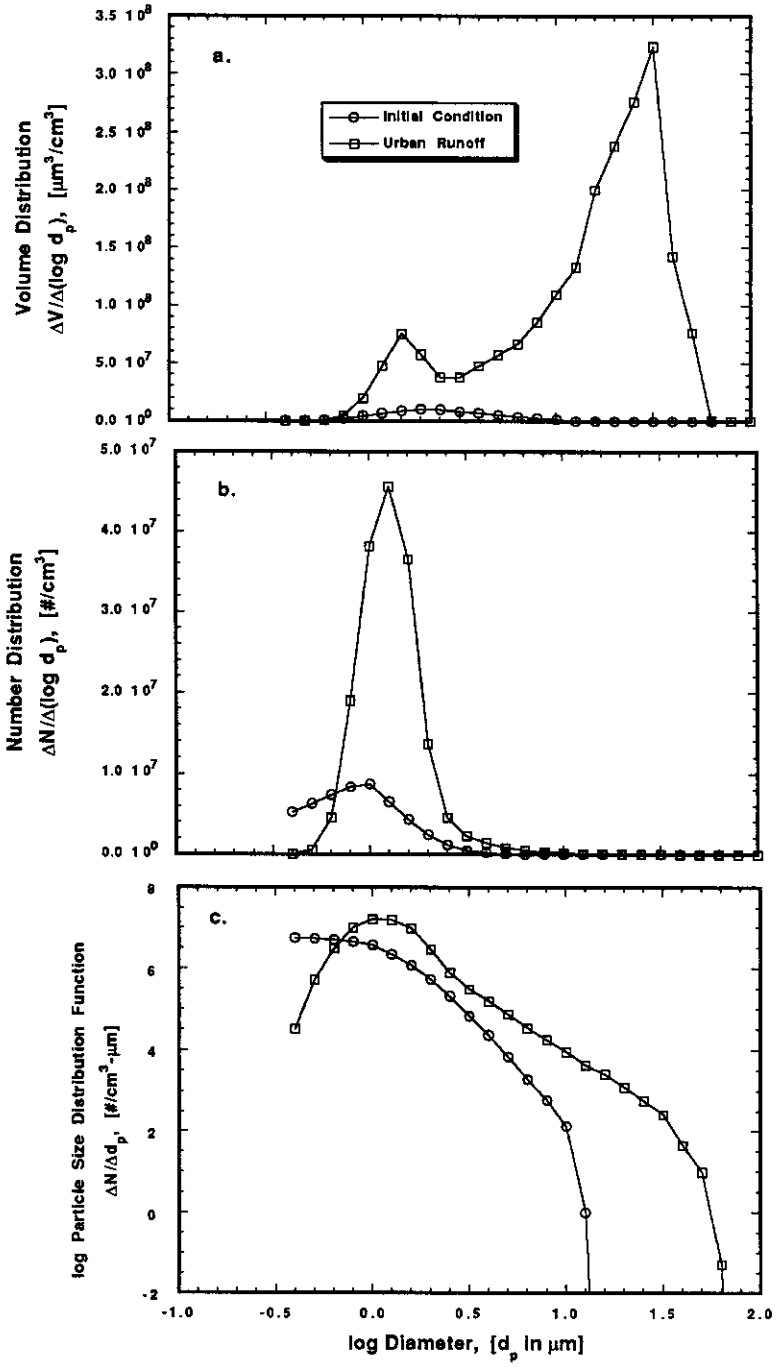

Figure 6.1 **Comparison of Particle Size Distributions in Upstream Inflow and in Lateral Tributaries**

6.3 ANNUAL-AVERAGE BEHAVIOR

6.3.1 Integral annual response

Steady-state integral response to the steady, annual-average conditions in Town Lake are presented and discussed in this section. As presented in Chapter 4, annual steady-state inflows to Town Lake were estimated on the basis of annual upstream releases, annual precipitation, tributary drainage areas, and watershed runoff coefficients. The mean longitudinal velocity varied, generally decreasing with distance, as shown in Figure 6.2(a). For comparison, the mean velocity corresponding to the uniform cross-section of the ideal rectangular system is also indicated. Incremental travel times through each section are inversely related to the velocities, as the sections are equally spaced. Higher than average velocities in the upper half of the reservoir leads to lower than average detention in that half of the system.

A critical measure of perturbation on the system, as demonstrated in Chapter 5, is the bed shear stress, τ_0. As described by a spatially-uniform (lumped) bed friction factor, the local shear velocity is linearly related to the local mean longitudinal velocity. The bed shear stress, however, is proportional to the square of the shear velocity. As shown in Figure 6.2(b), the bed shear stress thus exhibited a greater longitudinal variation than did the mean velocity.

For comparison, the constant shear stress corresponding to the uniform cross-section of the ideal rectangular system is also indicated in Figure 6.2(b). Note that the uniform system bed shear stress was 0.1067 dyne/cm^2 (g/cm-s). Because of the value chosen for the critical bed shear stress τ_c, set at a spatially-uniform 0.1 dyne/cm^2, the normalized excess shear stress $(\tau_0 - \tau_c)/\tau_c$ was always small in the uniform cross-

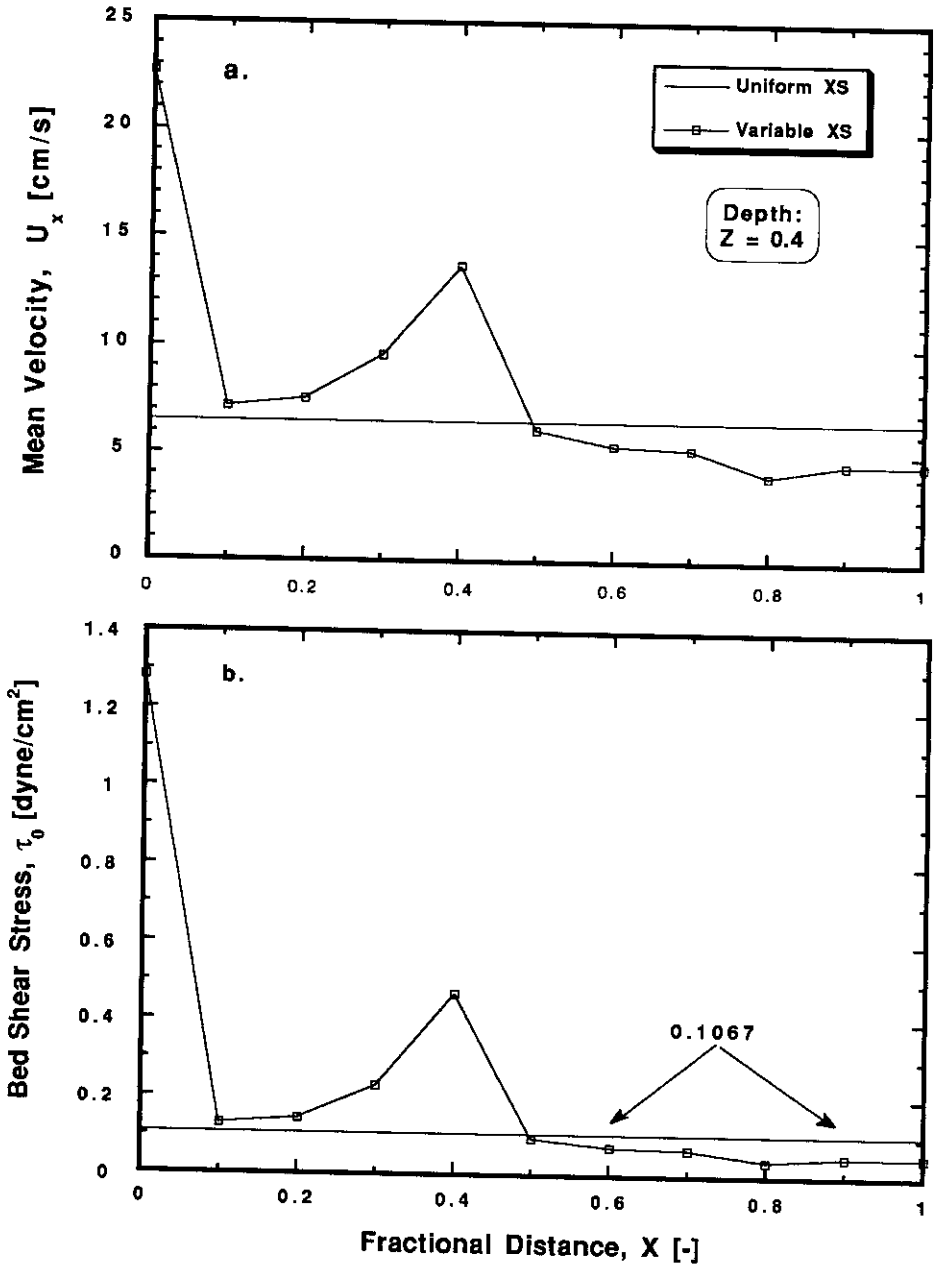

Figure 6.2 **Longitudinal Variation in Annual-Average Velocity and Shear Stress in Town Lake.** (uniform vs. variable cross-sections as noted)

section system. In the "real" system, with spatially variable cross sections and bed shear stress, the excess shear stress was highly variable. Lower segments of the lake produced no resuspension at all under the annual-average conditions, due to negative (zero) excess shear stress. Upper segments of the lake produced considerably more erosional flux in response to greater excess stress than under a uniform flow environment. Because of its location at the fixed concentration (upstream) boundary, neither erosional nor depositional fluxes were allowed at the computational node at $X = 0$.

Mass concentration response to the spatially varying bed shear stress was quite different than for the rectangular base cases. System responses at mid-depth, under conditions of standard coagulation and zero coagulation, are presented in Figure 6.3. In the upper sections of the lake, where relatively large excess shear and relatively small travel times existed, concentrations increased with distance, and the effects of coagulation were not apparent. In the lower sections of the lake, where relatively zero excess shear and relatively long travel times existed, concentrations decreased with distance, and the effects of coagulation were apparent.

Fluid and particle inflows and Town Lake responses are summarized in Table 6.1 for all of the steady-state simulations. Volumetric inflow rates are given for Lake Austin (Q_{head}) and the aggregate tributaries (Q_{tribs}). The suspended solids inflow rates are given for the combined Lake Austin (M_h) and aggregate tributaries (M_t). Ratios of main stem to tributary fluid and particle inflows are also presented. Mean hydraulic residence times for the lake, t_d, are also noted for annual and seasonal conditions. Note that the annual-average residence time is not the arithmetic or time average of the seasonal residence times, but a volumetric average for the year.

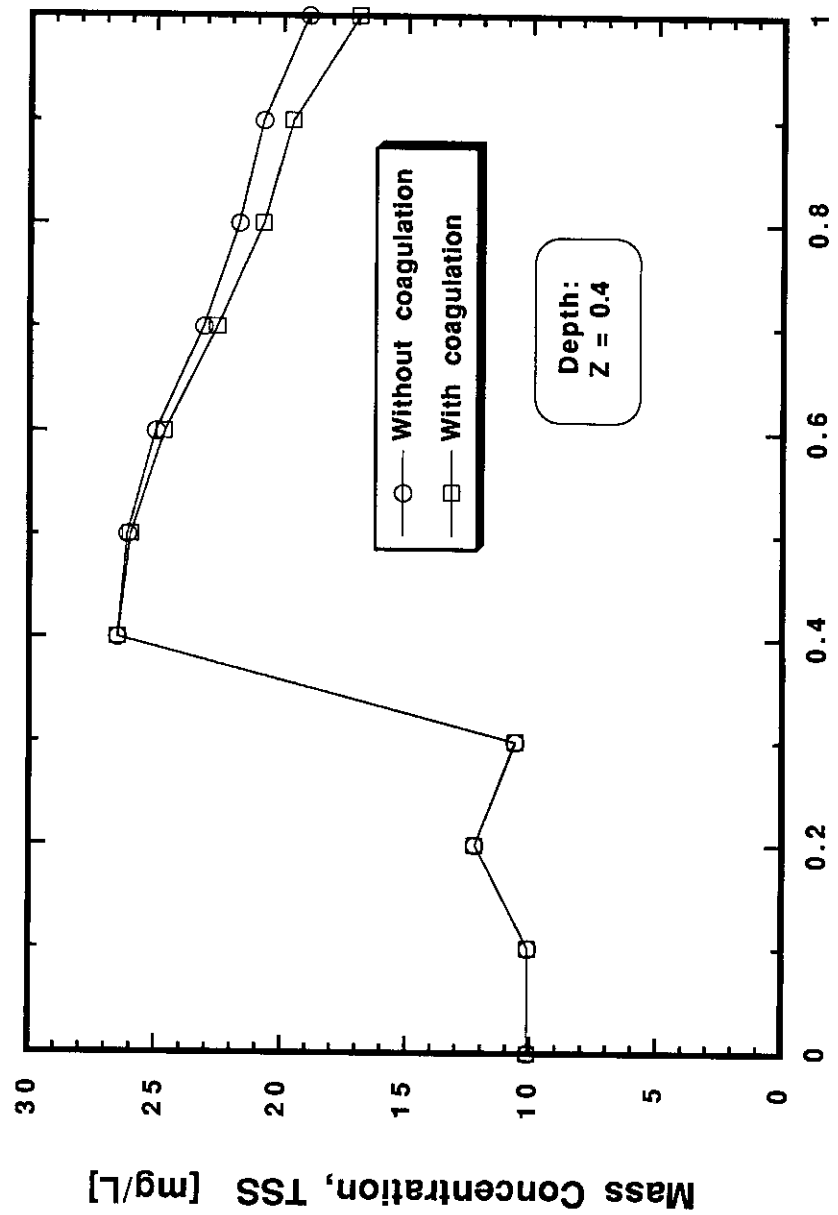

Figure 6.3 Effect of Coagulation on Longitudinal Evolution of Mass Response at Annual-Average Steady-State

Table 6.1

RESULTS OF TOWN LAKE ANNUAL AND SEASONAL STEADY-STATE ANALYSES

(Using system response concentrations at mid-depth outflow, [X, Z] of [1.0, 0.4])

	Condition	Base Case	Annual-w/o coag	Annual-w/ coag	Winter	Spring	Summer	Fall
Parameter	[Units]							
Q_{head}	[m^3/s]	43.04	43.04	43.04	20.88	84.49	56.58	10.21
Q_{tribs}	[m^3/s]	0.000	3.107	3.107	2.604	3.836	3.122	2.866
$Q_t / (Q_h + Q_t)$	[-]	0.000	0.067	0.067	0.111	0.043	0.052	0.219
M_{head}	[kg/d]	36,600	36,600	36,600	17,800	71,900	48,100	8,700
M_{trib}	[kg/d]	0.000	74,000	74,000	62,000	91,300	74,300	68,200
$M_t / (M_h + M_t)$	[-]	0.000	0.669	0.669	0.777	0.560	0.607	0.887
t_d	[d]	1.699	1.660	1.660	3.242	0.844	1.251	6.067
Response								
TNUM	[#/cm^3]	2.0657 e6	6.142 e6	1.982 e6	1.205 e6	3.409 e6	2.478 e6	1.15 e6
TAREA	[cm^2/L]	151.10	327.0	188.5	135.5	377.3	253.9	104.3
TSS	[mg/L]	10.259	18.98	16.97	12.48	42.06	25.88	8.224

Key:
(Parameters defined in text.)

TNUM = Integral (Total) Number Concentration
TAREA = Integral (Total) Area Concentration
TSS = Integral (Total Mass Concentration

For the annual-average conditions presented in Table 6.1, the effects of coagulation were marked in the mid-depth outflow integral concentrations. Despite the relatively short detention time in the reservoir, flocculation produced substantial reductions of number and area concentration when compared to sedimentation alone. Between the two conditions, the small numbers of larger particles remaining in the water column at the outflow led to relatively small differences in mass concentration. As a measure of influence on the particle size distribution, the number-, area-, and volume-average particle diameters in the flocculating system were considerably larger at the mid-depth outflow than their nonflocculative counterparts (25%, 55%, and 42%, respectively).

The two-dimensional isocontours of mass concentration for transport with coagulation vs. transport without coagulation are shown in Figure 6.4. As expected, both simulations indicated net sedimentation in the lower reaches of the system, with coagulation enhancing the kinetics of removal. There appeared to be a region ($0.3 \leq X \leq 0.4$) of significant flux(es) entering the system. In fact, substantial bed flux and tributary sources were both added at $X = 0.4$, the fifth computational node. This location corresponds to i) a narrowed cross-section of the reservoir (Figure 3.5) with higher velocity, shear velocity, bed shear stress, and resuspension mass flux and ii) the reach receiving inflows from the two major tributaries (large particle sources) to the lake, Barton Creek and Shoal Creek (Figures 3.1 and 3.2).

A comment concerning the finite difference approximations and contour construction is appropriate. Recall that contours fitted to simulation results for the discrete points were interpolated from discrete, nodal output. The dense gradients developed between $0.3 \leq X \leq 0.4$ are really artifacts of that interpolation. Although the

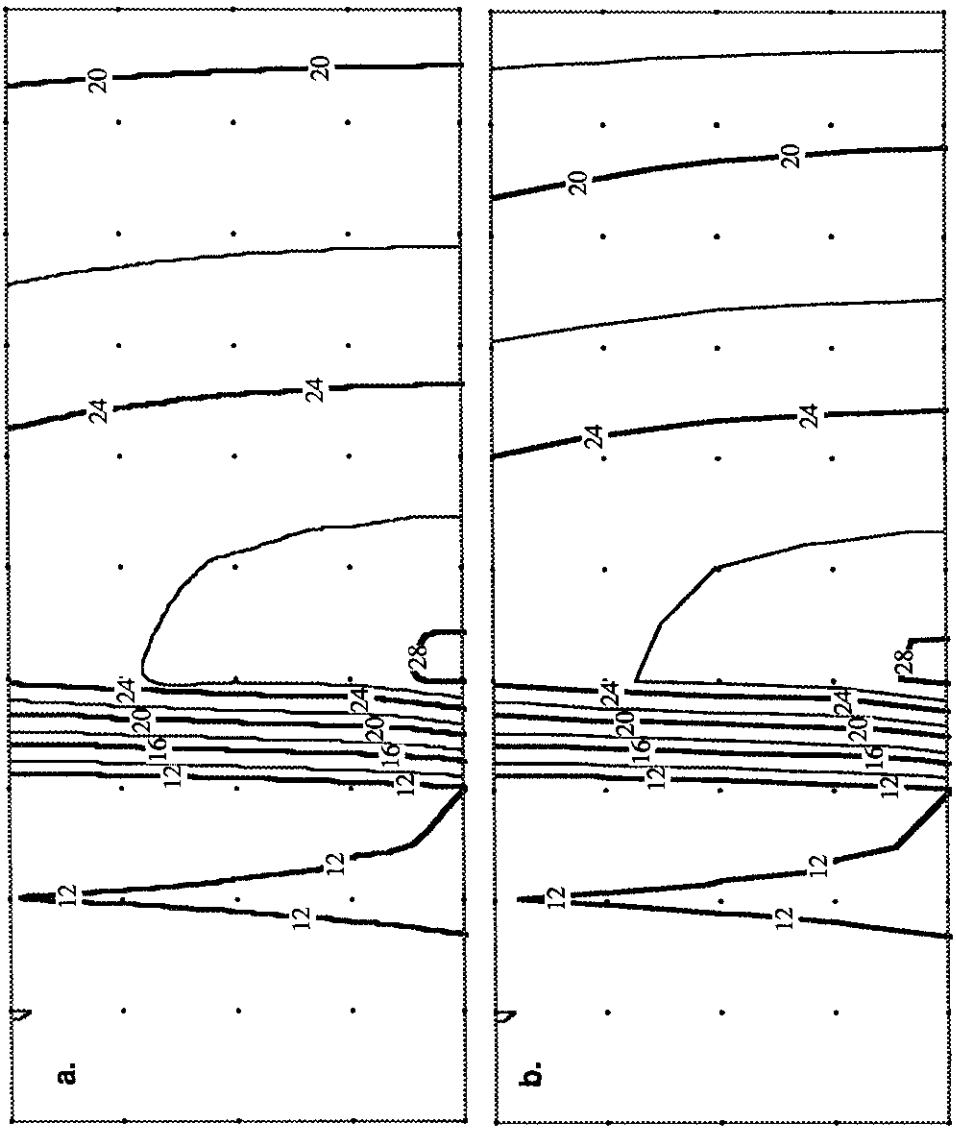

Figure 6.4 TSS Isocontours [mg/L] for Town Lake Annual-Average Conditions.
a. Without Coagulation b) With Coagulation

bed flux might increase in a continuous fashion in this region, we actually expect a discontinuous step response due to the tributary source. The apparent discrepancy is recognized as an artifact of the output treatment, and the results can be viewed appropriately. More on this interpolation is presented in Section 6.5.2.

As noted above, the tributary source terms were distributed over the top 30% of the water column ($0 \leq Z \leq 0.3$) at the longitudinal tributary grids, X = [0.0, 0.2, 0.4, 0.6, 0.8, 1.0]. Fluxes from both top and bottom boundaries thus resulted in more rapid achievement of vertical uniformity than if flux from one boundary had been distributed by vertical dispersion alone, as in the Chapter 5 simulations. The large mass-average particle settling velocities for the tributary inflows served to accelerate the rate of vertical homogenization compared to vertical bed-flux dispersion alone.

6.3.2 Discrete annual response

Examination of the particle size distribution responses in Town Lake to the annual-average conditions provides insight that is not available from the integral analyses. Longitudinal plots of the volume distribution, number distribution, and log particle size distribution function, shown in Figure 6.5, are discussed in this section.

The volume distributions (Figure 6.5a) illuminate the integral behavior discussed in the previous section. The upstream boundary ($X = 0.0$) volume distribution was almost the same as the assumed distribution for Lake Austin. A small inflow of runoff from the first drainage basin of Town Lake was combined in the model with the Lake Austin inflow, over the entire depth of the inflow water column, to produce the distribution seen. Despite the relatively small inflow fraction attributed to runoff, the volume distribution was modified to an extended, bimodal form.

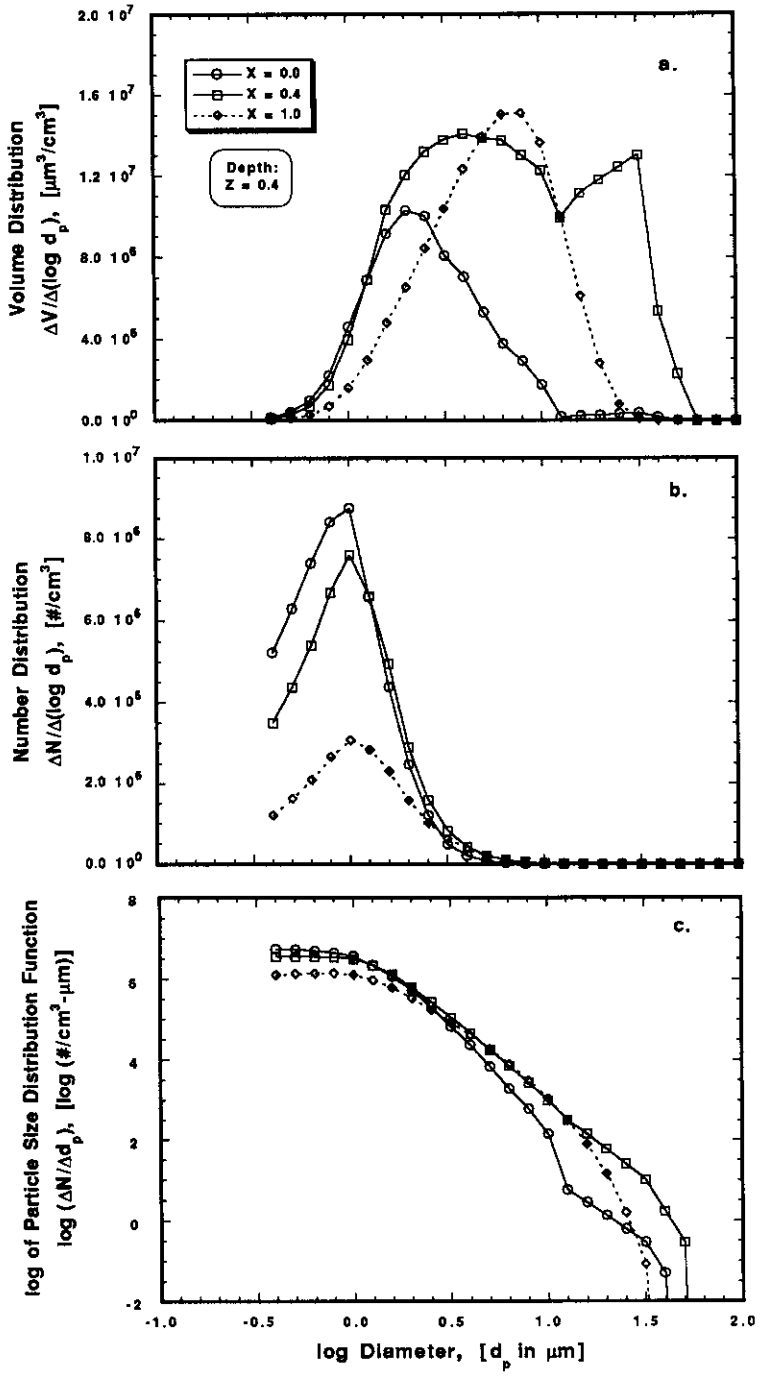

Figure 6.5 **Longitudinal Evolution of Annual-Average Particle Size Distributions in Town Lake**

Volume distribution modifications at mid-lake, X = 0.4, are obvious in Figure 6.5(b). The composite effects of adding small flows of the larger tributary distribution to the large flows of the smaller inflow distribution (*cf.* Figure 6.1a) are quite interesting. A detectable but minor reduction in the concentration of small ($\log d_p \leq 0.3$) inflow particle volume occurred during the travel to mid-lake. At the same time, large particles were appearing from the tributary inflows and the bed resuspension. The two influences can be distinguished by the modal diameters appearing in the distribution. The mode apparent at $\log d_p$ of 1.5 was surely due to the tributaries, which possessed the same mode. It is doubtful that the mode at $\log d_p$ of 0.6 could be the result of growth due to coagulation alone; in the ideal case simulation volume distributions (*cf.* Figure 5.11) the growth of the small-particle-rich distribution in the slower (upstream) lake was only from $\log d_p$ of 0.3 to 0.4 in the same distance and longer time. Resuspension can be identified, by elimination, as the source for the mid-sized particle ($0.4 \leq \log d_p \leq 1.1$) mound seen in the volume distribution.

The loss of particle mass from mid-lake to outflow, discussed in relation to the integral Figures 6.3 and 6.4, can be explicitly assigned to various mechanisms using Figure 6.5(a). Slower velocities in the lower half of the lake, with accompanying increase in residence time and decrease in resuspension, were expected to increase sedimentation. This downstream sedimentation would be expected in virtually any reservoir, and the sedimentation of particles $\log d_p \geq 1.1$ ($d_p \geq 12.6$ μm) was substantial. (An interesting observation, probably not coincidental, is that the largest particle found in the Lake Austin samples was also in the 12 μm size range.)

Coagulation in the lower half of the lake also helped to remove a large amount of particle volume by sedimentation. Most of the particle mass transferred out of the

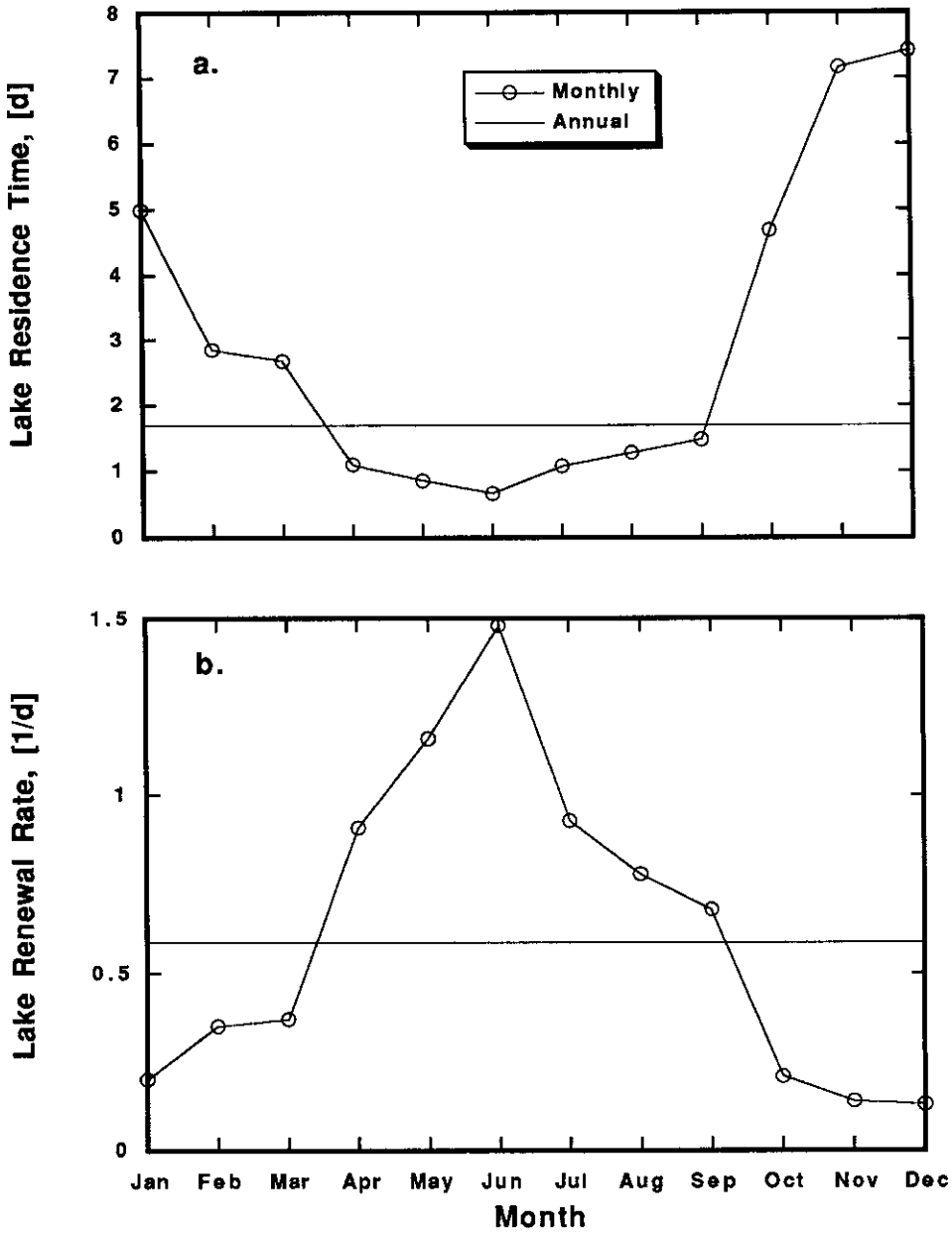

Figure 6.6 **Annual- and Monthly-Average Mean Residence Times and Renewal Rates for Town Lake**

March, and relatively shorter residence times occurred from April to September. For comparison with first-order removal rate coefficients, the inverse residence time (the renewal, or flushing, rate coefficient) was also calculated. Shown in Figure 6.6(b), the renewal rate provides another perspective on the seasonal time-variability of the transport regime.

As presented in Chapter 3, the Austin area has a bimodal rainfall distribution of heavy spring and moderate fall rains (see Table 3.3). There is also the distribution of residence times ranging from relatively 'short' to relatively 'long,' as shown in Figure 6.6(a). Four combinations of stormwater flowrates and residence time in the receiving system exist. These combinations are a) small absolute but large relative tributary inflow combined with long residence time, January through March, b) large absolute but small relative tributary inflow combined with short residence time, April through June, c) moderate absolute but small relative tributary inflow combined with short residence time, July through September, and d) moderate absolute but large relative tributary inflow combined with long residence, October through December. For this study, January through March is called "winter," April through June is called "spring," July through September is called "summer," and October through December is called "fall."

Referring to Table 6.1, the relative inflow contributions from the upstream reservoir vs. the immediate runoff sources is apparent. Urban runoff comprises greater than 10% of the total lake hydraulic inflow in two seasons, the winter and fall. The solids loading contribution from urban runoff is much greater, however, with the minimum seasonal runoff contribution in excess of 50% of the total.

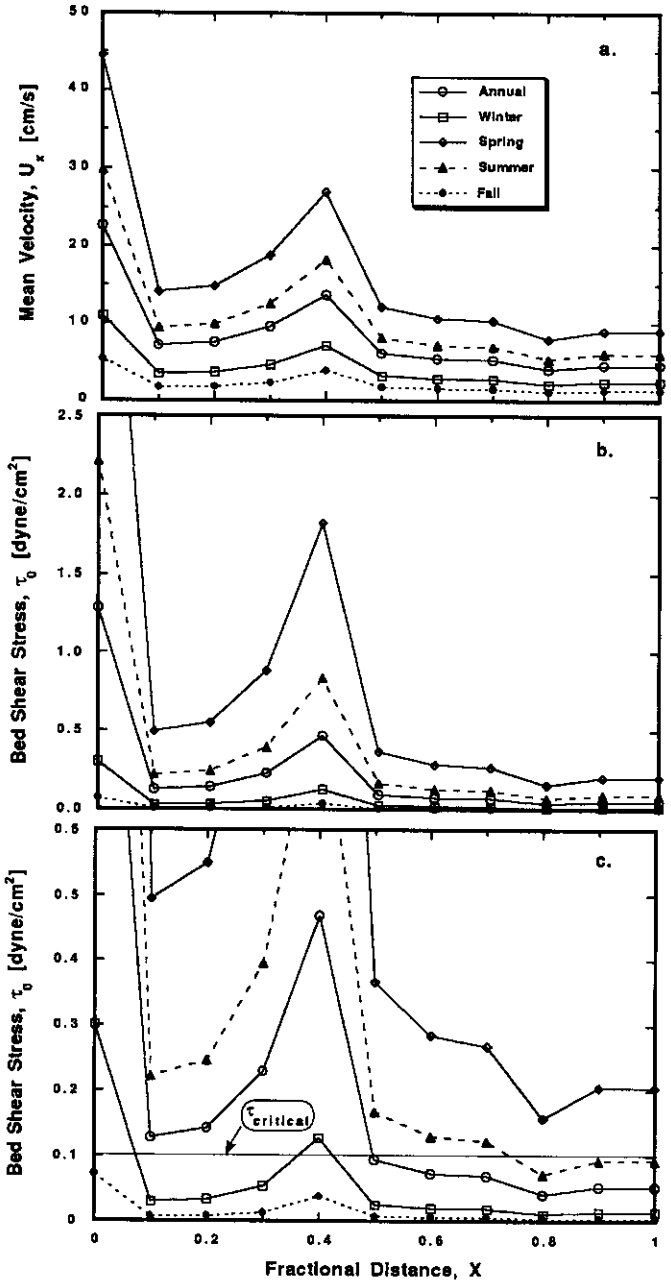

Figure 6.7 **Longitudinal Variation in Seasonal-Average Velocity and Bed Shear Stress in Town Lake**

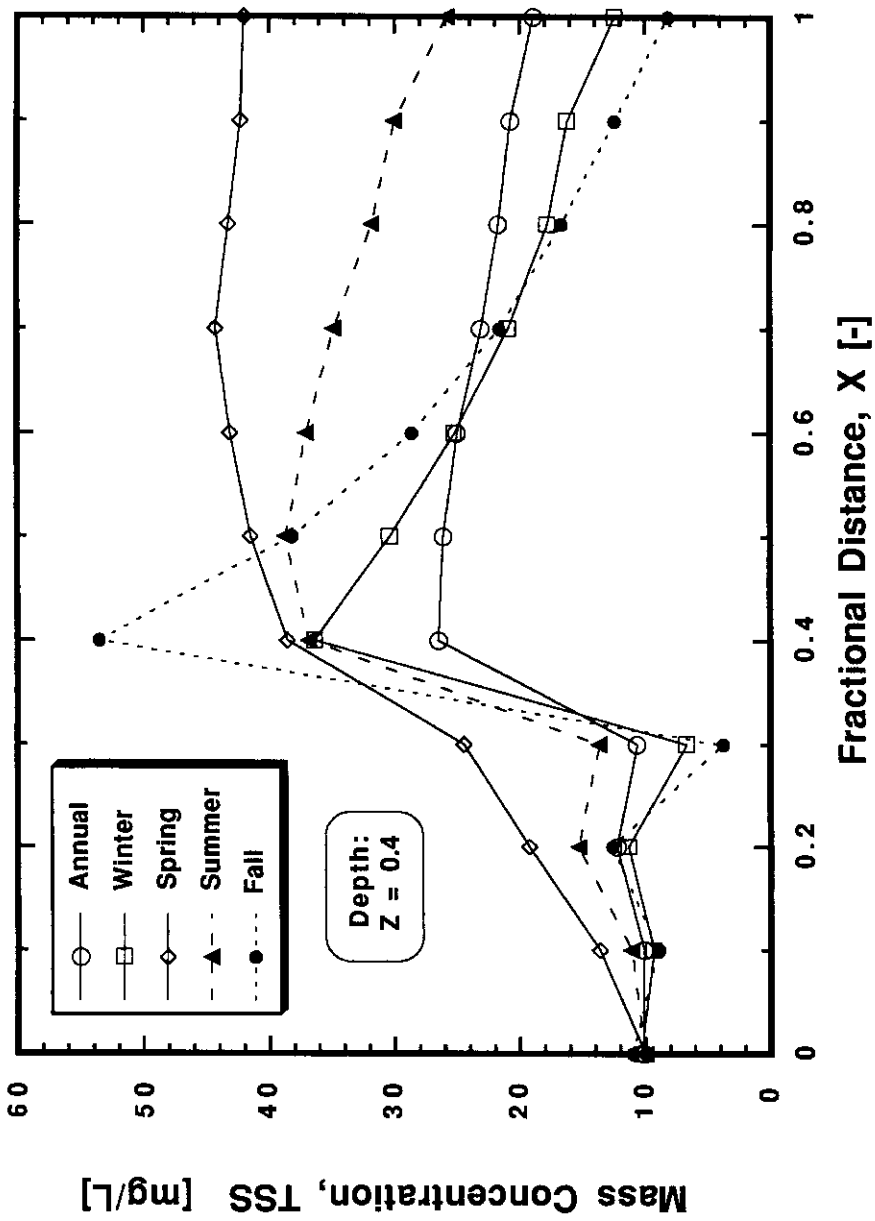

Figure 6.8 Seasonal and Spatial Variation of Suspended Solids in Town Lake

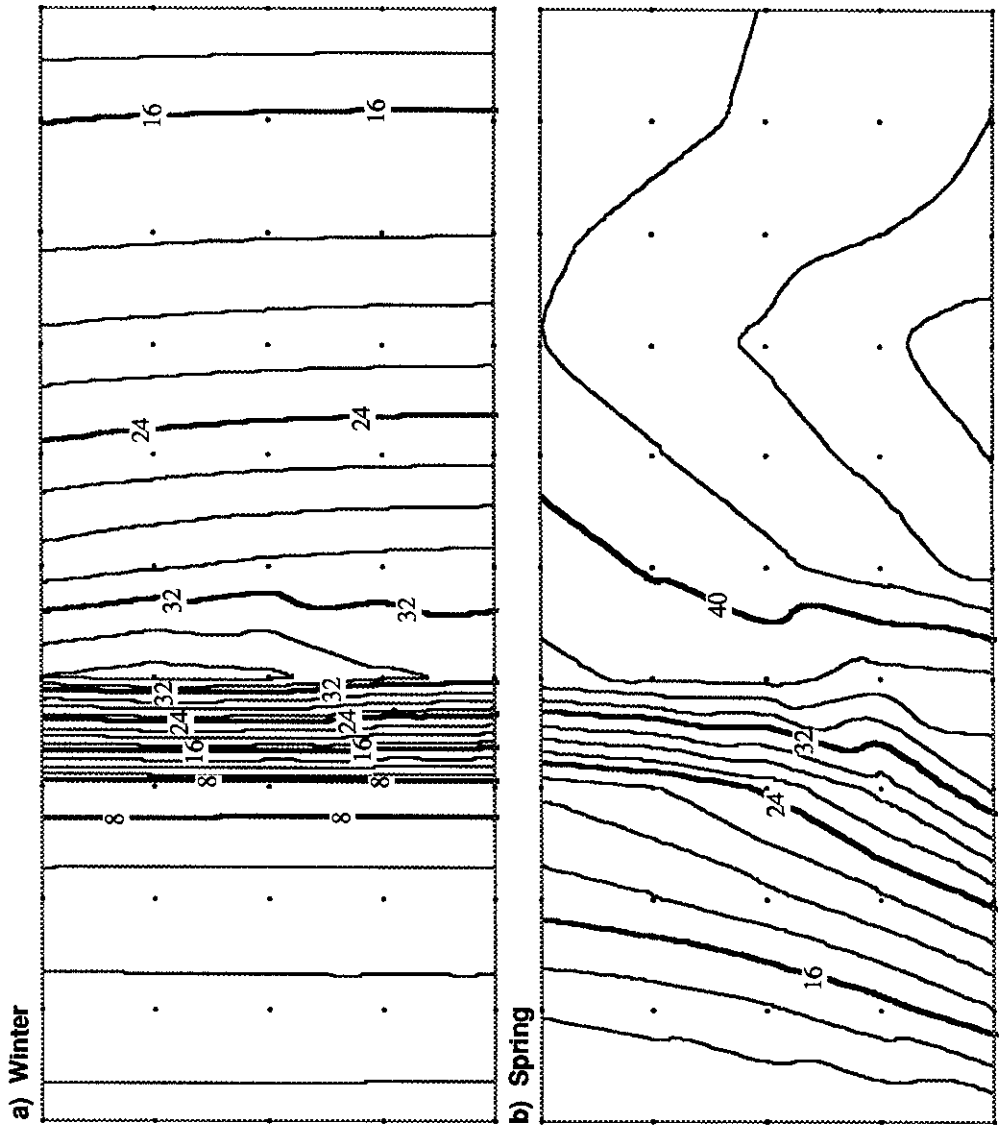

Figure 6.9 Isocontours of Two-Dimensional Variation in TSS in Town Lake by Season

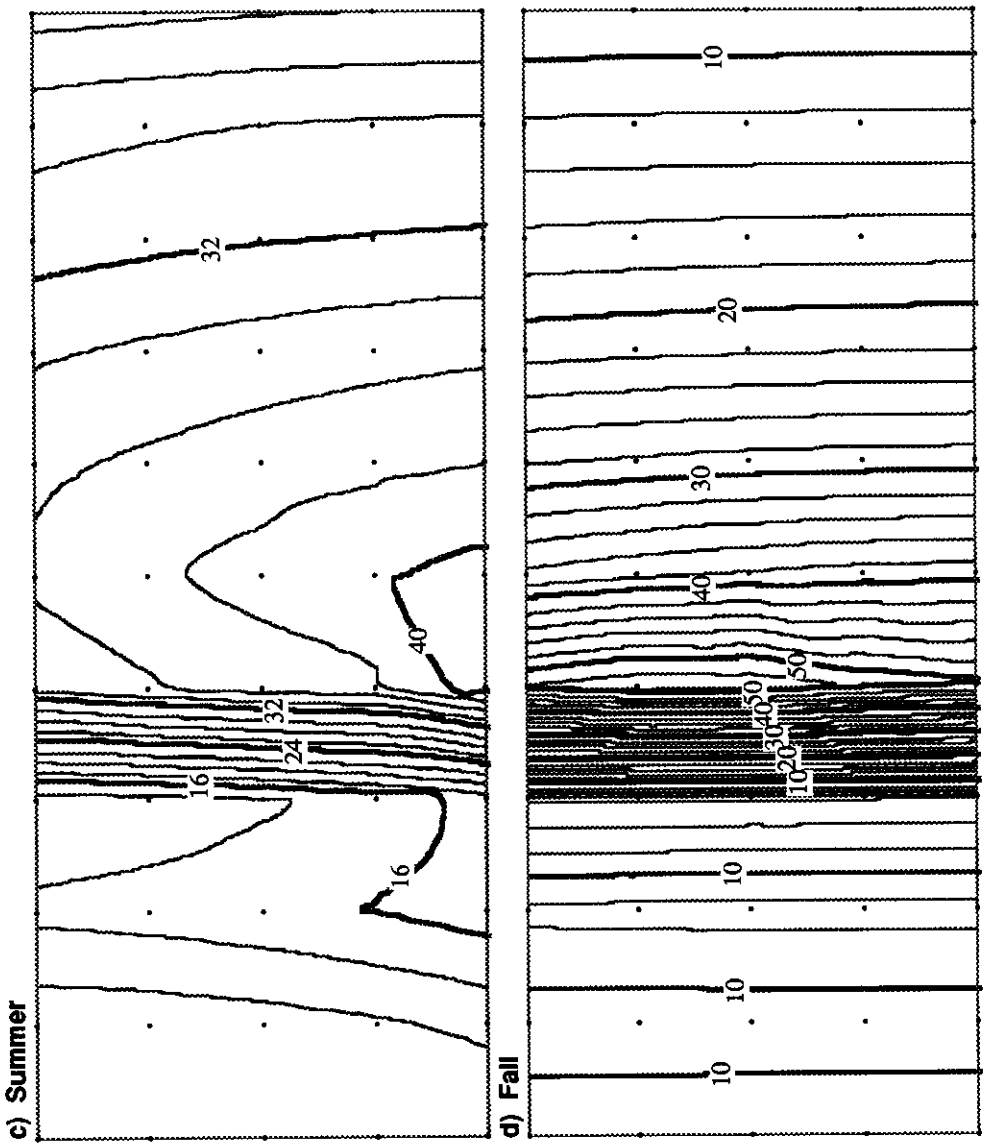
c) Summer
16
24
32
40
16
32
d) Fall
10
20
30
40
50
10
10
10
10
20
30
40
50

season. These tributary sources are apparent in Figure 6.8 in the concentration jumps at X = 0.2 and especially at X = 0.4.

Overall travel time through the system for the winter, labeled t_d in Table 6.1, was the second longest of any season, 3.2 d, and almost twice the annual average. The longer travel times allowed greater sedimentation, reducing system concentrations. It should be noted that longer detention in the winter resulted in decreases in all integral concentrations reported at mid-depth outflow, in comparison to the annual average responses, as shown in Table 6.1.

An interesting aspect revealed in the 2-D isocontour plot of winter TSS response (Figure 6.9a) concerns the tributary sources. Upstream boundary (X = 0.0) TSS concentrations were approximately 10 mg/L throughout the vertical; all of the seasons began with similar, though not identical, upstream boundary concentrations (see Figure 6.8). The major tributary surface source can be inferred from the isocontours in Figure 6.9(a); a substantial tributary source is seen in the upper water column at X = 0.4. The near-bed (Z = 0.8) concentration beneath that major tributary source was less than the water column concentration above it, despite the active resuspension immediately below at that location.

Spring

As noted in the discussion of Figure 6.7, upstream releases and storm runoff in spring produced the highest velocities, shear stresses, and resuspension of any season. Positive excess shear existed in every segment of the lake. The elevated mass concentrations, generally increasing with distance as seen in Figure 6.8, were thus expected. Because of the small relative tributary inflow contributions, and the relatively

small tributary load contribution, the perturbations of the system were dictated primarily by resuspension.

The resuspension-dominated regime present in the upper lake did, however, give way to a sedimentation-dominated region in the last three segments of the lake. This trend was evident in Figure 6.8, but the isocontour gradients in Figure 6.9(b) make the transition more visible. What was unique in this season's transition to a net sedimentation regime was that it was the only case thus far where sedimentation dominated at the same time that resuspension was occurring. Net sedimentation seen in the idealized base case and in the annual Town Lake case simulations only occurred in the absence of resuspension (*i.e.*, where $\tau_0 \leq \tau_c$). Net sedimentation in the lower lake during the spring season, represents a condition where the concentration of the water column suspension exceeds the carrying capacity of the fluid. Given that the vertical dispersion coefficient was assumed constant in the longitudinal and vertical directions for all seasons, this really means that a large sedimentation bed flux (due to large concentrations of fast-settling large particles resuspended from upstream locations) outbalanced a smaller resuspension bed flux (due to smaller excess bed shear stress).

Given the considerable resuspension taking place during spring, all of the integral concentration responses present at the mid-depth outflow, shown in Table 6.1, were maximums for the seasonal results. The particle size distributions at outflow were likewise shifted the most to the right (larger sizes), given the extensive contributions from the bed. This seasonal particle size distributions are presented in the next section. The short detention time in spring served more to advect existing particles out rather than flocculate them into larger flocs. The volume-average diameter of 8.8 μm would

have a Stokes velocity of 1.3 m/d, offering small chance to settle particles out of the 4.1 m deep lake during the 0.84 d mean detention time.

Summer

The summer conditions possessed the combination of high system velocities, high shear stress, and large resuspension, all primarily due to upstream inflow, as well as moderate tributary loadings. Excess shear stress, thus resuspension, existed in all but the lower two reaches of the lake. Relatively large mass concentrations at mid-depth were maintained throughout the mid- to lower lake, beginning at the narrow segment of the lake (X = 0.4), as shown in Figure 6.8. Because of the large flux of particles into the water column at the narrows, and despite the continuing resuspension in the following three segments, net sedimentation took place in the entire lower half of the lake. The rationale follows that discussed above for the spring results. The displacement of the net sedimentation region up the lake, compared with the spring behavior, was quite apparent in the mass isocontours of Figure 6.9(c). The intermediate position of the summer conditions produced unremarkable results for both the integral concentrations as shown in Table 6.1, as well as PSD-derived results.

Fall

The fall conditions produced both the largest and the smallest mid-depth responses in the system, as seen in Figure 6.8. Recall that resuspension did not occur in any section of the lake during the fall (Figure 6.7), due to inadequate bed shear stress. Referring to Table 6.1, the lake received minimum seasonal upstream inflow and overall loads. The travel time through the system was over 6 d.

Paradoxically, the low autumn velocities led to both low and high local particle mass concentrations. Lower velocities in the lake meant smaller dilution for the significant tributary load at mid-lake (X = 0.4). Concentration there jumped to over 50 mg/L. At the same time, longer travel times also allowed greater coagulation and sedimentation, reflected in rapidly decreasing concentrations in both the upper (TSS = 4 mg/L) and the mid- to lower lake. The nearly vertical mass isocontours for the fall (Figure 6.9d) demonstrate the insignificance of resuspension flux. The tributary source is evident at X = 0.4 via the accumulation of mass near the surface. The absence of resuspension and the relatively long residence time enabled settling of most of the large particles added by the tributary; the volume- (mass) average diameter at the outflow was only 5.2 μm.

6.4.2 Discrete seasonal response

The particle size distributions at the mid-depth outflow of Town Lake under quasi-steady seasonal forcing conditions are presented in Figure 6.10. As shown in Figure 6.5 and discussed in Section 6.3.2, the size distributions are a strong function of time and space, due to the spatial variation of internal and external loads and the kinetics of coagulation and sedimentation. Focusing on just the single point in the lake, however, does allow composite comparisons of net seasonal effects.

Integrating the volume distributions (Figure 6.10a) results in the same order of seasons as shown in the integral mass plots of Figure 6.8. The spring and summer conditions of greater resuspension and faster flow through the lake cause larger numbers of all size particles, as shown in Figure 6.10(b). The minimal residence times in the lake during these two seasons prevented relatively large particles from settling out of the water column. Modal diameters for the volume distributions ranged from the

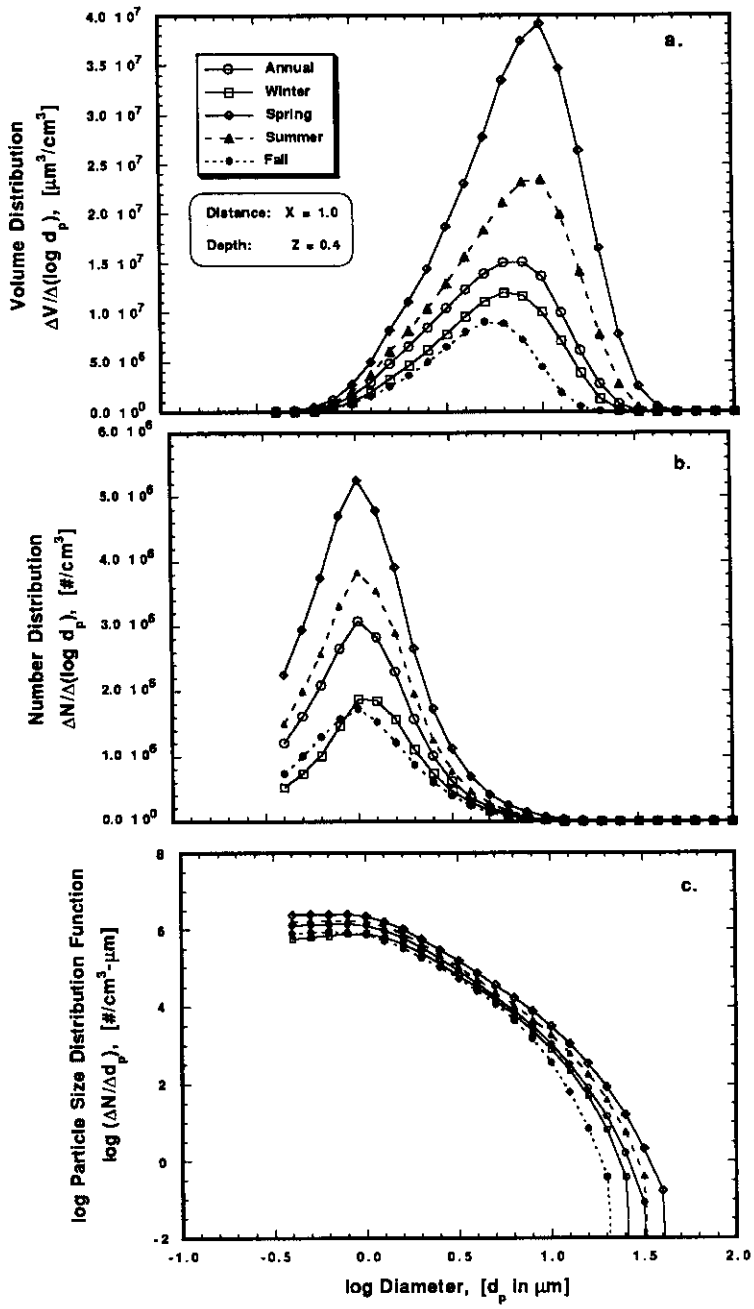

Figure 6.10 **Particle Size Distributions in Town Lake Outflow under Steady Seasonal Forcing**

minimum log d_p of 0.8 for the fall and winter to a maximum log d_p of 1.0 for the spring and summer. The magnitudes of the volume integrals and modal diameters, and their sequential orders, were positively related to the residence times (Table 6.1) and excess shear stresses (Figure 6.7). One is led to conclude that the relative resuspension loads were more of a determinant in the large particle presence than the relative tributary loads.

All of the seasonal outflow distributions were nonintersecting, with a single exception that was visible in two of the three distributions. The number distributions and the particle size distribution functions for the winter and fall clearly crossed each other at a log d_p value of -0.1 (intersection in the volume distribution was not resolved at smaller particles sizes). The fall distribution had a greater number of small particles and a lesser number of larger particles. As shown in Figure 6.7(c), resuspension was minimal in the winter and nonexistent under fall conditions. Since the fall residence time was nearly 90% longer than the winter residence time, one expects coagulation to bring about a greater reduction in small particle number concentrations. That the number concentrations of smaller particles were not less in the fall compared to the winter is a reflection, then, of two factors that can be derived from Table 6.1: the fall's absolute tributary solids loading was 10% larger than the winter's, and the fall's relative tributary/total solids contribution was approximately 15% larger. Despite the larger number of small particles present in the fall outflow, the larger particles were effectively removed by extended coagulation and sedimentation.

6.5 TIME-VARIABLE BEHAVIOR

6.5.1 Choice of conditions for storm event

All model simulations to this point have considered systems that have achieved steady-state concentration distributions in the water column. As previously implied, however, all of the simulation bed particle inventories were unsteady, due to net bed flux. In this section, simulation results are presented of time-variable system response to time-variable storm event forcing.

Conditions simulated for the storm event were based upon analysis of historical records. Although the Town Lake watershed is annually subject to approximately 80 storms with precipitation greater than or equal to 0.01 inches, appreciable runoff events only occur on the order of every 10 days. The ratio of the individual gauged tributary storm flowrates to their base flowrates is on the order of 100 to 300. Simplifying the hydrographs for the significant storms to a straight ramping up and ramping down with time, the rising limb lasts on the order of 2 to 10 hours, and the falling limb lasts on the order of 3 to 30 hours.

From the data just cited, conditions for the storm simulation were chosen. All tributaries were assumed to have a triangular hydrograph, with a rising limb duration of 6 hours and a falling limb duration of 18 hours. The simulated peak tributary flowrates were set at 221 times their annual average flowrates. An exception was the segment that included the Barton Creek watershed. Because of its (relatively) large, spring-fed base flow, its peaking factor was only 45 times. Localized storm conditions were envisioned to affect only the Town Lake watershed; flowrates into Town Lake from the upstream impoundment, Lake Austin, remained constant before, during, and after the storm.

This assumption is not critical for a 'typical' storm, since the storm flows and loads are dominated by the watershed runoff.

Changes in the inflow particle size distributions occur over the duration of a storm event. The typical watershed contaminant export response to a significant runoff event is a) greater number concentrations of all particle sizes compared to those originally present in the watershed outflow, b) appearance of particles with sizes larger than those originally present, and c) some nonlinear relationship as well as phase lags between the hydrologic and contaminant responses.

Stormwater concentration response of a watershed to excess precipitation might exhibit advanced and accelerated rising and falling relative to the stormwater flowrate response. This type of behavior, known as the 'first-flush effect,' was not modeled. Instead, it was assumed for simplicity that the hydrologic and contaminant responses follow similar time paths. Specifically, the rising and falling of the inflow number concentrations begin and end at the same times as the rising and falling of the tributary hydrographs. The scaling factor chosen for tributary storm concentrations was 2.0 for all particle sizes. The inflow size distribution was neither shifted nor extended to larger sizes because it was based upon a measured urban stormwater PSD.

An algorithm was developed to enable time- and space-dependent calculation of flowrates and inflow concentrations for each reach of the lake. As noted above, particle concentration scaling factors were set equal to 2.0 for each of the tributaries to the system, including the upstream inflow release from Tom Miller Dam. The hydrologic scaling factor was 221 for all tributaries, except the Barton Creek segment (45) and the dam release (1.0). The scaling subroutine was called only during the periods in which flow and concentration were ramping up and down.

The typical (*i.e.*, all except Barton/Shoal reach) tributary hydrologic flowrate ramp and particle flowrate load are shown in Figure 6.11. Both functions are presented as ratios of instantaneous to annual-average flowrate values. The tributary volumetric flowrate ramping was linear, as mentioned above. The particle flowrate function, however, had a second-order polynomial form because it was the product of the two first-order time functions for volumetric discharge and particle concentration.

The storm event began after a simulation of two detention times (3.40 d) of steady forcing on the system. The functions of Figure 6.11 have values of unity (not visible at the ordinate scale) except during the storm event. The initial period of two detention times allowed a physical and numerical steady-state response to develop in the water column. At the end of this numerical 'warm start,' *i.e.*, at the start of the storm, the system response was identical to the annual-average, steady-state results seen previously.

6.5.2 Integral storm response

As discussed with regard to Figure 6.11, the enormous flowrate and mass loading increases during storm events cause the in-lake flowrates and velocities to increase substantially during storms. Velocities in Town Lake at the time of peak storm inflows are presented in Figure 6.12. The actual velocities at peak inflow are compared to the annual-average velocities in Figure 6.12(a); the corresponding relative velocities, *i.e.*, storm velocities normalized to annual-average velocities, are shown in Figure 6.10(b). Recall that tributary inflows were placed at even distances X of [0.0, 0.2, 0.4, 0.6, 0.8, 1.0]; as such, the velocity differences seen in Figure 6.12(a) at the odd distances were not visible when put on a normalized scale in Figure 6.12(b).

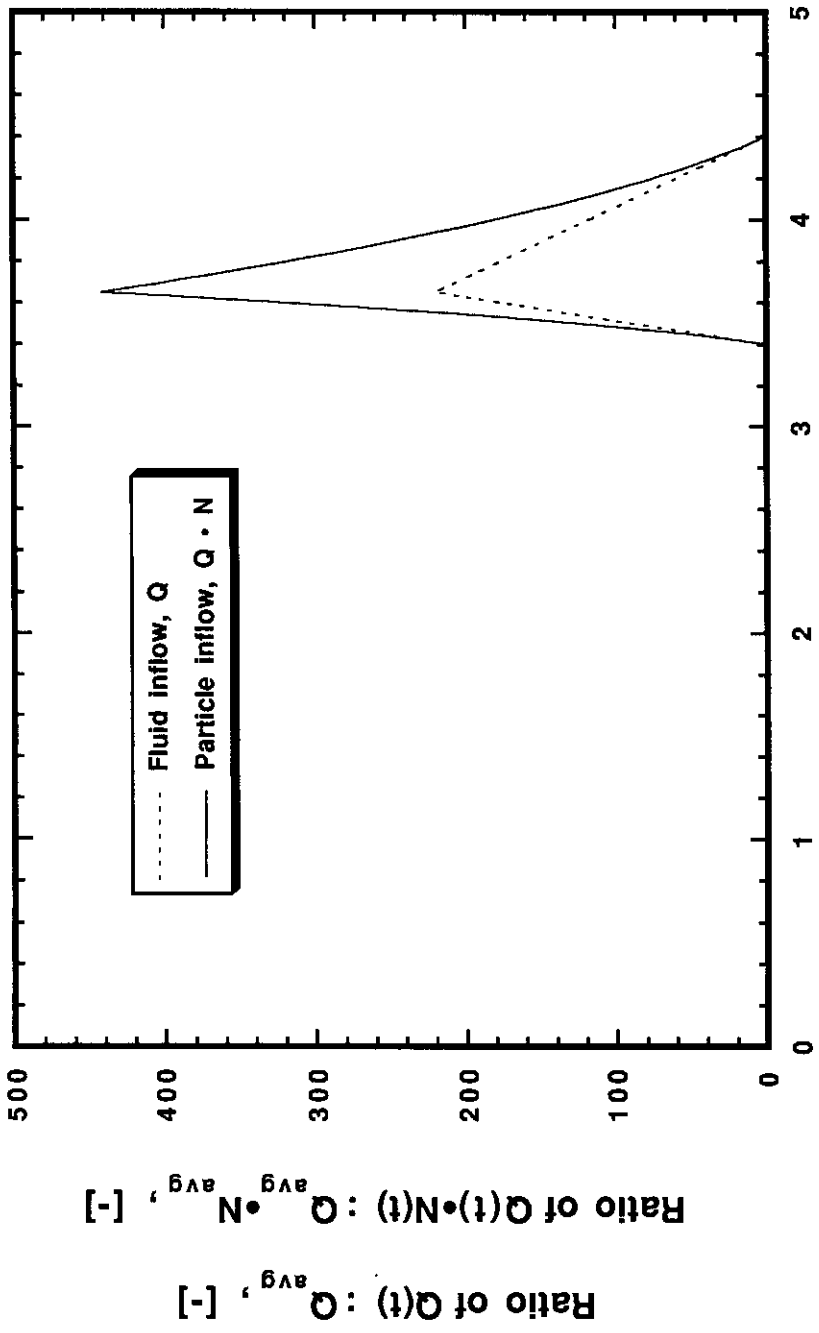

Figure 6.11 Ramping Functions for Stormwater Flowrates and Mass (Particle) Loading Rates

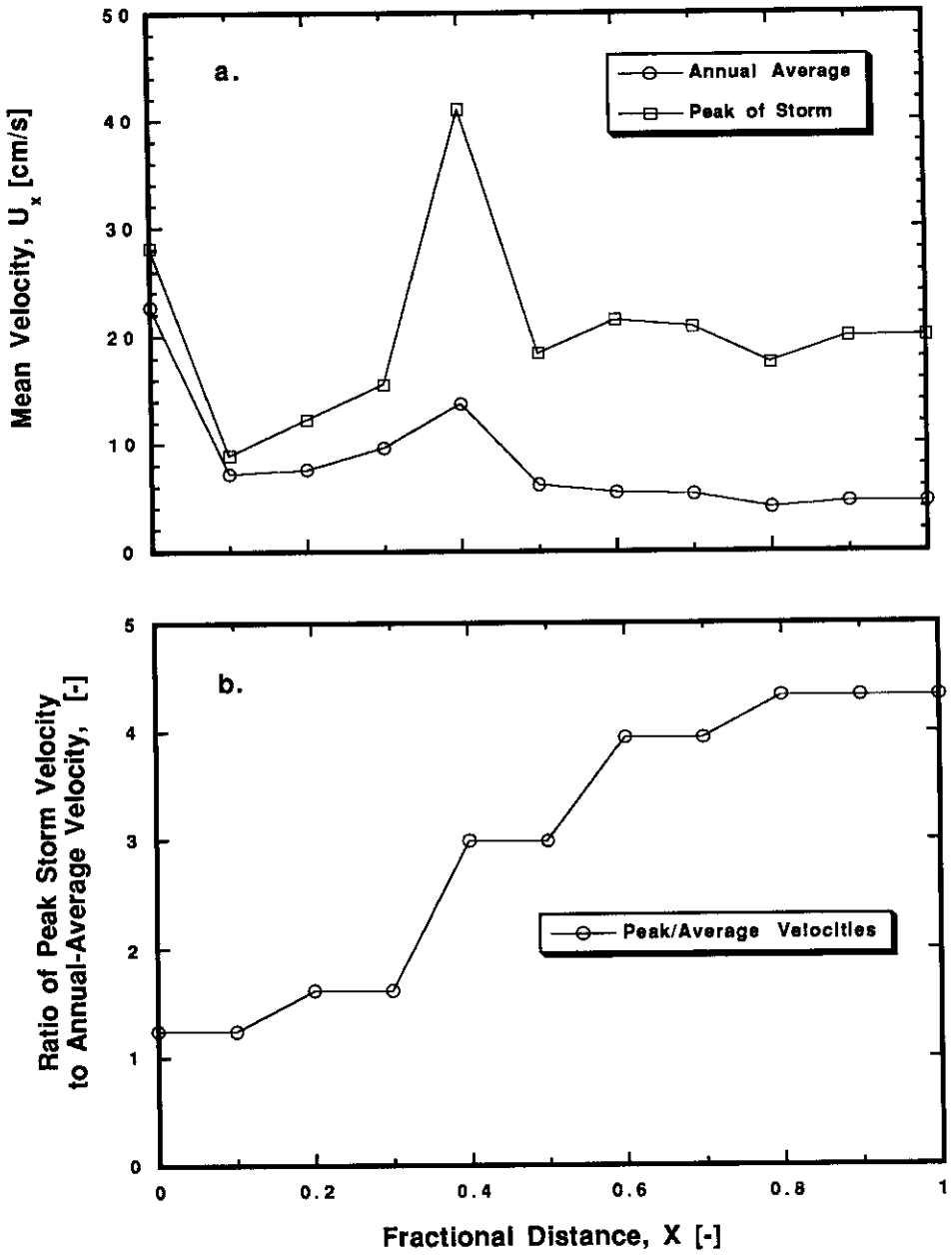

Figure 6.12 Spatial Variation of In-Lake Velocities under Steady Seasonal Forcing, Average vs. Storm. a) Absolute and b) Relative

Three points can be made regarding the in-lake velocities. First, recall that bed shear stresses stemming from average longitudinal velocities greater than approximately 6 cm/s produced resuspension. At the time of peak storm inflow, the tributary inflows served to maintain erosive velocities (bed shear stresses) throughout the entire lake according to Figure 6.10(a). Second, the relative sedimentation and resuspension fluxes were modified most in the downstream half of Town Lake. For the constant depth lake, substantially decreased residence times from mid-lake to the outflow would result in substantially less sedimentation flux to the bed. At the same time, the increased velocities would result in substantially larger (quadratic) bed shear stress and resuspension. Third, local effects can be expected in response to fluid acceleration and deceleration: acceleration should resuspend bed mass which can later be deposited downstream in a region of deceleration.

The first response to time-variable storm forcing was captured after six hours of increasing storm inflows and mass loading. Following the numerical 'warm start' of two residence times, as shown in Figure 6.9, the peak flows occurred at 6 hr or 0.25 d. At that time there were peak conditions of tributary flowrates, tributary particle concentrations, and thus tributary particle flowrates. The flowrates in the lake itself were also at a peak, producing peak velocities, peak bed shear stress, and minimum travel times, as discussed above.

Figure 6.13 contains the two-dimensional integral mass concentration isopleths at selected times during and after the simulated storm event. For reference, the system response at the onset of the storm event is shown in Figure 6.13(a), duplicating the annual steady-state response seen in Figure 6.3(a). The resultant system response at the time of peak inflow is shown in Figure 6.13(b). The in-lake mass concentrations

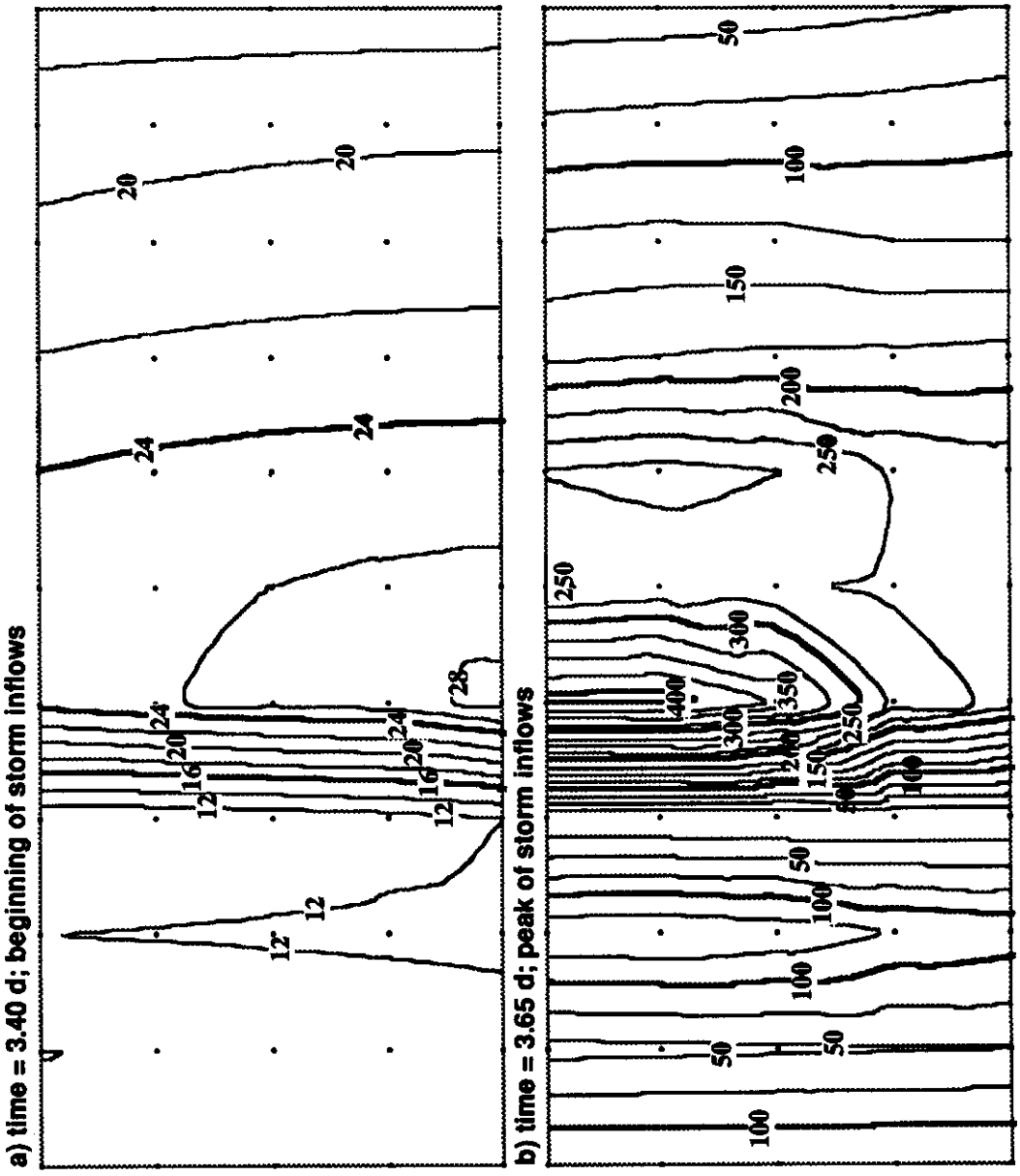

Figure 6.13 TSS Response of Town Lake During and After Storm

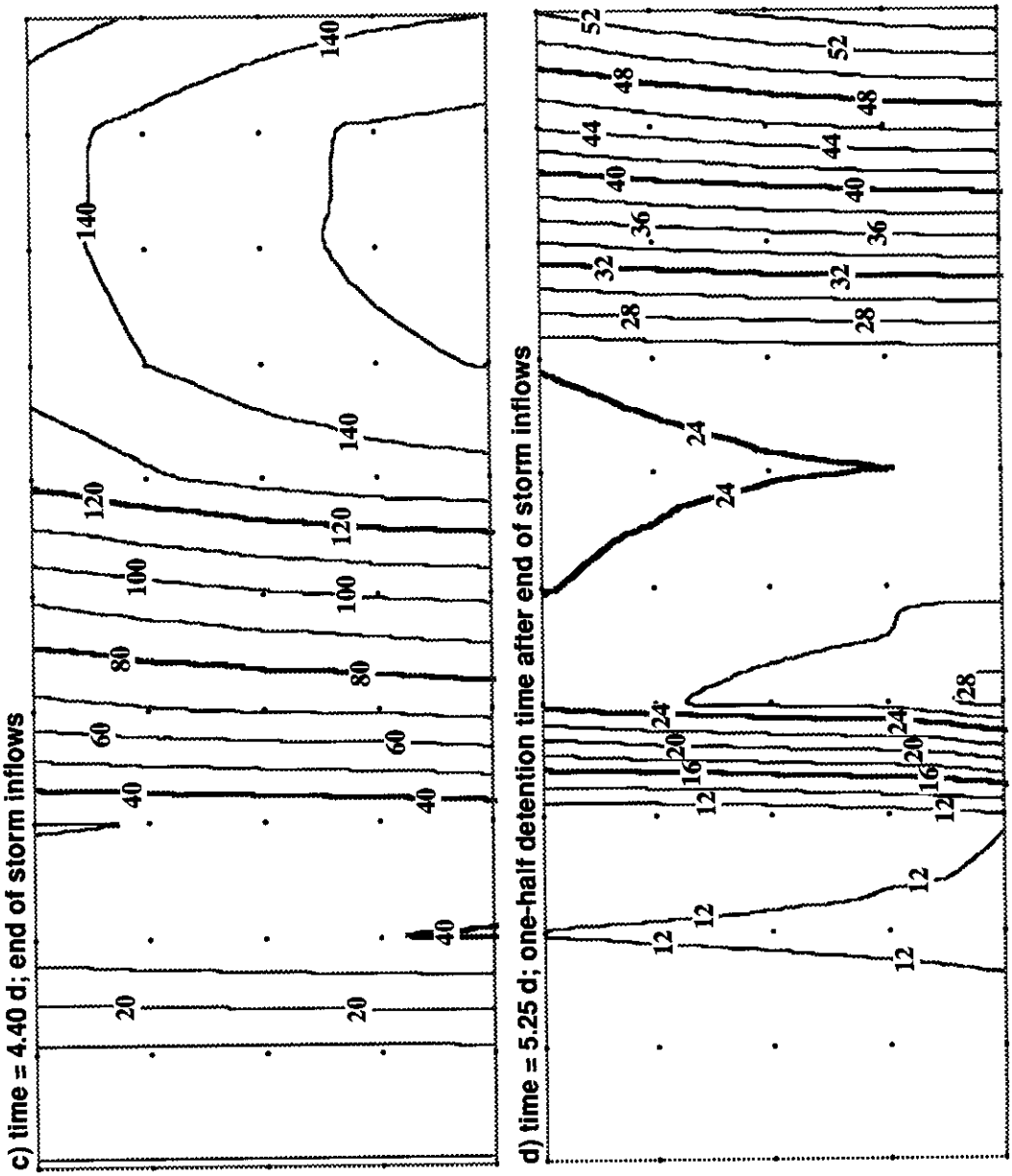
c) time = 4.40 d; end of storm inflows
d) time = 5.25 d; one-half detention time after end of storm inflows

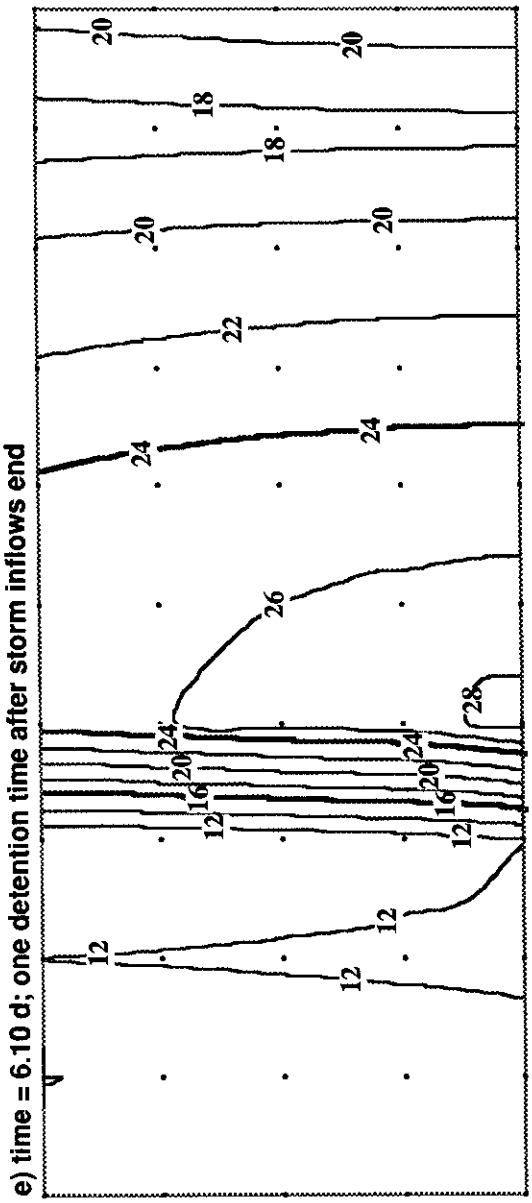
e) time = 6.10 d; one detention time after storm inflows end
20
20
18
18
20
20
22
24
24
26
28
24
20
16
12
24
20
16
12
12
12

distances X = [0.0, 0.2, 0.4, 0.6, and 0.8]. The large tributary particles (mass-average diameter of 19 μm) settled quickly, and removal rates were high.

Eighteen hours after the peak storm inflows, the tributaries had been ramped back down to their original pre-storm flowrates and concentrations. The system mass concentration response isopleths are shown in Figure 6.13(c). High concentrations in the water column were still present in the lower half of the lake; the large storm-induced tributary and bed resuspension loads that had heavily impacted the upstream half of the lake had not yet been advected out of the system. Since currents in the downstream half of the lake during the non-storm periods caused no resuspension (cf. Figure 6.10a), net sedimentation was evident in that region.

At one-half detention time after the end of storm inflows (Figure 6.13d) the upper lake ($X \leq 0.4$) had returned to pre-storm mass concentration profiles. Particles present in the lower half of the lake had not yet had adequate time to be advected or settled out of the water column. The interesting aspect of this profile was the positive longitudinal concentration gradient, particularly obvious in the lower third of the lake. The post-storm travel times were identical for the front and back of this cloud. Since the cloud had just passed over a non-resuspending bed, the particles present at the outflow represent the particles remaining (after coagulation and sedimentation) that were in suspension at one-half detention time upstream, at the end of the storm. Despite its being the most conducive region for sedimentation, the downstream outflow region had 'elevated' concentration relative to the primary tributary and bed impact areas.

After one detention time of post-storm reaction (Figure 6.13e) the system had nearly returned to the pre-storm initial condition (Figure 6.13a) for total mass concentration. The profiles are essentially identical for $X \leq 0.7$. At the downstream

outflow (X > 0.9), the concentrations were still somewhat elevated, compared to the initial conditions. The lagging of the storm displacement was likely caused by the last remnants of storm suspension; recall that fractional distance X does not correspond to fractional detention time in the nonrectangular lake.

6.5.3 Discrete storm response

Storm response of the lake can be judged in terms of time-variable and space-variable particle size distributions. The time-variable volume distributions at the mid-depth outflow location (1.0, 0.4) are presented in Figure 6.14. As the storm progressed, the volume distribution at the outflow was composed of both greater numbers of particles and larger sized particles. Following the storm, the outflow volume distributions and integral volumes returned to pre-storm values. As noted above, the outflow total volume was approaching the initial concentration after one detention time. Not shown in Figure 6.14 is the outflow volume distribution at 1.5 residence times after the storm, which was nearly indistinguishable, at all sizes, from the initial distribution.

The longitudinal profile of the volume distribution at mid-depth as the storm was ending is shown in Figure 6.15. At X = 0.4, the tributary inflow rates had already receded to their pre-storm magnitudes; the bimodal volume distribution there was the relic of the storm fluxes from the inflows that were upstream of mid-lake. The outflow distribution was largely composed of tributary storm particles.

6.5.4 Storm bed response

Presentation of the bed response to the storm event, expressed in terms of bulk bed volume per unit area of bed-water interface, is given in Figure 6.16. These units of

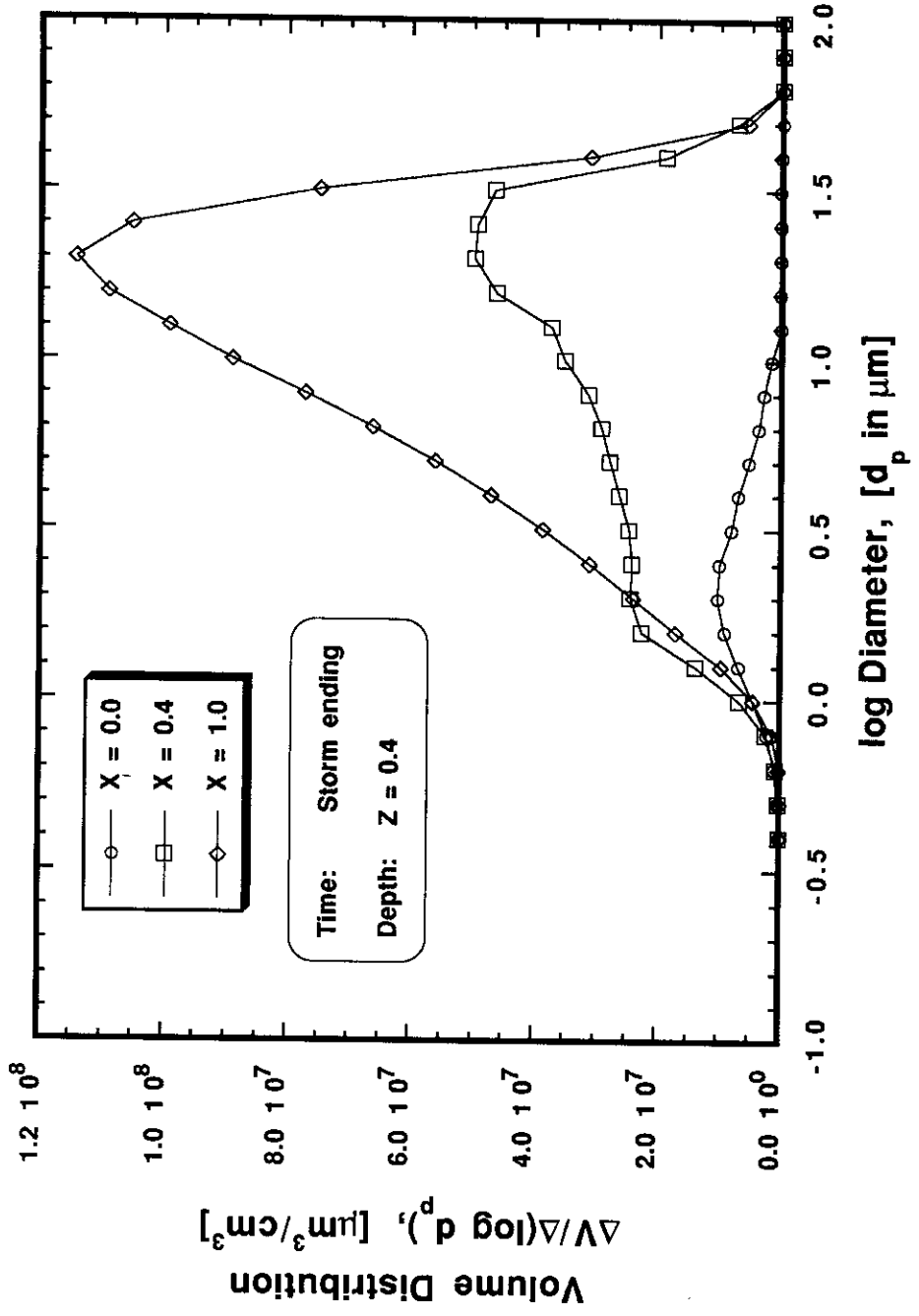

Figure 6.14 Longitudinal Profiles of Particle Volume Distribution at End of Town Lake Storm

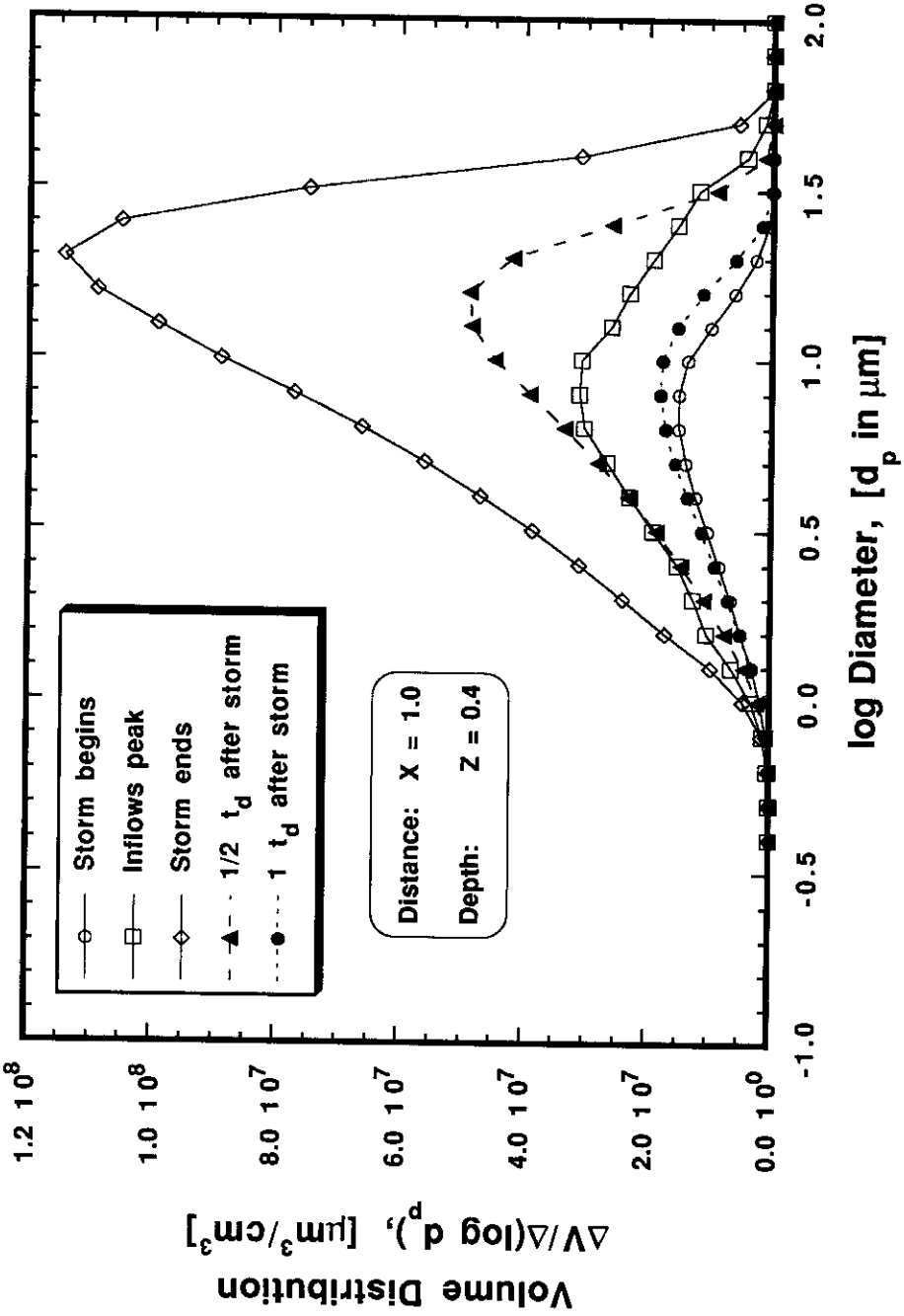

Figure 6.15 Time Variation of Particle Volume Distribution at Mid-Lake During and After Storm

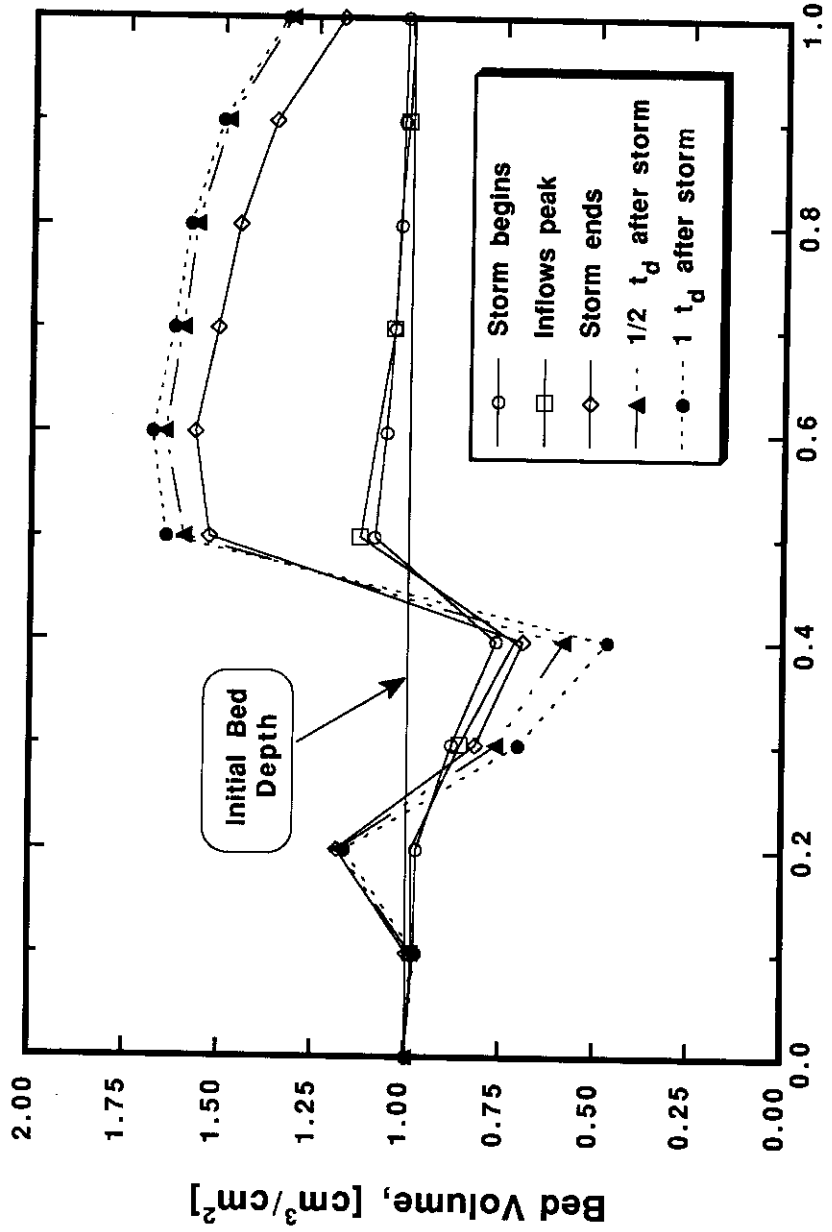

Figure 6.16 Active Bed Response to Town Lake Storm. (Initial time at t = 0; Storm begins after 3.4 d)

measurement can be translated as the active bed depth; a spatially uniform and temporally constant bed porosity is assumed, so the bed depth is also proportional to the particle mass in the bed. Recall that at the start of simulation, a uniform initial condition of 1.0 cm active bed depth is assumed for all sediment segments. After the numerical 'warm start,' the bed results at the beginning of the storm were identical to those from the annual average Town Lake simulation, as required. Given the boundary nature assigned to the numerical grid at X = 0.0, no resuspension flux or settling/ sedimentation fluxes were allowed at that grid. The bed depth therefore remained constant at the upstream boundary.

Consider first the bed depth just as the storm began. The time was two annual-average detention times, or 3.40 d, after the simulation began from uniform bed conditions. The bed depth was in response to the spatially varied bed shear stress; the relative bed shear stress and potential resuspension flux were indicated in Figure 6.7(c). Relatively small excess shear stresses at distances $0.1 \leq X < 0.3$ produced a relatively small scouring of the bed in the initial period. The increasing bed shear stress in the region $0.3 \leq X < 0.5$, which can also be thought of as a region of accelerating flow (velocity), resulted in larger amounts of net bed resuspension, evidenced by the deeper scouring of the bed. The scouring in the accelerating flow region was offset somewhat by larger sedimentation fluxes due to the resuspended particle mass in the water column, present from the upstream $0.1 \leq X < 0.3$ region.

The decelerating flow region had received net bed deposition, relative to the initial condition. This flow regime, which possessed no excess bed shear stress, was essentially the remainder of the system, $0.5 \leq X < 1.0$. The greatest net deposition was between $0.5 \leq X < 0.6$. As the first of the post-accelerating, erosive segments, this

decelerating flow segment was exposed to the largest water column concentrations, those concentrations (Figure 6.3) resulting from upstream resuspension and tributary loading. Thus the first decelerating region received the greatest relative deposition. Succeeding segments received smaller net deposition.

During the storm, regions of accelerating and decelerating flows were modified somewhat, altering the net particle deposition and scour. By the time the peak storm flows were entering the system (only six hours following the beginning of the storm), the bed profile changes had been fairly minor, as seen in Figure 6.16. Given the large, near-bed concentrations present throughout the lake (Figure 6.13b), sedimentation flux to the bed was substantially greater than at the start of the storm. The only changes in net sedimentation direction (positive, negative, neutral) were in segments $0.7 \leq X < 1.0$. Between $0.7 \leq X < 0.9$ resuspension over the period was just balanced by deposition, with essentially zero net sedimentation the result. In the region $0.9 \leq X \leq 1.0$, however, the accelerated in-lake storm flows, shown in Figure 6.12(a), caused a small net resuspension from the bed.

The recovery period following the storm produced dramatic changes in the bed profiles. At the time the storm inflows had ended, one day had elapsed since the start of the storm. Despite its accelerating conditions, the $0.2 \leq X < 0.3$ segment experienced substantial deposition as the result of increased upstream (Lake Austin) and tributary loadings. Erosion continued in the region $0.3 \leq X < 0.5$. The doubling of the bed inventory proceeding from $X = 0.4$ to $X = 0.5$ was in response to the joint conditions of upstream resuspension being advected downstream and substantial mass export from the Barton and Shoal Creek watersheds. Notice the gradual decline in the rate of net deposition proceeding downstream in $0.6 \leq X \leq 1.0$ as upstream mass was deposited

to the bed. Note also that the difference between the spatial integrals of net scour regions and net deposition regions reflects the boundary (upstream, tributary, and downstream) mass inflows and outflows.

The bed inventory continued to change after the bulk of the storm influences had advected through the system. These changes are seen in Figure 6.12 at times of one-half and one detention time after storm cessation. Changes to the longitudinal bed profile evidenced the same processes as at the beginning of the storm due to the identical in-lake hydraulic conditions and tributary loads. The depositional rates in the lower lake during the first half of the post-storm period reflected considerably greater net sedimentation than during non-storm periods, and can safely be attributed to the high near-bed concentrations just following the storm, as shown in Figures 6.13 (c) and (d). Given continuing base flow and base load conditions, one would expect the temporal changes in bed inventory along the lake to exactly follow the directions and rates demonstrated in the profile generated prior to the storm (modified slightly for the resuspension rate enhancement at the start of the simulation; this was caused by the uniform and 'under-saturated' initial condition assumed for the water column).

6.6 DISCUSSION

This section supplements the discussions accompanying the results of Chapter 6. It exists to address the more general questions concerning the model and its application that were not explicitly addressed as part of the simulation analyses. There are two general areas of interest. First is the reasonableness of the model and, specifically, its application to Town Lake. Second is the balance between strengths and limitations inherent in the model.

6.6.1 Reasonableness of model and application

The questions of model reasonableness can only be satisfactorily answered by a three prong approach: extensive testing and documentation of the model's theoretical and computational framework, comprehensive experiments designed to estimate process parameters, and field observations for model calibration and verification. Concerning the first task, this report documents the development, testing, and analysis of the physics and computations underlying the model. Very limited data exist, however, to estimate critical parameters for the Town Lake system; calibration data are even more limited.

The simulation results raise questions about the model application and the modeling approach itself. Given the *ad hoc* parameter estimation necessary for most of the particle and sediment related parameters, one wonders about the reasonableness of the model-predicted results.

The basic question concerning the simulations, specifically those termed 'steady-state' water column responses, might be 'If the bed is not at steady-state, how can the water column be?' This question addresses the fundamental question of modeling, *i.e.*, for what time and length scales are these approximations valid? The most direct answer, applicable to this research, is that the water column had achieved a response that balanced all fluxes; the water column had attained the time-invariant response to the forcing conditions, *i.e.*, the steady-state. The bed is coupled to the water column but is not at steady-state because fluxes over the bed are not in balance.

If the bed becomes devoid of solids due to its unsteady net loss by resuspension, then the water column fluxes would no longer be in balance. The water column response would again evolve through an unsteady phase of adjustment to the

boundary conditions and forces. The steady-state applicability of the water column results presented in Chapters 5 and 6 (given steady flows and parameters) begins at the time of initial flux balance in the water column (estimated to be somewhat larger than one detention time for the entire lake) and ends when the bed flux changes. Steady-state in the bed will only exist when there is a balance of fluxes over the bed-water interface.

Based upon the annual, seasonal, and storm results presented for the Town Lake sediment inventories, it is implied that certain seasons, *i.e.*, combinations of flow and mass loading conditions, can erode all solids from the bed. Bed inventories for the annual and seasonal conditions in Town Lake, after simulation of two annual-average detention times (3.4 d), are shown in Figure 6.17. Given the parameter suite chosen, the bed at X = 0.4 had been stripped of sediment in less than three and a half days during 'spring' conditions. Is that reasonable? Based on field reconnaissance of that reach, which is rather shallow and narrow, it is possible that the bed would have difficulty retaining solids. The same could be said of the first reach in Town Lake, which although it is not allowed to aggrade or degrade in this model (as a Dirichlet boundary), does have a rocky bottom.

There might be concern about whether the simulations, by ending prior to complete bed depletion, implicitly contain or endorse an 'infinite bed source' approach. The simulator establishes the current bed inventory as an explicit limit, however, on the allowable bed resuspension mass flux over any time step. As mentioned above, the spring results did contain the mid-lake bed segment that was essentially depleted (bed volume essentially constant over the final 1.7 d at 3×10^{-4} cm^3/cm^2). In this case it is apparent that this bed mass (3×10^{-4} cm^3/cm^2) was resuspended over each time step, with a fresh sediment layer deposited during the same time step by sedimentation; the

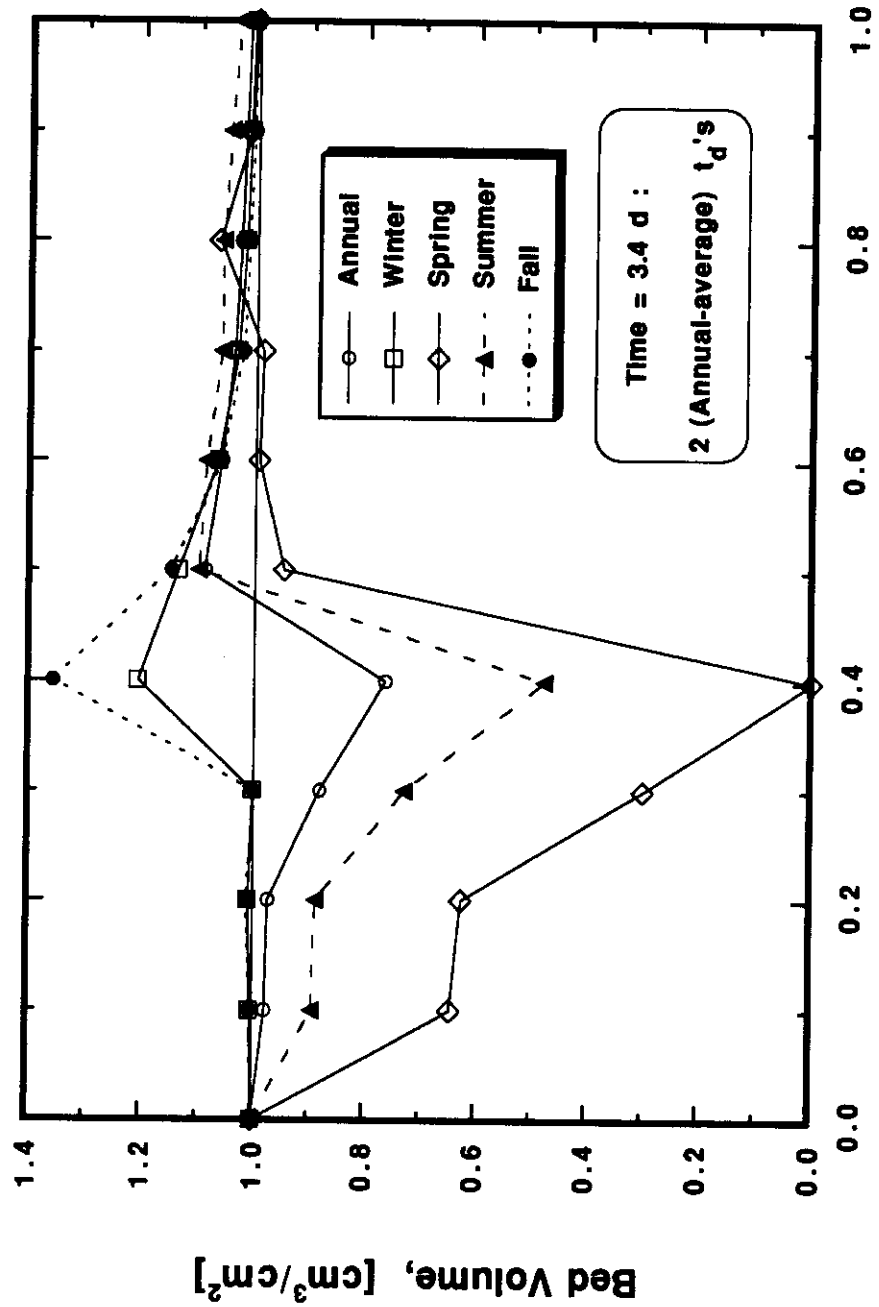

Figure 6.17 Short-Term Active-Bed Response to Longitudinal Variation in Local Resuspension and Deposition, by Season

potential resuspension flux (determined using equation 5.1 or 5.6) was greater than the actual mass flux, which was limited by the available mass in the bed.

Figure 6.7(c) contains a clear indication of which segments, in which seasons, can be expected to erode, based upon excess shear stress only. Excess shear stress conditions at the bed do not, however, dictate net resuspension of the entire bed. For example, despite substantial excess shear stress between $0.5 \leq X \leq 0.7$ during the summer, those segments experienced net sedimentation over the time scale of the simulation, as shown in Figure 6.17. A similar example is the net deposition in the eroding segment $X = 0.8$ during the spring.

Over the time scale of two mean detention times of steady flow, followed by the one day storm, and then by 1.5 mean detention times, there was not a perceptible change in the size distribution of the active bed particles. These observations were made for the bed PSD at $X = 0.5$ and were based on an output summary precision of five significant figures. That bed segment was the location of greatest storm and post-storm particle inventory change. Longer term simulations, with different size distributions and with greater precision in output, will be needed to analyze the interaction of bed and water column.

Although sufficient field observations from Town Lake are not available to calibrate the particle transport-transformation model, limited observations are available. Long-term water quality monitoring observations of suspension concentration measurements are given in Table 3.5 and Figure 3.8. These data, unstratified by season or antecedent storm conditions, can only be used to assess long-term predictions of the model, *i.e.*, the annual-average results. Given the rather extreme variance and limited resolution of the field data, one can say that a rough qualitative agreement exists

between the observations and predictions of Figures 3.8 and 6.3 and Tables 3.5 and 6.1.

The only possible test of field vs. model correlation at present is to consider the mean TSS concentration increases down the lake, observed (Figure 3.8 and Table 3.5) vs. predicted (Figure 6.3 and Table 6.1). Near the upstream boundary, the observed mean TSS concentration was 8.4 mg/L (1 standard deviation of ± 4.2 mg/L) at the Red Bud Trail bridge, or 12.7 mg/L (1 standard deviation of ± 25.2 mg/L) at the station TL-1, just downstream of Red Bud Isle. The estimated upstream model boundary condition was 10.26 mg/L. This correspondence was essentially predetermined, given two parameter estimates. First was the particle density, specified to match the observed particle volume distribution to the estimated mass concentration in Lake Austin. Second was the town Lake upstream inflow particle size distribution, specified (given particle density) to match the expected upstream mass concentration.

Outflow boundary concentrations reflect a marked evolution of the inflow particle size distribution, and observations and predictions there were not expected to match as closely as they do. At the downstream boundary, station TL-4 at Longhorn Dam, the mean TSS concentration was 17.0 mg/L (1 standard deviation of ± 24.9 mg/L). Remarkably, the estimated mid-depth outflow concentration was 16.98 mg/L. The agreement between outflow observations and predictions is excellent, but perhaps coincidental.

Given the many choices for parameters and no efforts at model calibration, there is certainly some degree of coincidence in the close agreement between outflow observations and predictions. For application of the particle transport-transformation model in engineering design or decision-making analysis, better definition of system

forcing is needed, especially particle and inflow rates. Site-specific influent and bed particle size distributions should be measured and characterized. Process rate data, particularly collision efficiencies of influent suspensions and sediment resuspension rate parameters, are needed.

6.6.2 Strengths and limitations of the model

The power of the model is vested in the ability to simulate size-dependent particle transport and fate, given specified flow fields. Both integral and discrete particle response of the system can be extracted using this approach. The discrete approach is expected to provide more accurate particle simulations than the traditional lumped mass approach under many conditions, but especially whenever the size distribution varies in space or when perturbations are forced on the system. It is expected that the particle model will provide a linkage to size-dependent particle-associated contaminants not currently available.

Regardless of the time frame (annual, season, storm), it is clear from Figures 6.16 and 6.17 that sediment transport down the lake by erosion and subsequent deposition was being simulated. The ability to see this process taking place, and to quantitatively analyze the competing mechanisms that lead to it, makes an entire class of sediment and particle-associated contaminant problems amenable to the analysis of size-dependent, differential transport.

At present, the capabilities of the model in analyzing Town Lake are limited by several factors. First, the model has not been adequately field-verified. Second, there is the requirement for a large amount of data and number of distributed parameters; many reasonable parameter estimates do exist for the lake, however. Third, the long-term simulation capabilities of the model, important in particle-associated fate studies, have

not been demonstrated. Fourth, computational expenses are significant, and improvements can and must be made to reduce these costs.

The limitations of the model for analyzing other natural systems include those factors mentioned for Town Lake, as well as two others. First, the model was built to simulate a rigid-lid, laterally-averaged, prismatic system of constant depth. Second, the capabilities of the model to handle transport in stratified or oscillatory flows has not been demonstrated.

On balance, the size-dependent framework developed for simulating particle fate is promising. It has been demonstrated to yield important insights not possible with other approaches. These insights are likely to be necessary in future studies where the complex behavior of the solid phase is important. The uncertainties and limitations that exist in the model all appear solvable and await research.

CHAPTER VII

SUMMARY AND RECOMMENDATIONS

7.1 SUMMARY

The behavior of particles in natural systems has traditionally been modeled as a lumped solid phase (total suspended solids) using first-order (linear) terms for sedimentation and resuspension. It has long been recognized, however, that discrete particle dynamics also includes coagulation, which is nonlinear and highly size-dependent. The contradiction between these two paradigms inspired this research.

In this study, a numerical model was developed for the purpose of evaluating the size-dependent processes that transport and transform discrete particles in natural systems. A finite difference representation of the laterally-averaged, two-dimensional, unsteady transport provided the model framework. Processes affecting particle transport and fate within the water column included advection and dispersion by the flow field, coagulation, and settling. Coupled exchange of discrete particles between the water column and the sediment bed by sedimentation and resuspension also was incorporated into the model. Particle-particle flocculation was treated as an independent process, acting in parallel with transport over small time steps. Explicit, numerically-integrated concentration changes due to transport and coagulation were superimposed for the combined system response.

The model was used to test the advantages of discrete particle modeling and the significance of size-dependent processes, coagulation in particular. Model development and initial use were accomplished using an idealized representation of Town Lake, an urban impoundment of the lower Colorado River in Austin, Texas. The idealized

system was characterized by a simple, uniform morphometry with steady, upstream loading only. Its use was for developmental purposes and fundamental studies. With this idealized system, the significance of various processes was examined, and sensitivity analyses of model parameters were conducted.

Prototype application of the model to Town Lake allowed more realistic analyses to be made of the lake and particle processes. Spatially-variable morphometry and spatially-distributed inflows and particle loading brought the simulation much closer to reality. Both steady (annual-average and seasonal-average) and unsteady (storm) conditions were assessed in Town Lake simulations.

7.2 CONCLUSIONS

The following conclusions have been drawn from the research conducted, as analyzed and reported above.

1. A general simulation model of discrete, size-dependent, particle transport and fate was developed, tested, and then applied to ideal and specific systems of interest. The model structure was two-dimensional (laterally-averaged) and unsteady, allowing spatially-distributed inflows and enabling the size-dependent coupling of the sediment bed and water column.

2. Mechanistic modeling of discrete, size-dependent, particle transport and fate demonstrated that competing processes significantly modified influent size distributions in all conditions examined.

3. Integral results, derived from discrete model simulations, enable insights concerning overall response to be gained. In certain cases, lumped concentration results appear to follow simple first-order transport/transformation models.

4. Modification of influent size distributions can be seen in both integral and discrete results, but the integral results are limited in usefulness for three reasons:
   a) integral results cannot be obtained without discrete particle modeling
   b) integral modeling cannot mechanistically preserve or reconcile the suspended phase volume, number, and surface area information available from the discrete distribution
   c) integral results provide little insight to the competing processes that determine particle behavior.

5. Process simulations were used to test the significance of size-dependency in the mechanisms of coagulation, sedimentation, and resuspension, alone and in combination. Although these tests were performed on the idealized system, the results are representative of the more realistic application to Town Lake and other similar natural systems. The importance of size-dependent modeling was demonstrated for all processes, *e.g.*, in

   - Coagulation

     Without coagulation, total inflow number and area concentrations remained essentially constant, but volume (mass) concentration increased almost 10% due to resuspension being greater than sedimentation.

     With only coagulation, total inflow volume concentration remained constant, but number and area concentrations were significantly reduced (approximately 60% and 30%, respectively).

- Resuspension

  Without resuspension, total inflow number, area, and volume (mass) concentrations were all reduced (approximately 60%, 40%, and 10%, respectively).

  With only resuspension, total inflow number concentration remained essentially constant, but volume and area concentrations were significantly increased (approximately 30% and 10%, respectively).

- Sedimentation

  Without sedimentation, total inflow volume (mass) concentration increased more than 30%, but number and surface concentrations were reduced significantly (approximately 60% and 25%, respectively).

  With only sedimentation, total inflow number concentration remained essentially constant, but volume and area concentrations both experienced small reductions.

6. Certain parameters emerged from the sensitivity analysis as critical to the predicted particle behavior. These included the influent size distribution, the collision efficiency and velocity gradient, and the resuspension-related parameters, *i.e.*, the shear velocity, the critical bed shear stress, and the mass flux rate constant.

7. Idealized and realistic conditions in Town Lake resulted in demonstrable particle coagulation. In the idealized system simulation, coagulation reduced the inflow particle number concentration by almost 60%, while the mass concentration changed little due to the offsetting effects of sedimentation and resuspension. In the realistic application to Town Lake, a simple upstream inflow vs. outflow comparison is neither possible nor applicable because of lateral tributary inflows;

substantial evidence of coagulation was clearly demonstrated, however, in the particle size distribution responses of all conditions tested.

8. Sediment transport down the lake by erosion and subsequent deposition has been simulated. The ability to analyze quantitatively the competing mechanisms and responses will make a class of sediment and particle-associated contaminant problems amenable to the analysis of size-dependent, differential transport.

9. The framework to link the particle model to a size-dependent, particle-associated contaminant transport and fate model has been outlined.

7.2.1 Generalizations

The model developed and the research conducted enabled simulation and analysis of a wide variety of potential systems. On the basis of the literature reviewed and the extensive simulations conducted, it is believed that the conclusions stated above serve to illustrate two principle generalizations, as indicated below.

First, coagulation is an important fate process for natural system particles under the following conditions:

a) Whenever unstable particles are present in the water column, (*e.g.*, in hard water, in water of low dissolved organic carbon, or in saline waters) AND

b) when the interparticle collision frequency is substantial (*e.g.*, a high concentration of particles, a size distribution of very small particles, a very broad size distribution of dense particles, or systems with large power input) AND

c) concentration changes due to flocculation are not overwhelmed by other processes.

The quantitative criterion that these three conditions are met in a given system is that the characteristic time for coagulation is comparable to or less than the characteristic times of competing processes. These time scales can be estimated even before explicit simulation.

Second, explicit modeling of discrete particle transport and coagulation should be used in simulating suspended solid phase behavior under the following conditions:

a) Whenever nonlinear particle behavior cannot be accurately described (in space or in time) by lumped (mass-average) linear behavior. Examples of these conditions include

i) large particle fluxes at a boundary, *e.g.*, high bed resuspension flux and in the vicinity of tributaries,

ii) whenever the size distribution, especially the volume distribution, changes substantially in the horizontal or vertical,

iii) conditions leading to unsteady forcing or unsteady kinetics.

b) When the lumped mass concentration cannot provide the information needed, such as

i) when the interest is in a number-related phenomenon such as light transmission or light scattering

ii) when the interest is in a surface-related phenomenon such as sorption.

7.3 RECOMMENDATIONS

In this research, new techniques developed to simulate the transport and transformation of discrete particles in natural aquatic systems have provided preliminary analyses of significant processes in ideal and prototype reservoirs. There remain

questions relevant to these processes that were not considered or that were revealed during the research. These questions relate to particle model testing and refinement, process experiments, and particle-associated model extensions.

Based upon the experiences and conclusions of this study, the following research could answer the outstanding questions:

- Extensive particle size distribution measurements in a lake and its tributaries under a variety of loading conditions are necessary for an adequate test of the model. The research reported herein was limited by a severe lack of data.
- Particle process experiments should be conducted to provide basic data on collision efficiencies. The collision efficiency tests would be done in standard coagulation/particle sizing experiments, but would extract the parameter using curvilinear trajectory hydrodynamics.
- Particle process experiments should be conducted to provide basic data on size-dependent resuspension kinetics. The flux experiments could be done in standard, small scale annular flumes, but would extract the parameters using time-dependent particle size measurements from bed and water column.
- The particle model should be applied to estuaries. Significant coagulation is known to occur in estuaries, and virtually all estuaries are experiencing sediment shoaling (navigation) and contaminant accumulation (environmental) problems.
- Optimization of particle computational algorithms could be conducted to make the model more efficient. The coagulation computations comprised approximately 90% of the total computational time, so the effort would begin there.

- Incorporation of a particle-contaminant model into the particle transport and transformation model developed in this research should be completed and tested. Size-dependent sorption studies should be conducted simultaneously to develop parameter estimates.

APPENDIX A

Size-Dependent, Particle-Associated,

Contaminant Transport Model

A.1. LITERATURE REVIEW

A.1.1 General Solute Sorption

Sorption is the sum of the interfacial (adsorption) and interphase (absorption) accumulation of a solute (Weber, 1972). In the context of aquatic surface phenomena, Westall (1987) distinguished between two-dimensional (interfacial) and three-dimensional (interphase) adsorption processes. Three-dimensional adsorption is envisioned as a solute-surface interaction, albeit within a three-dimensional surface matrix. Accumulations occur as the result of three types of interactions involving the solute: chemical reactions at the solid surface (a specific interaction such as surface hydrolysis, complexation, or ligand exchange), electrical interactions (nonspecific electrostatic or polarization effects), and solvent interactions (also nonspecific). Westall proposed both two- and three-dimensional models of adsorption for three classes of solutes: nonpolar organics, ionizable organics, and inorganics. The adsorption mechanism for nonpolar organics is hydrophobic repulsion rather than some force of attraction. Ionizable organics can interact by attraction/reaction as well as by hydrophobic repulsion. Inorganics interact primarily by attraction to the surface.

An important aspect of this research concerns the description of solute/sorbent distribution as a two-dimensional process. Certainly sorption also occurs in a three-dimensional manner, as mentioned above. Westall (1987) pointed out that a phenomenological test of the dimensionality of the solute/sorbent interaction is the response of the system to changes in ionic strength. If colloidal sorptive behavior changes with ionic strength, then a two-dimensional interaction between counterions and surface is evident. If the interaction of the solute is with a three-dimensional solid

phase, however, the interaction will be shielded from counterion effects by the solid matrix. An example where this concept is accepted is in the interpretation of electrophoretic mobilities; changes in electrophoretic mobility with ionic strength (or pH) do reflect a change in the surface potential (or charge) of the solid matrix.

The experimental representation of sorption as a partitioning or distribution between phases results in a distribution coefficient which is strictly phenomenological, and the partition coefficient is said to be conditional because it depends on the sorption conditions used during its determination. The porosity-corrected partition coefficient (Thomann and Mueller, 1987) used to describe the distribution of matter between solid and solution phases is normally expressed

$$K_p \equiv \frac{r}{C_d} . \qquad \textbf{(A.1)}$$

The sorbate concentration, r, is the mass sorbate/mass sorbent, [M/M], and the solute concentration, C_d, is the mass solute/volume suspension, [M/L^3]. This distribution relation is valid at any time and for any interaction between solute, solution, and solid. Values of K_p are normally reported as conditional equilibrium constants. The same definition is used to describe the sorption of both organics and inorganics. The interpretation and application of results from partitioning experiments are not as clear as the definition might indicate, however.

Development of reliable sorption models has been hampered by experimental difficulties in measuring sorbate concentration (which relies on the successful application of operationally defined phase separation) and in measuring the free solute concentration in equilibrium with the solid (with errors caused by solid/liquid separation difficulties, complexation of solute, loss of solute on experimental apparatus, and nonequilibrium measurements). The experimental difficulties arising in

sorption studies were summarized by Honeyman and Santschi (1988). Most applications rely on assumptions of local and reversible equilibrium. These assumptions further complicate the modeling of systems which are either not at equilibrium or are not completely reversible. Heterogeneous surface sites and competitive adsorption also confound the analysis.

A.1.2 Organic Solute Sorption

Deterministic sorption modeling from fundamental principles is not as complicated for organic sorption as it is for inorganic sorption. Westall (1987) stated that hydrophobic organic sorption is the most basic type of organic sorption to generalize and describe conceptually. This type of behavior is characterized by solute/solvent repulsion rather than solute/surface attraction. Many studies have related the extent of hydrophobic organic sorption to the organic content of the solid phase (Karickhoff, 1984). When sorption data have been normalized to the organic fraction of the solid, f_{OC}, it is generally found (Karickhoff, 1984) that a good empirical representation of behavior is

$$K_p = f_{OC} K_{OC} , \qquad (A.2)$$

where K_p is the conditional partition coefficient and K_{OC} is the organic carbon based partition coefficient.

A priori values of K_{OC} have been reported for hydrophobic organics as functions of solute aqueous solubility or solute octanol/water partition coefficient (Karickhoff, 1984). While results were presented as regression relations, Karickhoff argued that there does exist a thermodynamic basis for the relations, and data suggest a general applicability in the relations for uncharged hydrophobic organics of limited ($< 10^{-3}$ M) solubility. Karickhoff also presented data relating sorption to the relative ratio of swelling

clay to organic matter, indicating the increased importance of sorption by the mineral substrate when the relative organic content of the solid phase is very low.

The hydrophobic sorption process, with its direct relation to the mass of organic matter, can be conceived as a three-dimensional process if organic mass is independent of solid surface area. Analysis of data in Baccinni *et al.* (1982) shows, however, that the mass of organic matter sorbed onto natural particles can be dependent on the absolute surface area. In that study, the adsorption surface density of organic matter (mass organic carbon/surface area) on size-fractionated (silt and clay) samples of suspended lake particles was constant, within 50%. Thus, the organic mass sorbed was almost directly related to superficial surface area of the solid phase. This must be viewed in the light of a tenfold difference in the size fractions' mass mean diameter (5 μm vs. 0.5 μm), a threefold difference in the mass density of organic matter (mass organic matter/mass sorbent, *i.e.*, f_{oc}), a fourfold difference in the measured particle specific surface area A_s (surface area/mass sorbent), and the unknown effect of particle porosity. Thus, a two-dimensional surface sorption approach may be appropriate even for the mass (three-dimensional phase) sorption of organics by hydrophobic repulsion.

Partitioning of ionizable hydrophobic organics requires different treatment due to the surface binding of both nonpolar hydrophobic functional groups as well as polar ionic groups on the organic (Westall, 1987). Different approaches have related partitioning to the degree of organic solute ionization and charge, via pK_a and pH, and to solution/surface electrostatic effects, via ionic strength (Schellenberg, Leuenberger, & Schwarzenbach, 1985; Westall, Leuenberger, & Schwarzenbach, 1985).

Partitioning of hydrophobic ionic organic compounds is dependent on both hydrophobic and ionic functional groups, as for the ionizable organics above. In this

case, however, the charge on the organic is not related to pH. Westall (1987) presented sorption isotherms for an organic surfactant (linear alkylbenzenesulfonate) on metal oxide (alumina) which demonstrated that electrostatic interactions a) were stronger than hydrophobic repulsion, and b) controlled adsorption. Westall suggested that for natural surfaces, nonspecific hydrophobic effects would contribute much more to the total interaction than they did for the metal oxide surface.

It will be argued subsequently that specific chemical and electrostatic interactions can be described as two-dimensional surface phenomena. Thus, both the non-hydrophobic and hydrophobic interactions between surfaces and ionic or ionizable organics could be described, under certain conditions, by two-dimensional models.

A.1.3 Inorganic Solute Sorption

The sorption of inorganics to surfaces has been studied extensively, both through theoretical and experimental approaches. Since the inorganic solute/surface interaction is typically quite specific and dependent on several factors, the characterization is quite complex (Westall, 1987). Chemical equilibrium models describing sorption as a series of surface coordination reactions, analogous to thermodynamic solution complexation models, have been developed (Westall and Hohl, 1980). These models must include a representation of the electrostatic interactions between solute, surface, and solution, which accounts for the major differences between models. The combined physical/chemical model is called a surface complexation (or ionization) model (Dzombak and Morel, 1987a). The present status of these models is thoroughly reviewed for adsorption to hydrous metal oxide surfaces (Dzombak and Morel, 1987a; Westall, 1987) and for metal adsorption in general (Honeyman and Santschi, 1988). Adsorption to hydrous metal oxide surfaces has

received the most extensive treatment because these oxides are prevalent as coatings on all types of natural particles, have very high specific surface areas, and have very high affinities for ions due to their charged and reactive surface sites (Dzombak and Morel, 1987a).

Honeyman and Santschi (1988) noted that the success of surface complexation models in describing the effects of adsorbent site density and acidity, solute/surface affinity, complexing ligand interactions, ionic strength, and (sometimes) solute competition on metal/oxide surface binding has made them the reigning aquatic chemistry paradigm. On the other hand, Westall and Hohl (1980) showed that any of several different models could fit experimental data equally well, since they all rely heavily on experimentally determined parameters. Since each surface complexation model requires model-specific parameters, there is not a comprehensive thermodynamic data base for surface complexation analogous to that for solution complexation (Dzombak and Morel, 1987a). A simple yet widely applicable two-layer model was used as the framework for developing a thermodynamic data base of parameters for inorganic sorption on iron and aluminum oxides (Dzombak and Morel, 1987b).

Honeyman and Santschi (1988) identified several types of behavior which are not accurately predicted by surface complexation models. The anomalous effects are primarily related to solids concentration, solids aggregation, and surface site heterogeneity.

A.1.4 Sorption as a Surface Phenomenon

It has often been observed that sorption isotherms are linear at low concentrations. Karickhoff (1984) suggested that hydrophobic organics exhibit linear isotherms when the equilibrium dissolved solute concentration is $< 10^{-5}$ M and less

than one half the aqueous solubility. Ionizable and polar organics experience solution and surface interactions which preclude such simple generalization (Karickhoff, 1984). Dzombak and Morel (1987a) suggested that inorganic sorption to hydrous oxides is, in general, linear when the equilibrium dissolved solute concentration is $< 10^{-7}$ M. The concentration limit varies with solute and sorbent, as indicated below. The existence and applicability of such a linear sorption range simplify analysis considerably.

Although several models have been used to conceptually or empirically describe adsorption isotherms (Voice and Weber, 1983), and each of them can be reduced to linear behavior under certain conditions, the Langmuir isotherm is often chosen to describe linear sorption. The model is:

$$\Gamma = \Gamma_m \frac{K C_d'}{1 + K C_d'}, \qquad \textbf{(A.3)}$$

where

Γ = surface density, $\frac{\text{mass sorbate}}{\text{unit surface area}}$;

Γ_m = maximum surface density, $\frac{\text{mass sorbate}}{\text{unit surface area}}$;

K = ratio of adsorption to desorption rate constants; and

C_d' = solute concentration, $\frac{\text{mass solute}}{\text{volume solution}}$.

The Langmuir isotherm is based on assumptions of noninteracting surface sites of homogeneous size, character, and energy, with a maximum surface density corresponding to complete monolayer coverage. At low solute concentrations Γ is proportional to C_d, while at high solute concentration Γ approaches Γ_m. Γ_m can be thought of as a measure of the number of binding sites, and K is related to the enthalpy of adsorption, a measure of binding strength (Voice and Weber, 1983).

Observations in the nonlinear (higher) solute and sorbate concentration range frequently are not described by the Langmuir equation. Benjamin and Leckie (1981) proposed a multiple site model which could describe observed adsorption across a wide concentration range. At low concentrations (and surface densities), when all types of sites are in great excess, the model reduces to the Langmuir isotherm. Others have proposed surface precipitation mechanisms and models to explain observed solute behavior at high concentrations (*e.g.*, Farley, *et al.*, 1985). At present, no consensus exists as to which approach is more correct (Honeyman and Santschi, 1988).

At low concentrations, the Langmuir equation will be linear and of the form

$$\Gamma = (\Gamma_m K) C_d' . \qquad \textbf{(A.4)}$$

Log-log plots of Γ vs. C_d' will also be linear, have a slope of one, and follow

$$\log \Gamma = \log C_d' + \log (\Gamma_m K) . \qquad \textbf{(A.5)}$$

The particular definition of the upper limit of validity for the linear Langmuir equation varies substantially with adsorbate and adsorbent. Benjamin and Leckie (1981) presented experimental results for cation sorption onto amorphous iron hydroxide that delineated both linear and nonlinear ranges for copper, cadmium, zinc, lead, and mercury (Hg from others). The adsorbent concentration was large relative to environmental suspensions, 10^{-2} M (am)Fe_2O_3 or 1600 mg/L. At the upper limit of linear behavior, the maximum linear surface density, Γ^*, ranged from 10^{-5} to $10^{-2.4}$ mol Me/mol Fe, where "Me" is an abbreviation for the metal solute/sorbate. The corresponding maximum solute concentration for linear adsorption behavior, C_d^*, was less than 10^{-5} mol/L for each metal.

In an earlier study, Benjamin and Leckie (1980) examined other hydrous oxide metal adsorbents. They found that the surface density at the point of nonlinearity can be

extremely small, *e.g.*, as small as one molecule adsorbed per $10^{+7.7}$ potential sites. That conclusion presumes that every molecule of the crystalline solid is a potential site, however. The validity of the approximation depends on the crystal structure.

A.1.5 Solid Surface Area

The availability of solid surface area for adsorptive uptake is critical to the rate and extent of solute adsorption. For nonporous adsorbents, Weber (1972) stated that both the rate and extent of adsorption are inversely proportional to particle diameter. For porous adsorbents, Weber stated that rate would be inversely proportional to diameter when adsorption is controlled by diffusive film transport, and inversely proportional to diameter raised to a power greater than one when controlled by diffusive intraparticle pore transport. Finally, Weber said that the adsorption capacity of porous adsorbents could be inversely proportional to diameter if the solids were broken open to expose internal surfaces. For highly porous solids, the capacity would be independent of particle diameter.

The surface area of small particles is an elusive property to measure, and measured values are ambiguous. A characteristic measure of total (internal + external) surface area may be inferred from indirect measurements such as gas adsorption. The calculated value varies with the gas used (Mikhail and Brunauer, 1975) and the preparation of the solid (Jones and Bowser, 1978). Such areas do not necessarily represent the actual reactive surface areas of the particles (Lerman, 1979). In a similar vein, the geometric external surface areas of discrete particles can be estimated by transmission electron micrograph analysis (Nadeau, 1987), but accessible interior surfaces cannot be accounted for directly. Weiler and Mills (1965) compared total surface areas of marine sediments inferred from gas adsorption measurements with

those calculated from geometrical considerations. Particle size distributions were determined for selectively treated sediments using sieves, sedimentation tubes, and an early Coulter counter. Assuming spherical shape and complete closure of the distribution, and neglecting particle area due to particles removed by sieving, the surface areas calculated from geometrical considerations were one to two orders of magnitude lower than the values determined from gas measurements.

The specific surface area A_S of a solid is defined as the surface area per unit mass of adsorbent, typically reported in [m^2/g]. The values of A_S measured by gas adsorption for fine particle sorbents of natural and synthetic origin vary within some three orders of magnitude. Surface areas reported from gas or solute sorption studies range from 7 to 800 m^2/g for various clays (Ahlrichs, 1972; Jones and Bowser, 1978); 10 to 1500 m^2/g for various aluminosilicates (Ahlrichs, 1972; Kabata-Pendias and Pendios, 1984), 3 to 500 m^2/g for various hydrous metal oxides (Ahlrichs, 1972; Benjamin and Leckie, 1980; Chang, *et al.*, 1987; Sigg, 1987), and 3 to 150 m^2/g for various marine clay and ooze sediments (Weiler and Mills, 1965).

For nonporous particles, the surface area is simply the geometrical surface area. Regular geometric shapes yield simple estimates of surface area based on a small number of characteristic dimensions. The sphere is the most often assumed shape for small particles, and has a specific surface area of $A_s = 6/\rho_s d_p$, where d_p is the diameter and ρ_s is the density. Since a sphere has the smallest area to volume ratio possible for any solid, estimates of specific surface area made using measured or inferred particle diameter and the above relation will thus underestimate A_S for nonspherical particles. Likewise, if the solid is porous and its assumed density is overestimated, its true A_S

will again be underestimated. Similar relations between surface area and characteristic particle dimensions can be made for other geometries.

A.1.6 Sorption as a Function of Surface Area

Many studies of sorption as a function of specific surface area have been reported. Most of these studies have been laboratory investigations using a single homogeneous solid phase. Experiments discussed above with cation adsorption on hydrous metal oxide surfaces were of this type, *e.g.*, Dzombak and Morel (1987a) and Benjamin and Leckie (1980; 1981).

Langmuir behavior seems to offer an appropriate empirical model for the partitioning of solute to solid provided that small (system specific) adsorption densities exist, as discussed above. Linear partitioning and constant partition coefficients result when adsorbate concentration is directly related to solute concentration at equilibrium. Such relationships have been exhibited by cations on hydrous metal oxides, as presented above, as well as by hydrophobic ionic organics on prepared metal oxides (for example, by Westall, 1987).

Studies of ambient environmental sediment adsorbate vs. specific surface area are less abundant than studies of controlled laboratory adsorption. Sorption isotherms, predominantly linear, were presented by Hiraizumi *et al.* (1979) for PCB on a number of biotic and abiotic natural solids. Plots of BET specific surface area vs. reciprocal particle diameter d_p (based on sieve diameter) were linear only down to about 60 μm, indicating that floc, porous solids, or separation problems caused a departure from the strict geometrical relation between A_S and d_p for silt particles between 60 and 50 μm (the lower limit sieve of data presented). A log-log plot of the bulk properties of A_S and reciprocal number-mean diameter did, however, indicate a linear relationship with a

slope of unity, as would be expected. More to the point, though, is that a log-log plot of mass-based partition coefficient had a linear relation to specific surface area. As discussed below, this argues for a surface-based partition coefficient.

Other analyses of field samples for surface density vs. specific surface area have also supported a surface-based partition coefficient. Oliver (1973) analyzed bulk river sediments for metal adsorbate concentrations and specific surface areas and presented data showing linear relationships between adsorbate and surface area in the lower ranges of concentration and surface area.

Baccini *et al.* (1982) analyzed the adsorption of dissolved organic carbon (DOC) on particles as a function of particle concentration, size fraction, and specific surface area. Laboratory isotherms indicated that log-log plots of surface density vs. particle concentration of synthetic particles (γ-Al_2O_3) and bulk lake sediments resulted in linear plots of similar slope. Increasing the DOC concentration while holding constant the bulk lake particle concentration resulted in a slight increase in surface density, although the differences were not significant given the confidence intervals for the measurements. As mentioned above, one of the most relevant results found by Baccini *et al.* was that the sorbate surface density was nearly constant for the bulk and size-fractionated lake sediments, despite a threefold difference in organic mass fraction, a fourfold difference in specific surface areas, and a tenfold difference in mass-mean diameters. This shows that for a heterogeneous sediment exposed to a steady-state DOC concentration, it is the surface area which is controlling surface density. Baccini *et al.* also estimated from steric considerations that (for an assumed [DOC] = 2 mg/L) the solids would be saturated (complete monolayer coverage) at any suspended solids concentration less than 8 mg/L. The authors demonstrated competition between DOC,

anions, and metals for sorption. Given the last two results, low suspended solids concentrations might acquire multiple layer DOC adsorption and result in reduced inorganic sorption.

A.1.7 Particle Concentration Effects on Sorption

The assumptions of a linear adsorption isotherm and local (reversible and instantaneous) equilibrium result in a constant partition coefficient. This accepted concept was challenged by O'Connor and Connolly (1980), who proposed a solids concentration-dependent partition coefficient based on analysis of data from several studies. O'Connor and Connolly (1980) provided no mechanistic explanation for their model.

Since then, the solids effect, as it is called, has received considerable attention. A good summary of the experimental results for hydrophobic organics was given by Di Toro (1985). Hypotheses given to explain the phenomenon generally attribute the effect to either experimental artifact(s) or to particle-particle interaction.

The most popular rationalization advanced for the solids effect is not a new mechanism but the existence of experimental artifact. Voice *et al.* (1983) and Voice and Weber (1985) related the partition coefficient to nonseparable (third phase) dissolved organic matter. The latter paper (Voice and Weber, 1985) hypothesized that nonseparable, macromolecular organic matter complexed hydrophobic organics such that solid sorbents could sorb either the free hydrophobe, the complex, or both. Gschwend and Wu (1985) and Morel and Gschwend (1987) attributed the noted effect to incomplete separation of colloidal particles or organic complexes. The former (Gschwend and Wu, 1985) used laboratory experiments with sequential centrifugation and washing to show that nonseparable solids (as measured by dissolved solids,

turbidity, and DOC) are: (a) present in higher proportion to total solids at higher solids concentrations and (b) seemingly generated by resuspending large size fractions. Both Gschwend articles presented calculations to argue that a constant, mass-based partition coefficient exists, *i.e.*, the apparent solids effect could be explained as experimental artifact, provided that accurate accounting of nonseparable as well as separable solids is done. Baker *et al.* (1986) presented PCB distribution coefficients derived from an extensive field data set, along with suspended solids and DOC concentrations, to support a three phase model akin to the Gschwend approach. In another approach, Curl and Keoleian (1984) hypothesized that competitive adsorption between solute and an implicit adsorbate (unknown and unmeasured; present before the solids were exposed to quantitative solute) could also explain the effect.

The particle-particle interaction hypothesis has been offered by several researchers to explain the solids phenomenon. The most comprehensive and successful treatment of this sort is the empirical modeling of Di Toro and co-workers (1985; 1986). Di Toro (1985) proposed a "particle interaction model" which mathematically reproduced the solids effect (over the solids concentration range of 100 to 10,000 mg/L), as well as the adsorption/desorption hysteresis effect, for a very wide range of hydrophobic organics. The foundation for the model is a rate law describing particles (bare sites) combining with adsorbate (filled sites) to form free solute plus two bare particles sites. This adsorbate release effect is significant only at higher solids concentrations. The authors offered no physiochemical mechanism to explain the rate law; however, a traditional coagulation collision frequency analysis would provide exactly the effect proposed by Di Toro, *i.e.*, higher rates of particle-particle collisions at higher particle concentrations.

Chang *et al.* (1987) studied zinc adsorption using very low solids concentrations ([TiO_2] = 2 to 50 mg/L) and suggested that it was the degree of solid dispersion (aggregation) that caused the solids effect rather than the solids concentration, per se. The authors suggested that solids were more dispersed at lower concentrations, resulting in smaller particles with greater specific surface area and more available surface binding sites, hence greater adsorption on a sorbent mass basis. In a series of elegant adsorption and coagulation studies using phosphate and goethite (γ-FeOOH), Anderson *et al.* (1985) demonstrated that adsorption of PO_4^{3-} resulted in measurable changes in goethite aggregate size (larger), form (more ordered), and specific surface area (smaller). Anderson *et al.* concluded from data that greater coagulation at higher solids concentrations could explain their observations of lower, mass-based adsorption densities at those higher solids concentrations.

Since coagulation is a second order reaction (with respect to particle concentration) that results in somewhat less specific surface area and binding site density, and since two-dimensional sorption is dependent to some degree on binding site density, it is reasonable to expect coagulation to decrease adsorption. Honeyman (1984) showed with mixed sorbent experiments, however, that certain model binary sorbent systems resulted in adsorption densities that were greater than the sum of the individual adsorption densities (Honeyman also observed decreased densities with certain mixed sorbents). For the observations of increased densities, it was suggested (Honeyman and Santschi, 1988) that the increased sorption could have been due to a) surface modification of the weaker sorbent by the stronger sorbent or b) enhanced sorption of solute in the interfacial regions created during mixed-solid coagulation.

A.1.8 Contaminant Transport and Fate Modeling

Dissolved and sorbed contaminants are subject to a number of transfer and transformation processes which control the materials' fate and distribution. Discussions of the solution phase reaction and transfer processes typically incorporated in contaminant modeling are contained in Mills *et al.* (1985) and Mabey *et al.* (1982).

As illustrated by Imboden and Schwarzenbach (1985), appropriate contaminant modeling requires that only those processes important at the time and space scales of interest be modeled. Compilations of transfer and transformation rate coefficients (or methods for their estimation) for the USEPA's priority pollutants are available (Mabey, *et al.*, 1982; Mills, *et al.*, 1985; Schnoor, *et al.*, 1987). Hydrodynamic transport is system specific and must be characterized by studies of the river/lake under study.

As an important class of contaminant models, toxicant transport and fate models have been differentiated according to their spatial and temporal resolution as being one of three types (Di Toro, *et al.*, 1982). Partitioning models can only simulate steady-state equilibrium between spatially homogeneous compartments of the environment. Simplified fate models can simulate steady-state spatial variations in chemical concentration. Detailed fate models can simulate spatial as well as temporal variations in concentration. Increased data are needed for calibrating and testing the more detailed models. Succinct reviews of toxicant modeling were given by O'Connor (1988a; 1988b; 1988c) and Ambrose *et al.* (1988). A collection of short descriptions of publicly available toxicant models has been prepared (Versar, 1984).

A.1.9 Summary

The transport and transformation of the solid phase is dependent on the size of the particles comprising the solid phase. The sorption of contaminants onto particles is

also highly dependent on particle size. This dependency has been recognized in laboratory and field experiments by many investigators but has not been incorporated well into mathematical models for natural systems. The somewhat controversial solids effect on adsorption is also partially explainable by the size distributions, since adsorption is controlled primarily by the available surface area rather than mass. More realistic modeling of particle-associated contaminants is possible with a model which accounts for particle size distributions and their changes in time and space.

A.2. CONTAMINANT TRANSPORT AND FATE MODEL

A.2.1 Equations

The contaminant fate and transport model is based on the same framework as particle transport and reaction, Equation (4.3), viz.,

$$\frac{\partial C_T}{\partial t} + U_i \frac{\partial C_T}{\partial x_i} = E_{ii} \frac{\partial^2 C_T}{\partial x_i^2} + R(C_T) . \qquad \textbf{(A.6)}$$

The state variable modeled is the total bulk contaminant concentration, C_T. The total contaminant concentration is the sum of two conceptually separable phases of contaminant, *i.e.*,

$$C_T = C_d + C_p . \qquad \textbf{(A.7)}$$

C_d is the bulk dissolved contaminant concentration [mass of solute per volume of suspension], and C_p is the bulk particulate contaminant concentration [mass of sorbate per volume of suspension]. A third phase of nonseparable (colloidal) solids associated contaminant is operationally excluded. Bulk concentration dimensions are [mass contaminant/ bulk volume of suspension].

Contaminant transport and reaction are modeled in the same basic manner that was used for particles. The approach for the contaminant is modified, however, to allow for different forcing functions and transformation mechanisms for the two systems, *i.e.*, particles and particle-associated contaminant. Contaminant transport is linked to particle transport by a particle-contaminant interaction model. Contaminant removal by reaction acts in parallel with transport, just as coagulation did with particle transport. Obviously, particle reaction and contaminant reaction are not directly related.

Contaminant solute-sorbate speciation is determined by assuming linear and instantaneous adsorption equilibrium between dissolved contaminant and available particle surface area. The linear and instantaneous assumptions are valid when contaminant concentrations are low and the time scale of the adsorption/desorption reaction is much less than the time scale of the transport and decay processes; both conditions generally exist, though nonequilibrium situations do occur in natural systems (Honeyman and Santschi, 1988; Wu and Gschwend, 1986). The assumption of functional sorption dependence upon available surface area is the hypothesis advanced in this research, although the more traditional mass-based approach can also examined. The framework developed for coupling particle surface area and contaminants follows.

For any solid/sorbate/solute system there exists a condition of thermodynamic equilibrium. Equilibrium condition is described by the sorbent concentration [surface area of sorbent/volume of suspension], the sorbate concentration, Γ [mass of sorbed contaminant/available solid surface area], and the corresponding dissolved contaminant concentration, C_d' [mass of dissolved contaminant/solution volume]. Both Γ and C_d' are intrinsic properties of the system. At dilute concentrations, there is a linear relation

between solute and sorbate, analogous to the mass-based distribution approach of Equation (A.1), that is defined by the relation

$$\Omega' \equiv \frac{\Gamma}{C_d'} . \qquad \textbf{(A.8)}$$

Ω' is a conditional surface-based partition coefficient with dimensions of $[(M/L^2)/(M/L^3)]$.

To relate this partition coefficient to the bulk (suspension) dissolved contaminant concentration C_d, we must make an adjustment for the suspension porosity, Φ. Porosity Φ (volume solution/ bulk volume suspension) must be used to correct the dissolved concentration for the suspension volume occupied by solids. The correction is significant only for concentrated suspensions, say $\Phi < 0.95$. These suspension concentrations will occur only in the bed and the bed-water interface. The relation between the solution dissolved concentration and the suspension dissolved concentration is

$$C_d' = \frac{C_d}{\Phi} . \qquad \textbf{(A.9)}$$

A situation of zero porosity would only occur for a solid of no fluid void space, a condition of no interest in solid-solution exchange. Substituting the solution-suspension relation (A.9) for the dissolved concentration in the partition coefficient expression (A.8), we have another version of the partition coefficient,

$$\Omega' \equiv \frac{\Phi \Gamma}{C_d} . \qquad \textbf{(A.10)}$$

A porosity-corrected partition coefficient (termed Ω) is often preferred. The porosity-adjusted partition coefficient is fundamentally defined by

$$\Omega \equiv \frac{\Gamma}{C_d}. \qquad \textbf{(A.11)}$$

The porosity-adjusted (modeling) partition coefficient is related to the (experimental) partition coefficient in the following way:

$$\Omega \equiv \frac{\Gamma}{\Phi C_d'} \equiv \frac{\Omega'}{\Phi} \qquad \textbf{(A.12)}$$

It is necessary to note that experimental isotherms usually rely on measurement of the thermodynamically correct C_d' and thus result in estimates of Ω', while modeling is most often conducted with C_d as a state variable. The two views are related but not identical. Their parallel relationship is depicted in Figure A.1.

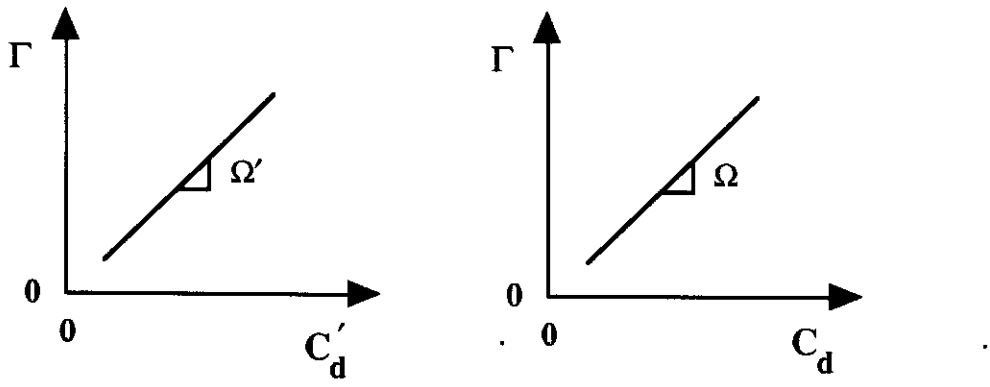

Figure A.1 Linear Surface Partition Coefficients

The newly defined surface-based distribution coefficient Ω is analogous to the conditional mass-based partition coefficient, K_p. In the traditional approach, K_p is defined as the quotient of the mass sorption density, r [mass of sorbate per mass of sorbent], and the suspension dissolved contaminant concentration, C_d :

$$K_p \equiv \frac{r}{C_d}. \qquad \textbf{(A.1)}$$

K_p has dimensions of $[(M/M)/(M/L^3)]$. As with the surface-based form (A.11), this partition coefficient is porosity-adjusted.

The analogies and differences between the mass density and surface density partition coefficients may be seen by comparing their definitions, equations (A.1) and (A.11). Sorbate mass density, r, is often expressed as

$$r = \frac{C_p}{M} \qquad \textbf{(A.13)}$$

or $C_p = rM$, where M is the mass of sorbent (particles) per bulk volume, *i.e.*, the suspension solids mass concentration. The limiting case of no sorbent (M = 0) is of no interest.

An analogous expression for the surface-based sorbate surface density, Γ, relates the sorbate density to the suspension solids surface area concentration S [particle surface area per bulk suspension volume]. Thus we have

$$\Gamma = \frac{C_p}{S}, \qquad \textbf{(A.14)}$$

or $C_p = \Gamma S$. A plot of mass density sorbate (r) vs. either C_d' or C_d would have the same appearance as the areal density sorbate (Γ) vs. solute graphs of Figure A.1. Corresponding slopes of the mass-based isotherms would be K_p' and K_p, respectively.

The relationship between the mass-based and surface-based partition coefficients is obtained by equating the expressions relating C_p to Γ, S, r, and M, then substituting partition coefficients for Γ and r. Then the mass-average partition coefficient is

$$\overline{K_p} = \frac{\Omega S}{M}. \qquad \textbf{(A.15)}$$

One may recognize the ratio of bulk surface area to bulk mass as the average specific surface area,

$$\frac{S}{M} = \overline{A_s} . \qquad \textbf{(A.16)}$$

For a suspension with particles of spherical geometry and uniform density, the average specific surface area is

$$\overline{A_s} = \frac{\sum_i n_i \pi (d_i)^2 \Big/ \sum_i n_i}{\sum_i n_i \pi \rho (d_i)^3 \Big/ 6 \sum_i n_i} = \frac{6 \sum_i n_i (d_i)^2}{\rho \sum_i n_i (d_i)^3} , \qquad \textbf{(A.17)}$$

where n_i is the number concentration [#/cm^3] of particles with size 'i.' The specific surface area can be characterized by a mean particle size such that

$$\overline{A_s} \cong \frac{6}{\rho \overline{d_p}} . \qquad \textbf{(A.18)}$$

The mean particle size for the specific surface area approximation (A.18) is neither the number-, area-, nor mass-average diameter; it is a nonlinear ratio of the area-average and mass-average diameters. It is apparent from (A.18), however, that average specific surface area is inversely related to mean particle size. If expressions (A.15), (A.16), and (A.18) are combined, then the bulk mass-based partition coefficient

$$\overline{K_p} = \Omega \left(\frac{6}{\rho \overline{d_p}} \right) \qquad \textbf{(A.19)}$$

is also inversely related to mean particle size.

When the particle size distribution shifts (in space or time), the bulk partition coefficient shifts in response to the shift in specific surface area, as reflected in the mean particle size. This indicates that the mass-based partition coefficient is itself a function of particle diameter. On a discrete size basis, the size-dependent mass-based partition coefficient is

$$K_{pk} = \Omega \frac{6}{\rho d_k} . \qquad \textbf{(A.20)}$$

Assuming the surface-based partition coefficient Ω is independent of size, equations (A.19) and (A.20) would indicate that the typical mass-based partition coefficient is a function of particle size. This would explain the size-dependent mass adsorption densities often observed, as reviewed in section A.1.4. Another frequent observation, the dependence of the mass-based partition coefficient on adsorbent or solids mass concentration, the so-called solids concentration effect, is described by this model in equation (A.15), provided the volumetric concentration of sorbent surface area is not linearly related to the volumetric concentration of sorbent mass. Recall that the variation between S and M is the coagulation premise of Anderson *et al.* (1985) and Chang *et al.* (1987), and indirectly, the peptization premise of Morel and Gschwend (1987).

Assuming a local equilibrium between solute and sorbate allows expression of the contaminant speciation in terms of the conditional partition coefficients. By relating the dissolved and particulate contaminant concentrations to the total contaminant concentration, one can reduce the number of state variables to be modeled from two or three to just one. The bulk dissolved and particulate mass or mole fractions are just

$$f_d = \frac{C_d}{C_T} \qquad \text{and} \qquad f_p = \frac{C_p}{C_T}. \tag{A.21}$$

Surface-based partitioning leads to expressions for the fractions of

$$f_d = \frac{1}{1 + \Omega S} = \frac{\Phi}{\Phi + \Omega' S} \tag{A.22}$$

and

$$f_p = \frac{\Omega S}{1 + \Omega S} = \frac{\Omega' S}{\Phi + \Omega' S}. \tag{A.23}$$

Conventional mass-based partitioning results in fractions of

$$f_d = \frac{1}{1 + \overline{K_p} M} = \frac{\Phi}{\Phi + \overline{K_p'} M} \qquad \textbf{(A.24)}$$

and $$f_p = \frac{\overline{K_p} M}{1 + \overline{K_p} M} = \frac{\overline{K_p'} M}{\Phi + \overline{K_p'} M} . \qquad \textbf{(A.25)}$$

From the definition of C_T as the sum of dissolved and particulate species (A.7), the sum of the mass fractions f_d and f_p is unity.

Total contaminant transport is conceptually driven by the fluid flow field as well as by the particle-associated contaminant transport relative to the fluid flow field. The particulate fraction f_p is used to modify the total contaminant transport equation,

$$\frac{\partial C_T}{\partial t} + U_i \frac{\partial C_T}{\partial x_i} = E_{ii} \frac{\partial^2 C_T}{\partial x_i^2} . \qquad \textbf{(A.26)}$$

We note at this point that total contaminant is partitioned between two species, enabling an expansion of any derivative of total concentration. For example, the time derivative can take any of the forms

$$\frac{\partial C_T}{\partial t} = \frac{\partial}{\partial t}(C_d + C_p) = \frac{\partial C_d}{\partial t} + \frac{\partial C_p}{\partial t} = \frac{\partial f_d C_T}{\partial t} + \frac{\partial f_p C_T}{\partial t} . \qquad \textbf{(A.27)}$$

Recall that for the fine particles considered, inertial effects are insignificant, so both the dissolved and particulate contaminant species follow the fluid flow. In addition to the flow field transport, particulate contaminant species transport due to particle fluxes must be superimposed on the total contaminant transport. Away from boundary fluxes, only the advective terms of the transport equation (A.26) are affected. Expanding the advective terms only we obtain

$$- U_i \left(\frac{\partial C_d}{\partial x_i} + \frac{\partial C_p}{\partial x_i} \right) = - U_x \left(\frac{\partial C_d}{\partial x} + \frac{\partial C_p}{\partial x} \right) - U_{zt} \left(\frac{\partial C_d}{\partial z} + \frac{\partial C_p}{\partial z} \right) . \qquad \textbf{(A.28)}$$

U_{zt} is the total vertical contaminant velocity, *i.e.*, the sum of fluid flow and contaminant motion relative to the fluid. Expanding the vertical advective transport terms alone, and distinguishing between which velocities apply to which species,

$$- U_{zt}\left(\frac{\partial C_d}{\partial z} + \frac{\partial C_p}{\partial z}\right) = - U_z \frac{\partial C_d}{\partial z} - (U_z + v_k)\frac{\partial C_p}{\partial z} . \qquad \textbf{(A.29)}$$

A simple rearrangement of the right hand side reveals that

$$- U_z\left(\frac{\partial C_d}{\partial z} + \frac{\partial C_p}{\partial z}\right) - v_k \frac{\partial C_p}{\partial z} = - U_z \frac{\partial C_T}{\partial z} - v_k \frac{\partial f_p C_T}{\partial z} . \qquad \textbf{(A.30)}$$

Therefore, total contaminant is transported in exactly the same manner as a neutrally buoyant tracer, with the superposition of a size-dependent settling term.

Use of the mass fraction f_p does enable a simplified calculation of total contaminant transport, but not to the extent expected. Because of its relation to sorbent surface concentration (A.23) or mass concentration (A.25), f_p is a function of two-dimensions in space. There is, at any point in space, an integral or total value of f_p due to the sum contribution of surface area or mass from all size particles. Because of its multiplication by size-dependent settling velocity v_k in (A.30), a size-dependent value of f_p at each point in space must also be considered.

A.2.2 Boundary Conditions and Solution

The boundary conditions and the solution method for the contaminant transport equation (A.26) parallel those used for the particles. The flux balance at the bed-water interface over short time scales during active sedimentation and resuspension might not require the inclusion of diffusive solute transfer.

The algorithms developed to describe size-dependent particle association and size-dependent, particle-associated contaminant transport are contained in subroutines DISTRB() and TRANSC(), respectively. The particle model is discussed in Chapter 3

and presented in Appendix E. These contaminant speciation and transport routines are presently bypassed in the particle transport and transformation model.

A.3 APPENDIX A REFERENCES

Ahlrichs, J.I. (1972). "The Soil Environment." In C.A.I. Goring and J.W. Hamaker (Ed.), Organic Chemicals in the Soil Environment (pp. 3-46). New York: Marcel Dekker.

Ambrose, R.B., Jr., Connolly, J.P., Southerland, E., Barnwell, T.O., Jr, & Schnoor, J.L. (1988). "Waste Allocation Simulation Models." Journal Water Pollution Control Federation, 60(9), 1646-1655.

Anderson, M.A., Tejedor-Tejedor, M.I., & Stanforth, R.R. (1985). "Influence of Aggregation on the Uptake Kinetics of Phosphate by Goethite." Environmental Science and Technology, 19(7), 632-637.

Baccinni, P., Greider, E., Steirli, R., & Goldberg, S. (1982). "The Influence of Natural Organic Matter on the Adsorption Properties of Mineral Particles in Lake Water." Schweizerische Zeitschrift fur Hydrologie, 44(1), 99-116.

Baker, J.E., Capel, P.D., & Eisenreich, S.J. (1986). "Influence of Colloids on Sediment-Water Partition Coefficients of Polychlorobiphenyl Congeners in Natural Waters." Environmental Science and Technology, 20(11), 1135-1143.

Benjamin, M.M. and Leckie, J.O. (1980). "Adsorption of Metals at Oxide Interfaces: Effects of the Concentrations of Adsorbate and Competing Metals." In R.A. Baker (Ed.), Contaminants and Sediments: Analysis, Chemistry, Biology (pp. 305-322). Ann Arbor, MI: Ann Arbor Science.

Benjamin, M.M. and Leckie, J.O. (1981). "Multiple-Site Adsorption of Cd, Cu, Zn, and Pb on Amorphous Iron Oxyhydroxide." Journal of Colloid and Interface Science, 79(1), 209-221.

Chang, C.C.Y., Davis, J.A., & Kuwabara, J.S. (1987). "A Study of Metal Ion Adsorption at Low Suspended-solid Concentrations." Estuarine, Coastal and Shelf Science, 24, 419-424.

Curl, R.L. and Keoleian, G.A. (1984). "Implicit-Adsorbate Model for Apparent Anomalies with Organic Adsorption on Natural Adsorbents." Environmental Science and Technology, 18(12), 916-922.

Di Toro, D.M. (1985). "A Particle Interaction Model of Reversible Organic Chemical Sorption." Chemosphere, 14(10), 1503-1538.

Di Toro, D.M., Donigan, A.S., Games, L.M., Lassiter, R.R., & Matsuoka, Y. (1982). "Synopsis of Discussion Session: Validation and Appraisal Testing." In K.L. Dickson, A.W. Maki, & J. Cairns Jr. (Ed.), Modeling the Fate of Chemicals in the Aquatic Environment (pp. 387-396). Ann Arbor, MI: Ann Arbor Science.

Di Toro, D.M., Mahony, J.D., Kirchgraber, P.R., O'Byrne, A.L., Pasquale, L.R., & Piccirilli, D.D. (1986). "Effects of Nonreversibility, Particle Concentration, and Ionic Strength on Heavy Metal Sorption." Environmental Science and Technology, 20(1), 55-61.

Dzombak, D.A. and Morel, F.M.M. (1987a). "Adsorption of Inorganic Pollutants in Aquatic Systems." Journal of Hydraulic Engineering, 113(4), 430-475.

Dzombak, D.A. and Morel, F.M.M. (1987b). "Development of a Data Base for Modelling Adsorption of Inorganics on Iron and Aluminum Oxides." Environmental Progress, 6(2), 133-137.

Farley, K.J., Dzombak, D.A., & Morel, F.M.M. (1985). "A Surface Precipitation Model for the Sorption of Cations on Metal Oxides." Journal of Colloid Interface Science, 112, 588-598.

Gschwend, P.M. and Wu, S. (1985). "On the Constancy of Sediment-Water Partition Coefficients of Hydrophobic Organic Pollutants." Environmental Science & Technology, 19(1), 90-96.

Hiraizumi, Y., Takahashi, M., & Nishimura, H. (1979). "Adsorption of Polychlorinated Biphenyl onto Sea Bed Sediment, Marine Plankton, and Other Adsorbing Agents." Environmental Science and Technology, 13(5), 580-584.

Honeyman, B.D. (1984). Cation and Anion Adsorption at the Oxide/Solution Interface in Systems Containing Binary Mixtures of Adsorbents: An Investigation of the Concept of Adsorptive Additivity. Unpublished doctoral dissertation, Stanford University.

Honeyman, B.D. and Santschi, P.H. (1988). "Metals in Aquatic Systems." Environmental Science and Technology, 22(8), 862-871.

Imboden, D.M. and Schwarzenbach, R.P. (1985). "Spatial and Temporal Distribution of Chemical Substances in Lakes: Modeling Concepts." In W. Stumm (Ed.), Chemical Processes in Lakes New York: John Wiley.

Jones, B.F. and Bowser, C.J. (1978). "The Mineralogy and Related Chemistry of Lake Sediments." In A. Lerman (Ed.), Lakes: Chemistry, Geology, Physics (pp. 179-236). New York: Springer-Verlag.

Kabata-Pendias, A. and Pendios, H. (1984). Trace Elements in Soils and Plants . CRC Press.

Karickhoff, S.W. (1984). "Organic Pollutant Sorption in Aquatic Systems." Journal of Hydraulic Engineering, 110(6), 707-735.

Lerman, A. (1979). Geochemical Processes: Water and Sediment Environments . New York: John Wiley & Sons.

Mabey, W.R., Smith, J.H., Podoll, R.T., Johnson, H.L., Mill, T., Chou, T.-W., Gates, J., Partridge, I.W., Jaber, H., & Vandenberg, D. (1982). Aquatic Fate Process Data for Organic Priority Pollutants (EPA-440/4-81- 014). USEPA.

Mikhail, R.S. and Brunauer, S. (1975). "Surface Area Measurements by Nitrogen and Argon Adsorption." Journal of Colloid and Interface Science, 52(3), 572-577.

Mills, W.B., Porcella, D.B., Ungs, M.J., Gherini, S.A., Summers, K.V., Mok, L., Rupp, G.L., Bowie, G.L., & Haith, D.A. (1985). Water Quality Assessment: A Screening Procedure for Conventional Pollutants in Surface and Ground Waters, Parts 1 and 2 (EPA-600/6-85-002 a,b). USEPA.

Morel, F.M.M. and Gschwend, P.M. (1987). "The Role of Colloids in the Partitioning of Solutes in Natural Waters." In W. Stumm (Ed.), Aquatic Surface Chemistry (pp. 405-422). New York: John Wiley & Sons.

Nadeau, P.H. (1987). "Relationships between the Mean Area, Volume and Thickness for Dispersed Particles of Kaolinites and Micaceous Clays and their Application to Surface Area and Ion Exchange Properties." Clay Minerals, 22(3), 351-356.

O'Connor, D.J. (1988a). "Models of Sorptive Toxic Substances in Freshwater Systems. I: Basic Equations." Journal of Environmental Engineering, 114(3), 507-532.

O'Connor, D.J. (1988b). "Models of Sorptive Toxic Substances in Freshwater Systems. II: Lakes and Reservoirs." Journal of Environmental Engineering, 114(3), 533-551.

O'Connor, D.J. (1988c). "Models of Sorptive Toxic Substances in Freshwater Systems. III: Streams and Rivers." Journal of Environmental Engineering, 114(3), 552-574.

O'Connor, D.J. and Connolly, J.P. (1980). "The Effect of Concentration of Adsorbing Solids on the Partition Coefficient." Water Research, 14, 1517-1523.

Oliver, B.G. (1973). "Heavy Metal Levels of Ottawa and Rideau River Sediments." Environmental Science & Technology, 7(2), 135-137.

Schellenberg, K., Leuenberger, C., & Schwarzenbach, R.P. (1985). "Sorption of Phenols by Natural Sediments and Aquifer Materials." Environmental Science & Technology, 18(9), 652-657.

Schnoor, J.L., Sato, C., McKechnie, D., & Sahoo, D. (1987). Processes, Coefficients, and Models for Simulating Toxic Organics and Heavy Metals in Surface Waters (EPA/600/3-87/015). USEPA.

Sigg, L. (1987). "Surface Chemical Aspects of the Distribution and Fate of Metal Ions in Lakes." In W. Stumm (Ed.), Aquatic Surface Chemistry (pp. 319-346). New York: John Wiley & Sons.

Thomann, R.V. and Mueller, J.A. (1987). Principles of Surface Water Quality Modeling and Control . New York: Harper & Row.

Versar, I. (1984). Catalogue of Waste Load Allocation Models for Toxic Compounds in Technical Guidance Manual for Performing Waste Load Allocations. Book 2, Streams and Rivers. Chapter 3, Toxic Substances. (EPA 440/4-84-022). USEPA.

Voice, T.C., Rice, C.P., & Weber, W.J., Jr. (1983). "Effects of Solids Concentration on the Sorptive Partitioning of Hydrophobic Pollutants in Aquatic Systems." Environmental Science and Technology, 17(9), 513-518.

Voice, T.C. and Weber, W.J., Jr. (1983). "Sorption of Hydrophobic Compounds by Sediments, Soils and Suspended Solids - I: Theory and Background." Water Research, 17(10), 1433-1441.

Voice, T.C. and Weber, W.J., Jr. (1985). "Sorbent Concentration Effects in Liquid/Solid Partitioning." Environmental Science and Technology, 19(9), 789-796.

Weber, W.J., Jr. (1972). "Adsorption." In W.J. Weber Jr. (Ed.), Physiochemical Processes for Water Quality Control (pp. 199-260). New York: Wiley-Interscience.

Weiler, R.R. and Mills, A.A. (1965). "Surface Properties and Pore Structure of Marine Sediments." Deep-Sea Research, 12, 511-529.

Westall, J. and Hohl, H. (1980). "A Comparison of Electrostatic Models for the Oxide/Solution Interface." Journal Colloid and Interface Science, 12, 265-294.

Westall, J.C. (1987). "Adsorption Mechanisms in Aquatic Surface Chemistry." In W. Stumm (Ed.), Aquatic Surface Chemistry (pp. 3-31). New York: John Wiley & Sons.

Westall, J.C., Leuenberger, C., & Schwarzenbach, R.P. (1985). "Influence of pH and Ionic Strength on the Aqueous-Nonaqueous Distribution of Chlorinated Phenols." Environmental Science & Technology, 19(2), 193-198.

Wu, S.-c. and Gschwend, P.M. (1986). "Sorption Kinetics of Hydrophobic Organic Compounds to Natural Sediments and Soils." Environmental Science and Technology, 20(7), 717-725.

APPENDIX B

Town Lake Watershed Areas

WATERSHED DEVELOPMENT, IMPERVIOUS COVER, AND RUNOFF COEFFICIENTS

Watershed-Year Land Use[1]	Impervious Cover (%)[2]	Dry Cr - 1980 Area (Ac)	Dry Cr - 1980 Area (%)	Dry Cr - 1980 Imperv (%)	Dry Cr - 2005 Area (Ac)	Dry Cr - 2005 Area (%)	Dry Cr - 2005 Imperv (%)	Johnson Cr - 1980 Area (Ac)	Johnson Cr - 1980 Area (%)	Johnson Cr - 1980 Imperv (%)	Johnson Cr - 2005 Area (Ac)	Johnson Cr - 2005 Area (%)	Johnson Cr - 2005 Imperv (%)	Barton Cr - 1980 Area (Ac)	Barton Cr - 1980 Area (%)	Barton Cr - 1980 Imperv (%)	Barton Cr - 2005 Area (Ac)	Barton Cr - 2005 Area (%)	Barton Cr - 2005 Imperv (%)
Residential Low	20	445	18.7	3.7	1124	47.3	9.4	0	0	0	0	0	0	631	1.9	0.4	1635	5.0	1.0
Medium	40	--	--	--	--	--	--	379	34.0	13.6	407	36.3	14.5	631	1.9	0.8	1635	5.0	2.0
High	60	--	--	--	--	--	--	63	5.6	3.4	68	6.1	3.6	--	--	--	--	--	--
Multi-Unit	70	--	--	--	--	--	--	189	17.0	11.9	204	18.2	12.7	--	--	--	--	--	--
(Total)		(445)			(1124)			(631)			(679)			(1262)			(3269)		
Commercial	50-80	62	2.6	1.7	128	5.4	3.5	26	2.3	1.5	31	2.8	1.8	30	0.09	0.06	144	0.4	0.3
Industrial	50-70	6	0.2	0.2	6	0.2	0.2	26	2.3	1.4	26	2.3	1.4	0	0	0	0	0	0
Street	100	105	4.4	4.4	255	10.7	10.7	213	19.1	19.1	215	19.2	19.2	228	0.7	0.7	401	1.2	1.2
Public	30	100	4.2	1.3	181	7.6	2.3	166	14.9	4.5	170	15.2	4.6	600	1.8	0.5	674	2.0	0.6
Undeveloped	8	1660	69.8	5.6	684	28.8	2.3	53	4.8	0.4	0	0	0	30,862	93.6	7.5	28,494	86.4	6.9
Total Basin		2378	100	16.9	2378	100	28.4	1115	100	55.8	1121	100	57.8	32,982	100	9.9	32,982	100	12.0
Planning Div. Area[1] (mi^2)		3.72			3.72			1.74			1.75			51.53			51.53		
Watershed Div. Area[3,8] (mi^2)		3.8			3.8			1.7			1.7			125.3			125.3		
Impervious Cover (%)[4,8]		13.1			23.2			47.4			49.2			7.0[6]			8.8[7]		
Runoff Coefficient[5,8]		0.15			0.19			0.33			0.35			0.12			0.13		

Appendix B (continued)

Watershed-Year Land Use[1]	Impervious Cover (%)[2]	W. Bouldin - 1980 Area (Ac)	W. Bouldin - 1980 Area (%)	W. Bouldin - 1980 Imperv (%)	W. Bouldin - 2005 Area (Ac)	W. Bouldin - 2005 Area (%)	W. Bouldin - 2005 Imperv (%)	Shoal Cr - 1980 Area (Ac)	Shoal Cr - 1980 Area (%)	Shoal Cr - 1980 Imperv (%)	Shoal Cr - 2005 Area (Ac)	Shoal Cr - 2005 Area (%)	Shoal Cr - 2005 Imperv (%)	Waller Cr - 1980 Area (Ac)	Waller Cr - 1980 Area (%)	Waller Cr - 1980 Imperv (%)	Waller Cr - 2005 Area (Ac)	Waller Cr - 2005 Area (%)	Waller Cr - 2005 Imperv (%)
Residential																			
Low	20	0	0	0	0	0	0	22.2	0.2	0.04	25.1	0.3	0.06	0	0	0	0	0	0
Medium	40	631	30.8	12.3	780	35.6	14.3	2219	25.0	10.0	2495	28.1	11.2	1812	31	12.4	2094	35.7	14.3
High	60	105	5.1	2.0	130	5.9	3.6	369	4.1	2.4	414	4.7	2.8	292	5	3.0	338	5.8	3.5
Multi-Unit	70	315	15.4	10.8	390	17.8	12.5	1110	12.5	8.8	1247	14.0	9.8	292	5	3.5	338	5.8	4.0
(Total)		(1051)			(1300)			(3720)			(4181)			(2396)			(2770)		
Commercial	50-80	221	10.8	7.0	265	12.1	7.9	799	9.0	5.8	970	10.9	7.1	386	6.6	4.3	477	8.1	5.3
Industrial	50-70	55	2.7	1.6	55	2.5	1.5	419	4.7	2.8	433	4.9	2.9	386	6.6	4.0	426	7.2	4.4
Street	100	369	18.0	18.0	375	17.1	17.1	1601	18.0	18.0	1606	18.1	18.1	1147	19.5	19.5	1149	19.6	19.6
Public	30	148	7.2	2.2	193	8.8	2.6	1122	12.6	3.8	1271	14.3	4.3	763	13.0	3.9	937	16.0	4.8
Undeveloped	8	205	10.0	0.8	0	0	0	1220	13.7	1.1	418	4.7	0.4	790	13.5	1.1	110	1.9	0.1
Total Basin		2049	100	54.7	2188	100	59.5	8884	100	52.7	8884	100	56.6	5869	100	51.7	5869	100	56.1
Planning Div. Area[1] (mi^2)		3.20			3.42			13.88			13.88			9.17			9.17		
Watershed Div. Area[3,8] (mi^2)		3.0			3.0			12.7			12.7			5.5			5.5		
Impervious Cover (%)[4,8]		46.4			50.6			46.4[6]			48.1[7]			42.0[6]			47.6[7]		
Runoff Coefficient[5,8]		0.33			0.365			0.27			0.285			0.34			0.37		

Appendix B (continued)

Watershed-Year Land Use[1]	Impervious Cover (%)[2]	E. Bouldin - 1980 Area (Ac)	Area (%)	Imperv (%)	E. Bouldin - 2005 Area (Ac)	Area (%)	Imperv (%)	Blunn Cr - 1980 Area (Ac)	Area (%)	Imperv (%)	Blunn Cr - 2005 Area (Ac)	Area (%)	Imperv (%)	Harper's Br - 1980 Area (Ac)	Area (%)	Imperv (%)	Harper's Br - 2005 Area (Ac)	Area (%)	Imperv (%)
Residential																			
Low	20	0	0	0	0	0	0	0	0	0	0	0	0	0	0	0	0	0	0
Medium	40	458	34.8	13.9	596	36.9	14.7	256	22.6	9.0	335	29.6	11.8	149	38.1	15.2	180	40.1	16.0
High	60	76.3	5.8	3.5	99	6.1	3.7	43	3.8	2.3	59	4.9	3.0	25	6.4	3.8	30	6.7	4.0
Multi-Unit	70	229	17.4	12.2	298	18.4	12.9	128	11.3	7.9	178	14.8	10.4	74	19.0	13.3	87	19.4	13.6
(Total)		(763)			(993)			(426)			(592)			(248)			(297)		
Commercial	50-80	89	6.8	4.4	152	9.4	6.1	95	8.4	5.4	144	12.0	7.8	46	11.8	7.6	64	14.2	9.3
Industrial	50-70	38	2.9	1.7	53	3.3	2.0	76	6.7	4.0	76	6.3	3.8	0	0	0	0	0	0
Street	100	254	19.3	19.3	260	16.1	16.1	189	16.7	16.7	195	16.2	16.2	76	19.4	19.4	76	16.9	16.9
Public	30	127	9.7	2.9	159	9.8	2.9	161	14.2	4.3	193	16.1	4.8	12	3.1	0.9	12	2.7	0.8
Undeveloped	8	45	3.4	0.3	0	0	0	186	16.4	1.3	0	0	0	9	2.3	0.2	0	0	0
Total Basin		1316	100	58.2	1617	100	58.4	1133	100	50.9	1200	100	57.8	391	100	60.4	449	100	60.6
Planning Div. Area[1] (mi^2)		2.06			2.53			1.77			1.88			0.61			0.70		
Watershed Div. Area[3,8] (mi^2)		1.9			1.9			1.4			1.4			0.6			0.6		
Impervious Cover (%)[4,8]		49.5			49.7			43.1			49.2			51.4			51.6		
Runoff Coefficient[5,8]		0.355			0.36			0.31			0.35			0.375			0.38		

Appendix B (continued)

Watershed-Year Land Use[1]	Impervious Cover (%)[2]	Tinnin Br - 1980 Area (Ac)	Area (%)	Imperv (%)	Tinnin Br - 2005 Area (Ac)	Area (%)	Imperv (%)
Residential							
Low	20	0	0	0	0	0	0
Medium	40	163	31.6	12.6	196	38.0	15.2
High	60	27	5.2	3.1	33	6.4	3.8
Multi-Unit	70	82	15.9	11.1	98	19.0	13.3
(Total)		(272)			(327)		
Commercial	50-80	52	10.1	6.6	57	11.0	7.2
Industrial	50-70	0	0	0	0	0	0
Street	100	86	16.7	16.7	88	17.0	17.0
Public	30	22	4.3	1.3	34	6.6	2.0
Undeveloped	8	84	16.3	1.3	10	1.9	0.2
Total Basin		516	100	52.7	516	100	58.6
Planning Div. Area[1] (mi^2)		0.81			0.81		
Watershed Div. Area[3,8] (mi^2)		--			--		
Impervious Cover (%)[4,8]		44.7			49.8		
Runoff Coefficient[5,8]		0.32			0.36		

Notes:
(1) Land use classes and areas from City of Austin (1982).
(2) City of Austin (1984b), from Hydroscience, Inc. (1976). Average of ranges used for commercial and industrial land types.
(3) City of Austin (1984a).
(4) Impervious cover calculated from linear regression of predicted vs. measured (aerial photos) impervious cover for City of Austin (1984b).
(5) Based on impervious cover/runoff coefficient relation presented in City of Austin (1984b).
(6) Measured (City of Austin, 1984b).
(7) Proportionate to 1980 measured/predicted.
(8) Values used in this study.

APPENDIX C

Town Lake Morphometry

MORPHOMETRY FOR TOWN LAKE

(USACE SURVEY, 1977)

X-SECTION	DOWNSTREAM DISTANCE	X-SECTION AREA	X-SECTION WIDTH AT SURFACE	SEGMENT DEPTH	SEGMENT VOLUME	SEGMENT SURFACE AREA
	(km)	(m^2)	(m)	(m)	(m^3)	(m^2)
1	.161	69	77	1.19	20,652	17,386
2	.193	187	139	1.35	6,029	4,460
3	.209	187	139	1.47	3,030	2,064
4	.241	189	118	1.47	6,061	4,128
5	.821	187	139	2.15	178,195	82,925
6	2.092	428	148	3.67	754,393	205,528
7	2.655	759	176	4.12	347,733	84,364
8	2.688	476	124	3.84	15,314	3,989
9	2.736	476	124	3.83	22,306	5,821
10	2.768	448	117	3.83	14,871	3,881
11	3.718	476	124	3.79	449,662	118,604
12	4.442	471	126	2.53	243,783	96,409
13	4.474	202	140	1.44	6,498	4,518
14	4.506	202	140	1.44	6,498	4,518
15	4.651	202	140	1.90	38,898	20,453
16	4.683	335	142	2.36	10,790	4,573
17	4.699	335	142	2.26	5,054	2,234
18	4.731	293	136	2.26	10,109	4,468
19	5.311	335	142	2.59	305,813	118,195
20	5.343	720	266	2.71	23,190	8,560
21	5.359	720	266	2.85	10,773	3,778
22	5.375	618	204	2.85	10,773	3,778
23	5.407	720	266	2.71	23,190	8,560
24	5.617	720	266	3.27	154,902	47,434
25	5.649	760	187	4.06	24,473	6,035
26	5.665	760	187	3.09	9,474	3,067
27	5.681	417	194	3.09	9,474	3,067
28	5.713	760	187	4.06	24,473	6,035
29	6.212	760	187	4.33	420,092	97,128
30	7.178	924	202	4.46	761,776	170,986
31	7.210	654	152	4.30	21,052	4,901
32	7.226	654	152	4.31	10,355	2,403
33	7.242	633	146	4.32	10,184	2,356
34	7.258	633	146	4.38	10,451	2,384
35	7.290	666	150	4.44	21,435	4,824
36	7.532	666	150	5.19	202,996	39,115
37	8.530	1,016	174	6.51	1,092,685	167,948
38	9.592	1,174	162	6.14	1,086,862	176,903
39	.000	872	171			

AVG AREA	AVG WIDTH	AVG DEPTH	TOTAL VOLUME	TOTAL AREA
(m^2)	(m^2)	(m)	(m^3)	(m^2)
541	163	4.12	6374000	1548000
(ft^2)	(ft^2)	(ft)	(ft^3)	(ft^2)
5826	534	13.51	225100000	16660000
			(ac-ft)	(ac)
			5168	382.5

APPENDIX D

Town Lake Hydrologic Inflows

In this appendix, the methods used to develop the hydrologic inflow rates for modeling Town Lake are described. Table 3.2 summarizes these results. References are provided at the end of the report.

D.1 Upstream Inflows

Releases from Lake Austin are dictated largely by the release schedule at Mansfield Dam, the outlet for Lake Travis. The flowrate measurements for the Lake Austin release from Tom Miller Dam were suspected of being inaccurate by the Lower Colorado River Authority (LCRA) at the time of this study, so the LCRA relies on flowrates from the Mansfield release for its Lake Austin release estimates (Robbins, 1985). Other inflows to and outflows from Lake Austin were added to the Travis release to close the water balance for the lake and estimate the upstream inflow to Town Lake.

The Lake Travis releases used in this study were prorated, 30-year monthly averages, developed as follows. The 30-year annual-average release from Lake Travis for 1952-1982 was 46.1 m^3/s (1,628 cfs), calculated from data provided by the LCRA (USGS, 1984). Average monthly release rates from LCRA for the 10-year period 1975-1984 (USGS; 1976-1984) were determined. During that period, the annual-average flowrate was 40.3 m^3/s. The 10-year monthly-average flowrates were then prorated (multiplied by the ratio of the 30-year to 10-year averages) to yield adjusted monthly-average release rates for the 30-year span.

Runoff from the Lake Austin watershed contributes to the inflow of water that eventually enters Town Lake. The methods for runoff estimation described in Section D.2 were applied for these monthly calculations.

As described in Section D.3, withdrawals for water supply from Lake Travis were expected to begin in 1989. These, combined with the increasing water supply withdrawals from Lake Austin, were subtracted from the Lake Austin inflows, as appropriate for the 2005 estimated outflows.

Rainfall directly onto the lake surface, minus the gross evaporation from the surface, produced monthly-average atmospheric inflows which were sometimes negative (net evaporation). These estimates are presented in Section D.4.

All of the monthly flowrates were combined to yield a net outflow from Lake Austin to Town Lake. The results for Lake Austin and other tributary inflows to Town Lake are contained in Table 3.2.

D.2 Tributaries Inflows

The methods used to estimate areas of and average rainfall-runoff coefficients for each sub-basin of the Town Lake watershed were discussed in Section 3.2. These data were used in combination with the monthly-average precipitation data shown in Table D.1 (see table for references and comparisons) to produce monthly-average flowrates for each basin. The rainfall data were taken from a long-term record of National Weather Service data from the station located in central Austin. Although different rainfall series were available, the period of record chosen for this study was 1951-1980, which corresponds closely to the period for the Travis release estimates.

D.3 Withdrawals

Water supply withdrawals represent a sizable diversion of clean water around Austin and Town Lake. These withdrawals reduce the flowrate through the lake so that contaminants remain in the system longer than they otherwise would.

The capacities of water treatment plants at Lake Austin, Town Lake, and Lake Travis, from 1980 through 2005, were obtained from the City of Austin (Benoit, 1985). A planning study (Metcalf & Eddy, 1985) provided the estimated annual-average withdrawal rates, *i.e.*, demand, for the total system in 1980 and 2005. The average percent of rated capacity for the total system was applied uniformly to each individual plant's rated capacity as a simplified expectation of the flowrate each was expected to withdraw. A summary of the rated, operating, and modeled withdrawal rates is given in Table D.2.

Annual-average withdrawal rates were apportioned into monthly-average withdrawal rates. Monthly-average rates for the period from May 1, 1984 to September 30, 1985 were obtained and examined for the two Lake Austin WTPs. The fraction of the total annual-average rate for the two plants was then determined for each month. These fractions were then applied to the estimated annual-average withdrawal rates for each individual plant in 1980 and 2005.

Annual-average diversions of Colorado river flow around Town Lake were estimated to be 5.8% in 1980 and 13.7% in 2005. As is now known, the Lake Travis water treatment plant has not materialized. The plant had been planned to meet municipal demands in the anticipated expansion of Austin's northwest corridor. Population growth in the metropolitan service region is likely to require additional withdrawals upstream of Town Lake, regardless of whether the Lake Travis plant is built. The long-term success of water conservation efforts in the city is unknown at this time. The uncertainty of the Lake Travis plant is somewhat academic, since the historical 1980 water supply withdrawal rates were used for modeling purposes.

D.4 Direct Rainfall and Evaporation

The last components of the water balance are the direct rainfall to and evaporation from the surface of Town Lake and Lake Austin. Multiplication of the monthly precipitation by the segment surface areas (Appendix C) gives the gross inflow rates to the segments. The monthly precipitation data used are presented in Table D.1. Reported pan evaporation rates for the area were reduced by the standard 30% to account for reservoir cooling effects. The adjusted gross evaporation rates, summarized in the same table, were also multiplied by segment surface areas to yield gross outflow rates from the surface of each segment.

D.5 Springs Flows

There are several springs in the drainage basin of Town Lake, but only the most significant has been quantified for flow and loading purposes. Barton Springs drains into Barton Creek and provides significant base flow. During dry periods, and when no water is being released from Tom Miller Dam, this can be the only flow into the lake.

The long-term average (1894-1982) flowrate for Barton Springs was 1.42 m^3/s (USGS, 1984). Monthly-average flowrates were estimated on the basis of monthly-average flowrates in 1982 (USGS, 1984) as:

$$Q_{li} = Q_{la} \times \frac{Q_{ai}}{Q_{aa}}, \qquad \textbf{(D.1)}$$

where

Q_{li} = long-term average flowrate for month i

Q_{la} = long-term annual-average flowrate

Q_{ai} = 1982 average flowrate for month i

Q_{aa} = 1982 annual-average flowrate.

Table D.1

SUMMARY OF AUSTIN RAINFALL AND EVAPORATION DATA

Month	Rainfall [in/month]			No. of Storms/Month[6]			Gross Evaporation [in/month]	
	(1,4)	(2)	(3)	P > 0.01 in[2]	P > 0.00 in[3]	Thunderstorms[2]	Pan[1]	Adjusted[4,5]
January	1.75	2.05	1.54	8	9.06	1	2.5	1.75
February	2.50	2.42	2.70	8	9.33	2	2.6	1.82
March	1.75	2.19	1.55	7	7.75	3	3.6	2.52
April	3.40	3.54	2.86	8	8.17	5	4.3	3.01
May	4.25	4.25	3.82	8	9.54	7	5.25	3.68
June	3.00	2.83	3.40	6	8.29	4	6.8	4.76
July	1.60	2.18	1.57	5	5.60	4	8.75	6.12
August	2.25	2.21	2.18	5	5.90	5	8.8	6.16
September	4.00	3.63	3.65	7	8.29	4	7.0	4.90
October	3.40	3.12	3.58	6	7.45	3	5.7	3.90
November	2.25	2.40	2.04	7	6.79	2	3.9	2.70
December	2.10	2.48	2.02	7	8.09	1	2.9	2.00
Annual	32.25	33.30	30.91	82	94.26	41	63.0	44.10

[1] Larkin and Bomar (1982). Period 1951-1980

[2] Gale Research Co. (1981). Period 1939-1978

[3] City of Austin and Engineering-Scinece, Inc. (1983). Period 1949-1974

[4] Used in Runoff Modeling.

[5] Adjusted Evaporation = 0.7 Pan Evaporation

[6] P is Precipitation in Inches per Storm

Table D.2
SUMMARY OF WATER TREATMENT PLANT WITHDRAWAL RATES

I. WATER TREATMENT PLANT CAPACITIES[1,2]

	1980	1985	1986	1987	1989	2005	Ultimate
Town Lake							
1. Green WTP [mgd]	33	45	45	45	45	45	45
Lake Austin							
2. Davis WTP [mgd]	90	90	120	120	120	120	120
3. Ullrich WTP [mgd]	33	33	33	140	140	140	140
Lake Travis[3]							
4. WTP #4 [mgd]	0	0	0	0	60	100	300
Total [mgd]	156	168	198	305	365	405	605

II. ANNUAL AVERAGE WITHDRAWALS FOR WATER SUPPLY[2]

	1980	1982-83	1995	2005
Withdrawal [mgd]	76.4	77.5	132.3	160.4
Average Capacity [%]	49.0	49.4	32.7	39.6

III. ANNUAL AVERAGE WITHDRAWALS BY TREATMENT PLANTS USED IN THIS STUDY

	Year	Capacity [mgd]	Capacity [%]	Average Withdrawal [mgd]
1. Town Lake	1980	33	49.0	16.2
	2005	45	39.6	17.8
2. Lake Austin	1980	123	49.0	60.3
	2005	260	39.6	103.0
3. Lake Travis[3]	1980	0	--	--
	2005	100	39.6	39.6

[1] Benoit (1985)
[2] Metcalf and Eddy (1985)
[3] Note: WTP #4 not operational (1991)

APPENDIX E

Transport Source Code (Fortran)

```
      PROGRAM TOWN
C This is code for Town Lake particle sims w/ lateral loads, with or w/o
C flow or load ramping: final version.
C Latest version:
C                - 1 apr   1991  2005.  removed all the BCN() writes in output
C Based on TOWNFIN.FOR (12/90), Based on TOWN7.FOR  Based on (BASE.FOR, 7/27/90)
C_____________________________________________________________________
      INTEGER   DIMNK,NK,NX,NZ,NM
      PARAMETER (DIMNK= 32, NK= 31, NX= 11, NZ= 6, NM= 10)
C
      INTEGER ITER,BAND1(10),BAND3(10),MAXFR1,MAXFR3,IBR,ISH,IDS
      INTEGER ICOAG,INFLAG,INRAMP,IQRAMP,IDISPZ,NOUT
C
C Real arrays used in both Fortran and C codes:
      REAL N1(DIMNK,NX,NZ), DP(DIMNK)
      REAL DELN1(DIMNK,NX,NZ)
C
C Real parameters used in both Fortran and C codes:
      REAL DELT,LV1ST,LVSTEP,TIME,GRAV,VISCOS,RHOW,RHOP
C
C Real arrays used in Fortran code only:
      REAL N2(DIMNK,NX,NZ),NSOURC(NK,NX,NZ)
      REAL NTRIB(NK,NX),NITRIB(NK),NIMAIN(NK),NMAIN(NK)
      REAL LDNDD1(NK),LDNDD2(NK),LDNDD3(NK),LDNDD4(NK),LDNDD(NK,NX,NZ)
      REAL CT1(NX,NZ), CT2(NX,NZ), FP(NK,NX,NZ), TOTFP(NX,NZ)
      REAL NUMIN(NK,NX),NUMOUT(NK,NX),NUMNET(NK,NX), TRNSFR(NX)
      REAL TSS(NX,NZ), DELTAD(NK), V(NK), TAREA(NX,NZ), TNUM(NX,NZ)
      REAL RFLUX(NX), BEDMAS(NX), BEDVOL(NX), POROS(NX), AREA(NX),B(NX)
      REAL MASSIN(NX), MASOUT(NX), OUTIME(NM)
C
      REAL UX(NX,NZ), UZ(NX,NZ), EX(NX,NZ), EZ(NX,NZ)
      REAL UXMEAN(NX), USTAR(NX), STRESB(NX)
      REAL Q(0:NX), QITRIB(0:NX), QTRIB(0:NX)
      REAL QSCALE(0:NX), NSCALE(0:NX)
      REAL CX(NX,NZ), CZ(NX,NZ), CZV(NK), DX(NX,NZ), DZ(NX,NZ)
      REAL TERMX(NX,NZ), TERMZ(NX,NZ)
C
C Real parameters used in Fortran code only:
      REAL DELX, DELZ, FRACT, DELA, TMAX
      REAL STRESC, RATEM, UXMAX, EXMEAN, EZMEAN, PI
      REAL CTW,CTB,KPM,KPA
      REAL TNRAMB,TNRAMU,TNRAMD,TQRAMB,TQRAMU,TQRAMD,TRMIN,TRMAX
C
C Real arrays and parameters used in C routines only:
      REAL FRAC(4,DIMNK), GAMMA(531), Y(DIMNK)
      REAL HMAX,TEMP,G,ALPHA
C
      CHARACTER*50   FILNAM
C
      COMMON/EROSON/ STRESC,RATEM
      COMMON/FLOC/   ALPHA,G,IBR,ISH,IDS
      COMMON/MEANS/  EXMEAN,EZMEAN,FRIC,IDISPZ,DEPTH
      COMMON/PART/   RHOP,RHOW,VISCOS,TEMP,GRAV,LV1ST,LVSTEP,PI
      COMMON/RAMP/   TNRAMB,TNRAMU,TNRAMD,TQRAMB,TQRAMU,TQRAMD,INRAMP,
     $               IQRAMP
      COMMON/STEPS/  DELX,DELZ,DELA,DELT,FRACT,TIME,TMAX,HMAX,NOUT,ITER
      COMMON/TAMNIT/ CTW,CTB,KPM,KPA
C
C_____________________________________________________________________
C PURPOSE: This program simulates particle and contaminant 2-D transport
C          and fate. In addition to Fortran subroutines, it calls two
C          coagulation subroutines in C.
C
C AUTHOR:  Jerry Culkin
C          Department of Civil Engineering
C          University of Texas at Austin
C
C PRECISION: Single.
C
C LANGUAGE: FORTRAN 77 except for FRCGAM() and COAG(), which are in C.
C
C REFERENCES: See subroutines.
C
C VARIABLE/PARAMETER DEFINITIONS:
C  ALPHA   - Chemical collision efficiency factor, [-]
C  CONA1   - Local conversion factor to convert proportional area in
C            [um^2/cm^3] to [cm^2/L]
C  CONA2   - Local conversion factor to convert proportional area-
C            partition fraction to actual area-partition fraction
C  CONM1   - Local conversion factor to convert proportional volume
C            in [um^3/cm^3] to absolute mass in [mg/L]
C  CONM2   - Local conversion factor to convert proportional mass-
C            partition fraction to actual mass-partition fraction
C  CONSTV  - Local conversion factor to Stokes settling velocity
C            in [cm/s]
C  COURNT  - Courant Number, [-]
C  CROSS   - Corrective term for 2-D FDE cross derivatives, [#-m/cm^3]
C  CTB     - Initial total contaminant conc in bed, [ug/L]
C  CTW     - Initial total contaminant conc in water, [ug/L]
C  CZV     - Vertical settling Courant Number, [-]
C  DELA    - Fraction of DELZ for vertical node at bed-water interface
C  DELCT   - Local Incremental Cp flux calculation, [ug/L-s]
C  DELNO   - Local change in number concentration at bed interface,
C            [#/cm^3]
C  DELT    - Time step size for numerical stability, [sec]
C  DELX    - Longitudinal grid spacing,(uniform), [cm]
C  DELZ    - Vertical grid spacing,(uniform), [cm]
C  DEPTH   - Average total water column depth, [cm]
C  DILUT   - Dilution factor for tributary concentration(k,i)
```

```
C  DIMNK    - NK + 1 to accomodate element shifts in C codes
C  DISPX    - Local dispersion component in X direction, [-]
C  DISPZ    - Local dispersion component in Z direction, [-]
C  DMHAF    - Local diameter at half log step below current size, [um]
C  DPHAF    - Local diameter at half log step above current size, [um]
C  ENGDIS   - Local energy dissipation, [cm^2/s^3]
C  EXJ      - Local longitudinal dispersion coefficient at depth j,
C              [cm^2/s]
C  EZJ      - Local vertical dispersion coefficient at depth j, [cm^2/s]
C  EXMAX    - Maximum longitudinal dispersion coefficient, [cm^2/s]
C  EZMAX    - Maximum vertical dispersion coefficient, [cm^2/s]
C  EXMEAN   - Mean longitudinal dispersion coefficient, [cm^2/s]
C  EZMEAN   - Mean vertical dispersion coefficient, [cm^2/s]
C  FDFULL   - Local Ratio of adjacent particle diameters, [-]
C  FDHALF   - Local Ratio of diameter half step above current to current
C              size
C  FRACT    - Safety factor used to set stable DELT, [ < 0.8]
C  FRIC     - Local Darcy-weisbach friction factor assigned, [-]
C  G        - Fluid velocity gradient, [1/s]
C  GRAV     - Acceleration due to gravity, [cm/s^2]
C  HMAX     - Maximum allowable time step in COAG, [s]
C  I,J,K    - Local Indices for X node, Z node, and particle size,
C              respectively
C  IBR      - Switch defining Brownian collision mechanism and trajectory
C              type
C  ICOAG    - Flag for coagulation routine calls (1=on)
C  IDS      - Switch defining differential sedimentation collision
C              mechanism and trajectory type
C  IDISPZ   - Switch for using uniform prescribed Ez (1=on)
C  INFLAG   - Switch for homogeneous number concentration as I.C. (1=on)
C  INRAMP   - Switch for ramping trib number concentrations (1=on)
C  IQRAMP   - Switch for ramping trib flowrates (1=on)
C  ISH      - Switch defining fluid shear collision mechanism and
C              trajectory type
C  ITER     - Number of iterations already taken
C  KARMAN   - Local von Karman's constant, [-]
C  KPA      - Surface-based, porosity-corrected partition coefficient,
C              [L/cm^2]
C  KPM      - Mass-based, porosity-corrected partition coefficient,
C              [L/kg]
C  K2, K3   - Local indices of size
C  LDSTEP   - log of ratio of adjacent particle diameters, [-]
C  LV1ST    - log(Volume of 1st particle size), vol in [um^3]
C  LVSTEP   - Delta log(Vp), log(V(k+1)/V(k))
C  M        - Output index for OUTIME():
C  MAXFR1   - Maximum value of any element in FRAC(1,DIMNK), [-]
C  MAXFR3   - Maximum value of any element in FRAC(3,DIMNK), [-]
C  NK       - Number of particle size classes
C  NM       - Maximum number of output times allowed after time zero
C  NOUT     - Number of actual output times after time zero output
C  NX       - Number of longitudinal (X) grids
C  NZ       - Number of vertical (Z) grids
C  PI       - The universal constant 3.141592
C  PEX      - Local Longitudinal Grid Peclet number, [-]
C  PEZ      - Local Vertical Grid Peclet number, [-]
C  RATEM    - Erosion rate constant, [s/cm]
C  REMAIN   - Remainder of ITER/1000. REMAIN=0. for every 1000 ITER.
C  RHOP     - Effective bulk density of floc, [g/cm^3]
C  RHOW     - Density of fluid, [g/cm^3]
C  SUMCP    - Local Cp flux accumulator, [ug/L-s]
C  STRESB   - Local Bed shear stress, [dyne/cm^2] = (g/cm-s^2]
C  STRESC   - Local Critical shear stress for erosion, [dyne/cm^2]
C  SUMARA   - Local Particle surface area conc accumulator for loop,
C              [um^2/cm^3]
C  SUMMAS   - Local Particle mass conc accumulator for loop, [um^3/cm^3]
C  SUMNUM   - Local Particle number conc accumulator for loop, [#/cm^3]
C  TMAX     - Maximum length of simulation, [s]
C  TEMP     - Temperature, [K]
C  TIME     - Elapsed time of simulation, [s]
C  TNRAMB   - Time to begin ramp up of inflow number concentrations, [s]
C  TNRAMD   - Time to ramp down of inflow number concentrations, [s]
C  TNRAMU   - Time to ramp up of inflow number concentrations, [s]
C  TQRAMB   - Time to begin ramp up of inflow flowrate, [s]
C  TQRAMD   - Time to ramp down of inflow flowrate, [s]
C  TQRAMU   - Time to ramp up of inflow flowrate, [s]
C  TRMAX    - Final time of ramp down of flowrate or trib concs, [s]
C  TRMIN    - Initial time of ramp up of flowrate or trib concs, [s]
C  UAVG     - Average velocity between top and bottom nodes where load is
C              distributed, [cm/s]
C  UXJ      - Local Longitudinal velocity at depth j, [cm/s]
C  UXMAX    - Max longitudinal velocity in vertical field, [cm/s]
C  UZMAX    - Max vertical velocity in field, [cm/s]
C  VISCOS   - Molecular viscosity of suspension, [g/cm-s]
C  VOLMAS   - Spherical volume to mass conversion factor
C  VMAX     - Maximum settling velocity of floc, [cm/s]
C  ZBOT     - Bottom depth where load is distributed, measured from bed,
C              [cm]
C  ZINT     - Vertical interval where load is distributed, [cm]
C  ZLOCAL   - Depth measured from bed, [cm]
C  ZSYSTM   - Depth measured from surface, [cm]
C  ZTOP     - Top depth where load is distributed, measured from bed, [cm]
C (AREA)    - Average cross-sectional area at grid, [m^2]
C (B)       - Average width of cross-section at grid, [m]
C (BAND1)
C (BAND3)
C (BEDMAS) - Total mass of solids in the interface layer per unit area
C              at node I, [g/cm^2]
C (BEDVOL) - Bulk volume of the interface layer per unit area at node
C              I, i.e., DEPTH(I), [cm^3/cm^2]
```

```
C {CZV}    - Settling Courant No. for size K particle, [-]
C {DELTAD} - Delta diameter about each floc size, [um]
C {DP}     - Equivalent spherical diameter of size k floc, elements
C              shifted in C code, [um]
C {GAMMA}  - Collision frequency function for 3 mechanisms, [ ]
C {LDNDD1} - Vector of initial PSD for water column, log([#/cm^3-um])
C {LDNDD2} - Vector of initial PSD for bed, log([#/cm^3-um])
C {LDNDD3} - Vector of initial PSD for main inflow, log([#/cm^3-um])
C {LDNDD4} - Vector of initial PSD for tributary, log([#/cm^3-um])
C {NIMAIN} - Initial number concentration distribution for main inflow,
C              from LDNDD3, [#/cm^3]
C {NITRIB} - Initial number concentration distribution for tributaries,
C              from LDNDD4, [#/cm^3]
C {NMAIN}  - Number concentration distribution for main inflow, [#/cm^3]
C {NSCALE} - Factor, peak tributary number concentrations divided by
C              initial tributary number concentrations, [-]
C {POROS}  - Bulk porosity of interface layer, [cm^3/cm^3]
C {Q}      - Total flowrate, [m^3/s]
C {QSCALE} - Factor, peak flowrate divided by initial flowrate, [-]
C {QITRIB} - Initial tributary flowrate, [m^3/s]
C {RFLUX}  - Total potential vertical bed mass flux at node I due
C              to resuspension; positive for flux out of bed.
C              Subject to bed mass availability. [g/cm^2-s]
C {STRESB} - Local Bed shear stress, [dyne/cm^2] = [g/cm-s^2]
C {TRNSFR} - Bulk resuspension transfer velocity, [cm/s]
C {USTAR}  - Local Shear velocity, [cm/s]
C {UXMEAN} - Mean longitudinal velocity, [cm/s]
C {V}      - Settling velocity of size class k, [cm/s]
C {Y}      - Working vector for concentration in C, overwritten for
C              each different (x,z) location, [#/cm^3]
C [CT1]    - Total contaminant concentration before transport, [ug/L]
C [CT2]    - Total contaminant concentration after transport, [ug/L]
C [CX]     - Courant Number in X, times width, [m]
C [CZ]     - Courant Number in Z, times width, [m]
C [DELN1]  - Change in number conc. due to coagulation over time step,
C              [#/cm^3]
C [DX]     - Dispersion Number in X, times width, [m]
C [DZ]     - Dispersion Number in Z, times width, [m]
C [EX]     - Dispersion coefficient in X, [cm^2/s]
C [EZ]     - Dispersion coefficient in Z, [cm^2/s]
C [FP]     - fraction of total contaminant sorbed to solid of size k,
C              [-]
C [FRAC]   - Fraction of particle floc in integer particle classes, [-]
C [LDNDD]  - Matrix of PSD, i.e., LdNdD, log([#/cm^3-um])
C [N1]     - Number concentration throughout water column & bed,[#/cm^3]
C [N2]     - Number concentration after transport but before
C              coagulation [#/cm^3]
C [NSOURC] - Concentration source at (i,j) due to tributary source,
C              [#/cm^3]
C [NTRIB]  - Number concentration for tributaries, [#/cm^3]
C [NUMIN]  - Number of size k flocs (per unit area) entering bed at
C              node I during DELT, [#/cm^2]
C [NUMNET] - Net number of size k flocs (per unit area) entering
C              interface at node I during DELT, [#/cm^2]
C [NUMOUT] - Number of size k flocs (per unit area) leaving
C              bed at node I during DELT, [#/cm^2]
C [TAREA]  - Total superficial surface area concentration of suspended
C              solids, [cm^2/L]
C [TERMX]  - Longitudinal combination of Ci & Di, times width, [m]
C [TERMZ]  - Vertical combination of Ci & Di, times width, [m]
C [TNUM]   - Total number concentration of suspended solids, [#/cm^3]
C [TSS]    - Total suspended solid mass concentration, [mg/L]
C [UX]     - Fluid velocity in X, [cm/s]
C [UZ]     - Fluid velocity in Z, [cm/s]
C
C REQUIRED ROUTINES:
C In Fortran:
C   - BEDXCH
C   - CONCIC
C   - DISTRB
C   - ERODE
C   - FLOWI
C   - IN
C   - OUTPT
C   - PARTCL
C   - RAMPQN
C   - SOURCE
C   - STABLE
C   - TOTAL
C   - TRANSC
C   - TRANSP
C
C In C:
C   - COAG
C   - FRCGAM
C
C The only external libraries explicitly called are those included by
C the C subroutines.
C
C-----------------------------------------------------------------------
      OPEN (UNIT =  5, ERR=98)
      OPEN (UNIT = 10, ERR=99)
      OPEN (UNIT = 11, ERR=99)
      OPEN (UNIT = 12, ERR=99)
      OPEN (UNIT = 13, ERR=99)
      OPEN (UNIT = 14, ERR=99)
C-----------------------------------------------------------------------
      PI   = 3.141592
      ITER = 0
```

```
      M    = 1
C M is an output counter for OUTIME():
C
      CALL IN (NK,NX,NZ,DIMNK,NM,QITRIB,AREA,NSCALE,QSCALE,LDNDD1,
     $         LDNDD2,LDNDD3,LDNDD4,BEDVOL,OUTIME,ICOAG,INFLAG,FILNAM)
C              ! Read and echo input data
C
      CALL PARTCL (NK,NX,NZ,DIMNK,LDNDD1,LDNDD2,LDNDD3,LDNDD4,DP,DELTAD,
     $             V,VMAX,N1,NITRIB,NIMAIN)
C                 ! Particle properties and key nodal ICs
      TIME  = 0.
C
      CALL CONCIC (NK,NX,NZ,DIMNK,V,N1,NITRIB,NTRIB,NIMAIN,NMAIN,DELN1,
     $             INFLAG,CT1)
C                 ! Calc initial concentrations at BC and in domain
C
CT      CALL DISTRB (NK,NX,NZ,DIMNK,N1,DP,TSS,TAREA,FP,TOTFP)
CT                  ! Contaminant diss/part fractions based on TAREA,KPA
C
      IF (ICOAG .EQ. 1) THEN
          CALL FRCGAM (NK,LVSTEP,TEMP,VISCOS,DP,G,GRAV,RHOP,RHOW,IBR,
     $                 ISH,IDS,FRAC,BAND1,BAND3,MAXFR1,MAXFR3,GAMMA)
      ENDIF
C                      ! C subroutine- assign frac[] and gamma[]
C
      CALL FLOWI (NX,NZ,Q,QITRIB,QTRIB,AREA,UXMEAN,USTAR,UX,UZ,EX,EZ,
     $            STRESB,B)
C                 ! Initial flow and dispersion fields
C
      CALL STABLE (NK,NX,NZ,UX,UZ,QSCALE,EX,EZ,CX,CZ,DX,DZ,TERMX,TERMZ,
     $             VMAX,V,CZV,B)
C                 ! Time step for stability
C
      CALL BCN (NK,NX,NZ,DIMNK,N1,NMAIN,NTRIB,Q,QTRIB)
C                 ! Initial upstream BC for concs
C
      CALL SOURCE (NK,NX,NZ,NTRIB,NSOURC,QTRIB,AREA)
C                 ! Initial Trib loading source terms
C
      CALL TOTAL (NK,NX,NZ,DIMNK,N1,DP,DELTAD,BEDVOL,BEDMAS,POROS,TSS,
     $            TAREA,TNUM,LDNDD,TIME)
C                 ! Calc total mass,area,number from [N1]
C
      CALL OUTPT (NK,NX,NZ,DIMNK,N1,TIME,BEDMAS,BEDVOL,TSS,TAREA,TNUM,
     $            LDNDD,POROS,CT1,FP,TOTFP,FILNAM,NSOURC,QTRIB,NTRIB)
C                 ! Prints Initial conditions
C
      TRMIN = AMIN1(TNRAMB,TQRAMB)
      TRMAX = AMAX1(TNRAMD,TQRAMD)
C
C Begin/continue time loop:
      DO 1000 ITER = 1,100000
          TIME = TIME + DELT
C
C         Check for status time. Write every 1000 iterations:
          REALIT = REAL(ITER)/ 1000.
          REMAIN = AMOD(REALIT,1.)
          IF (REMAIN .LT. 0.001) THEN
              WRITE (10,*) 'ITER/TIME    = ',ITER,' / ',TIME
          ENDIF
C
C Call ramping routines if unsteady tributary flow or conc ramps:
          IF (INRAMP .EQ. 0 .AND. IQRAMP .EQ. 0) GOTO 100
              IF (TIME .GT. TRMIN .AND. TIME .LE. TRMAX) THEN
                  CALL RAMPQN (NK,NX,NZ,DIMNK,NITRIB,NTRIB,NIMAIN,NMAIN,
     $                 Q,QITRIB,QTRIB,QSCALE,NSCALE,AREA,UXMEAN,USTAR,
     $                 UX,UZ,EX,EZ,CX,CZ,DX,DZ,TERMX,TERMZ,B)
C                      ! Ramps Q, Qtrib, Ntrib, and flow field
C
C
                   CALL BCN (NK,NX,NZ,DIMNK,N1,NMAIN,NTRIB,Q,QTRIB)
C                        ! New upstream BC for concs w/ new trib QxN
              ENDIF
  100     CONTINUE
C
          CALL SOURCE (NK,NX,NZ,NTRIB,NSOURC,QTRIB,AREA)
C                     ! Trib loading source terms
C
          CALL ERODE (NX,RHOW,USTAR,RFLUX,STRESB)
C                     ! Potential bed resuspension mass flux
C
          CALL BEDXCH (NK,NX,NZ,DIMNK,N1,DP,V,RFLUX,BEDMAS,N2,BEDVOL,
     $                 TSS,NUMIN,NUMOUT,NUMNET,MASSIN,MASOUT,TRNSFR)
C             ! Number and Mass inventories & exchange at bed interface
C
          CALL TRANSP (NK,NX,NZ,DIMNK,N1,N2,V,UX,UZ,EX,EZ,CX,CZ,
     $                 DX,DZ,TERMX,TERMZ,CZV,NUMNET,B)
C                     ! Particle transport
C
CT          CALL TRANSC (NK,NX,NZ,CT1,CT2,V,FP,UX,UZ,EX,EZ,CX,CZ,DX,DZ,
CT     $                 TERMX,TERMZ,CZV,BEDVOL,NUMIN,NUMOUT,TRNSFR,B)
CT                      ! Contaminant transport/reaction
C
          IF (ICOAG .EQ. 1) THEN
              CALL COAG (NK,NX,NZ,N1,HMAX,DELT,FRAC,BAND1,BAND3,MAXFR1,
     $                   MAXFR3,GAMMA,ALPHA,DELN1,Y)
          ENDIF
C                         ! Coagulation in parallel with transport & source
C
C         Reset initial condition concs for next time step as the final
```

```
C          concs & FPs from last time step. Any lateral trib sources are
C          added here in parallel with transport:
C
           DO 400 J = 1, NZ-1
               DO 300 I = 2, NX
                    DO 200  K = 1, NK
                         N1(K,I,J) = N2(K,I,J)+  NSOURC(K,I,J)
                         IF (N1(K,I,J) .LT. 0.0)  N1(K,I,J) = 0.0
  200               CONTINUE
  300           CONTINUE
  400       CONTINUE
C
C          Add coagulation conc changes, if applicable, to the concs
C          resulting from transport and lateral trib source:
           IF (ICOAG .EQ. 1) THEN
               DO 700 J = 1, NZ-1
                    DO 600 I = 2, NX
                         DO 500  K = 1, NK
                              N1(K,I,J) = N1(K,I,J) + DELN1(K,I,J)
                              IF (N1(K,I,J) .LT. 0.0)  N1(K,I,J) = 0.0
  500                    CONTINUE
  600               CONTINUE
  700           CONTINUE
           ENDIF
C
CT           DO 900 I = 2, NX
CT                DO 800 J = 1, NZ-1
CT                     CT1(I,J) = CT2(I,J)
CT                     IF (CT1(I,J) .LT. 0.0)  CT1(I,J) = 0.0
CT  800           CONTINUE
CT  900       CONTINUE
C
CT                CALL TOTAL (NK,NX,NZ,DIMNK,N1,DP,DELTAD,BEDVOL,BEDMAS,
CT     $                      POROS,TSS,TAREA,TNUM,LDNDD,TIME)
CT                CALL DISTRB (NK,NX,NZ,DIMNK,N1,DP,TSS,TAREA,FP,TOTFP)
C
C                                OUTPUT CONTROL
C Check for initial (debugging) iterations:
C            IF (ITER .LE. 3) THEN
C                WRITE (10,*) 'ITER/TIME    = ',ITER,' / ',TIME
C                WRITE (10,*) '*****************************OUTPUT Mark',
C     $                       'er*****************************'
C                WRITE (10,*)
C                CALL TOTAL (NK,NX,NZ,DIMNK,N1,DP,DELTAD,BEDVOL,BEDMAS,
C     $                      POROS,TSS,TAREA,TNUM,LDNDD,TIME)
C                CALL OUTPT (NK,NX,NZ,DIMNK,N1,TIME,BEDMAS,BEDVOL,TSS,
C     $                      TAREA,TNUM,LDNDD,POROS,CT1,FP,TOTFP,FILNAM,
C     $                      NSOURC,QTRIB,NTRIB)
C            ENDIF
C
C Check for final time and output times:
           IF (TIME .GE. TMAX) THEN
               GOTO 1100
           ENDIF
C
           IF (ABS(TIME - OUTIME(M)) .LE. DELT) THEN
               WRITE (10,*) '*****************************OUTPUT Mark',
     $                      'er*****************************'
               WRITE (10,*)
               WRITE (11,*)
               WRITE (10,*) 'ITER    =  ',ITER
               CALL TOTAL (NK,NX,NZ,DIMNK,N1,DP,DELTAD,BEDVOL,BEDMAS,
     $                     POROS,TSS,TAREA,TNUM,LDNDD,TIME)
               CALL OUTPT (NK,NX,NZ,DIMNK,N1,TIME,BEDMAS,BEDVOL,TSS,
     $                     TAREA,TNUM,LDNDD,POROS,CT1,FP,TOTFP,FILNAM,
     $                     NSOURC,QTRIB,NTRIB)
               M = M + 1
           ENDIF
C
 1000 CONTINUE
C
 1100 CONTINUE
C
      CLOSE(10)
      CLOSE(11)
      CLOSE(12)
      CLOSE(13)
      CLOSE(14)
      STOP
   98 WRITE (*,*)  'ERROR opening file for DATAIN'
   99 WRITE (*,*)  'ERROR opening file for DATAOUT'
C
      STOP
      END



C**********************************************************************
      SUBROUTINE IN (NK,NX,NZ,DIMNK,NM,QITRIB,AREA,NSCALE,QSCALE,LDNDD1,
     $               LDNDD2,LDNDD3,LDNDD4,BEDVOL,OUTIME,ICOAG,INFLAG,
     $               FILNAM)
C
      INTEGER NK,NX,NZ,DIMNK,NM,IBR,ISH,IDS,ICOAG,INFLAG,INRAMP,
     $        IQRAMP,IDISPZ,NSURF,NOUT
C
      REAL BEDVOL(NX),LDNDD1(NK),LDNDD2(NK),LDNDD3(NK),LDNDD4(NK)
      REAL QITRIB(0:NX),AREA(NX),NSCALE(0:NX),QSCALE(0:NX),OUTIME(NM)
C
```

```
      REAL DELX,DELZ,DELA,DELT,TIME,TMAX,HMAX
      REAL RHOP,RATEM,FRIC,RHOW,VISCOS,TEMP,GRAV
      REAL LV1ST,LVSTEP,ALPHA,G
      REAL CTW,CTB,KPM,KPA
      REAL TNRAMB,TNRAMU,TNRAMD,TQRAMB,TQRAMU,TQRAMD
C
      CHARACTER*50   FILNAM
C
      COMMON/EROSON/ STRESC,RATEM
      COMMON/FLOC/   ALPHA,G,IBR,ISH,IDS
      COMMON/MEANS/  EXMEAN,EZMEAN,FRIC,IDISPZ,DEPTH
      COMMON/PART/   RHOP,RHOW,VISCOS,TEMP,GRAV,LV1ST,LVSTEP,PI
      COMMON/RAMP/   TNRAMB,TNRAMU,TNRAMD,TQRAMB,TQRAMU,TQRAMD,INRAMP,
     $               IQRAMP
      COMMON/STEPS/  DELX,DELZ,DELA,DELT,FRACT,TIME,TMAX,HMAX,NOUT,ITER
      COMMON/TAMNIT/ CTW,CTB,KPM,KPA
C
C PURPOSE: This subroutine reads conditions for the simulation and echos
C          their values.
C
C INPUT PARAMETERS: DIMNK,NK,NX,NZ,NM are passed from MAIN
C                   All other variables are read in here.
C
C OUTPUT PARAMETERS: All variables read for simulation returned to MAIN;
C                    exception is NSURF, the number of 2-D concentration
C                    surfaces (output times) to be plotted from files
C                    12, 13 & 14 for TSS(i,j), TNUM(i,j) and TAREA(i,j)
C
C AUTHOR:   Jerry Culkin
C           Department of Civil Engineering
C           University of Texas at Austin
C
C LAST REVISED: 3 August 1990
C
C PRECISION: Single
C
C LANGUAGE: FORTRAN 77
C
C REFERENCES: None
C
C REQUIRED ROUTINES: None
C-----------------------------------------------------------------------
      READ (5,'(A)',ERR=311,END=381) FILNAM
C                                    ! Input file name and info
      READ (5,*,ERR=312,END=382) DELX,DELZ,DELA,FRACT,TMAX,HMAX,NOUT
      READ (5,*,ERR=313,END=383) LV1ST,LVSTEP,RHOP
      READ (5,*,ERR=314,END=384) RHOW,VISCOS,TEMP,GRAV
      READ (5,*,ERR=315,END=385) STRESC,RATEM,EXMEAN,EZMEAN,FRIC
      READ (5,*,ERR=317,END=387) (QITRIB(I),I = 0,NX)
      READ (5,*,ERR=317,END=387) (AREA(I),I = 1,NX)
      READ (5,*,ERR=318,END=388) (BEDVOL(I),I = 1,NX)
      READ (5,*,ERR=319,END=389) ALPHA,G,IBR,ISH,IDS
      READ (5,*,ERR=321,END=391) (LDNDD1(K),K = 1,NK)
      READ (5,*,ERR=322,END=392) (LDNDD2(K),K = 1,NK)
      READ (5,*,ERR=323,END=393) (LDNDD3(K),K = 1,NK)
      READ (5,*,ERR=323,END=393) (LDNDD4(K),K = 1,NK)
      READ (5,*,ERR=324,END=394) ICOAG,INFLAG,INRAMP,IQRAMP,IDISPZ
      READ (5,*,ERR=324,END=394) TNRAMB,TNRAMU,TNRAMD
      READ (5,*,ERR=324,END=394) TQRAMB,TQRAMU,TQRAMD
      READ (5,*,ERR=326,END=396) (NSCALE(I),I = 0,NX)
      READ (5,*,ERR=326,END=396) (QSCALE(I),I = 0,NX)
      READ (5,*,ERR=325,END=395) (OUTIME(M),M = 1,NOUT)
      READ (5,*,ERR=324,END=394) KPM,KPA,CTW,CTB
C
      CLOSE(5)
C
C Echo input values to be used in computation:
C
      WRITE (10,*) 'Input file info:  ',FILNAM
      WRITE (10,*)
      WRITE (11,*) 'Input file info:  ',FILNAM
      WRITE (11,*)
C Define NSURF, the number of "layers", i.e., the # of output times (plus
C  1 for time zero) of contour data, needed in Mac app 'NSURF':
      NSURF  = NOUT + 1
      WRITE (12,*) NSURF
      WRITE (13,*) NSURF
      WRITE (14,*) NSURF
C
      WRITE (10,15)
   15 FORMAT ('ECHO Dimensions HardWired in MAIN  :',/,
     $'      NK       NX       NZ     DIMNK     NM:')
      WRITE (10,25) NK,NX,NZ,DIMNK,NM
   25 FORMAT (5(TR5,I3))
C
      WRITE (10,35)
      WRITE (10,45,ERR=581)   DELX, DELZ, DELA, FRACT, TMAX, HMAX, NOUT
   35 FORMAT (/,'ECHO Parameters: ',/,
     $'     DELX         DELZ       DELA     FRACT      TMAX      HMAX      ',
     $'NOUT',/,
     $'     [cm]         [cm]                                  [s]      [s]')
   45 FORMAT (2F10.0,2F10.2,E11.4,2X,F7.1,I6)
C
      WRITE (10,55)
      WRITE (10,65,ERR=582)   LV1ST, LVSTEP, RHOP
   55 FORMAT (/,'ECHO Parameters: ',/,
     $'        LV1ST         LVSTEP       RHOP',/,
     $'        [um^3]        [um^3]     [g/cm^3]')
   65 FORMAT (4F12.4)
```

```
C
      WRITE (10,75)
      WRITE (10,65,ERR=583)   RHOW, VISCOS, TEMP, GRAV
   75 FORMAT (/,'ECHO Parameters: ',/,
     $'       RHOW       VISCOS       TEMP          GRAV',/,
     $'      [g/cm^3]   [g/cm-s]     [K]         [cm/s^2]')
C
      WRITE (10,85)
      WRITE (10,95,ERR=584)  STRESC,RATEM,EXMEAN,EZMEAN,FRIC
   85 FORMAT (/,'ECHO Parameters: ',/,
     $'    STRESC        RATEM          EXMEAN        EZMEAN        FRIC',/,
     $'  [dyne/cm^2]    [s/cm]        [cm^2/s]      [cm^2/s]      [-]')
   95 FORMAT (5E12.3)
C
      WRITE (10,103)
      WRITE (10,115,ERR=586) (QITRIB(I),I = 0,NX)
  103 FORMAT (/,'ECHO Initial Trib Flowrate, QTRIB(I), [m^3/s]:')
C
      WRITE (10,104)
      WRITE (10,115,ERR=586) (AREA(I),I = 1,NX)
  104 FORMAT (/,'ECHO Average Area, Area(I), [m^2]:')
C
      WRITE (10,105)
      WRITE (10,115,ERR=587) (BEDVOL(I),I = 1,NX,2)
  105 FORMAT (/,'ECHO INITIAL VALUES OF BEDVOL(I-odd), [cm^3/cm^2]:')
  115 FORMAT (5(E11.5,TR3))
C
C Echo coagulation (only) parameters:
      WRITE (10,125)
      WRITE (10,135,ERR=588)   ALPHA, G, IBR, ISH, IDS
  125 FORMAT (/,'ECHO Coagulation Parameters: ',/,
     $'       ALPHA          G       IBR  ISH  IDS',/,
     $'         [-]         [1/s]     [-]  [-]  [-]')
  135 FORMAT (2F12.2,3I5)
C
C Write initial PSDs for water, bed, and trib:
      WRITE (10,*)
      WRITE (10,145)
  145 FORMAT (/,'ECHO IC Water Column LDNDD1(K), [#/cm^3-um] :')
      WRITE (10,175,ERR=589) (LDNDD1(K), K = 1,NK)
      WRITE (10, 155)
  155 FORMAT (/,'ECHO IC Bed LDNDD2(K), [#/cm^3-um] :')
      WRITE (10,175,ERR=591) (LDNDD2(K), K = 1,NK)
      WRITE (10, 165)
  165 FORMAT (/,'ECHO IC Main Flow LDNDD3(K), [#/cm^3-um] :')
      WRITE (10,175,ERR=592) (LDNDD3(K), K = 1,NK)
  175 FORMAT (5(F11.5,TR2))
      WRITE (10, 177)
  177 FORMAT (/,'ECHO Tributary IC LDNDD4(K), [#/cm^3-um] :')
      WRITE (10,175,ERR=592) (LDNDD4(K), K = 1,NK)
C
C Echo COAGULATION SWITCH:
      WRITE (10,185,ERR=593)  ICOAG
  185 FORMAT (/,'ECHO Coagulation Switch (1= on):  ',I5)
C
C Echo CONC DISTRIBUTION SWITCH:
      WRITE (10,195,ERR=593)  INFLAG
  195 FORMAT (/,'ECHO Conc Distribution Switch (1= uniform):  ', I5)
C
C Echo BC Conc RAMP SWITCH:
      WRITE (10,205,ERR=593)  INRAMP
  205 FORMAT (/,'ECHO BC Conc Ramp Switch (1= on):  ',I5)
C
C Echo Flow RAMP SWITCH:
      WRITE (10,207,ERR=593)  IQRAMP
  207 FORMAT (/,'ECHO Flow Ramp Switch (1= on):  ',I5)
C
C Echo Ez SWITCH:
      WRITE (10,215,ERR=593)  IDISPZ
  215 FORMAT (/,'ECHO Mean Ez Override Switch (1= on): ',I5)
C
C Echo Contaminant Ramping scale coefficient and times:
      WRITE (10,245)
      WRITE (10,255,ERR=594) TNRAMB,TNRAMU,TNRAMD
  245 FORMAT (/,'ECHO Contaminant Ramping times',/,
     $'       TNRAMB       TNRAMU         TNRAMD',/,
     $'         [s]          [s]            [s]')
  255 FORMAT (3F13.0)
C
C Echo Flow Ramping scale coefficient and times:
      WRITE (10,265)
      WRITE (10,275,ERR=594) TQRAMB,TQRAMU,TQRAMD
  265 FORMAT (/,'ECHO Flow Ramping times',/,
     $'       TQRAMB       TQRAMU         TQRAMD',/,
     $'         [s]          [s]            [s]')
  275 FORMAT (3F13.0)
C
      WRITE (10,277)
      WRITE (10,115,ERR=596) (NSCALE(I),I = 0,NX)
  277 FORMAT (/,'ECHO Conc Scale Factors, [-]:')
C
      WRITE (10,279)
      WRITE (10,115,ERR=596) (QSCALE(I),I = 0,NX)
  279 FORMAT (/,'ECHO Flowrate Scale Factors, [-]:')
C
      WRITE (10,285)
  285 FORMAT (/,'ECHO OUTIME(M):')
      WRITE (10,295,ERR=595) (OUTIME(M), M = 1,NM)
  295 FORMAT (6(F11.0,TR2))
```

```
C
C Echo Contaminant Partition coefficients and ICs:
      WRITE (10,225)
      WRITE (10,235,ERR=594) KPM,KPA,CTW,CTB
  225 FORMAT (/,'ECHO Contaminant Partition Coefficients ',/,
     $'       KPM           KPA          CTW          CTB',/,
     $'      [L/kg]       [L/cm^2]      [ug/L]       [ug/L]')
  235 FORMAT (4E13.4)
C
      WRITE (10,*)
C
      RETURN
C_____________________________________________________________________
C I/O Error messages:
  311 WRITE (*,*)  'INPUT READ-ERROR READING FILENAME'
      STOP
  312 WRITE (*,*)  'INPUT READ-ERROR READING STEPS'
      STOP
  313 WRITE (*,*)  'INPUT READ-ERROR READING /PART-1'
      STOP
  314 WRITE (*,*)  'INPUT READ-ERROR READING /PART-2'
      STOP
  315 WRITE (*,*)  'INPUT READ-ERROR READING EROSON'
      STOP
  317 WRITE (*,*)  'INPUT READ-ERROR READING (Velocities) or (Areas)'
      STOP
  318 WRITE (*,*)  'INPUT READ-ERROR READING (BEDVOL)'
      STOP
  319 WRITE (*,*)  'INPUT READ-ERROR READING COAG'
      STOP
  321 WRITE (*,*)  'INPUT READ-ERROR READING (LdNdD)1'
      STOP
  322 WRITE (*,*)  'INPUT READ-ERROR READING (LdNdD)2'
      STOP
  323 WRITE (*,*)  'INPUT READ-ERROR READING (LdNdD)3 or (LdNdD)4'
      STOP
  324 WRITE (*,*)  'INPUT READ-ERROR READING Flags or Contams or Ramps'
      STOP
  325 WRITE (*,*)  'INPUT READ-ERROR READING (OUTIME):'
      WRITE (*,*)  'M = ', M
      STOP
  326 WRITE (*,*)  'INPUT READ-ERROR READING Scale Factors'
      STOP
  381 WRITE (*,*)  'No input file present or EOF while reading filename'
      STOP
  382 WRITE (*,*)  'END OF FILE ENCOUNTERED WHILE READING STEPS'
      STOP
  383 WRITE (*,*)  'END OF FILE ENCOUNTERED WHILE READING /PART-1'
      STOP
  384 WRITE (*,*)  'END OF FILE ENCOUNTERED WHILE READING /PART-2'
      STOP
  385 WRITE (*,*)  'END OF FILE ENCOUNTERED WHILE READING EROSON'
      STOP
  387 WRITE (*,*)  'END OF FILE ENCOUNTERED WHILE READING Veloc/Area'
      STOP
  388 WRITE (*,*)  'END OF FILE ENCOUNTERED WHILE READING BEDVOL'
      STOP
  389 WRITE (*,*)  'END OF FILE ENCOUNTERED WHILE READING COAG'
      STOP
  391 WRITE (*,*)  'END OF FILE ENCOUNTERED WHILE READING INITIAL PSD1'
      STOP
  392 WRITE (*,*)  'END OF FILE ENCOUNTERED WHILE READING INITIAL PSD2'
      STOP
  393 WRITE (*,*)  'END OF FILE ENCOUNTERED WHILE READING INITIAL PSD34'
      STOP
  394 WRITE (*,*)  'END OF FILE ENCOUNTERED WHILE READING Flags/Ct/Ramp'
      STOP
  395 WRITE (*,*)  'END OF FILE ENCOUNTERED WHILE READING Out Times'
      STOP
  396 WRITE (*,*)  'END OF FILE ENCOUNTERED WHILE READING Scale Factors'
      STOP
  581 WRITE (*,*)  'ECHO WRITE-ERROR WHILE WRITING STEPS'
      STOP
  582 WRITE (*,*)  'ECHO WRITE-ERROR WHILE WRITING /PART-1'
      STOP
  583 WRITE (*,*)  'ECHO WRITE-ERROR WHILE WRITING /PART-2'
      STOP
  584 WRITE (*,*)  'ECHO WRITE-ERROR WHILE WRITING EROSON'
      STOP
  586 WRITE (*,*)  'ECHO WRITE-ERROR WHILE WRITING Velocities/Areas'
      STOP
  587 WRITE (*,*)  'ECHO WRITE-ERROR WHILE WRITING BEDVOL'
      STOP
  588 WRITE (*,*)  'ECHO WRITE-ERROR WHILE WRITING COAG'
      STOP
  589 WRITE (*,*)  'ECHO WRITE-ERROR WHILE WRITING INITIAL PSD1'
      STOP
  591 WRITE (*,*)  'ECHO WRITE-ERROR WHILE WRITING INITIAL PSD2'
      STOP
  592 WRITE (*,*)  'ECHO WRITE-ERROR WHILE WRITING INITIAL PSD3 or PSD4'
      STOP
  593 WRITE (*,*)  'ECHO WRITE-ERROR WHILE WRITING Flags'
      STOP
  594 WRITE (*,*)  'ECHO WRITE-ERROR WHILE WRITING Contam'
      STOP
  595 WRITE (*,*)  'ECHO WRITE-ERROR WHILE WRITING Out Times'
      STOP
  596 WRITE (*,*)  'ECHO WRITE-ERROR WHILE WRITING Scale Factors'
      STOP
```

```
      END


C*********************************************************************
      SUBROUTINE PARTCL (NK,NX,NZ,DIMNK,LDNDD1,LDNDD2,LDNDD3,LDNDD4,DP,
     $                   DELTAD,V,VMAX,N1,NITRIB,NIMAIN)
C
      INTEGER  NK,NX,NZ,DIMNK
C
      REAL  DP(DIMNK),V(NK),DELTAD(NK),N1(DIMNK,NX,NZ),NITRIB(NK)
      REAL  NIMAIN(NK),LDNDD1(NK),LDNDD2(NK),LDNDD3(NK),LDNDD4(NK)
C
      REAL  RHOP,RHOW,VISCOS,TEMP,GRAV,PI
      REAL  LV1ST,LVSTEP,LDSTEP,FDFULL,FDHALF,DMHAF,DPHAF,VMAX
C
      COMMON/PART/   RHOP,RHOW,VISCOS,TEMP,GRAV,LV1ST,LVSTEP,PI
C
C PURPOSE: This routine assigns particle properties for each FLOC:
C           - floc diameter (equivalent spherical)
C           - floc settling velocity (equivalent spherical)
C           - delta diameter around floc
C           - initial bed concentrations based on input bed PSD
C           - (density - constant for now)
C
C INPUT PARAMETERS:
C  INFLAG   - Switch for homogeneous number concentration as I.C. (1=on)
C   LV1ST   - log(Initial particle volume), [um^3]
C   LVSTEP  - Delta log(Vp), [um^3]
C   RHOP    - Effective bulk density of floc, [g/cm^3]
C   RHOW    - Effective density of water, [g/cm^3]      (consistent w/
C   VISCOS  - Molecular viscosity of fluid, [g/cm-s]     the temp etc)
C   GRAV    - Gravitational acceleration, [cm/s^2]
C   NK      - Number of particle size classes
C   DIMNK   - NK + 1; accomodates array shift in C codes
C  (LDNDD1) - Vector of initial PSD for water column, log([#/cm^3-um])
C  (LDNDD2) - Vector of initial PSD for bed, log([#/cm^3-um])
C  (LDNDD3) - Vector of initial PSD for main inflow, log([#/cm^3-um])
C  (LDNDD4) - Vector of initial PSD for tributary, log([#/cm^3-um])
C
C OUTPUT PARAMETERS:
C   VMAX    - Maximum settling velocity, [cm/s]
C  (DELTAD) - Delta diamater around k floc, [um]
C  (DP)     - Equivalent spherical diameter of size k floc, elements
C               shifted in C code, [um]
C  (NIMAIN) - Initial number concentration distribution for main inflow,
C               from LDNDD3 or uniform, [#/cm^3]
C  (NITRIB) - Initial number concentration distribution for tributaries,
C               from LDNDD4 or uniform, [#/cm^3]
C  (V)      - Settling velocity for size k floc, [cm/s]
C  [N1]     - Initial concentration in domain, [#/cm^3]
C
C AUTHOR:   Jerry Culkin
C           Department of Civil Engineering
C           University of Texas at Austin
C
C LAST REVISED: 31 Jul 1990   1135
C
C PRECISION: Single
C
C LANGUAGE: FORTRAN 77
C
C REFERENCES: None
C
C REQUIRED ROUTINES: None
C_____________________________________________________________________
      WRITE (10,*)
      WRITE (10,*) '*****************************OUTPUT PARTCL*******',
     $'*****************************'
      WRITE (11,*)
C Define constants to simplify and convert LdNdD() to N1():
      LDSTEP = LVSTEP/ 3.
C               ! log (DP(k+1)/DP(k))
      FDFULL = 10**(LDSTEP)
C               ! DP increment Factor,full step
      FDHALF = 10**(LDSTEP/2.)
C               ! DP increment Factor,half step
      CONSTV = GRAV/(18.* VISCOS)* (RHOP- RHOW)* 1.E-8
C               ! Stokes settling velocity factor for result in [cm/s]
C
C Calc first elements for the array of diameters, settling velocities
C  (assume Stokes settling), and bed no. concentrations:
C
      K = 1
      DP(K) = (6./ PI* 10**LV1ST)**0.333333
C                 ! Initital Dp, [um]
      V(K)  = CONSTV* DP(K)**2
      DMHAF = DP(K)/ FDHALF
C                 ! Dp minus half log dp, [um]
      DPHAF = DP(K)* FDHALF
C                 ! Dp plus half log dp, [um]
      DELTAD(K)  = (DPHAF- DMHAF)
C
      N1(K,2,1)  = 10**LDNDD1(K)* DELTAD(K)
      N1(K,1,NZ) = 10**LDNDD2(K)* DELTAD(K)
      NIMAIN(K)  = 10**LDNDD3(K)* DELTAD(K)
      NITRIB(K)  = 10**LDNDD4(K)* DELTAD(K)
C
      IF (N1(K,2,1)  .LT. 1.0)  N1(K,2,1)  = 0.0
```

```
      IF (N1(K,1,NZ) .LT. 1.0)  N1(K,1,NZ) = 0.0
      IF (NIMAIN(K)  .LT. 1.0)  NIMAIN(K)  = 0.0
      IF (NITRIB(K)  .LT. 1.0)  NITRIB(K)  = 0.0
C Continue with particle loop through the PSD from size 2 thru NK to
C calculate diameters and velocities, as well as initial concentrations.
C Note: Loop limit of NK on LDNDD() results in nonzero initial
C concentrations for N1[NK-3,NK] :
      DO 100 K = 2,NK
           DP(K)     = DP(K-1)* FDFULL
           V(K)      = CONSTV* DP(K)**2
           DMHAF     = DP(K)/ FDHALF
           DPHAF     = DP(K)* FDHALF
           DELTAD(K)= (DPHAF- DMHAF)
C
           N1(K,2,1)  = 10**LDNDD1(K)* DELTAD(K)
           N1(K,1,NZ) = 10**LDNDD2(K)* DELTAD(K)
           NIMAIN(K)  = 10**LDNDD3(K)* DELTAD(K)
           NITRIB(K)  = 10**LDNDD4(K)* DELTAD(K)
C
           IF (N1(K,2,1)  .LT. 1.0)  N1(K,2,1)  = 0.0
           IF (N1(K,1,NZ) .LT. 1.0)  N1(K,1,NZ) = 0.0
           IF (NIMAIN(K)  .LT. 1.0)  NIMAIN(K)  = 0.0
           IF (NITRIB(K)  .LT. 1.0)  NITRIB(K)  = 0.0
  100 CONTINUE
C
C Define max V(k) for stability routine:
      VMAX = V(NK-3)
      WRITE (10,*) 'VMAX = ',VMAX,'    V(NK-3) = ',V(NK-3)
C
      WRITE (10,*)
      WRITE (10,5)
    5 FORMAT (' K',T5,'Dp[um]',T12,'DelDp[um]',T22,'Vk [cm/s]',T34,
     $'Nwat(k)    Nbed(k)    Nmain(k)    Ntrib(k), [#/cm^3]')
C
      DO 200 K = 1,NK
           WRITE (11,25) DP(K),DELTAD(K)
           WRITE(10,15) K,DP(K),DELTAD(K),V(K),N1(K,2,1),N1(K,1,NZ),
     $                  NIMAIN(K),NITRIB(K)
  200 CONTINUE
   15 FORMAT (I2,TR1,F6.2,TR1,F8.3,TR1,E10.3,TR1,E11.4,TR1,E11.4,TR1,
     $E11.4,TR1,E11.4)
   25 FORMAT (F10.2,TR5,F10.3)
C
      RETURN
      END


C*************************************************************************
      SUBROUTINE CONCIC (NK,NX,NZ,DIMNK,V,N1,NITRIB,NTRIB,NIMAIN,NMAIN,
     $                   DELN1,INFLAG,CT1)
C
      INTEGER  NK,NX,NZ,DIMNK,INFLAG
C
      REAL N1(DIMNK,NX,NZ),NITRIB(NK),NTRIB(NK,NX),NIMAIN(NK)
      REAL NMAIN(NK),DELN1(DIMNK,NX,NZ),CT1(NX,NZ)
C
      REAL CTW,CTB
C
      COMMON/TAMNIT/ CTW,CTB,KPM,KPA
C
C PURPOSE: This routine assigns initial domain, bed, U/S, and tributary
C          number and contaminant concentrations.
C
C INPUT PARAMETERS:
C  INFLAG  - Flag to set uniform concentrations (1=on)
C  NK      - Number of particle size classes
C  NX,NZ   - Number of longitudinal and vertical grids
C  CTB     - Initial total contaminant conc in bed, [ug/L]
C  CTW     - Initial total contaminant conc in water, [ug/L]
C  DIMNK   - NK + 1; accomodates array shift in C codes
C (NIMAIN) - Initial number concentration distribution for main inflow,
C              [#/cm^3]
C (V)      - Settling velocity, [cm/s]
C [CT1]    - Initial total contaminant concs, [ug/L]
C [NITRIB] - Initial number concentration for tributaries, [#/cm^3]
C
C OUTPUT PARAMETERS:
C (NMAIN)  - Number concentration distribution for main inflow,[#/cm^3]
C [DELN1]  - Initialize concentration changes (due to COAG in water
C             column) to zero, [#/cm^3]
C [N1]     - Initial concentration throughout water column & bed,
C             [#/cm^3]
C [NTRIB]  - Number concentration for tributaries, [#/cm^3]
C
C AUTHOR:   Jerry Culkin
C           Department of Civil Engineering
C           University of Texas at Austin
C
C LAST REVISED: 1 August 1990  1225 - new tribs
C               27 Sept 1430        - new NMAIN
C
C PRECISION: Single
C
C LANGUAGE: FORTRAN 77
C
C REFERENCES: None
C
C REQUIRED ROUTINES: None
```

```
C
CC      WRITE (10,*)
CC      WRITE (10,*) '*****************************OUTPUT CONCIC********',
CC     $'*****************************'
CC      WRITE (10,*)
C
C If flag for uniform (homogeneous) PSD on, then overwrite concs from
C  PARTCL. Note: manually set concentrations to 0.0 for last three size
C  classes.
C
      IF (INFLAG .EQ. 1) THEN
          DO 100 K = 1,NK-3
               NIMAIN(K) = 1.   ! Main flow IC
               NITRIB(K) = 1.   ! Trib flow IC
               N1(K,2,1) = 1.   ! Domain IC
  100     CONTINUE
          DO 200 K = 1,NK-3
               N1(K,1,NZ) = 10. ! Bed IC
  200     CONTINUE
      ENDIF
C
C     Assign IC particle concs(k,x,z) through DOMAIN:
      DO 500 J = 1, NZ-1
           DO 400 I = 2,NX
                DO 300 K = 1,NK-3
                     N1(K,I,J) = N1(K,2,1)
  300           CONTINUE
  400      CONTINUE
  500 CONTINUE
C
C     Assign IC particle concs(k,x,z) through BED:
      DO 700 I = 2,NX
           DO 600  K = 1,NK-3
                N1(K,I,NZ) = N1(K,1,NZ)
  600      CONTINUE
  700 CONTINUE
C
C     Assign IC particle concs(k,x,z) for U/S flow:
      DO 1200 K = 1,NK-3
                NMAIN(K) = NIMAIN(K)
 1200 CONTINUE
C
C     Assign IC particle concs(k,x,z) through tributaries:
      DO 1400 I = 1, NX
           DO 1300 K = 1, NK
                NTRIB(K,I) = NITRIB(K)
 1300      CONTINUE
 1400 CONTINUE
C
C     Zero the IC particle concs(k,x,z) in all 3 floc growth classes:
      DO 1700  J = 1,NZ
           DO 1600 I = 1,NX
                DO 1500  K = NK-2,NK
                     N1(K,I,J) = 0.
 1500           CONTINUE
 1600      CONTINUE
 1700 CONTINUE
C
C     Assign IC contaminant concs(x,z) uniformly through domain equal
C     to initial trib BC:
      DO 1900 J = 1, NZ-1
           DO 1800 I = 1,NX
                CT1(I,J) = CTW
 1800      CONTINUE
 1900 CONTINUE
C
      DO 2000 I = 1,NX
           CT1(I,NZ) = CTB
 2000 CONTINUE
C
C     Zero the IC coagulation array:
      DO 2300  J = 1,NZ
           DO 2200 I = 1,NX
                DO 2100  K = 1,NK
                     DELN1(K,I,J) = 0.
 2100           CONTINUE
 2200      CONTINUE
 2300 CONTINUE
C
      RETURN
      END


C*************************************************************************
      SUBROUTINE FLOWI (NX,NZ,Q,QITRIB,QTRIB,AREA,UXMEAN,USTAR,UX,UZ,EX,
     $                  EZ,STRESB,B)
C
      INTEGER  NX,NZ,IDISPZ
C
      REAL UX(NX,NZ), UZ(NX,NZ), USTAR(NX), UXMEAN(NX)
      REAL EX(NX,NZ), EZ(NX,NZ), AREA(NX), B(NX)
      REAL Q(0:NX), QITRIB(0:NX), QTRIB(0:NX), STRESB(NX)
C
      REAL FRIC,DELZ,DEPTH,KARMAN,ZLOCAL,ZSYSTM,EXMEAN,EZMEAN,RHOW
C
      COMMON/MEANS/  EXMEAN,EZMEAN,FRIC,IDISPZ,DEPTH
      COMMON/PART/   RHOP,RHOW,VISCOS,TEMP,GRAV,LV1ST,LVSTEP,PI
      COMMON/STEPS/  DELX,DELZ,DELA,DELT,FRACT,TIME,TMAX,HMAX,NOUT,ITER
```

```
C
C PURPOSE: This routine assigns fluid velocity and dispersion field
C          values, based on input magnitudes and distributions
C
C INPUT PARAMETERS:
C  IDISPZ  - Switch for using uniform prescribed Ez (1=on)
C  EXMEAN  - Mean longitudinal fluid dispersion coef, [cm^2/s]
C  EZAVG   - Average vertical fluid dispersion coef calc at I, [cm^2/s]
C  EZMEAN  - Mean vertical fluid dispersion coef imposed at I, [cm^2/s]
C  FRIC    - Darcy friction factor, [-]
C  RHOW    - Density of fluid, [g/cm^3]
C  ZLOCAL  - Depth measured from bed interface, [cm]
C  ZSYSTEM - Depth measured from surface, i.e., consistent w/ positive
C               z axis downward orientation, [cm]
C {AREA}   - Average cross-sectional area in reach, [m^2]
C {QITRIB} - Initial tributary flowrate, [m^3/s]
C
C OUTPUT PARAMETERS:
C  KARMAN  - von Karman constant
C  DEPTH   - Total water column depth, [cm]
C {B}      - Average width at cross-section, [m]
C {Q}      - Total flowrate, [m^3/s]
C {QTRIB}  - Tributary flowrate, [m^3/s]
C {STRESB} - Local Bed shear stress, [dyne/cm^2] = [g/cm-s^2]
C {USTAR}  - Shear velocity, [cm/s]
C {UXMEAN} - Mean longitudinal fluid velocity, [cm/s]
C [EX]     - Longitudinal fluid dispersion coefficient, [cm^2/s]
C [EZ]     - Average vertical fluid dispersion coefficient, [cm^2/s]
C [UX]     - Longitudinal fluid velocity, [cm/s]
C [UZ]     - Vertical fluid velocity, [cm/s]
C
C AUTHOR:   Jerry Culkin
C           Department of Civil Engineering
C           University of Texas at Austin
C
C LAST REVISED: 3 aug, 1990  1620. for new Q methods
C               1 oct, 1990  1745. for width calc
C
C PRECISION: Single
C
C LANGUAGE: FORTRAN 77
C
C REFERENCES: None
C
C REQUIRED ROUTINES: None
C-----------------------------------------------------------------------
      WRITE (10,*)
      WRITE (10,*) '************************** OUTPUT FLOWI() *******',
     $'**********************'
C
C Make initial parameters assignments. Set friction or shear velocity
C based on log velocity profile for fully developed turbulent flow.
C Initialize local and system depth scales with origins at bed and at
C surface.
      KARMAN = 0.40
      DEPTH  = (NZ - 2 + DELA) * DELZ
C
      DO 111 I = 0, NX
           QTRIB(I) = QITRIB(I)
  111 CONTINUE
C
C Velocity and dispersion coefficients for open channel shear flow w/
C  log velocity profile in defect form:
C
      Q(0) = QTRIB(0)
      DO 200 I = 1, NX
           B(I) = AREA(I)/ DEPTH* 100.
           Q(I) = Q(I-1) + QTRIB(I)
           UXMEAN(I) = Q(I)/ AREA(I)* 100.
           USTAR(I)  = UXMEAN(I)* SQRT(FRIC/8.)
           STRESB(I) = RHOW* USTAR(I)**2
           ZLOCAL    = DELA* DELZ
           ZSYSTM    = DEPTH- ZLOCAL
           EZAVG     = DEPTH* USTAR(I)/ 15.
           DO 100 J = NZ-1, 1, -1
                UX(I,J) = UXMEAN(I)+ USTAR(I)/ KARMAN* (1.+
     $                       LOG(ZLOCAL/ DEPTH))
                IF (UX(I,J) .LT. 0.0 )  UX(I,J) = 0.02* UXMEAN(I)
                UZ(I,J) = 0.0
                EZ(I,J) = EZAVG
                EX(I,J) = EXMEAN
                ZLOCAL  = ZLOCAL + DELZ
                ZSYSTM  = DEPTH- ZLOCAL
  100      CONTINUE
  200 CONTINUE
C
      IF (IDISPZ .EQ.1) THEN
          DO 400 J = 1,NZ-1
              DO 300 I = 1, NX
                  EZ(I,J) = EZMEAN
  300         CONTINUE
  400     CONTINUE
      ENDIF
C
C Write the initial tributary flowrates:
      WRITE (10,*)
      WRITE (10,*) 'Initial trib flowrates (I=0:NX), [m^3/sec]:'
      WRITE (10,115) (QTRIB(I),I = 0,NX)
C
```

```
C Write the initial system flowrates:
      WRITE (10,*)
      WRITE (10,*) 'Initial system flowrates (I-0:NX), [m^3/sec]:'
      WRITE (10,115) (Q(I),I = 0,NX)
C
C Write the initial mean velocity field:
      WRITE (10,*)
      WRITE (10,*) 'Initial mean velocity field (I), [cm/sec]:'
      WRITE (10,115) (UXMEAN(I),I = 1,NX)
C
C Write the initial shear velocity field:
      WRITE (10,*)
      WRITE (10,*) 'Initial Shear velocity field (I), [cm/sec]:'
      WRITE (10,115) (USTAR(I),I = 1,NX)
C
C Write the initial shear stress field:
      WRITE (10,*)
      WRITE (10,*) 'Initial Bed Shear stress, [dyne/cm^2] = [g/cm-s^2]:'
      WRITE (10,115) (STRESB(I),I = 1,NX)
C
C Write the initial longitudinal velocity field:
      WRITE (10,*)
      WRITE (10,*) 'Initial X-velocity field (I odd), [cm/sec]:'
      DO 500 J = 1,NZ
           WRITE (10,115) (UX(I,J),I = 1,NX,2)
  500 CONTINUE
C
C Write the longitudinal dispersion field:
      WRITE (10,*)
      WRITE (10,*) 'X-dispersion field (I odd), [cm^2/sec]:'
      DO 600 J = 1,NZ
           WRITE (10,115) (EX(I,J),I = 1,NX,2)
  600 CONTINUE
C
C Write the initial vertical dispersion field:
      WRITE (10,*)
      WRITE (10,*) 'Initial Z-dispersion field (I odd), [cm^2/sec]:'
      DO 700 J = 1,NZ
           WRITE (10,115) (EZ(I,J),I = 1,NX,2)
  700 CONTINUE
C
      WRITE (10,*)
  115 FORMAT (6(F10.4,TR3))
C
      RETURN
      END


C*************************************************************************
      SUBROUTINE STABLE (NK,NX,NZ,UX,UZ,QSCALE,EX,EZ,CX,CZ,DX,DZ,
     $                   TERMX,TERMZ,VMAX,V,CZV,B)
C
      INTEGER  NX,NZ,IQRAMP
C
      REAL UX(NX,NZ),UZ(NX,NZ),EX(NX,NZ),EZ(NX,NZ),TERMX(NX,NZ)
      REAL TERMZ(NX,NZ),CX(NX,NZ),CZ(NX,NZ),DX(NX,NZ),DZ(NX,NZ)
      REAL QSCALE(0:NX),V(NK),CZV(NK),B(NX)
C
      REAL VMAX,DELX,DELZ,DELA,DELT,EXMAX,EZMAX,FRACT
      REAL UXMAX,UZMAX,COURNT,CZVMAX,DISPX,DISPZ,PEX,PEZ
C
      COMMON/RAMP/   TNRAMB,TNRAMU,TNRAMD,TQRAMB,TQRAMU,TQRAMD,INRAMP,
     $               IQRAMP
      COMMON/STEPS/  DELX,DELZ,DELA,DELT,FRACT,TIME,TMAX,HMAX,NOUT,ITER
C
C PURPOSE: This subroutine determines the time step for necessary for
C          stable numerical solution (von Neumann sense) of the
C          transport (not including reaction) equations.
C
C INPUT PARAMETERS:
C  IQRAMP- Switch for ramping trib flowrates (1=on)
C  NX    - No. grids nodes in X
C  NZ    - No. grids nodes in Z
C  DELX  - Uniform mesh size in X, [cm]
C  DELZ  - Uniform mesh size in Z, [cm]
C  FRACT - Safety factor used to set stable DELT, [ < 0.8]
C  QSCALE- Factor, peak flowrate divided by initial flowrate, [-]
C  VMAX  - Maximum settling velocity of floc, [cm/s]
C (B)    - Average width of cross-section at grid, [m]
C (V)    - Settling velocity of size class k, [cm/s]
C (EX)   - Dispersion coefficient in X, [cm^2/s]
C (EZ)   - Dispersion coefficient in Z, [cm^2/s]
C (UX)   - Fluid velocity in X, [cm/s]
C (UZ)   - Fluid velocity in Z, [cm/s]
C
C OUTPUT PARAMETERS:
C  DELT  - Time step size for numerical stability, [sec]
C (CZV)  - Settling Courant No. for size K particle, [-]
C (CX)   - Courant Number in X, times width, [m]
C (CZ)   - Courant Number in Z, times width, [m]
C (DX)   - Dispersion Number in X, times width, [m]
C (DZ)   - Dispersion Number in Z, times width, [m]
C (TERMX)- Combination of Courant & Dispersion Numbers in X, times width, [m]
C (TERMZ)- Combination of Courant & Dispersion Numbers in Z, times width, [m]
C
C AUTHOR:  Jerry Culkin
C          Department of Civil Engineering
C          University of Texas at Austin
```

```
C
C LAST REVISED: 28 july, 1990 for flowrate adjustments
C               1  oct,  1990 to multiply (C, D, Term) by width
C
C PRECISION: Single
C
C LANGUAGE: FORTRAN 77
C
C REFERENCES: None
C
C REQUIRED ROUTINES: None
C_____________________________________________________________________
      WRITE (10,*)
      WRITE (10,*)
      WRITE (10,*) '*****************************OUTPUT STABLE*******',
     $'**********************'
      WRITE (10,*)
C
C Set minimum values to use in stability determinations:
      EXMAX = 1.
      EZMAX = 0.0001
      UXMAX = 0.01
      UZMAX = VMAX
C            ! Greatest particle settling velocity
C
C Find maximum values of dispersion and velocity in their fields:
      DO 200 J = 1,NZ-1
           DO 100 I = 1,NX
                EXMAX = AMAX1(EX(I,J),EXMAX)
                EZMAX = AMAX1(EZ(I,J),EZMAX)
                UXMAX = AMAX1(UX(I,J),UXMAX)
Ccc              UZMAX = AMAX1(UZ(I,J),UZMAX)
  100      CONTINUE
  200 CONTINUE
C
C Conservative correction for ramped flow:
      IF (IQRAMP .EQ. 1) THEN
          UXMAX = QSCALE(0)* UXMAX
          EZMAX = QSCALE(0)* EZMAX
      ENDIF
C
C Find 'stable' DELT:
      DELT = FRACT/ ((EXMAX/DELX**2 + EZMAX/DELZ**2)/2.0
     $              + UXMAX/DELX    + UZMAX/(DELA*DELZ))
C
C Calc Max Courant No. in X:
      COURNT = UXMAX* DELT/ DELX
C Calc Courant No. for fastest settling particle in bottom fluid layer:
      CZVMAX    = VMAX* DELT/ (DELZ* DELA)
C
C Calc relative indicators of dispersion:
      DISPX  = EXMAX* DELT /DELX**2
      DISPZ  = EZMAX* DELT /(DELZ)**2
      PEX    = COURNT/ DISPX
      PEZ    = CZVMAX/ DISPZ
C
C Calc dimensionless Courant & Dispersion Nos. and TERM combinations:
      DO 400 I = 1,NX
           DO 300 J = 1,NZ-1
                CX(I,J)    = UX(I,J)* DELT/ DELX * B(I)
                CZ(I,J)    = UZ(I,J)* DELT/ DELZ * B(I)
                DX(I,J)    = EX(I,J)* DELT/ DELX**2 * B(I)
                DZ(I,J)    = EZ(I,J)* DELT/ DELZ**2 * B(I)
                TERMX(I,J) = (B(I) - CX(I,J)**2/ B(I) - 6.* DX(I,J))
                TERMZ(I,J) = (B(I) - CZ(I,J)**2/ B(I) - 6.* DZ(I,J))
  300      CONTINUE
  400 CONTINUE
C
C Set settling Courant No. for particle using current time step size:
      DO 500 K = 1,NK
           CZV(K) = V(K)* DELT/ DELZ
  500 CONTINUE
C
      IF (TIME .EQ. 0.0) THEN
         WRITE (10,*) 'Calculated stable time-step = ',DELT,'[sec]'
         WRITE (10,*)
         WRITE (10,*) 'Max Courant No. in X    =',COURNT
         WRITE (10,*) 'Max Dispersion No. in X =',DISPX
         WRITE (10,*) 'Grid Peclet No. in X    =',PEX
         WRITE (10,*)
         WRITE (10,*) 'Max Settling Velocity   =',VMAX,' [cm/s]'
         WRITE (10,*) 'Max Courant No. in Z    =',CZVMAX
         WRITE (10,*) 'Max Dispersion No. in Z =',DISPZ
         WRITE (10,*) 'Grid Peclet No. in Z    =',PEZ
         WRITE (10,*)
C
         WRITE (10,*) 'GIVEN the following parameters:'
         WRITE (10,105) DELX,DELZ,DELA
  105 FORMAT (' DelX = ',F10.2,' & DelZ = ',F10.2,' [cm] & DELA = ',
     $        F10.3)
         WRITE (10,*) 'Max Ux = ',UXMAX,' & Max Uz = ',UZMAX,' [cm/s]'
         WRITE (10,*) 'Max Ex = ',EXMAX,' & Max Ez = ',EZMAX,' [cm^2/s]'
      ENDIF
      WRITE (10,*)
C
      RETURN
      END
```

```
C*********************************************************************
      SUBROUTINE RAMPQN (NK,NX,NZ,DIMNK,NITRIB,NTRIB,NIMAIN,NMAIN,
     $                   Q,QITRIB,QTRIB,QSCALE,NSCALE,AREA,UXMEAN,USTAR,
     $                   UX,UZ,EX,EZ,CX,CZ,DX,DZ,TERMX,TERMZ,B)
C
      INTEGER  NK,NX,NZ,DIMNK,IDISPZ,INRAMP,IQRAMP
C
      REAL   NITRIB(NK),NTRIB(NK,NX),NIMAIN(NK),NMAIN(NK)
      REAL   UX(NX,NZ), USTAR(NX), UXMEAN(NX), UZ(NX,NZ),EX(NX,NZ)
      REAL   EZ(NX,NZ),CX(NX,NZ), CZ(NX,NZ), DX(NX,NZ), DZ(NX,NZ)
      REAL   TERMX(NX,NZ), TERMZ(NX,NZ)
      REAL   Q(0:NX), QITRIB(0:NX), QTRIB(0:NX), AREA(NX), B(NX)
      REAL   QSCALE(0:NX), NSCALE(0:NX)
C
      REAL   DELX,DELZ,DELA,DELT,DEPTH,EZMEAN,FRIC,TIME,KARMAN
C
      COMMON/MEANS/  EXMEAN,EZMEAN,FRIC,IDISPZ,DEPTH
      COMMON/RAMP/   TNRAMB,TNRAMU,TNRAMD,TQRAMB,TQRAMU,TQRAMD,INRAMP,
     $               IQRAMP
      COMMON/STEPS/  DELX,DELZ,DELA,DELT,FRACT,TIME,TMAX,HMAX,NOUT,ITER
C
C PURPOSE: Compute the tributary flowrates, system flowrates, longitudinal
C          velocities, vertical dispersivities & their dimensionless
C          transport parameters.
C          Compute the main flow and tributary concs.
C
C INPUT PARAMETERS:
C  IDISPZ   - Switch for using uniform prescribed Ez (1=on)
C  INRAMP   - Switch for ramping trib number concentrations (1=on)
C  IQRAMP   - Switch for ramping trib flowrates (1=on)
C  NK       - Number of particle size classes
C  NX       - No. grids nodes in X
C  NZ       - No. grids nodes in Z
C  DELT     - Time step size for numerical stability, [sec]
C  DELX     - Uniform mesh size in X, [cm]
C  DELZ     - Uniform mesh size in Z, [cm]
C  DEPTH    - Total water column depth, [cm]
C  EZMEAN   - Mean vertical fluid dispersion coef, [cm^2/s]
C  FRIC     - Darcy friction factor, [-]
C  KARMAN   - von Karman constant
C  TIME     - Simulation Time, [s]
C  TNRAMB   - Time to begin ramp up of inflow number concentrations, [s]
C  TNRAMD   - Time to ramp down of inflow number concentrations, [s]
C  TNRAMU   - Time to ramp up of inflow number concentrations, [s]
C  TQRAMB   - Time to begin ramp up of inflow flowrate, [s]
C  TQRAMD   - Time to ramp down of inflow flowrate, [s]
C  TQRAMU   - Time to ramp up of inflow flowrate, [s]
C  {AREA}   - Average cross-sectional area in reach, [m^2]
C  {B}      - Average width of cross-section at grid, [m]
C  {NIMAIN} - Initial number concentration distribution for main inflow,
C             [#/cm^3]
C  {NITRIB} - Initial number concentration distribution for tributaries,
C             [#/cm^3]
C  {NSCALE} - Factor, peak tributary number concentrations divided by
C             initial tributary number concentrations, [-]
C  {QSCALE} - Factor, peak flowrate divided by initial flowrate, [-]
C  {QITRIB} - Initial tributary flowrate, [m^3/s]
C  [EX]     - Longitudinal fluid dispersion coefficient, [cm^2/s]
C  [UZ]     - Vertical fluid velocity, [cm/s]
C
C OUTPUT PARAMETERS:
C  {NMAIN}  - Number concentration distribution for main inflow,[#/cm^3]
C  {Q}      - Total flowrate, [m^3/s]
C  {QTRIB}  - Tributary flowrate, [m^3/s]
C  {USTAR}  - Shear velocity, [cm/s]
C  {UXMEAN} - Mean longitudinal fluid velocity, [cm/s]
C  [CX]     - Courant Number in X, times width, [m]
C  [CZ]     - Courant Number in Z, times width, [m]
C  [DX]     - Dispersion Number in X, times width, [m]
C  [DZ]     - Dispersion Number in Z, times width, [m]
C  [EZ]     - Average vertical fluid dispersion coefficient, [cm^2/s]
C  [TERMX]  - Combination of Courant & Dispersion Numbers in X, times width, [m]
C  [TERMZ]  - Combination of Courant & Dispersion Numbers in Z, times width, [m]
C  [UX]     - Longitudinal fluid velocity, [cm/s]
C
C AUTHOR:   Jerry Culkin
C           Department of Civil Engineering
C           University of Texas at Austin
C
C LAST REVISED: 31 july 1990 .    New ramping routine.
C               1  OCT  1990 .    Multiply (C, D, Term) by width.
C
C PRECISION: Single
C
C LANGUAGE: FORTRAN 77
C
C REFERENCES: None
C
C REQUIRED ROUTINES: None
C-----------------------------------------------------------------------
      KARMAN = 0.40
C For RAMPED FLOWS, reset longitudinal flowrates & velocities and
C vertical dispersion fields:
      IF (IQRAMP .EQ. 0) THEN
          GOTO 800
      ELSE
          DO 100 I = 0, NX
              IF (TIME .GT. TQRAMB .AND. TIME .LE. TQRAMU) THEN
```

```
                QTRIB(I) = QITRIB(I)* (1.+ (QSCALE(I)- 1.)*
     $                        (TIME- TQRAMB)/ (TQRAMU-TQRAMB))
              ELSEIF (TIME .GT. TQRAMU .AND. TIME .LE. TQRAMD) THEN
                QTRIB(I) = QITRIB(I)* (1.- (1.- QSCALE(I))*
     $                        (TQRAMD- TIME)/ (TQRAMD-TQRAMU))
              ELSE
                QTRIB(I) = QITRIB(I)
              ENDIF
  100       CONTINUE
C
C         Velocity and dispersion coefficients for open channel shear
C         flow w/ log velocity profile in defect form:
C
          Q(0) = QTRIB(0)
          DO 300 I = 1, NX
               Q(I)      = Q(I-1) + QTRIB(I)
               UXMEAN(I) = Q(I)/ AREA(I)* 100.
               USTAR(I)  = UXMEAN(I)* SQRT(FRIC/8.)
               ZLOCAL    = DELZ* DELZ
               ZSYSTM    = DEPTH- ZLOCAL
               DO 200 J = NZ-1, 1, -1
                    UX(I,J)    = UXMEAN(I)+ USTAR(I)/ KARMAN* (1.+
     $                           LOG(ZLOCAL/ DEPTH))
                    DX(I,J)    = EX(I,J)* DELT/ DELX**2 * B(I)
                    IF (UX(I,J) .LT. 0.0 ) UX(I,J) = 0.02* UXMEAN(I)
                    CX(I,J)    = UX(I,J)* DELT/ DELX* B(I)
                    TERMX(I,J) = (B(I) - CX(I,J)**2/ B(I) - 6.* DX(I,J))
                    ZLOCAL     = ZLOCAL + DELZ
                    ZSYSTM     = DEPTH- ZLOCAL
  200          CONTINUE
  300       CONTINUE
C
          IF (IDISPZ .EQ.1) THEN
              DO 500 J = 1,NZ-1
                   DO 400 I = 1, NX
                        CZ(I,J)    = UZ(I,J)* DELT/ DELZ* B(I)
                        EZ(I,J)    = EZMEAN
                        DZ(I,J)    = EZ(I,J)* DELT/ DELZ**2* B(I)
                        TERMZ(I,J) = (B(I) - CZ(I,J)**2/ B(I) - 6.
     &                               * DZ(I,J))
  400              CONTINUE
  500         CONTINUE
          ELSE
              DO 700 J = 1,NZ-1
                   DO 600 I = 1, NX
                        CZ(I,J)    = UZ(I,J)* DELT/ DELZ* B(I)
                        EZ(I,J)    = DEPTH* USTAR(I)/ 15.
                        DZ(I,J)    = EZ(I,J)* DELT/ DELZ**2* B(I)
                        TERMZ(I,J) = (B(I) - CZ(I,J)**2/ B(I) - 6.
     &                               * DZ(I,J))
  600              CONTINUE
  700         CONTINUE
              ENDIF
          ENDIF
  800 CONTINUE
C
C For RAMPED CONCENTRATIONS, reset trib concs and U/S concs:
          IF (INRAMP .EQ. 0) THEN
              GOTO 1900
          ELSE
C         Tributary concs:
              DO 1200 I = 1, NX
                   IF (TIME .GT. TNRAMB .AND. TIME .LE. TNRAMU) THEN
                        FACTN = 1.+ (NSCALE(I)- 1.)* (TIME- TNRAMB)/
     $                          (TNRAMU-TNRAMB)
                        DO 900 K = 1, NK
                             NTRIB(K,I) = NITRIB(K)* FACTN
  900                   CONTINUE
                   ELSEIF (TIME .GT. TNRAMU .AND. TIME .LE. TNRAMD) THEN
                        FACTN = 1.- (1.- NSCALE(I))* (TNRAMD- TIME)/
     $                          (TNRAMD-TNRAMU)
                        DO 1000 K = 1, NK
                             NTRIB(K,I) = NITRIB(K)* FACTN
 1000                   CONTINUE
                   ELSE
                        FACTN = 1.
                        DO 1100 K = 1, NK
                             NTRIB(K,I) = NITRIB(K)
 1100                   CONTINUE
                   ENDIF
 1200         CONTINUE
C
C         U/S concs (before tributary 1 load contribution added in BCN):
              IF (TIME .GT. TNRAMB .AND. TIME .LE. TNRAMU) THEN
                   FACTN = 1.+ (NSCALE(0)- 1.)* (TIME- TNRAMB)/
     $                     (TNRAMU-TNRAMB)
                   DO 1300 K = 1, NK
                        NMAIN(K) = NIMAIN(K)* FACTN
 1300              CONTINUE
              ELSEIF (TIME .GT. TNRAMU .AND. TIME .LE. TNRAMD) THEN
                   FACTN = 1.- (1.- NSCALE(0))* (TNRAMD- TIME)/
     $                     (TNRAMD-TNRAMU)
                   DO 1500 K = 1, NK
                        NMAIN(K) = NIMAIN(K)* FACTN
 1500              CONTINUE
              ELSE
                   FACTN = 1.
                   DO 1700 K = 1, NK
                        NMAIN(K) = NIMAIN(K)
```

```
 1700          CONTINUE
             ENDIF
          ENDIF
 1900 CONTINUE
C
      RETURN
      END



C*********************************************************************
      SUBROUTINE BCN (NK,NX,NZ,DIMNK,N1,NMAIN,NTRIB,Q,QTRIB)
C
      INTEGER  NK,NX,NZ,DIMNK
C
      REAL   N1(DIMNK,NX,NZ),NTRIB(NK,NX),NMAIN(NK)
      REAL   Q(0:NX), QTRIB(0:NX)
C
      REAL   TIME
C
      COMMON/STEPS/  DELX,DELZ,DELA,DELT,FRACT,TIME,TMAX,HMAX,NOUT,ITER
C
C PURPOSE: Compute the upstream BC concentrations at time zero and
C          subsequent calls if flow or conc ramping.
C
C INPUT PARAMETERS:
C  DIMNK    - Number of particle size classes + 1
C  NK       - Number of particle size classes
C  NX       - No. grids nodes in X
C  NZ       - No. grids nodes in Z
C  TIME     - Simulation time, [s]
C  {NMAIN}  - Number concentration distribution for main inflow,[#/cm^3]
C  {Q}      - Total flowrate, [m^3/s]
C  {QTRIB}  - Tributary flowrate, [m^3/s]
C
C OUTPUT PARAMETERS:
C  [N1]     - U/S boundary concentration for water column domain,[#/cm^3]
C
C AUTHOR:   Jerry Culkin
C           Department of Civil Engineering
C           University of Texas at Austin
C
C LAST REVISED: 27 SEPTEMBER 1990 1510.   New BC routine for U/S concs.
C               28 SEPTEMBER 1990 2045    TIME write added
C PRECISION: Single
C
C LANGUAGE: FORTRAN 77
C
C REFERENCES: None
C
C REQUIRED ROUTINES: None
C_____________________________________________________________________
C      WRITE (10,115) TIME
C  115 FORMAT (/,'BCN() called at Time = ',F10.2,' [s]',/)
      I = 1
      J = 1
      DO 100 K = 1,NK
            N1(K,1,1) = (Q(0)* NMAIN(K) + QTRIB(1)* NTRIB(K,1))/ Q(1)
  100 CONTINUE
      DO 300 J = 2,NZ-1
         DO 200 K = 1,NK
            N1(K,1,J) = N1(K,1,1)
  200    CONTINUE
  300 CONTINUE
C
      RETURN
      END


C*********************************************************************
      SUBROUTINE SOURCE (NK,NX,NZ,NTRIB,NSOURC,QTRIB,AREA)
C
      INTEGER  NK,NX,NZ,JNUM
C
      REAL   NSOURC(NK,NX,NZ),NTRIB(NK,NX)
      REAL   QTRIB(0:NX),AREA(NX)
C
      REAL   DELT,DELX,DELZ,DEPTH
C
      COMMON/MEANS/  EXMEAN,EZMEAN,FRIC,IDISPZ,DEPTH
      COMMON/STEPS/  DELX,DELZ,DELA,DELT,FRACT,TIME,TMAX,HMAX,NOUT,ITER
C
C PURPOSE: Compute the source strengths due to lateral tributary
C          particle inflows (flowrates x concentrations). The sources
C          are actually used in MAIN. Source changes of main inflow,
C          yielding  U/S BC (i.e., at i-1) are found in BCN().
C
C INPUT PARAMETERS:
C  NK     - Number of particle size classes
C  NX     - No. grids nodes in X
C  NZ     - No. grids nodes in Z
C  DELT   - Time step, [s]
C  DELX   - Uniform mesh size in X, [cm]
C  DELZ   - Uniform mesh size in Z, [cm]
C  DEPTH  - Average total water column depth, [cm]
C {AREA}  - Cross sectional area, [m^2]
C {Q}     - Total flowrate, [m^3/s]
C {QTRIB} - Tributary flowrate, [m^3/s]
```

```
C
C OUTPUT PARAMETERS:
C  FACT1  - Constant factor for fractional depth load zone, [-]
C  FACT2  - Constant for each longitudinal grid, [-]
C [NSOURC]- Concentration source at (k,i,j) due to tributary source,
C             [#/cm^3]
C
C AUTHOR:   Jerry Culkin
C           Department of Civil Engineering
C           University of Texas at Austin
C
C LAST REVISED: 28 sept 1990  2000. - new CV logic-6
C                uses (Delt*Qtrib/Volume)* Ntrib
C                results in Courant-type No. in source
C
C PRECISION: Single
C
C LANGUAGE: FORTRAN 77
C
C REFERENCES: None
C
C REQUIRED ROUTINES: None
C_____________________________________________________________________
C Note that tributary contributions for i=1 are necessarily separate as
C boundary conditions. They are computed in BCN().
C
C Specify volume of 2.5* DELZ depth for spreading the load over top 3
C grids. Put the 300 loop's bottom index at JNUM-3.
C Note that tributary contributions for i=1 are necessarily separate as
C boundary conditions:
C
      JNUM = 3
      RNUM = FLOAT(JNUM)
      FACT1 =  DEPTH/ ((RNUM- 0.5)* DELZ)* DELT/DELX* 100.
      DO 300 I = 2, NX
          FACT2  =  FACT1* QTRIB(I)/ AREA(I)
          DO 200 J = 1, JNUM
              DO 100 K = 1, NK
                  NSOURC(K,I,J) = FACT2* NTRIB(K,I)
  100         CONTINUE
  200     CONTINUE
  300 CONTINUE
C
      RETURN
      END


C*********************************************************************
      SUBROUTINE ERODE (NX,RHOW,USTAR,RFLUX,STRESB)
C
      INTEGER  NX
C
      REAL     RFLUX(NX),STRESB(NX),USTAR(NX)
C
      REAL     STRESC,RATEM,RHOW
C
      COMMON/EROSON/ STRESC,RATEM
C
C PURPOSE: This subroutine calculates POTENTIAL gross vertical mass flux
C          of particles due to resuspension at bed interface at each X
C          node.
C
C INPUT PARAMETERS:
C  NX      - Number of longitudinal grids
C  RATEM   - Erosion rate constant, [s/cm]
C  RHOW    - Water density, [g/cm^3]
C  STRESC  - Critical shear stress for erosion, [dyne/cm^2]
C [USTAR]  - Shear velocity, [cm/s]
C
C OUTPUT PARAMETERS:
C [RFLUX]  - Total POTENTIAL vertical bed mass flux at node I due
C              to resuspension, positive for flux out of bed.
C              Subject to bed mass availability. [g/cm^2-s]
C [STRESB] - Local Bed shear stress, [dyne/cm^2] = [g/cm-s^2]
C
C AUTHOR:   Jerry Culkin
C           Department of Civil Engineering
C           University of Texas at Austin
C
C LAST REVISED: 1 AUG, 1990.
C
C PRECISION: Single
C
C LANGUAGE: FORTRAN 77
C
C REFERENCES: None
C
C REQUIRED ROUTINES: None
C_____________________________________________________________________
C     WRITE (10,*)
C     WRITE (10,*) '*****************************OUTPUT ERODE********',
C    $'**********************'
C
      DO 100 I = 2,NX
          STRESB(I) = RHOW* USTAR(I)**2
          IF ((STRESB(I) - STRESC) .LE. 0.0) THEN
C             a) Zero or Negative effective shear stress:
              RFLUX(I) = 0.0
```

```
          ELSE
C             b) Positive effective shear stress:
              RFLUX(I) = RATEM* (STRESB(I) - STRESC)
          ENDIF
  100 CONTINUE
C
      RETURN
      END


C*********************************************************************
      SUBROUTINE DISTRB (NK,NX,NZ,DIMNK,N1,DP,TSS,TAREA,FP,TOTFP)
C
      INTEGER NK,NX,NZ,DIMNK
C
      REAL FP(NK,NX,NZ),TSS(NX,NZ),TAREA(NX,NZ),N1(DIMNK,NX,NZ)
      REAL TOTFP(NX,NZ),DP(DIMNK)
      REAL KPM,KPA,CONM1,CONA1,CONA2,PARTM,PARTA,RHOP,PI
C
      COMMON/PART/   RHOP,RHOW,VISCOS,TEMP,GRAV,LV1ST,LVSTEP,PI
      COMMON/TAMNIT/ CTW,CTB,KPM,KPA
C
C PURPOSE: This subroutine calculates the fraction of contaminant sorbed
C          to solid relative to total contaminant.
C
C INPUT PARAMETERS:
C  NK        - Number of particle sizes
C  DIMNK     - Number of particle sizes + 1
C  NX        - Number of longitudinal grids
C  NZ        - Number of vertical grids
C  [N1]      - Particle number concentration, [#/cm^3]
C  [TSS]     - Suspended solids mass concentrations at TIME, [mg/L]
C  [TAREA]   - Total superficial surface area concentration of suspended
C              solids, [cm^2/L]
C  [DP]      - Equivalent spherical floc diameter, [um]
C  RHOP      - Bulk floc density, [g/cm^3]
C  KPA       - Surface-based, porosity-corrected partition coefficient,
C              [L/cm^2]
C  KPM       - Mass-based, porosity-corrected partition coefficient,
C              [L/kg]
C
C OUTPUT PARAMETERS:
C  [FP]      - fraction of total contaminant sorbed to solid of size k,
C              [-]
C  CONA1     - Conversion factor to convert proportional area in
C              [um^2/cm^3] to [cm^2/L]
C  CONA2     - Conversion factor to convert proportional area-partition
C              fraction to actual area-partition fraction
C  CONM1     - Conversion factor to convert proportional volume in
C              [um^3/cm^3] to absolute mass in [mg/L]
C  CONM2     - Conversion factor to convert proportional mass-partition
C              fraction to actual mass-partition fraction
C
C AUTHOR:    Jerry Culkin
C            Department of Civil Engineering
C            University of Texas at Austin
C
C LAST REVISED:      22 June 1990         2250
C
C PRECISION:  Single
C
C LANGUAGE:   FORTRAN 77
C
C REFERENCES: None
C
C REQUIRED ROUTINES: TOTAL
C
C_____________________________________________________________________
C      WRITE (10,*)
C      WRITE (10,*) '*****************************OUTPUT DISTRB*******',
C     $'***********************'
C      WRITE (10,*)
C The surface area version:
      CONA1  = PI* 1.E-5
C
      DO 300 J = 1, NZ
           DO 200 I = 1, NX
                CONA2 = KPA/ (1.+ KPA* TAREA(I,J))
                TOTFP(I,J) = 0.
                DO 100 K = 1, NK
                     PARTA      =  N1(K,I,J)* DP(K)**2 * CONA1
                     FP(K,I,J)  =  PARTA* CONA2
                     TOTFP(I,J) =  TOTFP(I,J) + FP(K,I,J)
  100           CONTINUE
  200      CONTINUE
  300 CONTINUE
C
CM The mass version:
CM      CONM1  = PI* RHOP/ 6.* 1.E-6
CM
CM First adjust KPM units to match TSS units:
CM      KPM = KPM/1.E6
CM
CM      DO 600 J = 1, NZ
CM         DO 500 I = 1, NX
CM              CONM2 = KPM/ (1.+ KPM* TSS(I,J))
CM              TOTFP(I,J) = 0.
CM              DO 400 K = 1, NK
```

```
CM                    PARTM      =  N1(K,I,J)* DP(K)**3 * CONM1
CM                    FP(K,I,J)  =  PARTM* CONM2
CM                    TOTFP(I,J) =  TOTFP(I,J) + FP(K,I,J)
CM  400           CONTINUE
CM  500       CONTINUE
CM  600  CONTINUE
C
      RETURN
      END


C*********************************************************************
      SUBROUTINE BEDXCH (NK,NX,NZ,DIMNK,N1,DP,V,RFLUX,BEDMAS,N2,BEDVOL,
     &                   TSS,NUMIN,NUMOUT,NUMNET,MASSIN,MASOUT,TRNSFR)
C
      INTEGER  NK,NX,NZ,DIMNK
C
      REAL   N1(DIMNK,NX,NZ),N2(DIMNK,NX,NZ),V(NK),DP(DIMNK)
      REAL   RFLUX(NX),BEDMAS(NX),BEDVOL(NX)
      REAL   NUMIN(NK,NX),NUMOUT(NK,NX),NUMNET(NK,NX),TRNSFR(NX)
      REAL   MASSIN(NX), MASOUT(NX), TSS(NX,NZ)
C
      REAL   DELNO,MASNET,SUMNUM,VOLMAS,LV1ST,LVSTEP,PI
C
      COMMON/PART/   RHOP,RHOW,VISCOS,TEMP,GRAV,LV1ST,LVSTEP,PI
      COMMON/STEPS/  DELX,DELZ,DELA,DELT,FRACT,TIME,TMAX,HMAX,NOUT,ITER
C
C PURPOSE: This subroutine calculates particle deposition, bed inventory,
C          and vertical number concentration gradient for each size
C          at each X node.
C
C INPUT PARAMETERS:
C  DIMNK    - NK + 1 to accomodate element shifts in C codes
C             floc, [um]
C  NK       - Number of particle size classes
C  NX       - Number of longitudinal grids
C  NZ       - Number of vertical grids
C             interface layer at node I, J = NZ, t = t, [#/cm^3]
C  RHOP     - Particle bulk density, [g/cm^3]
C  DELT     - Time step, [s]
C {BEDMAS}- Total mass of solids in the interface layer per
C           unit area at node I, [g/cm^2]
C {BEDVOL}- Bulk volume of the interface layer per unit area at
C           node I, i.e., DEPTH(I), [cm^3/cm^2]
C {DP}     - Equivalent spherical diameter of size class k
C {RFLUX} - Total potential vertical bed mass flux at node
C           (I,NZ) due to resuspension, subject to bed mass
C           availability, [g/cm^2-s]
C {V}      - Settling velocity of size class k, [cm/s]
C [N1]     - Bulk number concentration of size class k in the
C [TSS]    - Total suspended solid mass concentration, [mg/L]
C
C OUTPUT PARAMETERS:
C {BEDVOL}- Bulk volume of the interface layer per unit area at
C           node I, i.e., BED DEPTH(I) [cm^3/cm^2]
C {BEDMAS}- Total mass of solids in the interface layer per
C           unit area at node I, [g/cm^2]
C {TRNSFR}- Bulk resuspension transfer velocity, [cm/s]
C [NUMIN] - Number of size k flocs (per unit area) entering
C              bed at node I during DELT, [#/cm^2]
C {NUMOUT]- Number of size k flocs (per unit area) leaving
C              bed at node I during DELT, [#/cm^2]
C {NUMNET}- Net number of size k flocs (per unit area) entering
C           interface at node I during DELT, [#/cm^2]
C [N2]     - Bulk number concentration of size class k particles at
C           t = t + DELT (calculated here for interface layer
C           only, [#/cm^3]
C
C AUTHOR:   Jerry Culkin
C           Department of Civil Engineering
C           University of Texas at Austin
C
C LAST REVISED:
C
C PRECISION: Single
C
C LANGUAGE: FORTRAN 77
C
C REFERENCES: None
C
C REQUIRED ROUTINES: None.
C_____________________________________________________________________
CB      WRITE (10,*)
CB      WRITE (10,*) '*****************************OUTPUT BEXCHN********',
CB     $'**********************'
CB      WRITE (10,*)
CB      WRITE (10,*) ' I     MASSIN [g]       MASOUT [g]'
C
C Volume to mass conversion factor:
      VOLMAS   = PI* RHOP/ 6.* 1.E-12
      DO 200 I = 2,NX
           MASSIN(I) = 0.0
           MASOUT(I) = 0.0
           TRNSFR(I) = RFLUX(I)/ TSS(I,NZ)* 1.E6
           DO 100 K = 1,NK
                BEDNUM      = N1(K,I,NZ)* BEDVOL(I)
C
                NUMIN(K,I) = DELT* V(K)* N1(K,I,NZ-1)
```

```
                NUMOUT(K,I)= DELT* TRNSFR(I)* N1(K,I,NZ)
                IF (NUMOUT(K,I) .GT. BEDNUM) THEN
                    NUMOUT(K,I) = N1(K,I,NZ)* BEDVOL(I)
                ENDIF
C
                NUMNET(K,I)= NUMIN(K,I)- NUMOUT(K,I)
                N2(K,I,NZ) = N1(K,I,NZ)+ NUMNET(K,I)/ BEDVOL(I)
C               { is this N2 calculation irrelevant- is it fixed by
C                 constant POROS and TSS(I,NZ) ?}
C
                MASSIN(I)  = MASSIN(I) + NUMIN(K,I)* DP(K)**3
                MASOUT(I)  = MASOUT(I) + NUMOUT(K,I)* DP(K)**3
  100       CONTINUE
C
C Convert net deposition [vol/cm^2] to [g/cm^2].
C Integrate mass flux for total solids mass in interface per unit area
C at time t + DELT (after deposition & resuspension).
C Calc total bulk volume of interface per unit area (DEPTH) at time
C t + DELT:
            MASSIN(I) = MASSIN(I)* VOLMAS
            MASOUT(I) = MASOUT(I)* VOLMAS
            BEDMAS(I) = BEDMAS(I) + MASSIN(I)- MASOUT(I)
C
            IF (BEDMAS(I) .LT. 1.E-6) THEN
                BEDMAS(I) = 0.0
            ENDIF
C
            BEDVOL(I)  = BEDMAS(I)/ TSS(I,NZ)* 1.E6
CB            WRITE (10,*) I, MASSIN(I), MASOUT(I)
  200 CONTINUE
C
      RETURN
      END



C**********************************************************************
      SUBROUTINE TRANSP  (NK,NX,NZ,DIMNK,N1,N2,V,UX,UZ,EX,EZ,
     $                    CX,C2,DX,DZ,TERMX,TERMZ,CZV,NUMNET,B)
C
      INTEGER NK,NX,NZ,DIMNK,ITER
C
      REAL  N1(DIMNK,NX,NZ),N2(DIMNK,NX,NZ)
      REAL  NUMNET(NK,NX)
C
      REAL  UX(NX,NZ),UZ(NX,NZ),EX(NX,NZ),EZ(NX,NZ),V(NK),CZV(NK)
      REAL  CX(NX,NZ),C2(NX,NZ),DX(NX,NZ),DZ(NX,NZ),B(NX)
      REAL  TERMX(NX,NZ),TERMZ(NX,NZ)
C
      REAL  DELX,DELZ,DELA,DELT
C
      COMMON/STEPS/  DELX,DELZ,DELA,DELT,FRACT,TIME,TMAX,HMAX,NOUT,ITER
C
C PURPOSE: This subroutine integrates the advection-dispersion equation
C          to find the number concentrations of particles given a
C          specified fluid flow/dispersion field. The parabolic PDE is
C          approximated by finite-difference equations in 2 dimensions,
C          with appropriate 2-point backward, 3-point central, and
C          4-point Leonard's method discretization of spatial deriva-
C          tives. The solution method is explicit. Boundary conditions
C          for U/S, D/S, air-water, & bed-water interfaces are written
C          into the discretizations.
C
C STATE VARIABLES:
C   N(K,I,J) - Number concentration of size k at longitudinal
C                    I and vertical J at time t.
C
C INPUT PARAMETERS:
C  NK        - Number of particle size classes
C  DIMNK     - NK + 1 to accomodate element shifts in C codes
C  NX        - Number of longitudinal grids
C  NZ        - Number of vertical grids
C  DELT      - Time step, [s]
C  DELX      - Longitudinal grid spacing, [cm]
C  DELZ      - Vertical grid spacing, [cm]
C  DELA      - Vertical grid spacing at bed-water interface [cm]
C {B}        - Average width of cross-section at grid, [m]
C {CZV}      - Settling Courant No. for size K particle, [-]
C {V}        - Settling velocity of size K particle, [cm/s]
C {N1}       - Initital number concentration, [#/cm^3]
C [NUMNET]   - Net number of size k flocs (per unit area) entering
C               interface at node I during DELT, [#/cm^2]
C [N2]       - Bulk number concentration of size class k particles at
C              t = t + DELT (calculated here for interface layer only,
C              [#/cm^3]
C [UX],[UZ] - Longitudinal and vertical velocities, [cm/s]
C {EX],[EZ] - Longitudinal and vertical dispersion coefficients,
C              [cm^2/s]
C [CX],[DZ] - Longitudinal and vertical Courant No., times width, [m]
C [DX],[DZ] - Longitudinal and vertical Dispersion No., times width, [m]
C [TERMX/Z] - Longitudinal and vertical combination of Ci & Di, [-]
C
C OUTPUT PARAMETERS:
C CROSS      - Corrective term for 2-D PDE cross derivatives, [#-m/cm^3]
C [N2]       - Number concentration after transport but before
C                coagulation [#/cm^3]
C
C AUTHOR: Jerry Culkin
```

```
C         Department of Civil Engineering
C         University of Texas at Austin
C
C LAST REVISED: 1 Oct   - new logic w/ (B) width
C               27 Sept - removed [NSOURC] for tributary loads; now in
C                         MAIN
C               1 Oct   - new logic w/ (B) width
C               2 Oct   - correct (B) problems in core
C
C PRECISION:  Single
C
C LANGUAGE:   FORTRAN 77
C
C REFERENCES: None
C
C REQUIRED ROUTINES: None
C
C
C-----------------------------------------------------------------------
C Air-water interface (top, horizontal water-column grid):
      J = 1
C Upstream boundary:
      I = 1
      DO 200 K = 1,NK
           N2(K,I,J) =  N1(K,I,J)
  200 CONTINUE
      I = 2
C
      DO 300 K = 1,NK
       N2(K,I,J) = N1(K,I,J)  +
     $  (N1(K,I+1,J)* (-CX(I+1,J)/2. + (CX(I+1,J)**2/2. + CX(I+1,J)
     &    /6. * TERMX(I+1,J))/B(I+1) + DX(I+1,J))
     $ + N1(K,I,J)* ((-CX(I,J)**2/B(I)-7./12.* CX(I,J)* TERMX(I,J))/B(I)
     $   - 2.*DX(I,J)- DELT* V(K)**2* B(I)/ EZ(I,J)- (CZ(I,J)+ CZV(K)
     &   *B(I)) - DZ(I,J))
     $ + N1(K,I-1,J)* (CX(I-1,J)/2. + (CX(I-1,J)**2/2.+ 5./12.
     &   *CX(I-1,J) * TERMX(I-1,J))/B(I-1) + DX(I-1,J))
     & + N1(K,I,J+1)* DZ(I,J+1))/ B(I)
  300 CONTINUE
C
      DO 500 I = 3,NX-1
       DO 400 K = 1,NK
        N2(K,I,J) = N1(K,I,J)  +
     $  (N1(K,I+1,J)* (-CX(I+1,J)/2. + (CX(I+1,J)**2/2.
     &   + CX(I+1,J)/6.* TERMX(I+1,J))/ B(I+1) + DX(I+1,J))
     $ + N1(K,I,J)* ((-CX(I,J)**2 - CX(I,J) *TERMX(I,J)/2.)/B(I)- 2.
     &   * DX(I,J)- DELT* V(K)**2* B(I)/ EZ(I,J)- (CZ(I,J)+ CZV(K)*B(I))
     &   - DZ(I,J))
     $ + N1(K,I-1,J)* (CX(I-1,J)/2. + (CX(I-1,J)**2/2. + CX(I-1,J)/2.
     $   * TERMX(I-1,J))/ B(I-1) + DX(I-1,J))
     $ + N1(K,I-2,J)* (-CX(I-2,J)* TERMX(I-2,J)/6.)/ B(I-2)
     & + N1(K,I,J+1)* DZ(I,J+1))/ B(I)
  400   CONTINUE
  500  CONTINUE
C
      I = NX
      DO 600 K = 1,NK
        N2(K,I,J) = N1(K,I,J)  +
     $  (N1(K,I,J)* ((-CX(I,J)**2  - CX(I,J)*TERMX(I,J)/2.)/ B(I)
     &   - 2.*DX(I,J) - DELT* V(K)**2* B(I)/ EZ(I,J)- (CZ(I,J)+ CZV(K)
     &   *B(I)) - DZ(I,J))
     $ + N1(K,I-1,J)* ((CX(I-1,J)**2+ 2./3.*CX(I-1,J)* TERMX(I-1,J))
     &   /B(I) + 2. * DX(I-1,J))
     $ + N1(K,I-2,J)* (-CX(I-2,J)* TERMX(I-2,J)/6.)/ B(I-2)
     & + N1(K,I,J+1)* DZ(I,J+1))/ B(I)
  600 CONTINUE
C
C-----------------------------------------------------------------------
C Second horizontal water column grid:
      J = 2
C Upstream boundary:
      I = 1
      DO 700 K = 1,NK
           N2(K,I,J) =  N1(K,I,J)
  700 CONTINUE
C
      I = 2
      DO 800 K = 1,NK
        N2(K,I,J) = N1(K,I,J)  +
     $  (N1(K,I+1,J)* (-CX(I+1,J)/2. + (CX(I+1,J)**2/2. + CX(I+1,J)/6.
     $   * TERMX(I+1,J))/ B(I+1) + DX(I+1,J))
     $ + N1(K,I,J)* ((-CX(I,J)**2- 7./12.*CX(I,J)* TERMX(I,J))/ B(I)
     &   - 2.*DX(I,J)- (CZ(I,J)+ CZV(K)*B(I)) - 2.*DZ(I,J))
     $ + N1(K,I-1,J)* (CX(I-1,J)/2. + (CX(I-1,J)**2/2. + 5./12.
     $   * CX(I-1,J)* TERMX(I-1,J))/ B(I-1) + DX(I-1,J))
     $ + N1(K,I,J+1)* DZ(I,J+1)
     $ + N1(K,I,J-1)* (CZ(I,J-1) + CZV(K)*B(I) + DZ(I,J-1))) / B(I)
  800 CONTINUE
C
      DO 1000 I = 3,NX-1
       DO 900 K = 1,NK
        N2(K,I,J) = N1(K,I,J)  +
     $  (N1(K,I+1,J)* (-CX(I+1,J)/2. + (CX(I+1,J)**2/2. + CX(I+1,J)/6.
     $   * TERMX(I+1,J))/ B(I+1) + DX(I+1,J))
     $ + N1(K,I,J)* ((-CX(I,J)**2 - CX(I,J)*TERMX(I,J)/2.)/ B(I)
     &   -2.*DX(I,J) - (CZ(I,J)+ CZV(K)*B(I)) - 2.*DZ(I,J))
     $ + N1(K,I-1,J)* (CX(I-1,J)/2. + (CX(I-1,J)**2/2. + CX(I-1,J)/2.
     $   * TERMX(I-1,J))/ B(I-1) + DX(I-1,J))
     $ + N1(K,I-2,J)* (-CX(I-2,J)* TERMX(I-2,J)/6.)/ B(I-2)
     $ + N1(K,I,J+1)* DZ(I,J+1)
     $ + N1(K,I,J-1)* (CZ(I,J-1) + CZV(K)*B(I) + DZ(I,J-1))) / B(I)
```

```
  900  CONTINUE
 1000 CONTINUE
C
      I = NX
      DO 1100 K = 1,NK
       N2(K,I,J) = N1(K,I,J)  +
     $ (N1(K,I,J)* ((-CX(I,J)**2 - CX(I,J)*TERMX(I,J)/2.)/ B(I)
     &   - 2.*DX(I,J) - (CZ(I,J)+ CZV(K)*B(I))  - 2.*DZ(I,J))
     $ + N1(K,I-1,J)* ((CX(I-1,J)**2 + 2./3.*CX(I-1,J)* TERMX(I-1,J))
     &   /B(I-1) + 2. * DX(I-1,J))
     $ + N1(K,I-2,J)* (-CX(I-2,J)* TERMX(I-2,J)/6.)/ B(I-2)
     $ + N1(K,I,J+1)* (DZ(I,J+1))
     $ + N1(K,I,J-1)* (CZ(I,J-1) + CZV(K)*B(I) + DZ(I,J-1))) / B(I)
 1100 CONTINUE
C
C Core of water column domain:
      DO 1700 J = 3,NZ-2
         I = 1
         DO 1200 K = 1,NK
            N2(K,I,J) =  N1(K,I,J)
 1200    CONTINUE
C
         I = 2
         DO 1300 K = 1,NK
         N2(K,I,J) = N1(K,I,J) +
     $    (N1(K,I+1,J)* (-CX(I+1,J)/2.+ (CX(I+1,J)**2/2.+ CX(I+1,J)/6.
     $    * TERMX(I+1,J))/ B(I+1) + DX(I+1,J))
     $ + N1(K,I,J)* ((-CX(I,J)**2- (CZ(I,J)+ CZV(K)*B(I))**2
     &    - 7./12. * CX(I,J)* TERMX(I,J) - (CZ(I,J) + CZV(K)*B(I))
     &    * (TERMZ(I,J)- 2.*CZ(I,J)*CZV(K)- CZV(K)**2* B(I))/2.)/ B(I)
     &    - 2.*DX(I,J) - 2.*DZ(I,J))
     $ + N1(K,I-1,J)* (CX(I-1,J)/2. + (CX(I-1,J)**2/2. + 5./12.
     $    * CX(I-1,J)* TERMX(I-1,J))/ B(I-1) + DX(I-1,J))
     $ + N1(K,I,J+1)* (-(CZ(I,J+1) + CZV(K)*B(I))/2. + ((CZ(I,J+1)
     $    + CZV(K)*B(I))**2/2. + (CZ(I,J+1) + CZV(K)*B(I))* (TERMZ(I,J+1)
     $    - 2. *CZ(I,J+1)*CZV(K) - CZV(K)**2*B(I))/6.)/ B(I) + DZ(I,J+1))
     $ + N1(K,I,J-1)* ((CZ(I,J-1) + CZV(K)* B(I))/2. + ((CZ(I,J-1)
     $    + CZV(K)* B(I))**2/2. + (CZ(I,J-1) + CZV(K)* B(I))
     &    * (TERMZ(I,J-1)- 2.*CZ(I,J-1)*CZV(K)- CZV(K)**2* B(I))/2.)/B(I)
     &    +  DZ(I,J-1))
     $ + N1(K,I,J-2)* ((-(CZ(I,J-2) + CZV(K)* B(I))* (TERMZ(I,J-2)
     $    - 2.*CZ(I,J-2)*CZV(K) - CZV(K)**2* B(I))/6.)/B(I))) / B(I)
 1300    CONTINUE
C
         DO 1500 I = 3,NX-1
            DO 1400 K = 1,NK
       N2(K,I,J) = N1(K,I,J) +
     $ (N1(K,I+1,J)* (-CX(I+1,J)/2. + (CX(I+1,J)**2/2. + CX(I+1,J)/6.
     $    * TERMX(I+1,J))/ B(I+1) + DX(I+1,J))
     $ + N1(K,I,J)* ((-CX(I,J)**2- (CZ(I,J) + CZV(K)*B(I))**2 -CX(I,J)
     &    /2.* TERMX(I,J) - (CZ(I,J) + CZV(K)* B(I))* (TERMZ(I,J)- 2.
     &    * CZ(I,J)* CZV(K) - CZV(K)**2*B(I))/2.)/ B(I) - 2.*DX(I,J)
     &    - 2.*DZ(I,J))
     $ + N1(K,I-1,J)* (CX(I-1,J)/2. + (CX(I-1,J)**2/2. + CX(I-1,J)/2.
     $    * TERMX(I-1,J))/ B(I-1) + DX(I-1,J))
     $ + N1(K,I-2,J)* ((-CX(I-2,J)* TERMX(I-2,J)/6.)/ B(I-2))
     $ + N1(K,I,J+1)* (-(CZ(I,J+1) + CZV(K)* B(I))/2.+ ((CZ(I,J+1)
     &    + CZV(K)* B(I))**2/2. + (CZ(I,J+1)+ CZV(K)*B(I))* (TERMZ(I,J+1)
     &    - 2.*CZ(I,J+1)* CZV(K) - CZV(K)**2* B(I))/6.)/ B(I)
     &    + DZ(I,J+1))
     $ + N1(K,I,J-1)* ((CZ(I,J-1)+ CZV(K)* B(I))/2.+ ((CZ(I,J-1)+ CZV(K)
     &    * B(I))**2/ 2.+ (CZ(I,J-1)+ CZV(K)* B(I))* (TERMZ(I,J-1)- 2.
     &    * CZ(I,J-1)*CZV(K)- CZV(K)**2* B(I))/2.)/ B(I)+ DZ(I,J-1))
     $ + N1(K,I,J-2)* ((-(CZ(I,J-2) + CZV(K)*B(I))* (TERMZ(I,J-2) - 2.
     $    * CZ(I,J-2)* CZV(K) - CZV(K)**2*B(I))/ 6.)/ B(I)))/ B(I)
C
C CROSS terms below added for cross derivatives; I eliminated two
C terms of i+2 and two terms of j+2 to fit entire area. Each pair
C was composed of both + and - components.
C Need to separate from calc above due to continuation line limits
       CROSS = CZV(K)/96.
     $ *(CX(I+1,J)* (3.*N1(K,I+1,J-2)
     $    - 19.*N1(K,I+1,J-1) + 7.*N1(K,I+1,J) + 9.*N1(K,I+1,J+1)
     $    + N1(K,I,J) - N1(K,I,J-1))
     $  - CX(I-1,J)* (3.*N1(K,I-1,J-2) - 19.*N1(K,I-1,J-1)
     $    + 7.*N1(K,I-1,J) + 9.*N1(K,I-1,J+1) + N1(K,I,J) + N1(K,I-2,J)
     $    - N1(K,I,J-1) - N1(K,I-2,J-1))
     $  + CX(I,J+1)* (3.*N1(K,I-2,J+1) - 19.*N1(K,I-1,J+1)
     $    + 7.*N1(K,I,J+1) + 9.*N1(K,I+1,J+1) + N1(K,I,J) - N1(K,I-1,J))
     $  - CX(I,J-1)* (3.*N1(K,I-2,J-1) - 19.*N1(K,I-1,J-1)
     $    + 7.*N1(K,I,J-1) + 9.*N1(K,I+1,J-1) + N1(K,I,J) + N1(K,I,J-2)
     $    - N1(K,I-1,J) - N1(K,I-1,J-2)))/ B(I)
C
      N2(K,I,J) =  N2(K,I,J) + CROSS
 1400       CONTINUE
 1500     CONTINUE
C
          I = NX
          DO 1600 K = 1,NK
       N2(K,I,J) = N1(K,I,J) +
     $ (N1(K,I,J)* ((-CX(I,J)**2 - (CZ(I,J)+ CZV(K)* B(I))**2- CX(I,J)
     &    / 2.* TERMX(I,J) - (CZ(I,J) + CZV(K)* B(I))/2.* (TERMZ(I,J)
     &    - 2.*CZ(I,J)* CZV(K) - CZV(K)**2* B(I)))/ B(I) - 2.*DX(I,J)
     &    - 2.*DZ(I,J))
     $ + N1(K,I-1,J)* ((CX(I-1,J)**2 + 2./3.*CX(I-1,J)* TERMX(I-1,J))
     &    / B(I-1)+ 2.*DX(I-1,J))
     $ + N1(K,I-2,J)* (-CX(I-2,J)* TERMX(I-2,J)/6.)/ B(I-2)
     $ + N1(K,I,J+1)* (-(CZ(I,J+1)+ CZV(K)* B(I))/ 2.+ ((CZ(I,J+1)
     &    + CZV(K)*B(I))**2/ 2.+ (CZ(I,J+1)+ CZV(K)* B(I))* (TERMZ(I,J+1)
```

```
     &    - 2.* CZ(I,J+1)*CZV(K)- CZV(K)**2* B(I))/6.)/ B(I)+ DZ(I,J+1))
     $ + N1(K,I,J-1)* ((CZ(I,J-1) + CZV(K)* B(I))/2.+ ((CZ(I,J-1)
     &    + CZV(K)* B(I))**2/ 2. + (CZ(I,J-1) + CZV(K)* B(I))/2.
     &    * (TERMZ(I,J-1)- 2.*CZ(I,J-1)* CZV(K) -CZV(K)**2* B(I)))/ B(I)
     &    + DZ(I,J-1))
     $ + N1(K,I,J-2)* ((-(CZ(I,J-2)+ CZV(K)* B(I))/6.*(TERMZ(I,J-2)
     $    - 2.*CZ(I,J-2)*CZV(K) - CZV(K)**2))/ B(I)))/ B(I)
 1600     CONTINUE
 1700 CONTINUE
C
C Bottom horizontal water column grid:
      J = NZ-1
      I = 1
      DO 1800 K = 1,NK
         N2(K,I,J) =  N1(K,I,J)
 1800 CONTINUE
C
      I = 2
      DO 1900 K = 1,NK
       N2(K,I,J) = N1(K,I,J)- NUMNET(K,I)/ (DELA*DELZ)
     $ + (N1(K,I+1,J)* (-CX(I+1,J)/2. + (CX(I+1,J)**2/2. + CX(I+1,J)/6.
     $    * TERMX(I+1,J))/ B(I+1) + DX(I+1,J))
     $ + N1(K,I,J)* ((-CX(I,J)**2- 7./12.*CX(I,J)* TERMX(I,J))/ B(I)
     &    - 2.*DX(I,J)- DZ(I,J))
     $ + N1(K,I-1,J)* (CX(I-1,J)/2. + (CX(I-1,J)**2/2. + 5./12.
     $    * CX(I-1,J)* TERMX(I-1,J))/ B(I-1) + DX(I-1,J))
     $ + N1(K,I,J-1)* (DZ(I,J-1)+ CZ(I,J-1)+ CZV(K)* B(I)))/ B(I)
 1900 CONTINUE
C
      DO 2100 I = 3,NX-1
         DO 2000 K = 1,NK
       N2(K,I,J) = N1(K,I,J)- NUMNET(K,I)/ (DELA*DELZ)
     $ + (N1(K,I+1,J)* (-CX(I+1,J)/2.+ (CX(I+1,J)**2/2. + CX(I+1,J)/6.
     $    * TERMX(I+1,J))/ B(I+1) + DX(I+1,J))
     $ + N1(K,I,J)* ((-CX(I,J)**2 - CX(I,J)*TERMX(I,J)/2.)/ B(I)
     &    - 2.* DX(I,J) - DZ(I,J))
     $ + N1(K,I-1,J)* (CX(I-1,J)/2. + (CX(I-1,J)**2/2. + CX(I-1,J)/2.
     $    * TERMX(I-1,J))/ B(I-1) + DX(I-1,J))
     $ + N1(K,I-2,J)* ((-CX(I-2,J)* TERMX(I-2,J)/6.)/ B(I-2))
     $ + N1(K,I,J-1)* (DZ(I,J-1)+ CZ(I,J-1)+ CZV(K)* B(I)))/ B(I)
 2000    CONTINUE
 2100 CONTINUE
C
      I = NX
      DO 2200 K = 1,NK
      N2(K,I,J) = N1(K,I,J)- NUMNET(K,I)/ (DELA*DELZ)
     $ + (N1(K,I,J)* ((-CX(I,J)**2 -CX(I,J)* TERMX(I,J)/2.)/ B(I)
     &    - 2.*DX(I,J)- DZ(I,J))
     $ + N1(K,I-1,J)* ((CX(I-1,J)**2 + 2./3.*CX(I-1,J)* TERMX(I-1,J))
     &    / B(I-1) + 2.*DX(I-1,J))
     $ + N1(K,I-2,J)* ((-CX(I-2,J)* TERMX(I-2,J)/6.)/ B(I-2))
     $ + N1(K,I,J-1)* (DZ(I,J-1)+ CZ(I,J-1)+ CZV(K)* B(I)))/ B(I)
 2200 CONTINUE
C
C Sediment-water interface, J = NZ.
C Note that N2(k,i,NZ) was determined explicitly from mass flux
C considerations in Subroutine BEXCHN.
C
      RETURN
      END


C**********************************************************************
      SUBROUTINE TRANSC (NK,NX,NZ,CT1,CT2,V,FP,UX,UZ,EX,EZ,CX,CZ,
     $                   DX,DZ,TERMX,TERMZ,CZV,BEDVOL,NUMIN,NUMOUT,
     $                   NUMNET,TRNSFR)
C
      INTEGER NK,NX,NZ
C
      REAL  CT1(NX,NZ),CT2(NX,NZ),FP(NK,NX,NZ)
      REAL  V(NK),CZV(NK)
      REAL  NUMIN(NK,NX),NUMOUT(NK,NX),NUMNET(NK,NX),TRNSFR(NX)
      REAL  BEDVOL(NX)
      REAL  UX(NX,NZ),UZ(NX,NZ),EX(NX,NZ),EZ(NX,NZ)
      REAL  CX(NX,NZ),CZ(NX,NZ),DX(NX,NZ),DZ(NX,NZ)
      REAL  TERMX(NX,NZ),TERMZ(NX,NZ)
C
      REAL  DELX,DELZ,DELA,DELT
C
      COMMON/STEPS/  DELX,DELZ,DELA,DELT,FRACT,TIME,TMAX,HMAX,NOUT,ITER
C
C PURPOSE: This subroutine integrates the advection-dispersion equation
C          to find the total contaminant concentration given a specified
C          fluid flow/dispersion field. Particle-associated flux is
C          superimposed on the advective and dispersive fluid fluxes.
C
C STATE VARIABLES:
C          CT(I,J) - Contaminant concentration at longitudinal I and
C                    vertical J at time t.
C
C INPUT PARAMETERS:
C  NX         - Number of longitudinal grids
C  NZ         - Number of vertical grids
C  DELCT      - Local Incremental Cp flux calculation, [ug/L-s]
C  DELT       - Time step, [s]
C  DELX       - Longitudinal grid spacing, [cm]
C  DELZ       - Vertical grid spacing, [cm]
C  DELA       - Vertical grid spacing at bed-water interface [cm]
C  SUMCP      - Local Cp flux accumulator, [ug/L-s]
```

```
C  [CT1]      - Inititial Contaminant concentration, [ug/L]
C  [NUMIN]    - Number of size k flocs (per unit area) entering
C                  bed at node I during DELT, [#/cm^2]
C  [NUMOUT]   - Number of size k flocs (per unit area) leaving
C                  bed at node I during DELT, [#/cm^2]
C  [NUMNET]   - Net number of size k flocs (per unit area) entering
C                  interface at node I during DELT, [#/cm^2]
C  [UX],[UZ] - Longitudinal and vertical velocities at node
C                  (I,J), [cm/s]
C  [EX],[EZ] - Longitudinal and vertical dispersion coefficients
C                  at node (I,J), [cm^2/s]
C  [CX],[DZ] - Longitudinal and vertical Courant No. at node
C                  (I,J)
C  [DX],[DZ] - Longitudinal and vertical Dispersion No.
C                  at node (I,J)
C  [TERMX/Z] - Longitudinal and vertical combination of Ci & Di
C                  at node (I,J)
C  [TRNSFR]  - Bulk resuspension transfer velocity, [cm/s]
C  [CZV]     - Settling Courant No. for size K particle
C  [V]       - Settling velocity of size K particle, [cm/s]
C
C OUTPUT PARAMETERS:
C          [CT2]     - Final Contaminant concentration, [ug/L]
C
C AUTHOR:   Jerry Culkin
C           Department of Civil Engineering
C           University of Texas at Austin
C
C LAST REVISED: 19 JUN        2030. remove CZV(K) in CT2(NX,NZ-1)!
C               11 JUN        2330. TYPE BEDVOL.
C                5 June       1050. New bed exchange logic
C               24 MAY, 1990  1030. Convert TRANSP for contaminant
C
C PRECISION:  Single
C
C LANGUAGE:   FORTRAN 77
C
C REFERENCES: None
C
C REQUIRED ROUTINES: None
C
C-----------------------------------------------------------------------
C Begin node by node calculations:
C Air-water interface (top, horizontal water-column grid):
      J = 1
C Upstream boundary:
      I = 1
      CT2(I,J) =  CT1(1,J)
      I = 2
C
      CT2(I,J) = CT1(I,J)
     $ + CT1(I+1,J)* (-CX(I+1,J)/2. + CX(I+1,J)**2/2. + CX(I+1,J)/6.
     $   * TERMX(I+1,J) + DX(I+1,J))
     $ + CT1(I,J)* (-CX(I,J)**2- 7./12.* CX(I,J)* TERMX(I,J)- 2.*DX(I,J)
     &   - CZ(I,J) - DZ(I,J))
     $ + CT1(I-1,J)* (CX(I-1,J)/2. + CX(I-1,J)**2/2.+ 5./12.*CX(I-1,J)
     $   * TERMX(I-1,J) + DX(I-1,J))
     $ + CT1(I,J+1)* DZ(I,J+1)
      SUMCP = 0.
      DO 200 K = 1,NK
         DELCT = FP(K,I,J)*CT1(I,J)* (-DELT* V(K)**2/ EZ(I,J)- CZV(K))
         SUMCP = SUMCP + DELCT
  200 CONTINUE
      CT2(I,J) = CT2(I,J) + SUMCP
C
      DO 400 I = 3,NX-1
         CT2(I,J) = CT1(I,J)
     $   + CT1(I+1,J)* (-CX(I+1,J)/2. + CX(I+1,J)**2/2. + CX(I+1,J)/6.
     $     * TERMX(I+1,J) + DX(I+1,J))
     $   + CT1(I,J)* (-CX(I,J)**2- CX(I,J) *TERMX(I,J)/2.- 2.* DX(I,J)
     &     - CZ(I,J) - DZ(I,J))
     $   + CT1(I-1,J)* (CX(I-1,J)/2. + CX(I-1,J)**2/2. + CX(I-1,J)/2.
     $     * TERMX(I-1,J) + DX(I-1,J))
     $   + CT1(I-2,J)* (-CX(I-2,J)* TERMX(I-2,J)/6.)
     $   + CT1(I,J+1)* DZ(I,J+1)
         SUMCP = 0.
         DO 300 K = 1,NK
            DELCT = FP(K,I,J)* CT1(I,J)* (-DELT* V(K)**2/EZ(I,J)-CZV(K))
            SUMCP = SUMCP + DELCT
  300    CONTINUE
         CT2(I,J) = CT2(I,J) + SUMCP
  400 CONTINUE

      I = NX
      CT2(I,J) = CT1(I,J)
     $ + CT1(I,J)* (-CX(I,J)**2 - CX(I,J)*TERMX(I,J)/2.- 2.*DX(I,J)
     &   - CZ(I,J) - DZ(I,J))
     $ + CT1(I-1,J)* (CX(I-1,J)**2+ 2./3.*CX(I-1,J)* TERMX(I-1,J) + 2.
     $   * DX(I-1,J))
     $ + CT1(I-2,J)* (-CX(I-2,J)* TERMX(I-2,J)/6.)
     $ + CT1(I,J+1)* DZ(I,J+1)
C
      SUMCP = 0.
      DO 500 K = 1,NK
         DELCT = FP(K,I,J)* CT1(I,J)* (- DELT* V(K)**2/ EZ(I,J)- CZV(K))
         SUMCP = SUMCP + DELCT
  500 CONTINUE
      CT2(I,J) = CT2(I,J) + SUMCP
C
```

```
C
C Second horizontal water column grid:
      J = 2
C Upstream boundary:
      I = 1
      CT2(I,J) =  CT1(1,J)
      I = 2
      CT2(I,J) = CT1(I,J)
     $ + CT1(I+1,J)* (-CX(I+1,J)/2. + CX(I+1,J)**2/2. + CX(I+1,J)/6.
     $    * TERMX(I+1,J) + DX(I+1,J))
     $ + CT1(I,J)* (-CX(I,J)**2- 7./12.*CX(I,J)* TERMX(I,J)- 2.*DX(I,J)
     &    - CZ(I,J)- 2.*DZ(I,J))
     $ + CT1(I-1,J)* (CX(I-1,J)/2. + CX(I-1,J)**2/2. + 5./12.
     $    * CX(I-1,J)* TERMX(I-1,J) + DX(I-1,J))
     $ + CT1(I,J+1)* DZ(I,J+1)
     $ + CT1(I,J-1)* (CZ(I,J-1)+ DZ(I,J-1))
C
      SUMCP = 0.
      DO 600 K = 1,NK
         DELCT = FP(K,I,J)* CT1(I,J)* (- CZV(K))
     &          + FP(K,I,J-1)* CT1(I,J-1)* CZV(K)
         SUMCP = SUMCP + DELCT
  600 CONTINUE
      CT2(I,J) = CT2(I,J) + SUMCP
C
      DO 800 I = 3,NX-1
         CT2(I,J) = CT1(I,J)
     $    + CT1(I+1,J)* (-CX(I+1,J)/2. + CX(I+1,J)**2/2. + CX(I+1,J)/6.
     $      * TERMX(I+1,J) + DX(I+1,J))
     $    + CT1(I,J)* (-CX(I,J)**2  - CX(I,J)*TERMX(I,J)/2. -2.*DX(I,J)
     $      - CZ(I,J)- 2.*DZ(I,J))
     $    + CT1(I-1,J)* (CX(I-1,J)/2. + CX(I-1,J)**2/2. + CX(I-1,J)/2.
     $      * TERMX(I-1,J) + DX(I-1,J))
     $    + CT1(I-2,J)* (-CX(I-2,J)* TERMX(I-2,J)/6.)
     $    + CT1(I,J+1)* DZ(I,J+1)
     $    + CT1(I,J-1)* (CZ(I,J-1)+ DZ(I,J-1))
C
         SUMCP = 0.
         DO 700 K = 1,NK
            DELCT = FP(K,I,J)* CT1(I,J)* (- CZV(K))
     &             + FP(K,I,J-1)* CT1(I,J-1)* CZV(K)
            SUMCP = SUMCP + DELCT
  700    CONTINUE
         CT2(I,J) = CT2(I,J) + SUMCP
  800 CONTINUE
C
      I = NX
      CT2(I,J) = CT1(I,J)
     $ + CT1(I,J)* (-CX(I,J)**2 - CX(I,J)*TERMX(I,J)/2.- 2.*DX(I,J)
     $    - CZ(I,J)- 2.*DZ(I,J))
     $ + CT1(I-1,J)* (CX(I-1,J)**2 + 2./3.*CX(I-1,J)* TERMX(I-1,J)
     $     + 2.* DX(I-1,J))
     $ + CT1(I-2,J)* (-CX(I-2,J)* TERMX(I-2,J)/6.)
     $ + CT1(I,J+1)* (DZ(I,J+1))
     $ + CT1(I,J-1)* (CZ(I,J-1)+ DZ(I,J-1))
C
      SUMCP = 0.
      DO 900 K = 1,NK
         DELCT = FP(K,I,J)* CT1(I,J)* (- CZV(K))
     &          + FP(K,I,J-1)* CT1(I,J-1)* CZV(K)
         SUMCP = SUMCP + DELCT
  900 CONTINUE
      CT2(I,J) = CT2(I,J) + SUMCP
C
C Core of water column domain:
      DO 1400 J = 3,NZ-2
         I = 1
         CT2(I,J) =  CT1(1,J)
         I = 2
         CT2(I,J) = CT1(I,J)
     $    + CT1(I+1,J)* (-CX(I+1,J)/2.+ CX(I+1,J)**2/2.+ CX(I+1,J)/6.
     $    * TERMX(I+1,J) + DX(I+1,J))
     $ + CT1(I,J)* (-CX(I,J)**2- CZ(I,J)**2 - 7./12.* CX(I,J)
     $    * TERMX(I,J)- CZ(I,J)* TERMZ(I,J)/2.- 2.*DX(I,J)- 2.*DZ(I,J))
     $ + CT1(I-1,J)* (CX(I-1,J)/2. + CX(I-1,J)**2/2. + 5./12.
     $    * CX(I-1,J)* TERMX(I-1,J) + DX(I-1,J))
     $ + CT1(I,J+1)* (-CZ(I,J+1)/2.+ CZ(I,J+1)**2/2.+ CZ(I,J+1)
     &    * TERMZ(I,J+1)/6.+ DZ(I,J+1))
     $ + CT1(I,J-1)* (CZ(I,J-1)/2. + CZ(I,J-1)**2/2.+ CZ(I,J-1)
     &    * TERMZ(I,J-1)/2.+ DZ(I,J-1))
     $ + CT1(I,J-2)* (-CZ(I,J-2)* TERMZ(I,J-2)/6.)
C
         SUMCP = 0.
         DO 1000 K = 1,NK
            DELCT = FP(K,I,J)* CT1(I,J)* (-CZV(K)**2- CZV(K)*(TERMZ(I,J)
     &              - 2.*CZ(I,J)*CZV(K)- CZV(K)**2)/2.)
     &            + FP(K,I,J+1)* CT1(I,J+1)* (-CZV(K)/2.+ CZV(K)**2/2.
     &              + CZV(K)* (TERMZ(I,J+1)- 2.*CZ(I,J+1)*CZV(K)
     &              - CZV(K)**2)/6.)
     &            + FP(K,I,J-1)* CT1(I,J-1)* (CZV(K)/2.+ CZV(K)**2/2.
     &              + CZV(K)* (TERMZ(I,J-1)- 2.*CZ(I,J-1)*CZV(K)
     &              - CZV(K)**2)/2.)
     &            + FP(K,I,J-2)* CT1(I,J-2)* (-CZV(K)* (TERMZ(I,J-2)
     &              - 2.*CZ(I,J-2)*CZV(K) - CZV(K)**2)/6.)
C
            SUMCP = SUMCP + DELCT
 1000    CONTINUE
         CT2(I,J) = CT2(I,J) + SUMCP
C
```

```
      DO 1200 I = 3,NX-1
         CT2(I,J) = CT1(I,J)
     $     + CT1(I+1,J)* (-CX(I+1,J)/2.+ CX(I+1,J)**2/2. + CX(I+1,J)/6.
     $       * TERMX(I+1,J) + DX(I+1,J))
     $     + CT1(I,J)* (-CX(I,J)**2- CZ(I,J)**2 -CX(I,J)/2.* TERMX(I,J)
     &       - CZ(I,J)* TERMZ(I,J)/2. - 2.*DX(I,J)- 2.*DZ(I,J))
     $     + CT1(I-1,J)* (CX(I-1,J)/2. + CX(I-1,J)**2/2. + CX(I-1,J)/2.
     $       * TERMX(I-1,J) + DX(I-1,J))
     $     + CT1(I-2,J)* (-CX(I-2,J)/6.* TERMX(I-2,J))
     $     + CT1(I,J+1)* (-CZ(I,J+1)/2. + CZ(I,J+1)**2/2.+ CZ(I,J+1)
     &       * TERMZ(I,J+1)/6.+ DZ(I,J+1))
     $     + CT1(I,J-1)* (CZ(I,J-1)/2. + CZ(I,J-1)**2/ 2.+ CZ(I,J-1)
     &       * TERMZ(I,J-1)/2.+ DZ(I,J-1))
     $     + CT1(I,J-2)* (-CZ(I,J-2)* TERMZ(I,J-2)/ 6.)
C
         SUMCP = 0.
         DO 1100 K = 1,NK
            DELCT = FP(K,I,J)* CT1(I,J)* (-CZV(K)**2- CZV(K)
     &           *(TERMZ(I,J)- 2.* CZ(I,J)* CZV(K)- CZV(K)**2)/2.
     &           + CZV(K)/96.* (CX(I+1,J)- CX(I-1,J)+ CX(I,J+1)-
     &             CX(I,J-1)))
     &         + FP(K,I,J+1)* CT1(I,J+1)* (-CZV(K)/2.+ CZV(K)**2/2.
     &           + CZV(K)* (TERMZ(I,J+1)- 2.*CZ(I,J+1)* CZV(K)
     &           - CZV(K)**2)/6.)
     &         + FP(K,I,J-1)* CT1(I,J-1)* (CZV(K)/2.+ CZV(K)**2/2.
     &           + CZV(K)* (TERMZ(I,J-1)- 2.*CZ(I,J-1)* CZV(K)
     &           - CZV(K)**2)/2. + CZV(K)/96. *(CX(I-1,J)- 7.
     &           * CX(I,J-1)))
     &         + FP(K,I,J-2)* CT1(I,J-2)* (-CZV(K)* (TERMZ(I,J-2)
     &           - 2.*CZ(I,J-2)* CZV(K)- CZV(K)**2)/6.- CZV(K)/96.
     &           * CX(I,J-1))
C
C Cross derivative terms for nodes not included in DELCT:
            CROSS = CZV(K)/96. *
     &       (CX(I+1,J) * (3.* FP(K,I+1,J-2)* CT1(I+1,J-2)
     &         - 19.*FP(K,I+1,J-1)* CT1(I+1,J-1)+ 7.* FP(K,I+1,J)
     &         * CT1(I+1,J)+ 9.* FP(K,I+1,J+1)*  CT1(I+1,J+1))
     &       - CX(I-1,J)* (3.* FP(K,I-1,J-2)*  CT1(I-1,J-2)- 19.
     &         * FP(K,I-1,J-1)* CT1(I-1,J-1)+ 7.* FP(K,I-1,J)
     &         * CT1(I-1,J)+ 9.* FP(K,I-1,J+1)* CT1(I-1,J+1)
     &         + FP(K,I-2,J)* CT1(I-2,J)- FP(K,I-2,J-1)* CT1(I-2,J-1))
     &       + CX(I,J+1)* (3.* FP(K,I-2,J+1)* CT1(I-2,J+1)- 19.
     &         * FP(K,I-1,J+1)* CT1(I-1,J+1)+ 7.* FP(K,I,J+1)
     &         * CT1(I,J+1)+ 9.* FP(K,I+1,J+1)* CT1(I+1,J+1)
     &         - FP(K,I-1,J)* CT1(I-1,J))
     &       - CX(I,J-1)* (3.* FP(K,I-2,J-1)* CT1(I-2,J-1)- 19.
     &         * FP(K,I-1,J-1)* CT1(I-1,J-1)+ 9.*FP(K,I+1,J-1)
     &         * CT1(I+1,J-1)- FP(K,I-1,J)* CT1(I-1,J)- FP(K,I-1,J-2)
     &         * CT1(I-1,J-2)))
C
            SUMCP = SUMCP + DELCT + CROSS
 1100    CONTINUE
         CT2(I,J) = CT2(I,J) + SUMCP
C
 1200  CONTINUE
C
      I = NX
      CT2(I,J) = CT1(I,J) +
     $   CT1(I,J)* (-CX(I,J)**2 - CZ(I,J)**2- CX(I,J) /2.* TERMX(I,J)
     $     - CZ(I,J)* TERMZ(I,J)/2.- 2.*DX(I,J) - 2.*DZ(I,J))
     $   + CT1(I-1,J)* (CX(I-1,J)**2 + 2./3.*CX(I-1,J)* TERMX(I-1,J)
     $     + 2.*DX(I-1,J))
     $   + CT1(I-2,J)* (-CX(I-2,J)* TERMX(I-2,J)/6.)
     $   + CT1(I,J+1)* (-CZ(I,J+1)/ 2.+ CZ(I,J+1)**2/ 2.+ CZ(I,J+1)
     &     * TERMZ(I,J+1)/6.+ DZ(I,J+1))
     $   + CT1(I,J-1)* (CZ(I,J-1)/2. + CZ(I,J-1)**2/ 2. + CZ(I,J-1)
     $     * TERMZ(I,J-1)/2.+ DZ(I,J-1))
     $   + CT1(I,J-2)* (-CZ(I,J-2)/6.* TERMZ(I,J-2))
C
      SUMCP = 0.
      DO 1300 K = 1,NK
         DELCT = FP(K,I,J)* CT1(I,J)* (-CZV(K)**2- CZV(K)
     &         * (TERMZ(I,J)- 2.*CZ(I,J)*CZV(K)- CZV(K)**2)/2.)
     &       + FP(K,I,J+1)* CT1(I,J+1)* (-CZV(K)/2.+ CZV(K)**2/2.
     &         + CZV(K)* (TERMZ(I,J+1)- 2.*CZ(I,J+1)*CZV(K)
     &         - CZV(K)**2)/6.)
     &       + FP(K,I,J-1)* CT1(I,J-1)* (CZV(K)/2.+ CZV(K)**2/2.
     &         + CZV(K)* (TERMZ(I,J-1)- 2.*CZ(I,J-1)*CZV(K)
     &         - CZV(K)**2)/2.)
     &       + FP(K,I,J-2)* CT1(I,J-2)* (-CZV(K)* (TERMZ(I,J-2)
     &         - 2.*CZ(I,J-2)*CZV(K) - CZV(K)**2)/6.)
C
         SUMCP = SUMCP + DELCT
 1300  CONTINUE
       CT2(I,J) = CT2(I,J) + SUMCP
C
 1400 CONTINUE
C_____________________________________________________________________
C Bottom horizontal water column grid:
      J = NZ-1
      I = 1
      CT2(I,J) =  CT1(I,J)
C
      I = 2
      CT2(I,J) = CT1(I,J)
     $ + CT1(I+1,J)* (-CX(I+1,J)/2. + CX(I+1,J)**2/2. + CX(I+1,J)/6.
     $   * TERMX(I+1,J) + DX(I+1,J))
     $ + CT1(I,J)* (-CX(I,J)**2- 7./12.*CX(I,J)* TERMX(I,J)- 2.*DX(I,J)
     &   - DZ(I,J))
```

```
     $ + CT1(I-1,J)* (CX(I-1,J)/2. + CX(I-1,J)**2/2. + 5./12.
     $   * CX(I-1,J)* TERMX(I-1,J) + DX(I-1,J))
     $ + CT1(I,J-1)* (DZ(I,J-1)+ CZ(I,J-1))
C
      SUMCP = 0.
      DO 1500 K = 1,NK
         DELCT = FP(K,I,J)* CT1(I,J)* (-CZV(K)/DELA)
     &         + FP(K,I,J-1)* CT1(I,J-1)* CZV(K)
     &         + FP(K,I,J+1)* CT1(I,J+1)* TRNSFR(I)/ DELA
C
         SUMCP = SUMCP + DELCT
 1500 CONTINUE
      CT2(I,J) = CT2(I,J) + SUMCP
C
      DO 1700 I = 3,NX-1
         CT2(I,J) = CT1(I,J)
     $    + CT1(I+1,J)* (-CX(I+1,J)/2. + CX(I+1,J)**2/2.
     $       + CX(I+1,J)/6.* TERMX(I+1,J) + DX(I+1,J))
     $    + CT1(I,J)* (-CX(I,J)**2  - CX(I,J)*TERMX(I,J)/2.
     $       -2.*DX(I,J)- DZ(I,J))
     $    + CT1(I-1,J)* (CX(I-1,J)/2. + CX(I-1,J)**2/2. + CX(I-1,J)/2.
     $      * TERMX(I-1,J) + DX(I-1,J))
     $    + CT1(I-2,J)* (-CX(I-2,J)* TERMX(I-2,J)/6.)
     $    + CT1(I,J-1)* (DZ(I,J-1)+ CZ(I,J-1))
C
         SUMCP = 0.
         DO 1600 K = 1,NK
            DELCT = FP(K,I,J)* CT1(I,J)* (-CZV(K)/DELA)
     &            + FP(K,I,J-1)* CT1(I,J-1)* CZV(K)
     &            + FP(K,I,J+1)* CT1(I,J+1)* TRNSFR(I)/ DELA
            SUMCP = SUMCP + DELCT
 1600    CONTINUE
         CT2(I,J) = CT2(I,J) + SUMCP
C
 1700 CONTINUE
C
      I = NX
      CT2(I,J) = CT1(I,J)
     $     + CT1(I,J)* (-CX(I,J)**2 -CX(I,J)* TERMX(I,J)/2.- 2.*DX(I,J)
     &       -  DZ(I,J))
     $     + CT1(I-1,J)* (CX(I-1,J)**2 + 2./3.*CX(I-1,J)* TERMX(I-1,J)
     $       + 2.*DX(I-1,J))
     $     + CT1(I-2,J)* (-CX(I-2,J)* TERMX(I-2,J)/6.)
     $     + CT1(I,J-1)* (DZ(I,J-1)+ CZ(I,J-1))
C
      SUMCP = 0.
      DO 1800 K = 1,NK
         DELCT = FP(K,I,J)* CT1(I,J)* (-CZV(K)/DELA)
     &         + FP(K,I,J-1)* CT1(I,J-1)* CZV(K)
     &         + FP(K,I,J+1)* CT1(I,J+1)* TRNSFR(I)/ DELA
C
         SUMCP = SUMCP + DELCT
 1800 CONTINUE
      CT2(I,J) = CT2(I,J) + SUMCP
C
C-----------------------------------------------------------------------
C Sediment-water interface:
      J = NZ
      I = 1
      CT2(I,J) =  CT1(I,J)
C
      I = 2
      SUMCP = 0.
      DO 1900 K = 1,NK
         DELCT = FP(K,I,J)* CT1(I,J)* (-TRNSFR(I)/ BEDVOL(I))
     &         + FP(K,I,J-1)* CT1(I,J-1)* CZV(K)/ BEDVOL(I)
         SUMCP = SUMCP + DELCT
 1900 CONTINUE
      CT2(I,J) = CT1(I,J) + SUMCP
C
      DO 2100 I = 3,NX-1
         SUMCP = 0.
         DO 2000 K = 1,NK
            DELCT = FP(K,I,J)* CT1(I,J)* (-TRNSFR(I)/ BEDVOL(I))
     &         + FP(K,I,J-1)* CT1(I,J-1)* CZV(K)/ BEDVOL(I)
            SUMCP = SUMCP + DELCT
 2000    CONTINUE
         CT2(I,J) = CT1(I,J) + SUMCP
 2100 CONTINUE
C
      I = NX
      SUMCP = 0.
      DO 2200 K = 1,NK
         DELCT = FP(K,I,J)* CT1(I,J)* (-TRNSFR(I)/ BEDVOL(I))
     &         + FP(K,I,J-1)* CT1(I,J-1)* CZV(K)/ BEDVOL(I)
         SUMCP = SUMCP + DELCT
 2200 CONTINUE
      CT2(I,J) = CT1(I,J) + SUMCP
C
      RETURN
      END



C**********************************************************************
      SUBROUTINE TOTAL (NK,NX,NZ,DIMNK,N1,DP,DELTAD,BEDVOL,BEDMAS,
```

```
     $                  POROS,TSS,TAREA,TNUM,LDNDD,TIME)
C
      INTEGER  NK,NX,NZ,DIMNK
C
      REAL  N1(DIMNK,NX,NZ),DP(DIMNK),DELTAD(NK)
      REAL  TSS(NX,NZ),TAREA(NX,NZ),TNUM(NX,NZ),LDNDD(NK,NX,NZ)
      REAL  BEDVOL(NX),BEDMAS(NX),POROS(NX)
C
      REAL  RHOP,CONA1,CONM1,SUMMAS,SUMARA,SUMNUM,PI
C
      COMMON/PART/   RHOP,RHOW,VISCOS,TEMP,GRAV,LV1ST,LVSTEP,PI
C
C
C PURPOSE: This routine derives integral property values for solids at
C           each node from heterogeneous number concentrations:
C           - total mass concentration
C           - total surface area concentration
C           - total number concentration
C           - PSD initial concentrations based on input PSD
C           - bed porosity
C           - bed volume
C
C INPUT PARAMETERS:
C  NK      - Number of particle size classes
C  NX      - Number longitudinal grids nodes
C  NK      - Number vertical grids nodes
C  DIMNK   - NK + 1; accomodates array shift in C codes
C  PI      - Value of pi
C  RHOP    - Effective bulk density of floc, [g/cm^3]
C  TIME    - Elapsed time, [s]
C (DP)     - equivalent spherical floc diameter, [um]
C (DELTAD) - delta diameter around floc, [um]
C (BEDVOL) - Bulk volume of the interface layer per unit area at
C             node I, i.e., Depth(I), [cm^3/cm^2]
C [N1]     - Number concentration of size k, [#/cm^3]
C
C OUTPUT PARAMETERS:
C  CONA1  - Conversion factor to convert proportional area in
C           [um^2/cm^3] to [cm^2/L]
C  CONM1  - Conversion factor to convert proportional volume in
C           [um^3/cm^3] to absolute mass in [mg/L]
C  SUMARA - Particle surface area conc accumulator for loop, [um^2/cm^3]
C  SUMMAS - Particle mass conc accumulator for loop, [um^3/cm^3]
C (POROS) - Volume of voids per total volume in the interface layer
C           at node I, [cm^3/cm^3]
C (BEDMAS)- Total mass of solids in the interface layer per unit area
C           at node I, [g/cm^2]
C (TSS)   - Total suspended solid mass concentration, [mg/L]
C [TAREA] - Total superficial surface area concentration of suspended
C           solids, [cm^2/L]
C [TNUM]  - Total initial number concentration of suspended solids,
C           [#/cm^3]
C [LDNDD] - Matrix of PSD, LdNdD, log([#/cm^3-um])
C
C AUTHOR:   Jerry Culkin
C           Department of Civil Engineering
C           University of Texas at Austin
C
C LAST REVISED: 15 Jun 1990  1430
C
C PRECISION: Single
C
C LANGUAGE: FORTRAN 77
C
C REFERENCES: None
C
C REQUIRED ROUTINES: None
C-----------------------------------------------------------------------
C Define constant to simplify and convert:
      CONM1  = PI* RHOP/ 6.* 1.E-6
      CONA1  = PI* 1.E-5
C
C Calculate initial number and proportional mass concentrations for bed:
      DO 300 J = 1,NZ
           DO 200 I = 1,NX
C Initialize mass and number counters for each (i,j):
                SUMMAS = 0.0
                SUMARA = 0.0
                SUMNUM = 0.0
                DO 100 K = 1,NK
                     SUMMAS = SUMMAS + N1(K,I,J)* DP(K)**3
                     SUMARA = SUMARA + N1(K,I,J)* DP(K)**2
                     SUMNUM = SUMNUM + N1(K,I,J)
  100           CONTINUE
C
C Convert the surrogates to actual mass, area, and number concs:
                TSS(I,J)   = SUMMAS * CONM1
                TAREA(I,J) = SUMARA * CONA1
                TNUM(I,J)  = SUMNUM
  200      CONTINUE
  300 CONTINUE
C
C Calculate PSDs:
      DO 600 J = 1,NZ
           DO 500 I = 1,NX
                DO 400 K = 1,NK
                     IF (N1(K,I,J) .LT. 0.25) THEN
                          LDNDD(K,I,J) = -10.0
                     ELSE
```

```
                        LDNDD(K,I,J) = LOG10( N1(K,I,J)/ DELTAD(K))
                    ENDIF
  400           CONTINUE
  500       CONTINUE
  600 CONTINUE
C
C Calculate bed porosity from bed TSS (BEDVOL is from IN, then BEDXCH).
C Calc bed mass, [g/cm^2]: this is redundant (BEDXCH) except at time 0!
      IF (TIME .LE. 1.E-6) THEN
          DO 700 I = 1,NX
              POROS(I)  = 1. - (TSS(I,NZ)/ RHOP * 1.E-6)
              BEDMAS(I) = BEDVOL(I)* RHOP* (1. - POROS(I))
  700     CONTINUE
      ENDIF
C
      RETURN
      END



C*********************************************************************
      SUBROUTINE OUTPT (NK,NX,NZ,DIMNK,N1,TIME,BEDMAS,BEDVOL,TSS,TAREA,
     $                  TNUM,LDNDD,POROS,CT1,FP,TOTFP,FILNAM,NSOURC,
     $                  QTRIB,NTRIB)
C
      INTEGER NK,NX,NZ,DIMNK,IMID,JMID
C
      REAL  N1(DIMNK,NX,NZ),CT1(NX,NZ),LDNDD(NK,NX,NZ),NSOURC(NK,NX,NZ)
      REAL  TSS(NX,NZ), TAREA(NX,NZ), TNUM(NX,NZ), NTRIB(NK,NX)
      REAL  BEDMAS(NX), BEDVOL(NX),FP(NK,NX,NZ),TOTFP(NX,NZ), POROS(NX)
      REAL  QTRIB(0:NX)
C
      REAL  TIME
C
      CHARACTER*50   FILNAM
C
C PURPOSE: This subroutine writes the values of indicated parameters
C          (at the end of simulation) to the open output file.
C
C INPUT PARAMETERS:
C  NK,NX,N2- Number of nodes
C  RHOP     - Bulk floc density, [g/cm^3]
C  TIME     - Elapsed time of simulation, [s]
C {BEDMAS} - Total mass of solids in the interface layer per unit area
C             at node I, [g/cm^2]
C {BEDVOL} - Bulk volume of the interface layer per unit area at node
C             I, i.e., DEPTH(I), [cm^3/cm^2]
C {DELTAD} - Delta diameter about each floc size, [um]
C {DP}     - Equivalent spherical diameter of size k floc, [um]
C {POROS}  - Volume of voids per total volume in the interface layer
C             at node I, [cm^3/cm^3]
C [CT1]    - Total contaminant concentration, [ug/L]
C [N1]     - The set of particle concentrations after transport AND
C             coagulation at TIME, [#/cm^3]
C [NSOURC] - Concentration source at (i,j) due to tributary source,
C             [#/cm^3]
C {TAREA}  - Suspended solids area concentrations at TIME, [cm^2/L]
C [TNUM]   - Suspended solids number concentrations at TIME, [#/cm^3]
C [TSS]    - Suspended solids mass concentrations at TIME, [mg/L]
C
C OUTPUT PARAMETERS:
C  All output is passed through, not modified.
C
C AUTHOR:  Jerry Culkin
C          Department of Civil Engineering
C          University of Texas at Austin
C
C Last Revision:  12 Jul  1990          TNUM() writes added
C                 14 Sept 1990          even writes added
C                 6 dec   1990          TAREA output added
C
C PRECISION: Single
C
C LANGUAGE: FORTRAN 77
C
C REFERENCES: None
C
C REQUIRED ROUTINES: None
C-----------------------------------------------------------------------
      WRITE (10,*)
      WRITE (10,5,ERR=99) TIME
      WRITE (11,*)
      WRITE (11,5,ERR=97) TIME
    5 FORMAT ('********************** OUTPUT at TIME = ',F11.0,' [sec]',
     $' ********************')
      WRITE (12,*) FILNAM, '  TSS at Time =',TIME
      WRITE (13,*) FILNAM, '  TNUM at Time =',TIME
      WRITE (14,*) FILNAM, '  TAREA at Time =',TIME
C
C Output the vertical profiles of number concentrations and PSDs at
C mid-domain. Nodes @ mid-domain are:
      IMID = (NX+1)/ 2 - 1
      JMID = NZ/ 2
C     (if odd NZ:       JMID = (NZ+1)/ 2 - 1)
C
C Output the longitudinal profile of mid-depth PSDs for odd I:
      WRITE (10,*)
      WRITE (10,201) IMID
```

```
  201 FORMAT ('VERTICAL profile of Conc/PSD @ Mid-domain, (K,',I2,',J',
     $'):')
C
C Write concentrations for each size class at surface at mid-domain:
      J = 1
      WRITE (10,*)
      WRITE (10,205) IMID,J
      WRITE (10,115,ERR=99) (N1(K,IMID,J), K = 1,NK)
  205 FORMAT ('Mid-domain No. Concs @ Surface, N(K,',I2,',',I2,'),',
     $' [#/cm^3] :')
C Write PSD at surface at mid-domain:
      WRITE (10,215) IMID,J
      WRITE (10,125,ERR=99) (LDNDD(K,IMID,1), K = 1,NK)
  215 FORMAT ('Mid-domain PSD @ Surface, LDNDD(K,',I2,',',I2,')')
C Write to PRN file the PSD at surface at mid-domain:
      WRITE (11,225) IMID,J
      DO 100 K = 1,NK
           WRITE (11,227,ERR=97) LDNDD(K,IMID,J)
  100 CONTINUE
  225 FORMAT ('LDNDD(K,',I2,',',I2,')')
  227 FORMAT (E14.5)
C
C Write concentrations for each size class at mid-depth at mid-domain:
      WRITE (10,229) IMID,JMID
      WRITE (10,115,ERR=99) (N1(K,IMID,JMID), K = 1,NK)
  229 FORMAT (/,'Mid-domain No. Concs @ MidDepth, N(K,',I2,',',I2,'),',
     $' [#/cm^3] :')
C Write PSD at middepth at mid-domain:
      WRITE (10,231) IMID,JMID
      WRITE (10,125,ERR=99) (LDNDD(K,IMID,JMID), K = 1,NK)
  231 FORMAT ('Mid-domain No. PSD @ MidDepth, LDNDD(K,',I2,',',I2,')')
C Write to PRN file the PSD at mid-depth at mid-domain:
      WRITE (11,225) IMID,JMID
      DO 200 K = 1,NK
           WRITE (11,227,ERR=97) LDNDD(K,IMID,JMID)
  200 CONTINUE
C
C Write concentrations for each size class above bed interface at
C mid-domain:
      J = NZ-1
      WRITE (10,235) IMID,J
      WRITE (10,115,ERR=99) (N1(K,IMID,J), K = 1,NK)
  235 FORMAT (/,'Mid-domain above Bed Interface, N(K,',I2,',',I2,'),',
     $' [#/cm^3] :')
C Write PSD above bed interface at mid-domain:
      WRITE (10,237) IMID,J
      WRITE (10,125,ERR=99) (LDNDD(K,IMID,J), K = 1,NK)
  237 FORMAT('Mid-domain PSD above B Interface, LDNDD(K,',I2,',',I2,')')
C Write to PRN file the PSD above bed interface at mid-domain:
      WRITE (11,225) IMID,J
      DO 300 K = 1,NK
           WRITE (11,227,ERR=97) LDNDD(K,IMID,J)
  300 CONTINUE
C
C Write concentrations for each size class at bed interface at
C mid-domain:
      J = NZ
      WRITE (10,245) IMID,NZ
      WRITE (10,115,ERR=99) (N1(K,IMID,NZ), K = 1,NK)
  245 FORMAT (/,'Mid-domain No. Concs @ Interface, N(K,',I2,',',I2,'),',
     $' [#/cm^3] :')
C Write PSD at bed interface at mid-domain:
      WRITE (10,247) IMID,NZ
      WRITE (10,125,ERR=99) (LDNDD(K,IMID,NZ), K = 1,NK)
  247 FORMAT ('Mid-domain PSD @ Interface, LDNDD(K,',I2,',',I2,')')
C Write to PRN file the PSD at bed interface at mid-domain:
      WRITE (11,225) IMID,NZ
      DO 400 K = 1,NK
           WRITE (11,227,ERR=97) LDNDD(K,IMID,NZ)
  400 CONTINUE
C
C Output the longitudinal profile of mid-depth PSDs for odd I:
      WRITE (10,*)
      WRITE (10,223) JMID
  223 FORMAT ('LONGITUDINAL profile of PSD @ Mid-depth, LDNDD(K,I,',I2,
     $'):')
C
      DO 600 I = 1,NX,2
           WRITE (10,225) I,JMID
           WRITE (10,125,ERR=99) (LDNDD(K,I,JMID), K = 1,NK)
           WRITE (11,225) I,JMID
           DO 500 K = 1,NK
                WRITE (11,227,ERR=97) LDNDD(K,I,JMID)
  500      CONTINUE
  600 CONTINUE
C
C Write first half of the total mass concentrations:
      WRITE (10,315)
      DO 700 J = 1,NZ
           WRITE (10,135,ERR=99) (TSS(I,J),I = 1,6)
  700 CONTINUE
  315 FORMAT (/,'TOT Mass concentration TSS(I=1,6), [mg/L]:')
C
C Write second half of the total mass concentrations:
      WRITE (10,317)
      DO 750 J = 1,NZ
           WRITE (10,135,ERR=99) (TSS(I,J),I = 6,11)
  750 CONTINUE
  317 FORMAT (/,'TOT Mass concentration TSS(I=6,11), [mg/L]:')
```

```
C
C Write the total number concentrations:
      WRITE (10,325)
      DO 800 J = 1,NZ
          WRITE (10,135,ERR=99) (TNUM(I,J),I = 1,NX,2)
  800 CONTINUE
  325 FORMAT (/,'TOT number concentration TNUM(I-odd), [#/cm^3]:')
C
C Define # grid points for TSS, TNUM, and TAREA contour plotting files.
C Note that J index is reversed to translate the physical coordinates
C (which are positive down) to graphical coordinates (which are positive
C up).
      NPOINT = (NX* (NZ-1))
      WRITE (12,*)  NPOINT,' 0'
      DO 1000 I = 1, NX
          DO 900 J = NZ-1,1,-1
              JREV = NZ - J
              WRITE (12,335) I, JREV, TSS(I,J)
  900     CONTINUE
 1000 CONTINUE
  335 FORMAT (I2,TR5,I2,TR5,F20.6)
C
C Convert (divide by 1e6) and then output TNUM() for contour:
      WRITE (13,*)  NPOINT,' 0'
      DO 1200 I = 1, NX
          DO 1100 J = 1,NZ-1
              JREV = NZ - J
              TNUM(I,J) = TNUM(I,J)/1.E6
              WRITE (13,335) I, JREV, TNUM(I,J)
 1100     CONTINUE
 1200 CONTINUE
C
C Output TAREA() for contour:
      WRITE (14,*)  NPOINT,' 0'
      DO 1250 I = 1, NX
          DO 1150 J = 1,NZ-1
              JREV = NZ - J
              WRITE (14,335) I, JREV, TAREA(I,J)
 1150     CONTINUE
 1250 CONTINUE
C
      WRITE (10,415)
      WRITE (10,425) (QTRIB(I),I = 0,NX)
  415 FORMAT (/,'Tributary Flowrates (I=0:NX), [m^3/s]:')
  425 FORMAT (5(E11.5,TR3))
C
      WRITE (10,435)
      WRITE (10,445) (NTRIB(1,I),I = 1,NX)
  435 FORMAT (/,'Tributary Concs (k=1,I=1:NX), [#/cm^3]:')
  445 FORMAT (5(E11.5,TR3))
C
      WRITE (10,437)
      WRITE (10,447) (NTRIB(15,I),I = 1,NX)
  437 FORMAT (/,'Tributary Concs (k=15,I=1:NX), [#/cm^3]:')
  447 FORMAT (5(E11.5,TR3))
C
      WRITE (10,455)
      WRITE (10,465) (NSOURC(1,I,1),I = 1,NX)
  455 FORMAT (/,'Tributary Source Strengths (k=1,I=1:NX,1), [#/cm^3]:')
  465 FORMAT (5(E11.5,TR3))
C
      WRITE (10,475)
      WRITE (10,485) (NSOURC(15,I,1),I = 1,NX)
  475 FORMAT (/,'Tributary Source Strengths (k=15,I=1:NX,1), [#/cm^3]:')
  485 FORMAT (5(E11.5,TR3))
C
      WRITE (10,355)
      WRITE (10,135,ERR=99) (BEDMAS(I),I = 1,NX)
  355 FORMAT (/,'Active bed mass per area BEDMAS(I), [g/cm^2]:')
C
      WRITE (10,365)
      WRITE (10,135,ERR=99) (BEDVOL(I),I = 1,NX)
  365 FORMAT (/,'Active bed volume per area,ie bed depth BEDVOL(I)',
     $', [cm^3/cm^2]:')
C
      IF (TIME .LE. 1.E-6) THEN
         WRITE (10,375)
         WRITE (10,135) (POROS(I), I = 1,NX)
  375 FORMAT (/,'Constant Bed Porosity POROS(I), [cm^3/cm^3] :')
      ENDIF
C
CT      WRITE (10,415)
CT      DO 1300 J = 1,NZ
CT          WRITE (10,115,ERR=99) (CT1(I,J),I = 1,NX,2)
CT 1300 CONTINUE
CT  415 FORMAT (/,'Tot Contaminant concentration CT(I-odd), [ug/L]:')
C
CT      DO 1500 K=1,NK
CT          WRITE (10,*) 'FP(K,I-odd,J) for K = ',K
CT          DO 1400 J = 1, NZ
CT              WRITE (10,115) (FP(K,I,J),I = 1,NX,2)
CT 1400     CONTINUE
CT 1500 CONTINUE
C
CT      WRITE (10,*)
CT      WRITE (10,*) 'TOTFP(I-odd,J):'
CT      DO 1600 J = 1, NZ
CT          WRITE (10,115) (TOTFP(I,J),I = 1,NX,2)
CT 1600 CONTINUE
```

```
C
      WRITE (10,*)
C
  115 FORMAT (5(E11.5,TR2))
  125 FORMAT (5(F11.4,TR2))
  135 FORMAT (6(E11.5,TR2))
C
      RETURN
   99 WRITE (10,*)  'OUTPT RESULTS WRITE-ERROR to FILE 10'
   97 WRITE (10,*)  'OUTPT RESULTS WRITE-ERROR to FILE 11'
  199 WRITE (10,*)  'OUTPT RESULTS WRITE-ERROR to CPR'
      STOP
      END
```

APPENDIX F

Coagulation Source Codes (C)

```
/* Subroutine FRCGAM32.c
*  Last revised 7/14/90 2310. -  [GAMMA] Dimensioned for 531.
*  Stripped down portion of Batch.c.
*  Subroutine FRCGAM.c is written in C and called by FORTRAN main.
*  Purpose is to calculate FRAC[][] and GAMMA[] for later use in COAG.c.
*
*  Arrays are dimensioned for NK+1 elements, i.e., waste the 0 elements, begin
*   w/ subscript 1 to use Han logic. This done for Fortran portability. These
*   two arrays must similarly be dimensioned for NK+1 in Fortran main.
*  Gammacalc() has been revised to accomodate particles larger than 200 um.
*/

#include <stdio.h>
#include <math.h>

FILE  *f1,*f2;

FRCGAM(NK,LVSTEP,TEMP,VISCOS,DIAM,G,GRAV,RHO,RHOW,IBR,ISH,IDS,FRAC,BAND1,BAND3,
       MAXFR1,MAXFR3,GAMMA)

/* INPUT POINTER ARGUMENTS:                                                  */
int   *NK;            /* Number of actual PARTICLE SIZE classes              */
float *LVSTEP;        /* log(V[k+1]/V[k])                                    */
int   *IBR,*ISH,*IDS; /* operative collision mechanisms and trajectory types */
float *TEMP;          /* Temperature, [K]                                    */
float *VISCOS;        /* Molecular viscosity of suspension, [g/cm-s]         */
float *RHO;           /* Density of flocs, [g/cm^3]                          */
float *RHOW;          /* Density of fluid, [g/cm^3]                          */
float *G;             /* Velocity gradient, [1/s]                            */
float *GRAV;          /* Acceleration due to gravity, [cm/s^2]               */
float DIAM[32];       /* Floc diameter, [um]                                 */

/* OUTPUT POINTER ARGUMENTS:                                                 */
int   *MAXFR1;
int   BAND1[10];
int   *MAXFR3;
int   BAND3[10];
float FRAC[32][4];    /* fraction of particle floc to integer particle classes */
float GAMMA[513];  /* binary collision frequency function values, [1/(s-#/cm^3)] */

{
int K;

f1 = fopen("FRAC","w");
f2 = fopen("GAMMA","w");

for (K = *NK; K >= 1; K--)             /* Array                              */
       DIAM[K] = DIAM[K-1];            /* shifting from Fortran to C         */

FRACCALC(NK,LVSTEP,FRAC,BAND1,BAND3,MAXFR1,MAXFR3);

GAMMACALC(TEMP,VISCOS,DIAM,G,GRAV,RHO,RHOW,IBR,ISH,IDS,NK,GAMMA);

fclose(f1);
fclose(f2);

for (K = 0; K < *NK; K++)             /* Array                               */
       DIAM[K] = DIAM[K+1];           /* shifting from C back into Fortran   */

}  /*  end of FRCGAM subroutine  */

/*********************************FRACCALC()*********************************/
FRACCALC(NK,LVSTEP,FRAC,BAND1,BAND3,MAXFR1,MAXFR3)

/* INPUT POINTER ARGUMENTS:                                                  */
int   *NK;            /* Number of PARTICLE SIZES                            */
float *LVSTEP;        /* log(V[k+1/V[k])                                     */

/* OUTPUT POINTER ARGUMENTS:                                                 */
int   *MAXFR1;
int   BAND1[10];
int   *MAXFR3;
int   BAND3[10];
float FRAC[32][4];   /* fraction of particle floc to integer particle classes */

{
int   I, IJ, JK, K, Q, JMAX, FR3, CELL;
float SUMV, X, V1, V2, STEP, VDIFF;

STEP    = *LVSTEP;
*MAXFR1 = floor(log10(2.00)/STEP);
                  /* max STEPs separation when I & J (J<I) create a K = I */

for (I= 1; I<= *MAXFR1; I++)
       BAND1[I] = floor(-1.0/ STEP* log10(pow(10.0, (I)* STEP)- 1.0));

BAND1[*MAXFR1+ 1] = -1;

/* column 1, frac[][1]. Note that elements [][0] left unassigned:
*/
VDIFF = pow(10.0,STEP*1.0)- pow(10.0,STEP*0.0);          /* V[K+1] - V[K] */
for (IJ= *NK-1; IJ> BAND1[1]; IJ--)
       {
        SUMV  = 1.0 + pow(10.0,STEP*(-IJ)*1.0);           /* V[I]+ V[J]    */
        CELL  = IJ+ 1;
        FRAC[CELL][1] = (pow(10.0,STEP*1.0)- SUMV)/ VDIFF;
       }

for (IJ= BAND1[1]; IJ>= 0; IJ--)
```

```
        {
         SUMV = 1.0+ pow(10.0, STEP* (-IJ)*1.0);
         for (Q= 1; Q<= *MAXFR1; Q++)
                {
                 if (IJ<= BAND1[Q] && IJ> BAND1[Q+1])
                        {
                         VDIFF          = pow(10.0,STEP* (Q+1)*1.0)
                                          - pow(10.0,STEP*Q*1.0);
                         CELL           = IJ+ 1;
                         FRAC[CELL][1] = (pow(10.0,STEP* (Q+1)*1.0)- SUMV)/ VDIFF;
                        }
                }
        }

/* column 2, frac[][2]:
*/
for (K= 1; K<= *NK; K++)
        FRAC[K][2] = 1.0+ pow(10.0,-STEP*(*NK- K));

/* column 3, frac[][3]:
*/
FR3 = 1, *MAXFR3 = 1;
for (K= 1; K<= *NK; K++)
        {
        V1        = pow(10.0,-STEP* (K));
        X         = log10(1.0- V1);
        JMAX      = floor(-X/ STEP* 1.0);
        BAND3[K] = JMAX;
        *MAXFR3   = *MAXFR3 + 1;                        /* used in Diffun()   */
        if (JMAX< K)
                goto NOMORE;
        for (JK= K; JK<= JMAX; JK++)
                {
                V2            = pow(10.0,-STEP* (JK));
                FRAC[FR3][3] = V1+ V2;
                FR3           = FR3+ 1;
                }
        }

NOMORE:  /* dummy statement */ ;
fprintf(f1,"NK= %d  LVSTEP= %f  MAXFR1= %d\n\n",*NK,STEP,*MAXFR1);
fprintf(f1,"K  FRAC[K][1]  FRAC[K][2]  FRAC[K][3]  BAND1[K]  BAND3[K]\n");
/* printf("\t\nNK= %d  LVSTEP= %f  MAXFR1= %d\n\n",*NK,STEP,*MAXFR1);
printf("\t  K   FRAC[K][1]  FRAC[K][2]  FRAC[K][3]  BAND1[K]  BAND3[K]\n"); */

for (K= 1; K <= *NK; K++)
     {
     fprintf(f1,"%3d %10.4f %10.4f %10.4f %10d %10d \n",
             K,FRAC[K][1],FRAC[K][2],FRAC[K][3],BAND1[K],BAND3[K]);
/*     printf("\t%3d %10.4f %10.4f %10.4f %10d %10d \n",
             K,FRAC[K][1],FRAC[K][2],FRAC[K][3],BAND1[K],BAND3[K]); */
     }
}

/*********************************FRACCALC()*********************************/

/*******************************GAMMACALC()*********************************/
GAMMACALC(TEMP,VISCOS,DIAM,G,GRAV,RHO,RHOW,IBR,ISH,IDS,NK,GAMMA)
                        /* CALCULATE Gamma FROM THREE TRANSPORT MECHANISMS  */

/* INPUT POINTER ARGUMENTS:                                                 */
int   *NK;              /* Number of PARTICLE SIZES                         */
int   *IBR,*ISH,*IDS; /* operative collision mechanisms and trajectory types  */
float *TEMP;            /* Temperature, [K]                                 */
float *VISCOS;          /* Molecular viscosity of suspension, [g/cm-s]      */
float *RHO;             /* Density of flocs, [g/cm^3]                       */
float *RHOW;            /* Density of fluid, [g/cm^3]                       */
float *G;               /* Velocity gradient, [1/s]                         */
float *GRAV;            /* Acceleration due to gravity, [cm/s^2]            */
float DIAM[32];         /* Floc diameter, [um]                              */

/* OUTPUT POINTER ARGUMENTS:                                                */
float GAMMA[436];  /* binary collision frequency function values, [1/(s-#/cm^3)] */

{
float BrCorr(), ShCorr(), DsCorr();
float BetaBr, BetaSh, BetaDs, CorrBr, CorrSh, CorrDs;
float Di, Dj, LAMDA, BRCOEF, DSCOEF;
float BOLTZ = 1.38E-16;
float PI    = 3.141592;
int   I, J, K;

BRCOEF = 2.0* BOLTZ* (*TEMP)/ (3.0* (*VISCOS));
DSCOEF = PI* (*GRAV)* (*RHO- *RHOW)/ (72.* (*VISCOS));

fprintf(f2,"\n  K  DIAM[I]  DIAM[J]  CorrBr  CorrSh  CorrDs  GAMMA[K]\n");
/* printf("\t\n K  DIAM[I]  DIAM[J]  CorrBr  CorrSh  CorrDs  GAMMA[K]\n"); */

/* Need to copy contents of DIAM[], written in Fortran main, to DIAM[]
*  usable in C. DIAM-Fort subscripting is (1:NK+1) and DIAM-C subscripting
*  is (0:NK), but we want the C subscripts to correspond to their actual
*  element order, e.g., element 1 having subscript 1:
*/
for (I= 1; I <= *NK; I++)
        {
        Di = DIAM[I];                   /* diameter of larger particle, [um]  */
        for (J= 1; J<= I; J++)
                {
                Dj    = DIAM[J];        /* diameter of smaller particle, [um] */
```

```
                LAMDA = Dj/ Di;         /* size ratio (less or equal to 1)    */

/* Brownian correction  */
                switch ((*IBR)+1)
                {
                case 1:                 /*  IBR=0, Brownian Motion not considered */
                        CorrBr = 0.;
                        break;
                case 2:                 /*  IBR=1, Rectilinear Brownian Motion    */
                        CorrBr = 1.;
                        break;
                case 3:                 /*  IBR=2, Curvilinear Brownian Motion    */
                        CorrBr = BrCorr(&Di,&LAMDA);
                        break;
                }
                BetaBr = CorrBr* BRCOEF* (1.0/Di + 1.0/Dj)* (Di+ Dj);

/* Fluid Shear correction  */
                switch ((*ISH)+1)
                {
                case 1:                 /*  ISH=0, Fluid Shear not considered  */
                        CorrSh = 0.;
                        break;
                case 2:                 /*  ISH=1, Rectilinear Fluid Shear     */
                        CorrSh = 1.;
                        break;
                case 3:                 /*  ISH=2, Curvilinear Fluid Shear     */
                        CorrSh = ShCorr(&Di,&LAMDA,G,VISCOS);
                        break;
                }
                BetaSh = CorrSh* (*G)/ 6.0* pow((Di+Dj),3.0)* 1e-12;

/* Differential Sedimentation correction  */
                switch ((*IDS)+1)
                {
                case 1:         /*  IDS=0, Differential Sedim not considered  */
                        CorrDs = 0.;
                        break;
                case 2:         /*  IDS=1, Rectilinear Differential Sedim     */
                        CorrDs = 1.;
                        break;
                case 3:         /*  IDS=2, Curvilinear Differential Sedim     */
                        CorrDs = DsCorr(&Di,&LAMDA);
                        break;
                }
                BetaDs = CorrDs* DSCOEF* pow((Di+Dj),3.0)*fabs((Di-Dj))* 1e-16;

/*              DRAG COEF NOT CONSIDERED YET*/

                K = I* (I-1)/ 2+ J;  /* subscript reflects element order,
                                        [1,NK], not storage subscript order [2,NK+1] */

                GAMMA[K] = BetaBr+ BetaSh+ BetaDs;

fprintf(f2," %3d  %6.2f %6.2f %6.3f %8.2e %8.2e %9.3e\n",
                                K,DIAM[I],DIAM[J],CorrBr,CorrSh,CorrDs,GAMMA[K]);
/* printf("\t %3d  %6.2f %6.2f %6.3f %8.2e %8.2e %9.3e\n",
                                K,DIAM[I],DIAM[J],CorrBr,CorrSh,CorrDs,GAMMA[K]); */
                }
        }
}

/*****************  Curvilinear Correction for Brownian motion ***************/
float BrCorr(Di,LAMDA)
float *Di, *LAMDA;                                      /* pointer to variables  */

{
float BOTSIZE, TOPSIZE, DELSIZE, ABOT, ATOP, correction, DI_UM, DL;
int   K, BOT, TOP;
static float BR[11][5]= {/* dia    a      b      c      d   */
                         {0.100, 1.025,-0.626, 0.516,-0.152},
                         {0.200, 1.007,-0.860, 0.870,-0.322},
                         {0.600, 0.976,-1.155, 1.342,-0.554},
                         {1.000, 0.962,-1.263, 1.522,-0.645},
        /*  BROWN */       {2.000, 0.943,-1.383, 1.725,-0.748},
                         {6.000, 0.916,-1.533, 1.991,-0.887},
                         {10.00, 0.905,-1.587, 2.087,-0.936},
                         {20.00, 0.891,-1.658, 2.221,-1.009},
                         {60.00, 0.871,-1.739, 2.371,-1.090},
                         {200.0, 0.863,-1.775, 2.439,-1.125},
                         {600.0, 0.850,-1.825, 2.500,-1.150}
                         };  /* coefficients for 600 added by eye */
DI_UM = *Di;
DL    = *LAMDA;
        for (K= 0; K<= 9; K++)
                {
                if(DI_UM< BR[K][0])
                        goto InterpolBr;
                }
InterpolBr:
        BOT     = K;
        TOP     = K- 1;
        BOTSIZE = BR[BOT][0];
        TOPSIZE = BR[TOP][0];
        DELSIZE = BOTSIZE- TOPSIZE;
        ABOT    = BR[BOT][1]+ BR[BOT][2]* DL+ BR[BOT][3]* DL*DL+ BR[BOT][4]*
                  DL*DL*DL;
        ATOP    = BR[TOP][1]+ BR[TOP][2]* DL+ BR[TOP][3]* DL*DL+ BR[TOP][4]*
                  DL*DL*DL;
```

```
        correction = ABOT + (ATOP- ABOT)/ DELSIZE* (BOTSIZE- DI_UM);
        return correction;
}

/******************  Curvilinear Correction for Fluid Shear ******************/
float ShCorr(Di,LAMDA,G,VISCOS)
float *Di,*LAMDA,*G,*VISCOS;                          /* pointer to variables  */

{
float HA, BOTHA, TOPHA, DELHA, TEMPO, ADLER, ABOT, ATOP, correction, DI_UM, DL;
int   K, BOT, TOP;
float PI  = 3.141592;
float HAM = 4.1E-13;
static float SH[11][5]= { /* HA     a       b       c       d    */
                          {10.00, 0.000, 0.000, 0.000, 0.000},
                          { 1.00,-1.128, 2.498,-2.042, 0.671},
                          { 0.00,-1.228, 2.498,-2.042, 0.671},
                          {-1.00,-1.482, 3.189,-3.468, 1.581},
                          {-2.00,-1.704, 3.116,-2.881, 1.121},
                          {-3.00,-2.523, 5.550,-6.098, 2.553},
        /*  SHEAR */      {-4.00,-3.723,10.039,-12.569,5.557},
                          {-5.00,-5.775,18.267,-24.344,10.992},
                          {-6.00,-7.037,20.829,-25.589,10.755},
                          {-7.00,-8.733,25.663,-30.703,12.555},
                          {-8.00,-9.733,30.663,-35.703,14.555}
                          };

        DI_UM = *Di;
        DL    = *LAMDA;

        HA = log10(HAM/ (18.0* PI* (*VISCOS)* DI_UM* DI_UM* DI_UM* 1E-12* (*G)));
        for (K= 0; K<= 10; K++)
                {
                if(HA > SH[K][0])
                        goto InterpolSh;
                }
InterpolSh:
        BOT   = K;
        TOP   = K- 1;
        BOTHA = SH[BOT][0];
        TOPHA = SH[TOP][0];
        DELHA = TOPHA - BOTHA;
        ABOT  = SH[BOT][1]+ SH[BOT][2]* DL+ SH[BOT][3]* DL*DL+ SH[BOT][4]*
                DL*DL*DL;
        ATOP  = SH[TOP][1]+ SH[TOP][2]* DL+ SH[TOP][3]* DL*DL+ SH[TOP][4]*
                DL*DL*DL;
        TEMPO = ATOP- (ATOP- ABOT)/ DELHA* (TOPHA- HA);
        ADLER = pow(10.0,TEMPO*1.0);

        correction = ADLER* 8.0/ pow(1.0+ DL,3.0);
        return correction;
}

/********** Curvilinear Correction for Differential Sedimentation *************/
float DsCorr(Di,LAMDA)
float *Di, *LAMDA;                                    /* pointer to variables  */

{
float BOTSIZE, TOPSIZE, DELSIZE, ABOT, ATOP, correction, DI_UM, DL, TEMPO;
int   K, BOT, TOP;
static float DS[8][5]= { /* dia    a       b       c       d    */
                         {0.000, 0.000, 0.000, 0.000, 0.000},
                         {4.000,-1.212, 0.991,-1.661, 1.103},
        /*  SEDIM */     {10.00,-1.966, 2.520,-3.725, 2.001},
                         {20.00,-2.447, 3.647,-5.417, 2.817},
                         {60.00,-3.002, 4.547,-6.762, 3.454},
                         {100.0,-3.132, 4.547,-6.762, 3.454},
                         {200.0,-3.928, 6.423,-9.449, 4.614},
                         {600.0,-3.928, 6.423,-9.449, 4.614}
                         };  /* coefficients for 600 repeated
                                by GWC as if the limiting case*/
        DI_UM = *Di;
        DL    = *LAMDA;
        for (K= 0; K<=7; K++)
                {
                if(DI_UM < DS[K][0])
                        goto InterpolDs;
                }
InterpolDs:
        BOT     = K;
        TOP     = K-1;
        BOTSIZE = DS[BOT][0];
        TOPSIZE = DS[TOP][0];
        DELSIZE = BOTSIZE- TOPSIZE;
        ABOT    = DS[BOT][1] + DS[BOT][2]* DL+ DS[BOT][3]* DL*DL+ DS[BOT][4]*
                  DL*DL*DL;
        ATOP    = DS[TOP][1]  +DS[TOP][2]* DL+ DS[TOP][3]* DL*DL+ DS[TOP][4]*
                  DL*DL*DL;
        TEMPO   = ABOT+ (ATOP- ABOT)/ DELSIZE* (BOTSIZE- DI_UM);

        correction = pow(10.0,TEMPO*1.0);
        return correction;
}
/*********************************GAMMACALC()*********************************/
/* Subroutine FRCGAM32.c
*  Last revised 7/14/90 2310. -  [GAMMA] Dimensioned for 531.
*  Stripped down portion of Batch.c.
*  Subroutine FRCGAM.c is written in C and called by FORTRAN main.
```

```
*  Purpose is to calculate FRAC[][] and GAMMA[] for later use in COAG.c.
*
*  Arrays are dimensioned for NK+1 elements, i.e., waste the 0 elements, begin
*   w/ subscript 1 to use Han logic. This done for Fortran portability. These
*   two arrays must similarly be dimensioned for NK+1 in Fortran main.
*  Gammacalc() has been revised to accomodate particles larger than 200 um.
*/

#include <stdio.h>
#include <math.h>

FILE  *f1,*f2;

FRCGAM(NK,LVSTEP,TEMP,VISCOS,DIAM,G,GRAV,RHO,RHOW,IBR,ISH,IDS,FRAC,BAND1,BAND3,
       MAXFR1,MAXFR3,GAMMA)

/* INPUT POINTER ARGUMENTS:                                                  */
int   *NK;             /* Number of actual PARTICLE SIZE classes             */
float *LVSTEP;         /* log(V[k+1]/V[k])                                   */
int   *IBR,*ISH,*IDS; /* operative collision mechanisms and trajectory types */
float *TEMP;           /* Temperature, [K]                                   */
float *VISCOS;         /* Molecular viscosity of suspension, [g/cm-s]        */
float *RHO;            /* Density of flocs, [g/cm^3]                         */
float *RHOW;           /* Density of fluid, [g/cm^3]                         */
float *G;              /* Velocity gradient, [1/s]                           */
float *GRAV;           /* Acceleration due to gravity, [cm/s^2]              */
float DIAM[32];        /* Floc diameter, [um]                                */

/* OUTPUT POINTER ARGUMENTS:                                                 */
int   *MAXFR1;
int   BAND1[10];
int   *MAXFR3;
int   BAND3[10];
float FRAC[32][4];    /* fraction of particle floc to integer particle classes */
float GAMMA[513];  /* binary collision frequency function values, [1/(s-#/cm^3)] */

{
int K;

f1 = fopen("FRAC","w");
f2 = fopen("GAMMA","w");

for (K = *NK; K >= 1; K--)             /* Array                              */
       DIAM[K] = DIAM[K-1];            /* shifting from Fortran to C         */

FRACCALC(NK,LVSTEP,FRAC,BAND1,BAND3,MAXFR1,MAXFR3);

GAMMACALC(TEMP,VISCOS,DIAM,G,GRAV,RHO,RHOW,IBR,ISH,IDS,NK,GAMMA);

fclose(f1);
fclose(f2);

for (K = 0; K < *NK; K++)              /* Array                              */
       DIAM[K] = DIAM[K+1];            /* shifting from C back into Fortran  */

}  /*  end of FRCGAM subroutine  */

/*********************************FRACCALC()*********************************/
FRACCALC(NK,LVSTEP,FRAC,BAND1,BAND3,MAXFR1,MAXFR3)

/* INPUT POINTER ARGUMENTS:                                                  */
int   *NK;             /* Number of PARTICLE SIZES                           */
float *LVSTEP;         /* log(V[k+1/V[k])                                    */

/* OUTPUT POINTER ARGUMENTS:                                                 */
int   *MAXFR1;
int   BAND1[10];
int   *MAXFR3;
int   BAND3[10];
float FRAC[32][4];   /* fraction of particle floc to integer particle classes */

{
int   I, IJ, JK, K, Q, JMAX, FR3, CELL;
float SUMV, X, V1, V2, STEP, VDIFF;

STEP    = *LVSTEP;
*MAXFR1 = floor(log10(2.00)/STEP);
                    /* max STEPs separation when I & J (J<I) create a K = I */

for (I= 1; I<= *MAXFR1; I++)
       BAND1[I] = floor(-1.0/ STEP* log10(pow(10.0, (I)* STEP)- 1.0));

BAND1[*MAXFR1+ 1] = -1;

/* column 1, frac[][1]. Note that elements [][0] left unassigned:
*/
VDIFF = pow(10.0,STEP*1.0)- pow(10.0,STEP*0.0);          /* V[K+1] - V[K] */
for (IJ= *NK-1; IJ> BAND1[1]; IJ--)
       {
        SUMV  = 1.0 + pow(10.0,STEP*(-IJ)*1.0);           /* V[I]+ V[J]    */
        CELL  = IJ+ 1;
        FRAC[CELL][1] = (pow(10.0,STEP*1.0)- SUMV)/ VDIFF;
       }

for (IJ= BAND1[1]; IJ>= 0; IJ--)
       {
        SUMV = 1.0+ pow(10.0, STEP* (-IJ)*1.0);
        for (Q= 1; Q<= *MAXFR1; Q++)
              {
```

```
                if (IJ<= BAND1[Q] && IJ> BAND1[Q+1])
                        {
                         VDIFF          = pow(10.0,STEP* (Q+1)*1.0)
                                          - pow(10.0,STEP*Q*1.0);
                         CELL           = IJ+ 1;
                         FRAC[CELL][1] = (pow(10.0,STEP* (Q+1)*1.0)- SUMV)/ VDIFF;
                        }
                }
        }

/* column 2, frac[][2]:
*/
for (K= 1; K<= *NK; K++)
        FRAC[K][2] = 1.0+ pow(10.0,-STEP*(*NK- K));

/* column 3, frac[][3]:
*/
FR3 = 1, *MAXFR3 = 1;
for (K= 1; K<= *NK; K++)
        {
        V1        = pow(10.0,-STEP* (K));
        X         = log10(1.0- V1);
        JMAX      = floor(-X/ STEP* 1.0);
        BAND3[K] = JMAX;
        *MAXFR3   = *MAXFR3 + 1;                        /* used in Diffun()   */
        if (JMAX< K)
                goto NOMORE;
        for (JK= K; JK<= JMAX; JK++)
                {
                V2              = pow(10.0,-STEP* (JK));
                FRAC[FR3][3] = V1+ V2;
                FR3             = FR3+ 1;
                }
        }

NOMORE:  /* dummy statement */ ;
fprintf(f1,"NK= %d  LVSTEP= %f  MAXFR1= %d\n\n",*NK,STEP,*MAXFR1);
fprintf(f1,"K  FRAC[K][1]  FRAC[K][2]  FRAC[K][3]  BAND1[K]  BAND3[K]\n");
/* printf("\t\nNK= %d  LVSTEP= %f  MAXFR1= %d\n\n",*NK,STEP,*MAXFR1);
printf("\t  K   FRAC[K][1]  FRAC[K][2]  FRAC[K][3]  BAND1[K]  BAND3[K]\n"); */

for (K= 1; K <= *NK; K++)
     {
     fprintf(f1,"%3d %10.4f %10.4f %10.4f %10d %10d \n",
             K,FRAC[K][1],FRAC[K][2],FRAC[K][3],BAND1[K],BAND3[K]);
/*     printf("\t%3d %10.4f %10.4f %10.4f %10d %10d \n",
             K,FRAC[K][1],FRAC[K][2],FRAC[K][3],BAND1[K],BAND3[K]); */
     }
}

/*********************************FRACCALC()*********************************/

/*********************************GAMMACALC()********************************/
GAMMACALC(TEMP,VISCOS,DIAM,G,GRAV,RHO,RHOW,IBR,ISH,IDS,NK,GAMMA)
                        /* CALCULATE Gamma FROM THREE TRANSPORT MECHANISMS  */

/* INPUT POINTER ARGUMENTS:                                                 */
int   *NK;              /* Number of PARTICLE SIZES                         */
int   *IBR,*ISH,*IDS; /* operative collision mechanisms and trajectory types  */
float *TEMP;            /* Temperature, [K]                                 */
float *VISCOS;          /* Molecular viscosity of suspension, [g/cm-s]      */
float *RHO;             /* Density of flocs, [g/cm^3]                       */
float *RHOW;            /* Density of fluid, [g/cm^3]                       */
float *G;               /* Velocity gradient, [1/s]                         */
float *GRAV;            /* Acceleration due to gravity, [cm/s^2]            */
float DIAM[32];         /* Floc diameter, [um]                              */

/* OUTPUT POINTER ARGUMENTS:                                                */
float GAMMA[436];  /* binary collision frequency function values, [1/(s-#/cm^3)] */

{
float BrCorr(), ShCorr(), DsCorr();
float BetaBr, BetaSh, BetaDs, CorrBr, CorrSh, CorrDs;
float Di, Dj, LAMDA, BRCOEF, DSCOEF;
float BOLTZ = 1.38E-16;
float PI    = 3.141592;
int   I, J, K;

BRCOEF = 2.0* BOLTZ* (*TEMP)/ (3.0* (*VISCOS));
DSCOEF = PI* (*GRAV)* (*RHO- *RHOW)/ (72.* (*VISCOS));

fprintf(f2,"\n  K  DIAM[I]  DIAM[J]  CorrBr  CorrSh  CorrDs  GAMMA[K]\n");
/* printf("\t\n K  DIAM[I]  DIAM[J]  CorrBr  CorrSh  CorrDs  GAMMA[K]\n"); */

/* Need to copy contents of DIAM[], written in Fortran main, to DIAM[]
*  usable in C. DIAM-Fort subscripting is (1:NK+1) and DIAM-C subscripting
*  is [0:NK], but we want the C subscripts to correspond to their actual
*  element order, e.g., element 1 having subscript 1:
*/
for (I= 1; I <= *NK; I++)
        {
        Di = DIAM[I];                   /* diameter of larger particle, [um]  */
        for (J= 1; J<= I; J++)
                {
                Dj    = DIAM[J];        /* diameter of smaller particle, [um] */
                LAMDA = Dj/ Di;         /* size ratio (less or equal to 1)    */

/* Brownian correction  */
                switch ((*IBR)+1)
```

```
                {
                case 1:                 /*  IBR=0, Brownian Motion not considered */
                        CorrBr = 0.;
                        break;
                case 2:                 /*  IBR=1, Rectilinear Brownian Motion    */
                        CorrBr = 1.;
                        break;
                case 3:                 /*  IBR=2, Curvilinear Brownian Motion    */
                        CorrBr = BrCorr(&Di,&LAMDA);
                        break;
                }
                BetaBr = CorrBr* BRCOEF* (1.0/Di + 1.0/Dj)* (Di+ Dj);

/* Fluid Shear correction  */
                switch ((*ISH)+1)
                {
                case 1:                 /*  ISH=0, Fluid Shear not considered  */
                        CorrSh = 0.;
                        break;
                case 2:                 /*  ISH=1, Rectilinear Fluid Shear     */
                        CorrSh = 1.;
                        break;
                case 3:                 /*  ISH=2, Curvilinear Fluid Shear     */
                        CorrSh = ShCorr(&Di,&LAMDA,G,VISCOS);
                        break;
                }
                BetaSh = CorrSh* (*G)/ 6.0* pow((Di+Dj),3.0)* 1e-12;

/* Differential Sedimentation correction  */
                switch ((*IDS)+1)
                {
                case 1:                 /*  IDS=0, Differential Sedim not considered  */
                        CorrDs = 0.;
                        break;
                case 2:                 /*  IDS=1, Rectilinear Differential Sedim     */
                        CorrDs = 1.;
                        break;
                case 3:                 /*  IDS=2, Curvilinear Differential Sedim     */
                        CorrDs = DsCorr(&Di,&LAMDA);
                        break;
                }
                BetaDs = CorrDs* DSCOEF* pow((Di+Dj),3.0)*fabs((Di-Dj))* 1e-16;

/*              DRAG COEF NOT CONSIDERED YET*/

                K = I* (I-1)/ 2+ J;  /* subscript reflects element order,
                                        [1,NK], not storage subscript order [2,NK+1] */

                GAMMA[K] = BetaBr+ BetaSh+ BetaDs;

fprintf(f2," %3d  %6.2f %6.2f %6.3f %8.2e %8.2e %9.3e\n",
                                K,DIAM[I],DIAM[J],CorrBr,CorrSh,CorrDs,GAMMA[K]);
/* printf("\t %3d  %6.2f %6.2f %6.3f %8.2e %8.2e %9.3e\n",
                                K,DIAM[I],DIAM[J],CorrBr,CorrSh,CorrDs,GAMMA[K]); */
                }
        }
}

/*****************  Curvilinear Correction for Brownian motion ****************/
float BrCorr(Di,LAMDA)
float *Di, *LAMDA;                                      /* pointer to variables  */

{
float BOTSIZE, TOPSIZE, DELSIZE, ABOT, ATOP, correction, DI_UM, DL;
int   K, BOT, TOP;
static float BR[11][5]= {/* dia    a      b      c      d   */
                         {0.100, 1.025,-0.626, 0.516,-0.152},
                         {0.200, 1.007,-0.860, 0.870,-0.322},
                         {0.600, 0.976,-1.155, 1.342,-0.554},
                         {1.000, 0.962,-1.263, 1.522,-0.645},
        /*  BROWN */     {2.000, 0.943,-1.383, 1.725,-0.748},
                         {6.000, 0.916,-1.533, 1.991,-0.867},
                         {10.00, 0.905,-1.587, 2.087,-0.936},
                         {20.00, 0.891,-1.658, 2.221,-1.009},
                         {60.00, 0.871,-1.739, 2.371,-1.090},
                         {200.0, 0.863,-1.775, 2.439,-1.125},
                         {600.0, 0.850,-1.825, 2.500,-1.150}
                         };  /* coefficients for 600 added by eye */
DI_UM = *Di;
DL    = *LAMDA;
        for (K= 0; K<= 9; K++)
                {
                if(DI_UM< BR[K][0])
                        goto InterpolBr;
                }
InterpolBr:
        BOT     = K;
        TOP     = K- 1;
        BOTSIZE = BR[BOT][0];
        TOPSIZE = BR[TOP][0];
        DELSIZE = BOTSIZE- TOPSIZE;
        ABOT    = BR[BOT][1]+ BR[BOT][2]* DL+ BR[BOT][3]* DL*DL+ BR[BOT][4]*
                  DL*DL*DL;
        ATOP    = BR[TOP][1]+ BR[TOP][2]* DL+ BR[TOP][3]* DL*DL+ BR[TOP][4]*
                  DL*DL*DL;

        correction = ABOT + (ATOP- ABOT)/ DELSIZE* (BOTSIZE- DI_UM);
        return correction;
}
```

```
/******************  Curvilinear Correction for Fluid Shear ******************/
float ShCorr(Di,LAMDA,G,VISCOS)
float *Di,*LAMDA,*G,*VISCOS;                          /* pointer to variables  */

{
float HA, BOTHA, TOPHA, DELHA, TEMPO, ADLER, ABOT, ATOP, correction, DI_UM, DL;
int   K, BOT, TOP;
float PI  = 3.141592;
float HAM = 4.1E-13;
static float SH[11][5]= { /* HA     a       b       c       d    */
                          {10.00, 0.000, 0.000, 0.000, 0.000},
                          { 1.00,-1.128, 2.498,-2.042, 0.671},
                          { 0.00,-1.228, 2.498,-2.042, 0.671},
                          {-1.00,-1.482, 3.189,-3.468, 1.581},
                          {-2.00,-1.704, 3.116,-2.881, 1.121},
                          {-3.00,-2.523, 5.550,-6.098, 2.553},
        /*  SHEAR */      {-4.00,-3.723,10.039,-12.569,5.557},
                          {-5.00,-5.775,18.267,-24.344,10.992},
                          {-6.00,-7.037,20.829,-25.589,10.755},
                          {-7.00,-8.733,25.663,-30.703,12.555},
                          {-8.00,-9.733,30.663,-35.703,14.555}
                          };

        DI_UM = *Di;
        DL    = *LAMDA;

        HA = log10(HAM/ (18.0* PI* (*VISCOS)* DI_UM* DI_UM* DI_UM* 1E-12* (*G)));
        for (K= 0; K<= 10; K++)
                {
                if(HA > SH[K][0])
                        goto InterpolSh;
                }
InterpolSh:
        BOT   = K;
        TOP   = K- 1;
        BOTHA = SH[BOT][0];
        TOPHA = SH[TOP][0];
        DELHA = TOPHA - BOTHA;
        ABOT  = SH[BOT][1]+ SH[BOT][2]* DL+ SH[BOT][3]* DL*DL+ SH[BOT][4]*
                DL*DL*DL;
        ATOP  = SH[TOP][1]+ SH[TOP][2]* DL+ SH[TOP][3]* DL*DL+ SH[TOP][4]*
                DL*DL*DL;
        TEMPO = ATOP- (ATOP- ABOT)/ DELHA* (TOPHA- HA);
        ADLER = pow(10.0,TEMPO*1.0);

        correction = ADLER* 8.0/ pow(1.0+ DL,3.0);
        return correction;
}

/********** Curvilinear Correction for Differential Sedimentation *************/
float DsCorr(Di,LAMDA)
float *Di, *LAMDA;                                    /* pointer to variables  */

{
float BOTSIZE, TOPSIZE, DELSIZE, ABOT, ATOP, correction, DI_UM, DL, TEMPO;
int   K, BOT, TOP;
static float DS[8][5]= { /* dia    a       b       c       d    */
                         {0.000, 0.000, 0.000, 0.000, 0.000},
                         {4.000,-1.212, 0.991,-1.661, 1.103},
        /*  SEDIM */     {10.00,-1.966, 2.520,-3.725, 2.001},
                         {20.00,-2.447, 3.647,-5.417, 2.817},
                         {60.00,-3.002, 4.547,-6.762, 3.454},
                         {100.0,-3.132, 4.547,-6.762, 3.454},
                         {200.0,-3.928, 6.423,-9.449, 4.614},
                         {600.0,-3.928, 6.423,-9.449, 4.614}
                         };  /* coefficients for 600 repeated
                                by GWC as if the limiting case*/
        DI_UM = *Di;
        DL    = *LAMDA;
        for (K= 0; K<=7; K++)
                {
                if(DI_UM < DS[K][0])
                        goto InterpolDs;
                }
InterpolDs:
        BOT     = K;
        TOP     = K-1;
        BOTSIZE = DS[BOT][0];
        TOPSIZE = DS[TOP][0];
        DELSIZE = BOTSIZE- TOPSIZE;
        ABOT    = DS[BOT][1] + DS[BOT][2]* DL+ DS[BOT][3]* DL*DL+ DS[BOT][4]*
                  DL*DL*DL;
        ATOP    = DS[TOP][1]  +DS[TOP][2]* DL+ DS[TOP][3]* DL*DL+ DS[TOP][4]*
                  DL*DL*DL;
        TEMPO   = ABOT+ (ATOP- ABOT)/ DELSIZE* (BOTSIZE- DI_UM);

        correction = pow(10.0,TEMPO*1.0);
        return correction;
}
/*********************************GAMMACALC()*********************************/


/* Program COAG32.c                    Last revised 7/19/90 1935.
*
*   Removed all references to FILE3 because it was gigantic and unused.
*   Purpose is to calculate DeltaY[][][] for particle coagulation.
*   Subroutine COAG.c is written in C and called by FORTRAN main.
*
```

```
*   Particle class array indices are from [1 to n] in the Han logic, rather than
*   [0 to n-1], so these arrays are dimensioned here for [n+1]. Particle conc
*   array is shifted on entry/exit to allow access to subscripts from [0,n] and
*   is needed for Fortran transfer compatability.
*
*   GAMMA array is dimensioned 1 element larger than needed to allow for skip of
*   element 0, i.e., (32* (32/2 - 1) + 1). [GAMMA] dimensioned for 513.
*
*   Note that the variable order for multidimensional array in C is reversed
*   relative to its Fortran representation.
*/

#include <stdio.h>
#include <math.h>

COAG (NK,NX,NZ,N1,HMAX,DELT,FRAC,BAND1,BAND3,MAXFR1,MAXFR3,GAMMA,ALPHA,
      DELN1,Y)

/* INPUT POINTER ARGUMENTS:
*/
int   *NK;            /* Number of actual PARTICLE SIZE classes              */
int   *NX;            /* Number of Longitudinal nodes                        */
int   *NZ;            /* Number of Vertical nodes                            */
float N1[6][11][32]; /* number conc before transport or rxn., [#/cm^3]      */
float *HMAX;          /* Max. allowable timestep for coag integration, [s]   */
float *DELT;          /* Reaction time, ie, time step taken in transport, [s] */
float *ALPHA;         /* Collision efficiency  */
float FRAC[32][4];    /* Fraction of particle floc to integer particle
                                                  classes       - from FRCGAM  */
float GAMMA[513];     /* Binary collision frequency function values,
                                                [1/(s-#/cm^3)] - from FRCGAM  */
int   *MAXFR1;        /* from FRCGAM.c  */
int   BAND1[10];      /* from FRCGAM.c  */
int   *MAXFR3;        /* from FRCGAM.c  */
int   BAND3[10];      /* from FRCGAM.c  */

/* OUTPUT POINTER ARGUMENTS:
*/
float DELN1[6][11][32];/* change in number conc due to coagulation,[#/cm^3-s]*/
float Y[30];           /* working vector of conc(x,z) to examine in main.for  */

/************************************COAG()*************************************/
{
int   dimNK = *NK;
int   dimNX = *NX;
int   dimNZ = *NZ;
int   k, i, j;
float DY[32];      /* Derivative array used in calculations, [#/cm^3]          */
float TTRY;        /* Time step used for next integration step, [s]            */
float Tadjust;     /* NOTE**  this is passed but NOT changed for simple Euler  */
                   /* Actual (adjusted) time step for integration, [s]         */
float T    = 0.;   /* Elapsed simulation time during rxn step, [s]             */
                   /* T is reset to 0. for each node integration               */
int   CALL = 0;    /* No. of calls to Diffun() during simulation               */

for (j = 0; j < dimNZ-1; j++)    /* skips j= dimNZ-1, the bed: no coagulation    */
    for (i = 1; i < dimNX; i++) /* skips i= 0, the U/S boundary: no coagulation */
       {
        T = 0.0;                /* reinitialize time for next integration      */

/* Need to copy contents of 3-D array N1[j][i][k], written in Fortran main, to
*  1-D vector Y[k], independent of location in C. DIAM-Fort subscripting is
*  (1:NK+1) and DIAM-C subscripting is [0:NK], but we want the C subscripts to
*  correspond to their actual element order, e.g., element 1 having subscript 1:
*/
        for (k = dimNK; k >= 1; k--)
             Y[k] = N1[j][i][k-1];                    /* I.C. on concentration */

/*        Commented out:
          Diffun(Y,NK,ALPHA,FRAC,GAMMA,MAXFR1,MAXFR3,BAND1,BAND3,CALL,DY);
          This call can be used to get information on derivatives at system
          time (not same as T)=0., w/o changing Y, if so desired.
*/
INTEGRATE:
/* Determine a timestep from current reaction time, desired time for output,
*  and max timestep constraint:
*/

/* Comment out code to reverse and speed the block
*        if ((*DELT- T) >= *HMAX)
*             TTRY = *HMAX;
*        else if ((*DELT- T) < *HMAX)
*             TTRY = *DELT;
*/
        if ((*DELT- T) <= *HMAX)
             TTRY = *DELT;
        else if ((*DELT- T) > *HMAX)
             TTRY = *HMAX;

/* Integrate concentration in time using Euler's method (NOT adjusted by
   Predictor-Corrector method!):
*/
        Euler_PCM(&T,Y,&TTRY,DY,NK,ALPHA,FRAC,GAMMA,MAXFR1,MAXFR3,BAND1,
                  BAND3,&CALL,&Tadjust);

        T += TTRY;
        if(T< *DELT)
             goto INTEGRATE;
```

REFERENCES

Abbott, M.B. 1979. Computational Hydraulics: Elements of the Theory of Free Surface Flows. London: Pitman Publishing Limited.

Adler, P.M. 1981. "Interaction of Unequal Spheres 1. Hydrodynamic Interaction: Colloidal Forces." *Journal of Colloid and Interface Science*, 84(2), 461-474.

Ali, W., O'Melia, C.R., and Edzwald, J.K. 1984. "Colloidal Stability of Particles in Lakes: Measurement and Significance." *Water Science Technology*, 17, 701-712.

Annandale, G.W. 1987. Reservoir Sedimentation. New York: Elsevier.

Ariathurai, R. and Arulanandan, K. 1978. "Erosion Rates of Cohesive Sediments." *Journal of the Hydraulics Division, ASCE*, 104(HY2), 279-283.

Ariathurai, R. and Krone, R.B. 1976. "Finite Element Model for Cohesive Sediment Transport." *Journal of the Hydraulics Division, ASCE*, 102(HY3), 323-338.

Armstrong, N.E., Johnson, C., Wallace, I.E., Culkin, G.W., and Gordon, N.H. 1985. Managing Water Quality in Lake Austin and Town Lake. University of Texas at Austin, Center for Research in Water Resources.

Basco, D.R. 1984. An Implicit, Wiggle-Free, and Accurate Finite-Difference Algorithm for the One-Dimensional Transport-Diffusion Equation. (EL-84-4). US Army Corps of Engineer Waterways Experiment Station.

Bedford, K.W. and Abdelrhman, M. 1987. "Analytical and Experimental Studies of the Benthic Boundary Layer and Their Applicability to Near-Bottom Transport in Lake Erie." *Journal of Great Lakes Research*, 13(4), 628-648.

Blumberg, A.F. 1986. "Turbulent Mixing Processes in Lakes, Reservoirs, and Impoundments." In W.G. Gray (Ed.), Physics-Based Modeling of Lakes, Reservoirs, and Impoundments (pp. 79-105). New York: American Society of Civil Engineers.

Boyce, F.M. 1974. "Some Aspects of Great Lakes Physics of Importance to Biological and Chemical Processes." *Journal Fisheries Research Board of Canada*, 31(5), 689-730.

Brune, G.M. 1953. "Trap Efficiency of Reservoirs." *Transactions, American Geophysical Union*, 34(3), 407-418.

Camp, T.R. and Stein, P.C. 1943. "Velocity Gradients and Internal Work in Fluid Motion." *Journal Boston Society Civil Engineering*, 30, 219-237.

Chase, R.R.P. 1979. "Settling Behavior of Natural Aquatic Particulates." *Limnology and Oceanography*, 24, 417-426.

City of Austin 1982. Demographic and Land Use Projections and Distribution for the Growth Management Scenario to 2005. City of Austin Planning Department.

City of Austin 1984a. Lake Austin/Town Lake Water Quality Data Analysis. City of Austin Department of Public Works, Watershed Management Division.

City of Austin 1984b. Longhorn Dam and Town Lake. City of Austin Electric Department.

City of Austin 1984c. Stormwater Quality Modeling for Austin Creeks. Austin Department of Public Works, Watershed Management Division.

City of Austin and Engineering-Science, Inc. 1983. Final Report of the Nationwide Urban Runoff Program in Austin, Texas. (NTIS No. PB83-211102). USEPA.

Clark, M.M. 1985. "Critique of Camp and Stein's RMS Velocity Gradient." *Journal of Environmental Engineering*, 111(6), 741-754.

Csanady, G.T. 1978. "Water Circulation and Dispersal Mechanisms." In A. Lerman (Ed.), Lakes: Chemistry, Geology, Physics (pp. 21-64). New York: Springer-Verlag.

Culkin, G.W. 1986. Assessment of Toxicant Impacts in an Urban Receiving System. Unpublished M.S. thesis, University of Texas at Austin.

Cushing, R. 1990. Direct Filtration: Ripening from a Particle Perspective. Unpublished M.S. technical report, University of Texas at Austin.

Davis, R.W. 1984. "Finite Difference Methods for Fluid Flow." In J. Noye and C. Fletcher (Eds.), Computational Techniques and Applications (pp. 51-69). Amsterdam: Elsevier Science Publishers B.V.

Davis, R.W. and Moore, E.F. 1982. "A Numerical Study of Vortex Shedding from Rectangles. *Journal of Fluid Mechanics*, 116, 475-506.

Dobbins, W.E. 1943. "Effect of Turbulence on Sedimentation." *American Society of Civil Engineers, Transactions*, Paper No. 2218, 629-678.

Edzwald, J.K., Upchurch, J.B., and O'Melia, C.R. 1974. "Coagulation in Estuaries." *Environmental Science and Technology*, 8(1), 58-63.

Ellis, J.B., Hamilton, R., and Roberts, A.H. 1982. "Sedimentary Characteristics of Suspensions in London Stormwater." *Sedimentary Geology*, 33, 147-154.

Eppler, B., Neis, U., and Hahn, H.H. 1975. "Engineering Aspects of the Coagulation of Colloidal Particles in Natural Waters." *Progress in Water Technology*, 7(2), 207-216.

Espey, Huston, and Associates. 1976. The Effect of Projected Urban Land Development on the Quantity and Quality of Storm Water Runoff into Lake Austin. Document No. 7629. Prepared for Wallace, McHarg, Roberts and Todd and City of Austin Planning Department.

Farley, K.J. and Morel, F.M.M. 1986. "Role of Coagulation in the Kinetics of Sedimentation." *Environmental Science Technology*, 20(2), 187-195.

Fischer, H.B., List, E.J., Koh, R.C.Y., Imberger, J., and Brooks, N.H. 1979. Mixing in Inland and Coastal Waters. New York: Academic Press.

Frenette, M. and Julien, P.Y. 1986. "Advances in Predicting Reservoir Sedimentation." In S.Y. Wang, H.W. Shen, and L.Z. Ding (Eds.), River Sedimentation, Volume III (pp. 26-46). University, MS: The University of Mississippi.

Friedlander, S.K. 1965. "The Similarity Theory of the Particle Size Distribution of the Atmospheric Aerosol." In K. Spurny (Ed.), Aerosols, Physical Chemistry and Applications (pp. 115-130). Czechoslovakian Academy of Science.

Friedlander, S.K. 1977. Smoke, Dust and Haze: Fundamentals of Aerosol Behavior New York: Wiley.

Fukuda, M.K. and Lick, W. 1980. "The Entrainment of Cohesive Sediments in Freshwater." *Journal of Geophysical Research*, 85(C5), 2813-2824.

Gerritsen, J. and Bradley, S.W. 1987. "Electrophoretic Mobility of Natural Particles and Cultured Organisms in Freshwaters." *Limnology and Oceanography*, 32(5), 1049-1058.

Gibbs, R.J. 1983a. "Effect of Natural Organic Coatings on the Coagulation of Particles." *Environmental Science and Technology*, 17(4), 237-240.

Gibbs, R.J. 1983b. "Coagulation Rates of Clay Minerals and Natural Sediments." *Journal of Sedimentary Petrology*, 54(4), 1193-1203.

Gibbs, R.J. 1985. "Estuarine Flocs: Their Size, Settling Velocity and Density." *Journal of Geophysical Research*, 90(C2), 3249-3251.

Hahn, H.H. and Stumm, W. 1970. "The Role of Coagulation in Natural Waters." *American Journal of Science*, 268, 354-368.

Hahn, H.H., Kaser, F., and Klute, R. 1980. "Modeling Particulate Transport on Impounded Rivers." In M.C. Kavanaugh and J.O. Leckie (Eds.), Particulates in Water: Characterization, Fate, Effects, and Removal (pp. 213-231). Washington, D.C.: American Chemical Society.

Hakanson, L. and Jansson, M. 1983. Principles of Lake Sedimentology. Berlin-Heidelberg: Springer-Verlag.

Hall, R.W. and Chapman, R.S. 1985. Two-Dimensional Quickest: Solution of the Depth-Averaged Transport-Dispersion Equation (EL-85-3). US Army Corps of Engineer Waterways Experiment Station.

Han, M. 1989. Mathematical Modeling of Heterogeneous Flocculent Sedimentation. Unpublished Ph.D. Dissertation, University of Texas at Austin.

Happel, J. and Brenner, H. 1983. Low Reynolds Number Hydrodynamics. Boston: Martinus Nijhoff Publishers.

Hayter, E.J. 1987. Finite Element Hydrodynamic and Cohesive Sediment Transport Modeling System (EPA-600/3-83-045, revised). USEPA.

Holley, E.R. 1969. "Unified View of Diffusion and Dispersion." *Journal of the Hydraulics Division*, ASCE, 95(HY2), 621-631.

Holley, E.R. and Jirka, G.H. 1986. Mixing in Rivers. (E-86-11). U.S. Army Engineer Waterways Experiment Station.

Hunt, J.R. 1980. "Prediction of Oceanic Particle Size Distributions from Coagulation and Sedimentation Mechanisms." In M.C. Kavanaugh and J.O. Leckie (Eds.), Particulates in Water: Characterization, Fate, Effects, and Removal (pp. 243-257). Washington, D.C.: American Chemical Society.

Hunter, K.A. 1980. "Microelectrophoretic Properties of Natural Surface-Active Organic Matter in Coastal Seawater." *Limnology and Oceanography*, 25(5), 807-822.

Hunter, K.A. and Liss, P.S. 1979. "The Surface Charge of Suspended Particles in Estuarine and Coastal Waters." *Nature*, 282, 20-27.

Hunter, K.A. and Liss, P.S. 1982. "Organic Matter and the Surface Charge of Suspended Particles in Estuarine Waters." *Limnology and Oceanography*, 27(2), 322-335.

Hydroscience, Inc. 1976. Water Quality Management Planning Methodology for Urban and Industrial Stormwater Needs. Prepared for Texas Water Quality Board, Arlington, Texas.

Imberger, J., et al. 1987. Special Section: "Mixing in Stratified Fluids." *Journal Geophysical Research*, 92(C5), 5229-5495.

Imberger, J. and Hamblin, P.F. 1982. "Dynamics of Lakes, Reservoirs, and Cooling Ponds." *Annual Review Fluid Mechanics*, 14, 153-187.

Imboden, D.M. and Lerman, A. 1978. "Chemical Models of Lakes." In A. Lerman (Ed.), Lakes: Chemistry, Geology, Physics (pp. 341-356). New York: Springer-Verlag.

Imboden, D.M. and Schwarzenbach, R.P. 1985. "Spatial and Temporal Distribution of Chemical Substances in Lakes: Modeling Concepts." In W. Stumm (Ed.), Chemical Processes in Lakes. New York: John Wiley.

Jaluria, Y. and Torrance, K.E. 1986. Computational Heat Transfer. Washington, D.C.: Hemisphere Publishing Corporation.

Jobson, H.E. and Sayre, W.W. 1970. "Vertical Transfer in Open Channel Flow." *Journal of the Hydraulics Division, ASCE*, (HY3), 703-724.

Kajihara, M. 1971. "Settling Velocity and Porosity of Large Suspended Particles." *Journal Oceanography Society of Japan*, 27, 158-162.

Kawana, K. and Tanimoto, T. 1976. "Temporal Variation of Suspended Matter Near the Sea Bottom in Hiro Bay." *Mer*, 14, 47-52.

Kawana, K. and Tanimoto, T. 1979. "Suspended Particles Near the Bottom in Osaka Bay." *Journal of the Oceanographical Society of Japan*, 35, 75-81.

Kraus, E.B. and Turner, J.S. 1967. "A One-Dimensional Model of the Seasonal Thermocline: The General Theory and Its Consequences." *Tellus*, 19, 98-105.

Kuo, J.-T. and Thomann, R.V. 1983. "Phytoplankton Modeling in the Embayments of Lakes." *Journal of Environmental Engineering*, 109(6), 1311-1332.

Kuo, J.-T. and Thomann, R.V. 1985. Closure of 'Phytoplankton Modeling in the Embayments of Lakes'. *Journal of Environmental Engineering*, 111(1), 116-117.

Lam, D.C.L. 1986. "Basic Equations for Pollutant and Heat Transports in Lakes." In W.G. Gray (Ed.), Physics-Based Modeling of Lakes, Reservoirs, and Impoundments (pp. 17-78). New York: American Society of Civil Engineering.

Lapidus, L. and Pinder, G.F. 1982. Numerical Solution of Partial Differential Equations in Science and Engineering. New York: John Wiley and Sons.

Lavelle, J.W. and Mofjeld, H.O. 1987. "Bibliography on Sediment Threshold Velocity." *Journal of Hydraulic Engineering*, 113(3), 389-393.

Lawler, D.F. 1979. A Particle Approach to the Thickening Process. Unpublished Ph.D. dissertation, University of North Carolina at Chapel Hill.

Lawler, D F. 1987. "Particle Size Distributions: Measurements in Flocculation." In Proceedings of American Water Works Association conference on Influence of Coagulation on the Selection, Operation, and Performance of Water Treatment Facilities, Kansas City, MO., AWWA Seminar Proceedings No. 20014.

Lawler, D.F. and Wilkes, D.R. 1984. "Flocculation Model Testing: Particle Sizes in a Softening Plant." *Journal of the American Water Works Association*, 76(7), 90-97.

Lawler, D.F., O'Melia, C.R., and Tobiason, J.E. 1980. "Integral Water Treatment Plant Design: From Particle Size to Plant Performance." In M.C. Kavanaugh and J.O. Leckie (Eds.), Particulates in Water: Characterization, Fate, Effects, and Removal (pp. 213-231). Washington, D.C.: American Chemical Society.

Leonard, B.P. 1979. "A Stable and Accurate Convective Modelling Procedure Based on Quadratic Upstream Interpolation." *Computer Methods in Applied Mechanics and Engineering*, 19, 59-98.

Leonard, B.P., Vachtsevanos, G.J., and Abood, K.A. 1978. "Unsteady-State, Two-Dimensional Salinity Intrusion Model for an Estuary." In C.A. Brebbia (Ed.), Applied Numerical Modeling (pp. 113-123). New York: John Wiley and Sons.

Lerman, A. 1979. Geochemical Processes: Water and Sediment Environments. New York: John Wiley and Sons.

Lick, W. 1982. "Entrainment, Deposition, and Transport of Fine-Grained Sediments in Lakes." *Hydrobiologia*, 91, 31-40.

Ludwick, J.C., and Domurat, G.W. 1982. "A Deterministic Model of the Vertical Component of Sediment Motion in a Turbulent Fluid." *Marine Geology*, 45, 1-15.

Lyklema, J. 1978. "Surface Chemistry of Colloids in Connection with Stability." In K.J. Ives (Ed.), The Scientific Basis of Flocculation (pp. 3-36). Sijthoff and Noordhoff.

Lynch, D.R. 1986. Basic Hydrodynamic Equations for Lakes. In W.G. Gray (Ed.), Physics-Based Modeling of Lakes, Reservoirs, and Impoundments (pp. 17-53). New York: American Society of Civil Engineers.

McCave, I.N. 1984. "Size Spectra and Aggregation of Suspended Particles in the Deep Ocean." *Deep Sea Research*, 31(4), 329-352.

O'Melia, C.R. 1972. "Coagulation and Flocculation." In W.J. Weber Jr. (Ed.), Physicochemical Processes for Water Quality Control (pp. 61-109). New York: Wiley-Interscience.

O'Melia, C.R. and Bowman, K.S. 1984. "Origins and Effects of Coagulation in Lakes." *Schweizerische Zeitschrift fur Hydrologie*, 46(1), 64-85.

Overbeek, J.T. 1977. "Recent Developments in the Understanding of Colloid Stability." *Journal of Colloid and Interface Science*, 58(2), 408-422.

Panton, R.L. 1984. Incompressible Flow. New York: Wiley-Interscience.

Partheniades, E. 1986. "The Present State of Knowledge and Needs for Future Research on Cohesive Sediment Dynamics." In S.Y. Wang, H.W. Shen, and L.Z. Ding (Eds.), River Sedimentation, Volume III (pp. 3-25). University, MS: University of Mississippi.

Press, W.H., Flannery, B.P., Teukolsky, S.A., and Vetterling, W.T. 1986. Numerical Recipes, The Art Scientific Computing. New York, NY: Cambridge University Press.

Pruppacher, H.R., and Klett, J.D. 1978. The Microphysics of Clouds and Precipitation. Dordrecht: Reidel.

Raggio, G., and Jirka, G.H. 1988. "Fine Contaminated Sediment Erosion/Deposition in the Buffalo River, New York." In Abt, S.R. and Gessler, J. (Eds.), Proceedings First National Conference on Hydraulic Engineering, Colorado Springs, Colorado: American Society of Civil Engineers, 850-856.

Richardson, W.L., Smith, V.E., and Wethington, R. 1983. "Dynamic Mass Balance of PCB and Suspended Solids in Saginaw Bay - A Case Study." In D. Mackay, S. Paterson, S.J. Eisenreich, and M.S. Simmons (Eds.), Physical Behavior of PCBs in the Great Lakes (pp. 329-366). Ann Arbor, MI: Ann Arbor Science.

Roache, P.J. 1982. Computational Fluid Dynamics (Revised printing, 1985). Albuquerque, NM: Hermosa Publishers.

Saad, N., Pope, G.A., and Sepehrnoori, K. 1989. "Application of Higher Order Methods in Compositional Simulation" (Submitted for publication). *Society of Petroleum Engineers.*

Saffman, P.G. and Turner, J.S. 1956. "On the Collision of Drops in Turbulent Clouds." *Journal of Fluid Mechanics*, 1, 16-30.

Santschi, P. 1986. "Radionuclides as Tracers for Sedimentation and Remobilization Processes in the Ocean and in Lakes." In P.G. Sly (Ed.), Sediment and Water Interactions (pp. 437-449). New York: Springer-Verlag.

Sayre, W.W. 1969. "Dispersion of Silt Particles in Open Channel Flow." *Journal of the Hydraulics Division, ASCE*, 95(HY3), 1009-1038.

Shanahan, P. and Harleman, D.R.F. 1984. "Transport in Lake Water Quality Modeling." *Journal of Environmental Engineering*, 110(1), 42-57.

Shanahan, P. and Harleman, D.R.F. 1985. Discussion of 'Phytoplankton Modeling in the Embayments of Lakes'. *Journal of Environmental Engineering*, 111(1), 113-115.

Sheng, Y.P. 1986a. "Finite-Difference Models for Hydrodynamics of Lakes and Shallow Seas." In W.G. Gray (Ed.), Physics-Based Modeling of Lakes, Reservoirs, and Impoundments (pp. 146-228). New York: American Society of Civil Engineers.

Sheng, Y.P. 1986b. "Modeling Bottom Boundary Layer and Cohesive Sediment Dynamics in Estuarine and Coastal Waters." In A.J. Mehta (Ed.), Estuarine Cohesive Sediment Dynamics (pp. 360-400). New York: Springer-Verlag.

Sheng, Y.P. 1986c. "Numerical Modeling of Coastal and Estuarine Process Using Boundary-Fitted Grids." In S.Y. Wang, H.W. Shen, and L.Z. Ding (Eds.), River Sedimentation, Volume III. University, MS: University of Mississippi, 1426-1442.

Sheng, Y.P. and Lick, W. 1979. "The Transport and Resuspension of Sediments in a Shallow Lake." *Journal of Geophysical Research*, 84(C4), 1809-1826.

Sly, P.G. 1978. "Sedimentary Processes in Lakes." In A. Lerman (Ed.), Lakes: Chemistry, Geology, Physics (pp. 65-89). New York: Springer-Verlag.

von Smoluchowski, M.Z. 1917. "Versuch Einer Mathematischen Theorie der Koagulations- kinetic Kolloider Losungen." *Zeitschrift fur Physikalische Chemie*, 92, 129-158.

Stefan, H.G. and Demetracopoulos, A.C. 1981. "Cells-In-Series Simulation of Riverine Transport." *Journal of Hydraulics Division, ASCE*, 107(HY6), 675-697.

Tambo, N. and Watanabe, Y. 1979. "Physical Characteristics of Flocs 1: The Floc Density Function and Aluminum Floc." *Water Research*, 13, 409-419.

Thomann, R.V. and Mueller, J.A. 1987. Principles of Surface Water Quality Modeling and Control. New York: Harper and Row.

TNRIS. 1983. Selected ambient water quality data for the Lower Colorado River basin from Texas Natural Resource Inventory System.

Tritton, D.J. 1977. Physical Fluid Dynamics. Berkshire, England: Van Nostrand Reinhold (UK) Co. Ltd.

Tsai, C., Iacobellis, S., and Lick, W. 1987. "Flocculation of Fine-Grained Lake Sediments Due to a Uniform Shear Stress." *Journal of Great Lakes Research*, 13(2), 135-146.

Uchrin, C.G., and Weber, W.J., Jr. 1980. "Modeling of Transport Processes for Suspended Solids and Associated Pollutants in River-Harbor-Lake Systems." In R.

Baker (Ed.), Contaminants and Sediments (pp. 407-425). Ann Arbor Science: Ann Arbor, MI.

USEPA. 1983. Results of the Nationwide Urban Runoff Program, Volume I-Final Report (NTIS No. PB86-185552). USEPA.

USEPA. 1984. Report to Congress: Nonpoint Source Pollution in the U.S.. USEPA, Office of Water Program Operations, Water Planning Division.

Vanoni, V.A. (Ed.). 1975. Sedimentation Engineering. New York: American Society of Civil Engineers, 745 pp.

Wallace, I.E. 1986. The Effects of Urbanization on Toxicant Concentrations in Lake Austin and Town Lake, Texas. Unpublished M.S. thesis, University of Texas at Austin,

Wang, S.Y., Shen, H.W., and Ding, L.Z. (Eds.). 1986. River Sedimentation, Volume III. University, MS: University of Mississippi, 1822 pp.

Weilenmann, U., O'Melia, C.R., and Stumm, W. 1989. "Particle Transport in Lakes: Models and Measurements." *Limnology and Oceanography*, 34(1), 1-18.

Weitz, D.A. and Oliveria, M. 1984. "Fractal Structures Formed by Kinetic Aggregation of Aqueous Gold Colloids." *Physical Review Letters*, 52(16), 1433-1436.